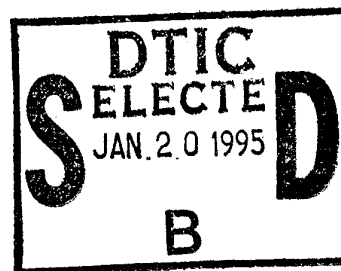


R&D6307-PA-01

PROJECT

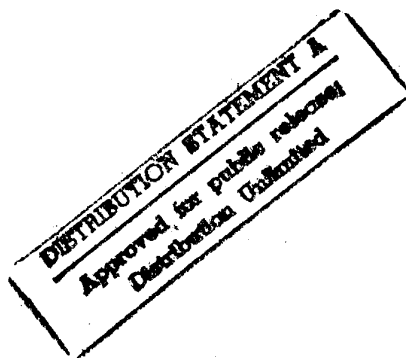
"SYNTHESIS AND APPLICATIONS
OF LARGE HETEROMETALLIC CLUSTER SYSTEMS"



CONTRACT NO: DAJA45 - 90 - C - 0034

NINTH INTERIM REPORT

15 JANUARY 1994



DTIC QUALITY INSPECTED 3

19950117 036

1. Executive Summary

This report contains technical details of organometallic chemistry of Lanthanides and Fullerenes, as presented as PhD thesis by Mr D. N Weldon, one of the postgraduate students sponsored in part by this project.

2. Staffing

No major staffing changes have taken place in the reporting period.

3. Technical Details

See enclosed thesis.

Accession For	
NTIS GRA&I	<input checked="" type="checkbox"/>
DTIC TAB	<input type="checkbox"/>
Unannounced	<input type="checkbox"/>
Justification	
By: <i>Performs</i>	
Distribution:	
Availability Codes	
Dist	Avail and/or Special
<i>A-1</i>	

**Organometallic Chemistry of Lanthanides
and Fullerenes.
Nonlinear Optical, Spectroscopic, and Electron
Microscopic Studies of Large Carbon Systems.**

by

Declan N. Weldon

A thesis submitted for the degree of
Doctor of Philosophy
in the University of Dublin

Department of Chemistry
University of Dublin
Trinity College
Dublin 2

December 1993

ABSTRACT

A brief introduction to the field of lanthanide organometallics is given covering the chemistry of Ln(II) and Ln(III) compounds. Chapter 1 reports the synthesis and characterisation of a range of new oxygen chelating ligands for use in organolanthanide chemistry. The synthesis and characterisation of the ligands 2-chloro(1,3,6-trioxaheptyl)benzene (L1), (1,3,6-trioxaheptyl)benzene (L2), 4,6-dichloro-1,3-bis(1,3,6-trioxaheptyl)benzene (L3), and 1,3-bis(1,3,6-trioxaheptyl)aminobenzene (L4) is described. A wide range of lanthanide starting materials (LnCl₃, LnCp₃, LnCp₂Cl) in various oxidation states [Ln(0), Ln(II), Ln(III)] were reacted with the lithium and sodium salts of the ligands. These salt elimination reactions gave products which demonstrate a number of different coordination modes depending on the nature of the lanthanide used and the ligand. The novel benzyl alcohol with the long ether side-chain (L2) provided the best characterised derivatives.

Chapter 2 deals with ytterbium and europium compounds in the (II) oxidation state. Preparation of these highly sensitive materials from the metal usually involves a range of activation methods. Activation of the metal with liquid ammonia was found to give greater yields and cleaner products than other methods. The chemistry of a new cyclopentadienyl Yb(II) derivative was investigated through its reactions with various metal carbonyls. A new synthetic route to an Yb-Fe ladder polymer is shown as well as the synthesis of the Eu-Fe analogue.

The relatively new field of fullerene chemistry is introduced. The synthesis of gram quantities of fullerenes is demonstrated using a novel fullerene generator which generates higher yields than the traditional steel generator described by Krätschmer and Huffman. The organometallic chemistry of C₆₀ is discussed in chapter 3 along with a description of a series of reactions involving Pt(PPh₃)₄, Pd(PPh₃)₄, Ir(CO)I(PPh₂Me)₂, W(MeCN)₃(CO)₃, Mo(MeCN)₃(CO)₃ and Yb. A Raman study was used to probe the bonding situation of the products from the palladium reactions. A study of possible η⁶-C₆₀ bonding using Mo(MeCN)₃(CO)₃ and W(MeCN)₃(CO)₃ produced η²-derivatives which were found to be highly unstable.

Almost all of the organometallic chemistry of fullerenes has concentrated on C₆₀. Chapter 4 describes the synthesis of a number of C₇₀ organometallic compounds. Pt(PPh₃)₄, Pd(PPh₃)₄, Ir(CO)I(PPh₂Me)₂, W(MeCN)₃(CO)₃, Mo(MeCN)₃(CO)₃ were used in this study to generate C₇₀ organometallic derivatives analogous to the C₆₀ products. To date only two organometallic derivatives have been reported in the literature despite the availability of gram quantities of this fullerene. C₇₀ offers a

greater variety of coordination sites than C₆₀ and this has led to difficulties in obtaining isomerically pure compounds.

Nonlinear optical studies of fullerenes have attracted much attention. Chapter 4 describes a study of the nonlinear optics of the organometallic derivatives of C₆₀ and C₇₀ synthesised in the course of this work. The bulk parameter of the third order nonlinear susceptibility ($\chi^{(3)}$) was determined for these materials using the technique known as Z-scan. All of the compounds displayed optical limiting properties and this has been explained in terms of reverse saturable absorption. The same technique was employed to measure the susceptibility of the Yb-Fe ladder polymer described in chapter 2.

The morphology of nanotubes derived from graphite through the plasma/arc technique was studied using high and low resolution transmission microscopy. A number of features of these systems are addressed in the course of this study including negative curvature, irradiation effects, helicity, capping, and bundling. A video recording of the irradiation effects provides a unique possibility to view this process on an atomic scale. A resonance Raman study of nanoparticles demonstrated a dispersive effect. A subtle change in the i.r spectrum of nanoparticles compared to graphite is interpreted.

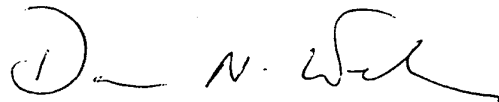
To my Parents and Family.

For Madeline and Christopher.

DECLARATION

The work described in this thesis has not been submitted in part or as whole for a degree in this or any other university. Except where acknowledgement is given, all the work described is original and was carried out by the author alone.

I agree that Trinity College may lend or copy this thesis on request.

A handwritten signature in black ink, appearing to read 'D. N. Weldon', with a stylized flourish at the end.

D.N. WELDON

ACKNOWLEDGEMENTS

I would like to thank Professor D.J. Cardin for his guidance, supervision and especially his friendship. Many thanks.

The academic staff of the Chemistry department especially Dr. C.J. Cardin and Professors Lloyd, McMurray and Corish for their assistance and patience, deserve a round of applause.

Special thanks to the technical and secretarial staff whose skills make it all come together. To Fred Cowzer for doing what he does best.

I am indebted to my colleagues in the Inorganic Research Lab. and the Opto-Electronics group for their wisdom and friendship. To Andy, Brendan, Feargal, Chris, Xia, Mick, Barry, Pat, Joe, Shay, Debbie, Maire, Sylvia, Marika, John, Michel, Karl, Adrian, Kathleen, Fryad, Hugh, Anna, Des, Pat, Joe, J.P, Morgan and John L.

I am grateful to Professor Werner Blau for his encouragement, enthusiasm, trust and friendship.

To Andy, Sharon and Stephanie for being Andy, Sharon and Stephanie.

Special thanks to Prof. Hans Kuzmany, Dr. Henny Zandbergen and David John for their expertise.

I would like to acknowledge the Kriebel Fund, Bayer Chemicals and the U.S. Army for financial assistance during the course of this work.

None of this would have been possible without the fantastic support and encouragement of my parents, sisters and brothers. Special thanks also to my extended family and to Irene and Mick.

To Madeline and Christopher for their love, support, humour and for reminding me that life exists outside of the lab.

Table of Contents

Introduction:	Section 1: Lanthanides	1
	Section 2: Fullerenes	8
	Section 3: Nonlinear Optics	11
	Section 4: Nanotubes	14
	Experimental Techniques	15
	References	18
Chapter 1	New Ligands for Organo-lanthanide Chemistry	23
	1. Synthesis of and reactions involving 2-Chloro(1,3,6-trioxaheptyl)benzene (L1)	26
	2. Synthesis of and reactions involving 2-(1,3,6-trioxaheptyl)benzylalcohol (L2)	28
	3. Synthesis of and reactions involving 4,6-dichloro-1,3-bis(1,3,6-trioxaheptyl)benzene (L3)	33
	4. Synthesis of and reactions involving (1,3-bis(1,3,6-trioxaheptyl)2-aminobenzene) (L4)	35
	Experimental	38
	References	49
Chapter 2	Organometallic Lanthanide(II) Chemistry	52
	1. Introduction	53
	2. Synthesis and reactions of YbCp_2^{I}	54
	3. Reaction of YbCp_2^{I} with $\text{Co}_2(\text{CO})_8$	55
	4. Reaction of YbCp_2^{I} with $\text{Fe}_3(\text{CO})_{12}$	56
	5. Reaction of YbCp_2^{I} with MeCN	57
	6. Reactions involving Lanthanides and transition metals	58
	7. Reaction of Eu with $\text{Fe}_3(\text{CO})_{12}$	60
	8. Experimental	61
	References	66

Chapter 3 Synthesis and Purification of Fullerenes and the Organometallic
Chemistry of C_{60} 68

1. Production of C_{60} and C_{70}	69
2. Chemistry of C_{60}	72
3. Metal-Alkene bonding	77
4. Palladium (0) and platinum (0) chemistry	80
5. Reaction of $Pd(PPh_3)_4$ with C_{60}	82
6. Reaction of excess $Pd(PPh_3)_4$ with C_{60}	83
7. Synthesis of $C_{60}Pd_x$	84
8. Raman studies on palladium C_{60} organometallics	86
9. Addition reactions of Ir(I) compounds	88
10. Reaction of C_{60} with $IrI(CO)(PPh_2Me)_2$	90
11. Reaction of x s $IrI(CO)(PPh_2Me)_2$ with C_{60}	92
12. Reaction of $Mo(MeCN)_3(CO)_3$ with C_{60}	93
13. Reaction of $W(MeCN)_x(CO)_{6-x}$ with C_{60} ($X=3,2$)	96
14. Reaction of C_{60} with activated Yb	97
Experimental	100
References	107

Chapter 4 Organometallic Chemistry of C_{70}

1. Introduction	112
2. Reaction of C_{70} with $Pd(PPh_3)_4$	115
3. Reaction of C_{70} with $Pt(PPh_3)_4$	116
4. Reaction of C_{70} with $IrI(CO)(PPh_2Me)_2$	117
5. Reaction of C_{70} with $Mo(MeCN)_3(CO)_3$	118
6. Reaction of C_{70} with $W(CO)_x(MeCN)_{6-x}$ ($X=3,2$)	118
Experimental	120
References	122

Chapter 5 Nonlinear Optics of Fullerenes and Metallofullerenes 123

1. Introduction	124
2. Aims of study	126
3. Z-Scan Technique	127
4. Absorption spectra	129
5. Experimental	132

Chapter 5 contd.	
6. Results	132
7. Discussion	133
8. Im($\chi^{(3)}$) determination of Yb-Fe polymer	134
9. References	135
Chapter 6 Nanoparticles, Morphology and Spectroscopy	137
Introduction	138
1. Raman spectroscopy of nanoparticles	139
2. Resonance Raman spectroscopy of nanoparticles	141
3. I.r spectroscopy of nanoparticles	144
Spectroscopy conclusions	145
4. Microscopy of nanoparticles	145
5. Curved nanotubes	147
6. HREM study of curved nanotubes	148
7. Buckybundles	149
8. Electron irradiation of nanoparticles	150
9. Capping and helicity	153
10. Conclusions	155
Experimental	156
References	158

Abbreviations

thf	: tetrahydrofuran
tlc	: thin layer chromatography
dme	: dimethoxyethane
MEM	: 2-methoxyethoxymethyl
EDTA	: ethylene diamine tetra(acetic acid)
CpH	: cyclopentadiene
Cp ₂ ¹	: Yb(CpCH ₂ (CH ₃) ₂ CH ₂ (CH ₃) ₂ Cp)
Cp*H	: Pentamethyl cyclopentadiene
Ln	: lanthanides
T.M.	: transition metal
TDAE	: tetrakis(dimethylamino)ethylene
LUMO	: lowest unoccupied molecular orbital
HOMO	: highest occupied molecular orbital
NLO	: nonlinear optics
THG	: third harmonic generation
DFWM	: degenerate four-wave mixing
TPA	: two photon absorption
RSA	: reverse saturable absorption
i.r	: infra-red
uv/vis	: ultra-violet/visible (spectrum)
b.p	: boiling point
nmr	: nuclear magnetic resonance
m.p	: melting point
FAB	: fast atom bombardment (mass spectroscopy)
TEM	: transmission electron microscopy
HREM	: high resolution electron microscopy

INTRODUCTION

Section I: Lanthanides.

The Rare-Earth elements comprise the fourteen elements from Ce to Lu but are commonly taken to include La and sometimes Sc and Y as well. The electronic configurations of the free atoms (Table 1.1A) are determined only with difficulty because of the complexity of their atomic spectra but it is generally agreed that they are nearly all $[\text{Xe}] 4f^n 5d^0 6s^2$. Normally on descending a group in the periodic table the covalent and ionic radii increase due to the filling of extra shells of electrons. On moving across a period, the covalent and ionic radii decrease because the nuclear charge is increased and since the extra orbital electrons shield this charge imperfectly all the electrons are pulled in closer. The shielding effect of electrons decreases from $s < p < d < f$. Though the contraction in size from element to element is small, the additive effect over the fourteen elements from Ce to Lu is about 0.2 \AA i.e. radial size decreases gradually and monotonically from La(III) (1.061 \AA) to Lu(III) (0.848 \AA). The 4f orbitals differ from the valence orbitals of other metallic elements in their relatively limited radial extension. Because the 4f orbitals do not extend significantly beyond the filled 5f and 5p of the xenon inert core, a trivalent lanthanide ion looks like a closed shell inert gas electron cloud with a tripositive charge as far as its interaction with ions or groups is concerned. This has a major effect on the chemical and physical properties of these metals and their complexes. This small radial extension of the lanthanides valence orbitals means that the metals' interactions with ligands are smaller than those with transition metal complexes, which is why the chemistry tends to be more ionic. Another effect of this limited radial extension of the 4f orbitals is that the chemistry of the trivalent lanthanide ions can be similar in many systems regardless of the $4f^n$ configuration. The most common oxidation state of the lanthanides is (III). Though all of the lanthanides can be prepared in the (II) oxidation state in alkaline earth-metal matrices, only Eu(II) is stable in aqueous solution for any length of time. Similarly, four lanthanides have now been synthesized as solid compounds in the (IV) oxidation state, but only one ion, Ce(IV), is stable in aqueous solution⁽¹⁾. Though lanthanide redox properties partly reflect such electronic factors as the inherent stability of the unfilled, half-filled and completely filled f-shell, it also appears that chemical factors such as solvation energies play an important role in determining the stability of various oxidation states.

Atomic number	Name	Symbol	Atomic Config.	Oxidation states	Radius M ³⁺ (Å)
57	Lanthanum	La	5d ¹ s ²	(III)	1.061
58	Cerium	Ce	4f ¹ 5d ¹ 6s ²	(III), (IV)	1.034
59	Praseodymium	Pr	4f ³ 6s ²	(III), (IV)	1.013
60	Neodymium	Nd	4f ⁴ 6s ²	(III), (IV)	0.995
61	Promethium	Pm	4f ⁵ 6s ²	(III)	0.979
62	Samarium	Sm	4f ⁶ 6s ²	(III), (II)	0.964
63	Europium	Eu	4f ⁷ 6s ²	(III), (II)	0.950
64	Gadolinium	Gd	4f ⁷ 5d ¹ 6s ²	(III)	0.938
65	Terbium	Tb	4f ⁹ 6s ²	(III), (IV)	0.923
66	Dysprosium	Dy	4f ¹⁰ 6s ²	(III)	0.908
67	Holmium	Ho	4f ¹¹ 6s ²	(III)	0.894
68	Erbium	Er	4f ¹² 6s ²	(III)	0.881
69	Thulium	Tm	4f ¹³ 6s ²	(III), (II)	0.869
70	Ytterbium	Yb	4f ¹⁴ 6s ²	(III), (II)	0.858
71	Lutetium	Lu	4f ¹⁴ 5d ¹ 6s ²	(III)	0.848

Table.1.1A Properties of Lanthanide atoms and ions.

In the Pearson terminology, lanthanides are hard acids.⁽²⁾ As successive electrons are removed from a neutral lanthanide atom, the stabilising effect is in the order 4f>5d>6s, this being the order in which the orbitals penetrate through the inert core of electrons towards the nucleus. By the time an ionic charge of +3 has been reached, the preferential stabilisation of the 4f orbitals is such that in all cases the 6s and 5d orbitals have been emptied and in most cases the electrons remaining in the 4f orbitals are themselves so far embedded in the inert core as to be immovable by chemical means. Ce and Pr are exceptions because their 4f orbitals are still at a comparatively high energy and can therefore lose a further electron.

The large ionic radii of the lanthanide ions give rise to complexes with coordination numbers higher than those normally found in transition metal chemistry. Lanthanide ion coordination numbers of 8 are very common and some as large as 12 have been observed. Obviously the ionic radii for the (II) ions are larger (by about 0.08 - 0.15 Å) than the corresponding (III), and the (IV) lanthanide radii are smaller by about 0.08 - 0.11 Å.

The absence of 5d electrons and the inertness of the lanthanides 4f shell makes π -backbonding energetically unfavourable and simple carbonyls for instance, have only been obtained in argon matrices at 8-12K. Essentially ionic cyclopentadienyls are well known and an increasing number of σ -bonded Ln-C compounds have been reported. The most striking difference in chemistry between the metals arises with the four elements for which non-trivalent oxidation states are accessible under normal reaction conditions Ce(IV)-4f⁰,

Eu(II)-4f⁷ , Yb(II)-4f¹⁴ and Sm(II)-4f⁶.

The past decade has seen a period of vigorous activity in the field of lanthanide organometallic chemistry.^(3a-3r) Early studies on organolanthanide complexes namely the cyclopentadienyl complexes confirmed that these were rather ionic and suggested that organolanthanide compounds would merely be trivalent versions of alkali and alkaline-earth metal compounds. In contrast to the diverse chemistry observed for a row of transition elements the lanthanide elements were thought to have a very similar chemistry. Most lanthanide chemistry has centred on the trivalent state. Of the few lanthanide elements which have readily accessible non-trivalent oxidation states Ce(IV), Eu(II), Sm(II) and Yb(II), none have both the (IV) and the (II) oxidation states readily available on the same metal. Hence within the lanthanide series the two-electron processes common in transition-metal chemistry such as oxidative addition and reductive elimination are not possible at a single lanthanide metal centre. In addition to this apparently limited chemistry the organolanthanide complexes are experimentally more difficult than most transition-metal systems. Almost all organolanthanides are extremely air and moisture sensitive and even the metal trihalide starting materials are hydrolytically unstable (all lanthanide compounds are strongly oxophilic). Purification and isolation of organolanthanide compounds is difficult because the compounds decompose on chromatographic supports, generally cannot be sublimed in high yield, and frequently undergo ionic redistribution reactions giving mixtures during recrystallisation attempts. Moreover, the paramagnetism of many of the metals limits characterisation by nmr spectroscopy.

Two generalisations on organolanthanide stability are usually followed to obtain isolable organolanthanide complexes. First, electrostatic interactions must be optimised by using stable organic anions to balance the charge on the metal cation. Secondly, additional stability often can be gained by choosing large bulky groups which can completely occupy the coordination sphere and sterically block decomposition pathways. The most prevalent ligands in organolanthanide chemistry C₅H₅⁻ and C₈H₈⁻ meet these requirements. Lu, Er and Yb have been investigated more extensively than the others because their small size makes steric saturation of the metal co-ordination less difficult and hence provides more tractable complexes.

Since the electrostatic charge balance requirement for stability must be met in organolanthanide complexes, the determining factor in stability/reactivity is often steric. Several basic generalisations appear to apply to trivalent organolanthanides based on current data. High reactivity and limited stability are associated with free co-ordination sites i.e, steric unsaturation and with terminal as opposed to bridging, ligands. High reactivity or limited stability can be caused by insufficient ligand bulk around the metal (steric unsaturation) or by excessive ligand bulk (steric "oversaturation") when it leads to structures with open co-ordination positions and terminal ligands. The three classes of organolanthanide complexes, sterically saturated, sterically unsaturated and sterically oversaturated compounds display different types of reactivity due to the differences in

terminal vs bridging groups and the relative availability of open co-ordination positions. This can be illustrated by the metalation reactivity of organoanthanide hydrides with ethers, hydrocarbons and pyridine. The sterically saturated hydrides $[(C_5H_4R)Ln(\mu-H)(thf)]_2$, $R=H$ or CH_3 ; $Ln=Er, Y$ or Lu) are stable to ethers⁽⁴⁾; metalate only rather acidic hydrocarbons such as terminal alkynes, and undergo 1,2- LnH addition rather than metalation when reacted with pyridine. In contrast the sterically oversaturated $[(C_5Me_5)_2LuH]_n$ complex decomposes ethers⁽⁵⁾, metalates pyridine to form a $(C_5Me_5)_2Lu(\eta^2-NC_5H_4)$ complex, and is such a powerful metalation reagent that not only benzene and Me_4Si are metalated, but even CH_4 . The sterically unsaturated $[(Cp^*)_2Sm(\mu-H)]_2$ ⁽⁶⁾ has intermediate reactivity-it decomposes ether and metalates pyridine, but metalates arenes only slowly.

Given that all this reactivity involves the same, nominally ionic, $Ln-H$ bond, it is clear that steric factors influence trivalent organoanthanide chemistry to a great extent. Obviously the thermodynamic difference in bond strengths and the differences in the charge/radius ratio from one metal to another will also affect the chemistry. However in many cases these factors are likely to be sufficiently similar that it is the steric parameters which will largely govern the observed variations in reactivity.

Although divalent lanthanide ions for almost all the elements in the series have been generated by irradiating trivalent ions doped into CaF_2 ,⁽⁷⁾ only three elements have divalent states which are chemically accessible in organometallic systems under normal conditions: Eu , Sm and Yb . It is only for these elements that X-ray crystallographic structures of divalent organoanthanide complexes are available.

The aqueous reduction potentials for the $Ln(II) - Ln(III)$ couple are reported to be 0.35V for Eu , -1.1V for Yb and -1.5V for Sm (vsNHE)⁽¹⁾ indicating that $Eu(II)$ should be the most stable and $Sm(II)$ the most reactive in terms of reducing power. Complexes of the smaller $Yb(II)$ ion could be the most stable in terms of steric saturation of the metal co-ordination sphere and $Sm(II)$ the most reactive in this regard. $Sm(II)$ is most desirable not only in terms of high reactivity, but also when nmr characterisation is considered. Sm provides the only $Ln(II)-Ln(III)$ system in which both oxidation states have complexes which are nmr-accessible. Despite room temperature magnetic moments of 3.4-3.8 μB for $Sm(II)$ and 1.3-1.9 μB for $Sm(III)$,⁽⁸⁾ 1H nmr resonances are reasonably sharp and are found within 10ppm of the normal 0-10ppm region where diamagnetic resonances are located. This is not true for $Eu(II)$, $Eu(III)$ or $Yb(III)$ which have room temperature magnetic moments in the ranges 7.4-8.0, 3.4-4.2 and 4.2-4.9 μB , respectively. Of course, diamagnetic $Yb(II)$ provides nmr complexes having normal nmr parameters.

Divalent organoanthanide complexes differ in appearance from trivalent species in that their colours are more intense and these colours vary as the ligand set is changed. For trivalent species these colours arise from Laporte forbidden 4f-4f transitions.⁽⁹⁾ Due to the limited radial extension of the 4f orbitals, crystal field splitting is very small and hence the colours vary little as the ligand set is changed. Another consequence of the limited radial extension is that little vibronic coupling occurs to relax the Laporte-forbidden nature of the

transitions. Hence the colours of the complexes are pale. In contrast the colours of the divalent lanthanide ions are attributed to Laporte allowed 4f-5d transitions. The variation in colour with ligand environment is greatest with Sm(II) and Yb(II). Organometallic Sm(II) compounds can be green or purple and Yb(II) species can be yellow, red, blue, green or purple. Eu(II) organometallics, on the other hand are almost always yellow, orange or red.

There are numerous examples where the metal gets oxidised and forms a sterically saturated trivalent species which contains a new ligand involving the most electronegative of the donor atoms available in the system. As expected, reactivity parallels reduction potential, with Sm(II) more reactive than Yb(II) which is more reactive than Eu(II).

Although the majority of divalent organolanthanide structures are similar to their Ln(III) analogues, the remarkable $(C_5Me_5)_2Ln$ complexes ($Ln = Sm, Eu$) are not.⁽¹⁰⁾ The bent, sterically unsaturated structures are unexpected on the basis of both electrostatic and steric arguments and this structure occurs regardless of the 4f electron configuration or reduction potential of the metal. This unusual geometry may signal the existence of an entire series of unanticipated structural possibilities for divalent lanthanides.

Compounds with covalent bonds between lanthanide elements and metals and/or metals are receiving increasing interest. The number of clearly characterised derivatives is not great. First examples in this area are organometallic compounds with lanthanide-to-transition metal bonds, prepared by salt elimination methods (Fig.1.3) or by the reaction of finely divided lanthanide metals with organometallic compounds of transition metals.

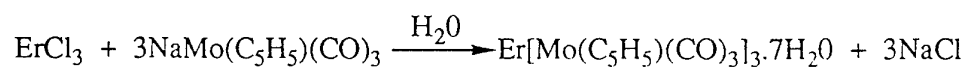
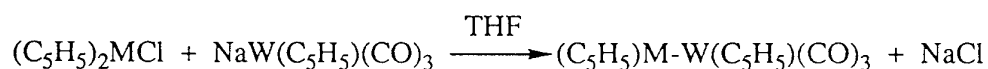


Fig.1.3 Salt elimination methods.

The bonding in these compounds is not completely understood but i.r data for the tungsten compound suggests isocarbonyl linkages.⁽¹¹⁾ The i.r data for the erbium compound does not show isocarbonyl links.⁽¹²⁾ However its structure must be under some doubt in view of the fact that the reaction was carried out using water as a solvent !

Recently however Magomedov *et al.*⁽¹³⁾ have reported a compound containing a lutetium-ruthenium bond. This compound is well characterised and provides the first example of a transition metal-lanthanide bond in an organometallic system. More recently Shore and Deng⁽¹⁴⁾ have synthesized a remarkable compound with a ladder polymer structure which contains an ytterbium-iron bond in each repeat unit.

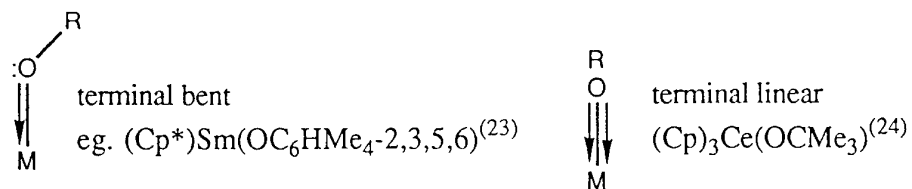
It is clear that the bonding in all of the compounds so far studied is predominantly ionic and that covalent interactions between ligand molecular orbitals and metal valence atomic orbitals are considerably smaller than in d-block organometallics. With the exception

of the results for lanthanide carbonyls in argon matrices at 4K, there is no evidence that the lanthanide ions in isolable organometallics can engage in appreciable π -bonding to uncharged ligands. Much of the organometallic chemistry of the lanthanides appears to be reminiscent of alkaline earth organometallic chemistry. The lack of covalency means that directional bonding is relatively unimportant. The ionicity of the bonding causes organolanthanides to be rather nucleophilic. Fisher⁽¹⁵⁾ has performed calculations that suggest that the lanthanide 5d orbitals, which are less contracted than the 4f orbitals, have the best prospects for metal-ligand overlap and covalent bonding. For divalent lanthanides, the 5d orbitals range from about 0.24eV(La(II)) to about 5eV(Yb(II)) higher in energy than the 4f orbitals. For the trivalent ions, the 5d orbitals are from about 6eV(Ce(III)) to about 12eV(Yb(III)) higher in energy than the 4f orbitals. In all cases the 6s and 6p are higher in energy than the 5d levels.⁽¹⁶⁾ Hayes and Thomas⁽¹⁷⁾ from a study of lanthanide tris(cyclopentadienyl) concluded that the covalent bonding probably involves the metal 5d orbitals to the greatest extent and that about 0.1 to 0.3 electrons are transferred from the three cyclopentadienyls to the metal. They also suggest that the Lewis acidity of the LnCp₃ complexes is due to the empty 5d_{z²}. Clearly the bonding situation in organolanthanide compounds is by no means fully understood and further work in this field is necessary to shed more light on the problem.

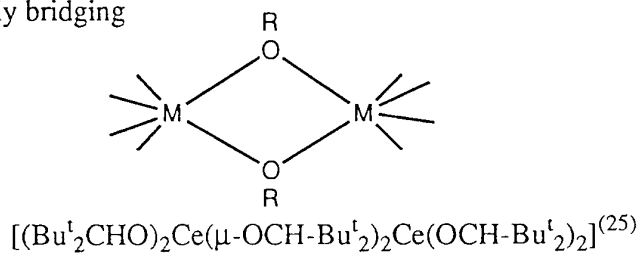
Alkoxy and Aryloxy Chemistry of Lanthanides.

There are only two sizeable reviews to date which deal exclusively with Ln-O-C derivatives,^(18, 19) even though research in this area has progressed rapidly in the past decade. Although behaving generally as either one-electron ligands (\cdot OR) or two electron donors (:OR-) with notable flexibility, these can function sometimes in a non-innocent manner showing more than one electronic and structural configuration (Fig.1.4) with a variable (terminal, μ^2 or μ^3 -bridging) behaviour. In view of their oxophilic nature, aryloxy ligands prefer to be oxygen bonded with the lanthanides,^(20,21) although η^5 -bonding with another phenyl ring intramolecularly in the case of ytterbium has been observed by Deacon *et al.*⁽²²⁾ The most convenient route to the alkoxy/aryloxy derivatives is by the salt elimination method. The favoured salt is potassium over sodium and lithium as the halides are less soluble than the corresponding sodium or lithium halides and therefore can be removed from the reaction mixture more easily. Although crystallographic studies of some lanthanide alkoxides have been reported, such studies are in general frustrated by factors such as unsuitable crystals, twinning problems, high solubility in common organic solvents including the parent alcohol as well as the extreme sensitivity to atmospheric moisture.

(a) Terminal (M-OR)



(b) Doubly bridging



(c) Triply bridging

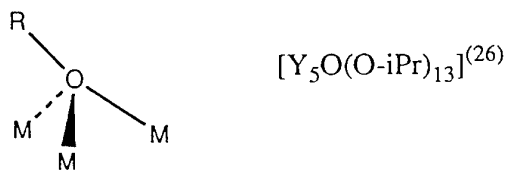


Fig.1.4 Modes of co-ordination of oxygen containing ligands.

In addition to diamagnetic species such as Sc, Y, La and Lu (in III oxidation state), Ce(IV) as well as Yb(II), some paramagnetic lanthanide complexes (e.g., Sm(III)) exhibit rather sharp signals in their ^1H and ^{13}C nmr spectra at ambient temperatures.⁽¹²⁾ This is due to the rapidity of electronic spin lattice relaxation in these systems. Some species such as Gd(III) give highly broadened resonances due to their long relaxation time.⁽²⁷⁾ Special irradiation multipulse techniques are being developed to resolve this type of problem.

Section 2: Fullerenes.

In 1985 Kroto *et al.* observed a stable carbon molecular ion consisting of sixty carbon atoms in the mass spectrum of laser ablated graphite.⁽²⁸⁾ Research into this phenomenon continued at a relatively slow pace until early in 1990 when Huffman and Krätschmer reported⁽²⁹⁾ evidence for the presence of this C₆₀ species in carbon dust prepared from vaporised graphite and presented a method for producing gram scale quantities of a whole range of new closed cage carbon structures. This family of new carbon structures were called 'fullerenes' after the architect Buckminster-Fuller who patented designs for geodesic domes based on five and six membered ring units.

Four methods for producing fullerenes have been reported (a) laser ablation of a graphite disc⁽²⁸⁾ (b) resistive heating of graphite electrodes⁽³⁰⁾ (c) plasma/arc consumption of graphite rods and⁽²⁹⁾ (d) an oxidising benzene flame⁽³¹⁾. The most common method employed for producing fullerenes is the Huffman-Krätschmer carbon arc system in which a graphite electrode is vapourised in a low pressure helium atmosphere by passing an electric current (a.c. or d.c.) through two graphite electrodes thus generating an arc. The soot subsequently produced by this method contains appreciable amounts of C₆₀, C₇₀ and higher fullerenes. The two most common methods for fullerene production, resistive heating and arc heating, give different product distributions. Resistive heating of graphite by the UCLA group yielded soot, the Fullerene content of which was 65% C₆₀, 30% C₇₀ and 5% of higher fullerenes⁽³²⁾. The arc/plasma unit used in this study produces soot which contains approximately 60% C₆₀, 37% C₇₀ and the remaining 3% of mainly C₈₄. Achiba *et al.*⁽³³⁾ who produced soot by arc heating isolated a significant amount of C₈₂.

Kroto⁽³⁴⁾ postulated the cage structures for C₆₀ and C₇₀ based on an 'isolated pentagon' rule. Pentagon incorporation into a graphitic sheet causes that sheet to curl up and enables some of the peripheral dangling bonds to join. Incorporation of further pentagons can cause the structure to eventually close. Smalley⁽³⁵⁾ suggests that the energetically most favoured form of any open graphitic sheet is one which (a) is made up solely of pentagons and hexagons and (b) has as many pentagons as possible whilst (c) avoiding adjacent pentagons. These three criteria are necessary to comply with the "isolated pentagon rule". All higher fullerenes isolated and characterised by Diederich *et al.*⁽³⁶⁾ and Achiba *et al.*⁽³³⁾ obey the isolated pentagon rule i.e. all twelve pentagons are fully annealed by hexagons yielding corannulene/pyracyclene type structures. To date there is no other explanation of fullerene growth that is compatible with the observation that the overall yield of C₆₀ can be as high as 20% of all the condensing vapour. Since C₆₀ is not energetically favoured over C₇₀ or the larger fullerenes or even bulk graphite this high yield formation of C₆₀ must be explained by a very efficient path in the kinetics of cluster growth before the clusters get too large. Studies⁽³⁷⁾ of the isotope distribution of C₆₀ produced from 1:1 mixtures of ¹²C and ¹³C graphite powders show beyond any reasonable doubt that C₆₀ under the conditions of arc synthesis is formed by the aggregation of small carbon

fragments. Heath⁽³⁸⁾ has proposed a mechanism in which graphitic sheets grow from small carbon radicals and then coalesce as quickly as possible to form fullerenes as small as C_{28} . These small fullerenes have no dangling bonds but contain adjacent pentagons. This model then explains the abundance of C_{60} by the fact that it is a special stopping place in the growth kinetics since it is the first that avoids the highly reactive adjacent pentagon configuration. Smalley dismisses the Heath 'all fullerene growth model' on the evidence of the facile synthesis of the endohedral metal fullerene complexes.⁽³⁵⁾ The 'all fullerene growth model' does not, according to Smalley, lend itself to the facile production of endohedral fullerenes, due to the fact that the metal atom may be too large (e.g., La) to fit on the inside of the small fullerenes and too difficult to insert once the fullerene is closed. These carbon cages with a metal inside (denoted using $M@C_n$) can be easily prepared by doping a graphite rod with the metal halide or oxide before vapourisation. The most abundant species isolated so far are the endohedral complexes of C_{82} e.g. $La@C_{82}$.

C_{60} is a three dimensional cage structure comprising of twelve pentagons and twenty hexagons (Fig.1.2.1). There are two types of carbon double bonds possible (a) a carbon double bond between two six membered rings (6:6 fusion) and (b) a carbon double bond between a pentagon and a hexagon (5:6 fusion), these can be envisaged as inter-pentagon double bonds or intra-pentagon double bonds. Close examination of the structure reveals that C_{60} is made up of a number of pyracyclene units and on the basis that pyracyclene is a $4n\pi$ system it was hypothesised that each unit would provide a driving force for the capture of up to two electrons either by direct electron transfer to give a $4n+2 \pi$ electron dianion or in the form of a lone pair to give a 'cyclopentadienide' monoadduct. C_{70} is similar to C_{60} except that there is an extra band of five hexagons around the centre of the C_{60} structure giving it a 'rugby ball' appearance. There are five distinct types of carbon environment in C_{70} (Fig.1.2.2).

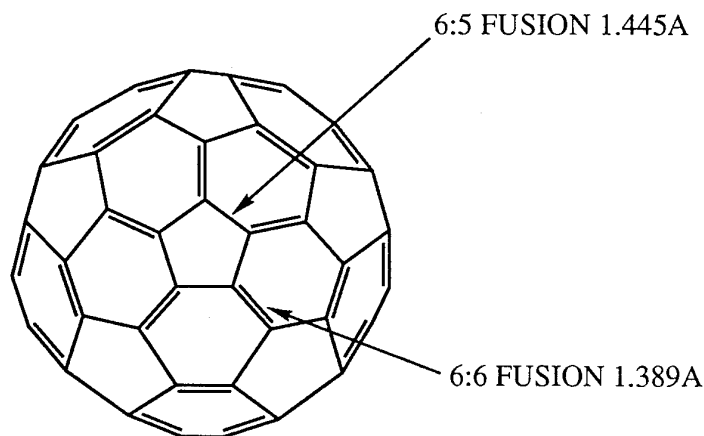


Fig.1.2.1 Buckminsterfullerene (C_{60})

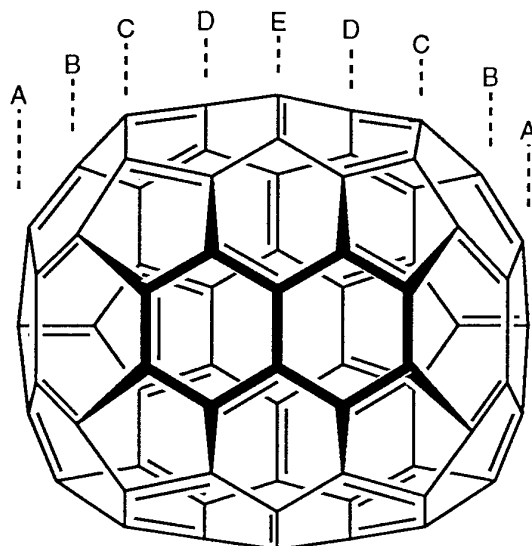


Fig.1.2.2 C_{70}

C_{60} and C_{70} are probably the most extensively characterised molecules to date despite being only relatively new. Kroto and Krätschmer provided mass spectrograms of the soot from ablated/arced graphite showing C_{60}^+ (720 amu) and C_{70}^+ (840 amu) as the most abundant peaks among a range of fullerene products. Kroto realised early on in the search for C_{60} ⁽³⁹⁾ that the ^{13}C nmr should contain only one peak since all the carbon atoms are equivalent and that C_{70} should show five peaks. ^{13}C nmr experiments by Taylor and Kroto showed clearly the expected result for the cage structures.⁽⁴⁰⁾ C_{60} has a single resonance at 143ppm (ref. to TMS) whilst C_{70} has five, 130ppm(10C), 144ppm(20c), 146ppm(10C), 147ppm(20C) and 150ppm(10C) (see Fig.1.2.2). This was the most convincing proof for the proposed cage structures of these molecules. Hawkins⁽⁴¹⁾ then provided the first crystal structure containing a C_{60} osmate ester. This was followed by the first organometallic derivatives of C_{60} synthesised by Fagan *et al.*⁽⁴²⁾. Balch *et al.*⁽⁴³⁾ obtained a crystal structure containing the C_{70} molecule. The synthesis of a number of organometallic derivatives of C_{60} and C_{70} is described in Chapters 3 and 4. Research in the field of fullerenes spans most sciences and a list of review articles is published in reference (45).

Section 3: Non-Linear Optics (NLO) of fullerenes.

The interaction of light with matter is usually characterised by several phenomena: these include light absorption, refraction, scattering and luminescence. All of these were classically regarded to be wavelength dependent, but independent of light intensity. The availability of the laser as a source of high intensity coherent light has opened a field where the characteristic optical properties of materials become a function of intensity. The study of this field is called non-linear optics.

The first developments have already given rise to non-linear optical devices such as frequency doubling crystals useful in laser experimentation. But new applications in the field of telecommunications, computers and optical signal processing devices are expected in the future.

In classical optics, a polarisation induced when light interacts with matter is described by (1.3.1)

$$\underline{P} = \chi \underline{E} \quad (1.3.1)$$

where \underline{E} is the electric field strength, $\chi = n^2 - 1$ and n is the complex refractive index of the material. Hence, \underline{P} is linearly dependant on \underline{E} . With the introduction of lasers, the polarisation induced by a high intensity light source may be found to be non-linear. This can be expressed as a series expansion in the electric field \underline{E} (1.3.2)

$$\underline{P} = \chi^{(1)}\underline{E} + \chi^{(2)}\underline{E}\underline{E} + \chi^{(3)}\underline{E}\underline{E}\underline{E} + \dots \quad (1.3.2)$$

where, $\chi^{(1)}$, the classical linear susceptibility, is called the first-order susceptibility, $\chi^{(2)}$ the second order and $\chi^{(3)}$ the third order (non-linear) susceptibility. $\chi^{(n)}$ are bulk material parameters which describe the degree of response of the material to high intensity radiation. In terms of the classical electric dipole oscillator model, the higher order terms in the expansion may be considered to be the result of the anharmonic behaviour of the oscillator representing the bound electrons of the atom. These higher order terms represent perturbations to the harmonic case and as such, decrease in magnitude with increasing order.

It is important to note that material symmetry and structure are of prime consideration in dealing with non-linear susceptibilities. Firstly, in materials with centrosymmetric structure, the relationship (1.3.3)

$$P(\underline{E}) = P(-\underline{E}) \quad (1.3.3)$$

should hold, so the even order susceptibilities may only be observed in non-centrosymmetric materials. Exploitation of this term is subject, therefore, to strict material requirements and this has led to a flurry of activity in crystal design and growth, producing such materials as the so-called beta barium borates, which have large second order

susceptibilities. Furthermore, the coefficients $\chi^{(n)}$ are tensorial in nature, $\chi^{(3)}$ for example is a fourth rank tensor. The third-order non-linearity can therefore be defined as a tensor with 81 separate tensor components, but in an isotropic medium, inversion symmetry reduces this to 21 nonzero elements, of which four can be different and only three can be independent. In the dipolar approximation, the polarisation induced in an atom or molecule can be written as⁽⁴⁷⁾(1.3.4)

$$\underline{P} = \alpha \underline{E} + \beta \underline{E} \cdot \underline{E} + \gamma \underline{E} \cdot \underline{E} \cdot \underline{E} + \quad (1.3.4)$$

where, α , β and γ are known as polarisability, first hyperpolarisability and the second hyperpolarisability respectively and the terms involving β and γ describe the microscopic second order and the third order nonlinear optical effects. Corresponding to the non-linear optical susceptibility $\chi^{(3)}$ in a macroscopic or bulk medium the second hyperpolarisability γ in the molecular level can be written as a simple model (1.3.5)

$$|\gamma| = \frac{|\chi^{(3)}|}{N_A C L} \quad (1.3.5)$$

In this equation, N_A is Avogadro's constant, C is the molar concentration and L is the Lorentz local field factor, which for practical purposes is taken to be that of a spherical or randomly coiled molecule, given by (1.3.6)

$$L = (n^2 + 2)/3 \quad (1.3.6)$$

n is the refractive index of the solvent.

Nonlinearity in a material may be observed as a number of different processes which can be identified. Due to a large modulation of the refractive index of the material, thermal processes are the nonlinear effect most frequently observed, especially in absorbing materials⁽⁴⁶⁾. This modulation is due to the temperature dependence of the refractive index from only weak absorption of incident radiation. The general order of values for thermal nonlinearity is around $10^{-18} \text{ m}^2/\text{V}^2$.⁽⁴⁶⁾

The nonlinear dependence of the refractive index of a transparent material on the incident light intensity giving rise to a third order nonlinear process is called the optical Kerr effect. The range of values for this effect is 10^{-15} - $10^{-20} \text{ m}^2/\text{V}^2$. The response time of the materials which show an optical Kerr effect is normally of the order of picoseconds.⁽⁴⁷⁾ Organic systems which are highly polarisable due to a π -electron backbone, have demonstrated nonlinearities which provide the possibility for optical switching applications.

Caro and Grower⁽⁴⁸⁾ have proposed approximate behaviour for a two level system where the nonlinearity is a consequence of a change in the material absorption coefficient as a result of saturation of the ground state absorption. This model explains to a close approximation the absorptive effects in a nonlinear regime. The ground state repopulation

time which is of the order of nanoseconds determines the response time of the nonlinearity.

In most materials the transmittance increases with the incident intensity. However the decrease of the transmission with increasing intensity can be observed when the absorption cross-section of the ground state is smaller than that of the excited state. This behaviour has been observed experimentally in semiconductors⁽⁴⁹⁾, dyes⁽⁵⁰⁾ and organometallic materials.⁽⁵¹⁾ This effect should prove useful in making devices such as optical limiters for the protection of eyes, optical sensors and switches.

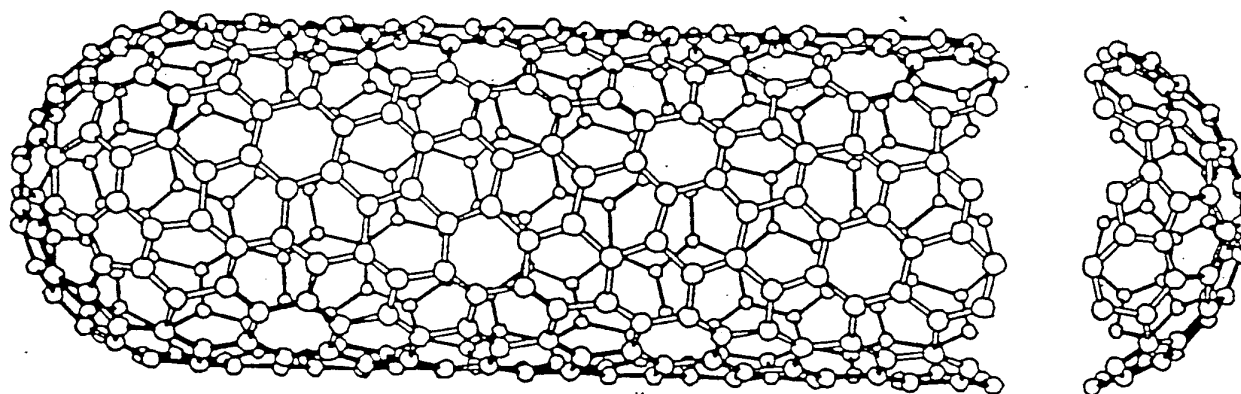
The study of non-linear phenomena in fullerenes has received considerable interest since bulk amounts became available. Cardin and Blau have reviewed the area.⁽⁵²⁾ Similar to organic conjugated polymers and inorganic semiconductors, fullerenes exhibit various types of third order nonlinear effects, such as third harmonic generation, two photon absorption, optical limiting, self focussing and self-defocussing. The latter properties are based on an intensity dependent refractive index.⁽⁵²⁾ The Z-scan technique has been used by our group to demonstrate⁽⁵³⁾ intensity dependent absorption and resonant optical non-linearity in solutions of C₆₀ and C₇₀. More recently we have published a paper on the low power optical response of fullerene solutions.⁽⁵⁴⁾

With picosecond laser pulses, off-resonant third order nonlinearities of up to 10^{-34} esu per molecule have been reported in fullerenes. When the laser is tuned to a frequency within the electronic absorption bands of the material, a resonant enhancement of the nonlinearity is observed. In fullerenes, this manifests itself as an intensity dependent absorption, leading to efficient optical limiting behaviour via the saturation of the molecule's lowest triplet state⁽⁵⁵⁾.

The two references quoted in (56) provide a background to the subject of Nonlinear Optics. The third order nonlinear susceptibility of a range of organometallic fullerene derivatives were measured and the results are discussed in Chapter 5.

Section 4: Nanotubes.

Since the discovery of carbon nanotubes⁽⁵⁷⁾ several reports have suggested the practical usefulness of this material in composites, catalysts and molecular wires⁽⁵⁸⁾. Theorists have also concluded that the electronic properties depend on the structure and diameter of these tubes⁽⁵⁹⁾, making them possible candidates in the electronics industry. The structure of these tubular assemblies of carbon consists of concentric cylinders of hollow carbon hexagonal networks, arranged around one another, often with a helical twist⁽⁵⁷⁾ (Fig.1.4.1). The tips of the tubes are almost always closed with the presence of pentagons which are positive surface disclinations ($+60^\circ$) in the hexagonal lattice. Heptagons (-60° disclinations) are also seen as important entities in the growth of tubes as they provide negative curvature for the transformation of conical shapes into tubes, and other transformations.⁽⁶⁰⁾ The actual process through which the tubes nucleate and grow is still a matter of debate. The production of nanotubes is carried out under the same conditions as that for fullerenes, indeed both can be produced at the same time. Whilst fullerenes are found in the soot produced from the vaporization of graphite the fullerenes are found in the core of a deposit attached to the negative electrode. The proposed formation mechanism(s) are discussed in Chapter 6 along with a study of the morphology and spectroscopy of nanotubes and nanoparticles.



EXPERIMENTAL TECHNIQUES

All manipulations of air-sensitive compounds were carried out using Schlenk tubes inside a dry-box with typical levels of $O_2 < 5\text{ppm}$ and $H_2O < 2\text{ppm}$. These levels were maintained using a combination of molecular sieve and BASF O_2 removal catalyst. The circulating gas inside the box was Argon which was found to cause less problems with static than Nitrogen. When materials were removed from the dry-box they were stored inside Schlenk tubes. Degassing, distillation, solvent removal and sublimations were carried out on a vacuum line attached to 2-stage rotary pump with a mercury-diffusion pump. Unless otherwise stated all solvents used were dried and degassed by the conventional methods (eg. hexane over sodium and benzophenone). Degassing was carried out using the conventional three cycle freeze-thaw technique. Rigorous drying and degassing of all solvents and starting materials is necessary when working with lanthanide organometallics especially the Ln^{2+} compounds, some were found to be explosive and many are pyrophoric. When working with these materials the solvents were subjected to extra cycles in the drying/degassing routines.

The 1H and ^{13}C nmr spectra were recorded on either a Bruker 80MHz or 300MHz machine. For non-sensitive materials the common deuterated solvent used was $CDCl_3$ using TMS as a reference when necessary. For sensitive materials the deuterated solvents were dried and de-oxygenated using the same techniques as for ordinary solvents and where necessary were stored over molecular sieve inside the dry-box.

Infra-red spectra were recorded on a Perkin-Elmer 800 series machine using KBr or CsI discs, thin films on NaCl and NaCl solution cells. For sensitive materials a novel sandwiching technique was used for recording samples as discs. Two blank discs were first pressed in the normal manner and then the sample disc was prepared. The sample disc was then sandwiched in between the two blanks and the sandwich was then gently pressed. This process produces a single disc but the air-sensitive compound has a barrier of KBr or CsI over its' surface which delays exposure to oxygen long enough for a spectrum to be recorded.

Uv/vis/nir spectra were recorded on a Pye-Unicam SP8-200 and a Perkin Elmer machine (nir) usually in 1mm or 1cm quartz cuvettes. For air-sensitive solutions a 1mm cell attached to a small reservoir (10cm^3) and a Youngs' tap was used. Samples could be degassed and/or reactions carried out in this apparatus.

Metal analysis was performed for the lanthanides using a combination of two techniques (A) Direct complexometric titration of lanthanide solutions using EDTA and (B) Uv/vis/nir spectroscopic determination. These are standard procedures for most researchers in the Organolanthanide field.⁽⁶¹⁾

(A) Direct Complexometric Titration of Lanthanide Solutions:

Introduction. The quantity of lanthanide(Ln) present in an aqueous solution may be determined by direct titration with EDTA. The stoichiometry of the product in this reaction is 1:1, therefore a simple technique exists to determine the %Ln in a preweighed sample. Other reagents required are xylenol orange(indicator) and hexamethylenetetramine(HMTA, buffer). The %Ln in the sample may be calculated by the following formula:

$$\%Ln = \left[\frac{M. V. (At. Wt)}{\text{Sample Wt.}} \right] .100$$

M=0.01 M EDTA

V=vol(cm³) of EDTA used

At.Wt.=Atomic weight of Ln

Sample Wt in mg.

Procedure: Standard analytical techniques were employed in all of the titrations. All equipment was thoroughly cleaned with detergent, rinsed and then washed with fresh aqua regia. The equipment was then rinsed thoroughly with de-ionised water before being dried in an oven.

A standard solution of EDTA was prepared by dissolving 3.772g of Na₂EDTA.2H₂O in de-ionised water (500cm³). This solution was then transferred to a 1L volumetric flask and made up to 1L. The 0.01M solution was transferred to a polyethylene bottle immediately to avoid possible leaching of metals from the glass surface.

A solution of the indicator (xylenol orange) was prepared by dissolving 0.1g of the tetrasodium salt of xylenol orange in de-ionised water (100cm³).

The sample under investigation was loaded into a preweighed flask and the weight determined by subtraction. The accuracy of the balance in the dry-box was not adequate (0.01g) for this purpose. The sample was quickly hydrolysed outside the dry-box with de-ionised water and a few drops of conc. HCl were added to completely dissolve the Ln. If a cloudy suspension resulted from the hydrolysis/acidification procedure the pyrolysis of a fresh sample was employed. A weighed sample of the Ln was loaded onto a small pyrex dish and placed inside a furnace. The temperature was slowly raised to circa. 350 °C and maintained for several hours until no black traces remained in the sample. After pyrolysis the samples were dissolved with de-ionised water and HCl.

A few drops of indicator were added to the Ln solution which turned yellow. Solid HMTA buffer was added to neutralise HCl until the solution turned purple. The solution was then titrated with EDTA until the purple colour started to fade. More buffer was added to maintain the purple colour until a sharp colour change from purple to yellow occurred. The volume of EDTA required was noted and the %Ln was calculated.

For the lanthanides the f-f electronic transitions are orbitally forbidden just as in d-d

transitions. This "forbiddenness" can be partially relaxed by a mechanism which depends on the effect of the crystal field in distorting the symmetry of the metal ion. The crystal field effects in Ln^{3+} ions are very much smaller than in transition metal ions and they therefore cannot produce the same relaxation of the selection rule. The absorption bands for the f-f transitions are therefore much sharper than those for d-d transitions and provide a useful means of characterising, and quantitatively estimating Ln^{3+} ions. Elemental analysis of the lanthanides can therefore be performed on air sensitive compounds by dissolving a weighed amount of the material in hydrochloric acid to generate the Ln^{3+} chloride. This is then made up to a known volume using a volumetric flask with distilled water. A uv/vis/nir spectrum is then recorded and using the Lambert-Beer law the concentration of the Ln(III) ion in the solution can be found. This is then used to calculate the percentage Ln in the weighed amount of material.

In utilising the rare earth absorption bands for analytical purposes, the first problem is to choose the most suitable bands for use as index peaks and determine their extinction coefficients. This work has already been carried out by Stewart and Kato.⁽⁶²⁾ This publication gives a comprehensive list of index peaks and interference corrections. The index peaks which were used in this study are shown in Table 1.1B series of standards was made up from commercial lanthanide chlorides to test the procedure. The results were found to be in excellent agreement with those published. In some cases a 1mm quartz cell was used as a limiting factor in working with aqueous solutions in the 900nm-1400nm range are the small absorption bands of water at approx.955nm and1190nm.

Table 1.1B Index peaks for Lanthanide analysis.

Element	λ_{max} nm	ϵ Extinction coeff.
Neodymium	575.5	6.34
Neodymium	742.5	6.22
Samarium	401.6	3.30
Europium	394.3	2.90
Holmium	536.5	4.55
Holmium	641	2.04
Erbium	523.5	3.55
Erbium	654	2.04
Ytterbium	973	2.10
Praseodymium	444.0	10.1

The accuracy of this method can be as good as 0.5%. when working with stable compounds. The limiting factor in this study was the balance inside the dry-box which weighed to two places of decimals and therefore had an error of 5% when weighing 100mg amounts. Where possible larger amounts of the compound were used. For all the compounds analysed a second reading was taken at a different index peak.

References.

- 1 L.R. Morss, *Chem. Rev.*, 1976, **76**, 827.
- 2 R.G. Pearson, *Hard and Soft Acids and Bases*, Dowden, Hutchinson and Ross, Stroudsburg, Pa., 1973.
- 3 (a) W.J. Evans, *J. Organomet. Chem.*, 1983, **250**, 217. (b) D.J. Cardin and R.J. Norton, *Organomet. Chem.*, 1983, **11**, 232. (c) H. Schumann, *Comments on Inorg. Chem.*, 1983, **2**, 247. (d) R.D. Rogers and L.M. Rogers, *J. Organomet. Chem.*, 1990, **380**, 51. (e) J.D. Miller, *Annu. Rep. Prog. Chem., Sect. A: Inorg. Chem.*, 1985, **81**, 325. (f) J.D. Miller, *Annu. Rep. Prog. Chem., Sect. A: Inorg. Chem.*, 1986, **82**, 347. (g) M.J. Winter, *Organomet. Chem.*, 1986, **14**, 225. (h) H. Schumann, *Angew. Chem. Int. Ed. Engl.*, 1984, **23**, 474. (i) H. Schumann, *J. Organomet. Chem.*, 1985, **281**, 95. (j) R.D. Rogers and L.M. Rogers, *J. Organomet. Chem.*, 1991, **416**, 201. (k) R.D. Ernst and T.J. Marks, *J. Organomet. Chem.*, 1987, **318**, 29. (l) M.J. Winter, *Organomet. Chem.*, 1987, **15**, 229. (m) M.J. Winter, *Organomet. Chem.*, 1989, **18**, 200. (n) M.J. Winter, *Organomet. Chem.*, 1989, **17**, 206. (o) W.J. Evans, *Polyhedron*, 1987, **6**, 803. (p) I.P. Beletskaya and G.Z. Suliemanov, *Metalloorg. Khim.*, 1989, **1**, 10. (q) G.X. Xu, J. Ren, C.H. Huang and J.G. Wu, *Pure & appl. Chem.*, 1988, **60**, 1145. (r) Q. Shen, W. Chen, Y. Jin and C. Shan, *Pure & Appl. Chem.*, 1988, **60**, 1251.
- 4 W.J. Evans, H. Meadows and J. Atwood, *J. Am. Chem. Soc.*, 1984, **106**, 4554.
- 5 P.J. Watson, *J. Am. Chem. Soc.*, 1982, **104**, 6471.
- 6 W.J. Evans, T.T. Peterson, M.D. Rausch, W.E. Hunter and J. Atwood, *Organometallics*, 1985, **4**, 554.
- 7 D.S. McLure, Z. Kiss, *J. Chem. Phys.*, 1963, **39**, 3251 and N.B. Kheer, *Inorg. Chim. Acta.*, 1984, **94**, 241.
- 8 W.J. Evans, *J. Am. Chem. Soc.*, 1981, **103**, 6507.
- 9 T. Moeller, *Comprehensive Inorg. Chem.*, 1973, **4**, 44.

- 10 W.J. Evans, *J. Am. Chem. Soc.*, 1984, **106**, 4270.
- 11 A.E. Crease and P. Legzdins, *J. Chem. Soc. Chem. Commun.*, 1973, 775.
- 12 A.E. Crease and P. Legzdins, *J. Chem. Soc. Dalton Trans.*, 1973, 1501.
- 13 G.K.I. Magomedov, *Metalloorg. Khim.*, 1990, **3**, 706.
- 14 H. Deng and S. Shore, *J. Am. Chem. Soc.*, 1991, **113**, 8538.
- 15 R.D. Fisher, *Angew. Chem.*, 1965, **77**, 1019.
- 16 G.H. Dieke, *Spectra and Energy Levels of Rare Earth Ions in Crystals*, Interscience, 1969, 49.
- 17 R.G. Hayes and J.L. Thomas, *Organomet. Chem. Rev.*, 1971, **A**, 7, 1.
- 18 R.C. Mehrotra, P.N. Kapoor, J.M. Batwara, *Coord. Chem. Rev.*, 1980, **31**, 67
- 19 R.C. Mehrotra, A. Singh, U.M. Tripathi, *Cem. Rev.*, 1991, **91**, 1287.
- 20 P.B. Hitchcock, M.F. Lappert, A. Singh, *J. Chem. Soc., Chem. Commun.*, 1983, 1499.
- 21 P.B. Hitchcock, M.F. Lappert, R.G. Smith, *Inorg. Chim. Acta*, 1987, **139**, 183.
- 22 G.B. Deacon, S. Nickel, P. McKinnon, E.R.T. Tiekink, *Austr. J. Chem.*, 1990, **43**, 1245.
- 23 W.J. Evans, T.P. Hanusa, K.R. Levan, *Inorg. Chim. Acta*, 1985, **110**, 191.
- 24 W.J. Evans, T.J. Deming, J.W. Ziller, *Organometallics*, 1989, **8**, 1582.
- 25 H.A. Stecher, A. Sen, A.L. Rheingold, *Inorg. Chem.*, 1989, **28**, 3280.
- 26 O. Poncelet, W.J. Sartain, L.G. Pfalzgraf, K. Foulting, K.B. Caulton, *Inorg. Chem.*, 1989, **28**, 263.
- 27 T.J. Marks, R.D. Ernst, *Comprehensive Organometallic Chemistry*; G.

- Wilkinson and F.G.A. Stone, Eds: 1988, **3**, 178.
- 28 H.W. Kroto, J.R. Heath, S.C. O'Brien, R.F. Curl and R.E. Smalley, *Nature*, 1985, **318**, 162.
- 29 W. Kratschmer, L.D. Lamb, K. Fostiropoulos and D.R. Huffman, *Nature*, 1990, **347**, 354.
- 30 R. Taylor, J.P. Hare, A. Abdul-Sada and H. Kroto, *J. Chem. Soc. Chem. Commun.*, 1990, 1423.
- 31 J.B. Howard, J.T. McKinnon, Y. Marovsky, A. Lafleur and M.E. Johnson, *Nature*, 1991, **352**, 139.
32. F. Diederich, R.L. Whetten, *Acc. Chem. Res.*, 1992, **25**, 119.
- 33 K. Kikuchi, N. Nakahara, M. Honda, S. Suzuki, K. Saito, H. Shiromaru, K. Yamauchi, I. Ikemoto, S. Hino and Y. Achiba, *Chem. Lett.*, 1991, 1607.
- 34 H.W. Kroto, *Nature*, 1987, **329**, 529 and T.G. Schmaltz, W.A. Seitz, D.J. Klein and G.E. Hite, *J. Am. Chem. Soc.*, 1988, **110**, 1113.
- 35 R.E. Smalley, *Acc. Chem. Res.*, 1992, **25**, 98.
- 36 F. Diederich, R.L. Whetten, C. Thilgen, R. Ettl, I. Chao and M. Alvarez, *Science*, 1991, **254**, 1768.
- 37 G. Meijer and D.S. Bethune, *J. Phys. Chem.*, 1990, **93**, 7800.
- 38 J.R. Heath, *Fullerenes : synthesis, properties and chemistry of large carbon clusters* (ACS Symp. Ser., no. 48), Ed. G.S. Hammond & V.J. Kuck, p1-23, Am. Chem. Soc.
- 39 H.K. Kroto, *Angew. Chem. Intl. Ed. (Engl.)*, 1992, **31**, 111.
- 40 R. Taylor, J.P. Hare, A.K. Abdul-Sada, H.W. Kroto, *J. Chem. Soc. Chem. Commun.*, 1990, 1423.
- 41 J.M. Hawkins, T.A. Lewis, S.D. Loren, A. Meyer, J.R. Heath, Y. Shibato and R.J. Saykally, *J. Org. Chem.*, 1990, 6250.

- 42 P.J. Fagan, J.C. Calabrese and B. Malone, *Science*, 1991, **252**, 1160.
- 43 A.L. Balch, V.J. Catalano and J.W. Lee, *J. Am. Chem. Soc.*, 1991, **113**, 8953.
- 45 P.J. Fagan, B. Chase, J.C. Calabrese, D.A. Dixon, R. Harlow, P.J. Krusic, N. Matsuzawa, F.N. Tebbe, D.L. Thorn, E. Wasserman, *Carbon*, 1992, **30**, 1213.
- 46 W.M. Dennis, W. Blau and D.J. Bradley, *Opt. Eng.*, 1986, **25**, 538.
- 47 G.M. Carter, J.V. Hizyniewicz, M.K. Thakur, T.R. Chen and S.E. Meyler, *Appl. Phys. Lett.*, 1986, **49**, 998.
- 48 R.G. Caro and M.C. Gower, *IEEE J. Q. Elec.*, 1980, **18**, 1376.
- 49 H.J. Eichler, F. Massmann and C.H. Zaki, *Opt. Commun.*, 1982, **40**, 302.
- 50 H.E. Lessing and A. von Jena, *Chem. Phys. Lett.*, 1978, **59**, 249.
- 51 W. Blau, H. Byrne, W.M. Dennis, *Opt. Commun.*, 1985, **56**, 25 and L.W. Tutt and S. McGahon, *Opt. Commun.*, 1990, **15**, 700.
- 52 W. Blau and D.J. Cardin, *Mod. Phys. Lett. B*, 1992, **6**, 1351.
- 53 F.Z. Henari, J. Callaghan, H. Stiel, W. Blau and D.J. Cardin, *Chem. Phys. Lett.*, 1992, **199**, 144.
- 54 F.Z. Henari, S. MacNamara, O. Stevenson, J. Callaghan, D. Weldon and W. Blau, *Adv. Mater.* (accepted Nov. 1993).
- 55 (53) and L.W. Tutt, A. Kost, *Nature*, 1992, **356**, 255.
- 56 *Nonlinear Optics, Materials and Devices*, 1986, Eds. C. Flytzanis and J.L. Oudar, Springer Verlag and *Nonlinear Optical Properties of Organic and Polymeric Materials*, 1983, A.C.S. Symp. Ser. No. 233, Washington.
- 57 S. Iijima, *Nature*, 1991, **354**, 56.
- 58 P. Calvert, *Nature*, 1992, **357**, 365 and P. Ross, *Sci. Am.*, 1991, **265**, No.6,

16.

59 A. Oshiyama, S. Saito, N. Hamada and Y. Miyamoto, *J. Phys. Chem. Solids*, 1992, **53**, 11.

60 S. Iijima, T. Ichihashi and Y. Ando, *Nature*, 1992, **356**, 776.

61 G. Deacon private communication.

62 D. Stewart and D. Kato, *Analyt. Chem.*, 1958, **30**, No.2, 164.

CHAPTER 1

New Ligands for Organo-Lanthanide Chemistry.

Introduction.

The question of covalency in organometallic compounds of the lanthanides could not be resolved in terms of a 'monohapto' sigma bond by the synthesis of the cyclopentadienyl, indenyl, cyclooctatetraenyl, allyl or even alkynyl complexes.

The reaction of LaCl_3 or PrCl_3 with phenyllithium yields products which are not simply phenyls. The air sensitive solids are suggested to be $\text{LiM}(\text{C}_6\text{H}_5)_4$ ⁽¹⁾. They are soluble in benzene when first obtained from thf solution, but after drying under vacuum they are insoluble in benzene. The original product should be a thf complex, which polymerises on removal of thf.

The probable polymeric nature of these compounds led to the use of some other ligands which should stabilise organolanthanide compounds like bulky alkyl or aryl groups(Fig. 1.1),

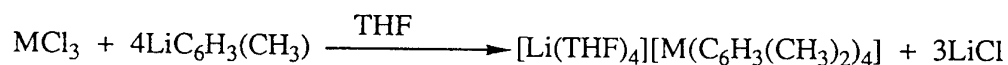


Fig. 1.1

The compounds are quite unstable, smouldering on contact with air. A considerable stabilisation of organolanthanide complexes with three M-C σ bonds can be achieved by the use of chelated organic ligands. The reaction of $\text{LiCH}_2\text{C}_6\text{H}_4\text{-o-N}(\text{CH}_3)_2$ with ScCl_3 led to the isolation of thermally stable, air sensitive, pale yellow $\text{Sc}[\text{CH}_2\text{C}_6\text{H}_4\text{N}(\text{CH}_3)_2]_3$.⁽²⁾

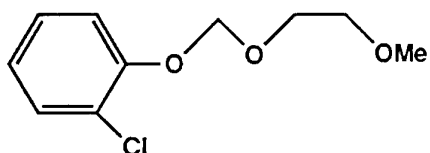
Other types of bulky alkyl groups have been used by Lappert and co-workers for the preparation of organolanthanide complexes. Sc and Y compounds with the groups $\text{CH}_2\text{Si}(\text{CH}_3)_3$ ⁽⁴⁾, $\text{CH}[\text{Si}(\text{CH}_3)_3]_2$ ⁽³⁾ and $\text{CH}_2\text{Si}(\text{CH}_3)_2\text{C}_6\text{H}_4\text{-o-OCH}_3$ ⁽⁴⁾ have been isolated from the reaction of the appropriate reagent with ScCl_3 and YCl_3 . The complexes were obtained in good yield as analytically pure, air sensitive, colourless crystals from pentane with two molecules of thf co-ordinated.

The work described in this part of the thesis is concerned with the synthesis of new ligands for organolanthanide chemistry. For this purpose a number of features have been borne in mind: (a) lanthanide ions are comparatively large in comparison with those of the first transition metal series, (b) the high co-ordination numbers expected for stable complexes, (c) the 'hard' character of the metals, and their consequent preference for hard donor atoms, and (d) their relative flexibility with regard to stereochemical requirements (if any) imposed by the ligand.⁽⁵⁾ Similar ligands have been developed and studied in the context of lanthanide chemistry,

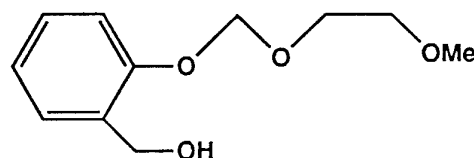
however they have certain limitations, for example, crown ethers have been studied extensively but these do not allow the incorporation of a lanthanide-carbon sigma bond.⁽⁶⁾ We also developed ligands which contained nitrogen and oxygen functional groups for reaction with lanthanides. The stabilising effect of chelating amino-aromatic ligands has been demonstrated for a variety of transition metal ions.⁽⁷⁾

The approach we have followed in designing the desired ligands has been to attach a polyether side-chain, or two such chains, to an aromatic nucleus and, where appropriate to study its' lithiation. Unlike the crown ethers the molecules described here have maximised their flexibility in geometrical terms, by not being ring-closed, but leaving the polyether side-chains free. In order to increase the chelating potential of the ligand a convenient reagent was used known as 2-methoxyethoxymethyl chloride (MEM). This reagent was developed as a versatile protecting group for hydroxyl moieties, as it can be removed by strong Lewis acids, with formation initially of $\text{CH}_2(\text{OH})_2$ and $\text{MeOCH}_2\text{CH}_2\text{OH}$.⁽⁸⁾

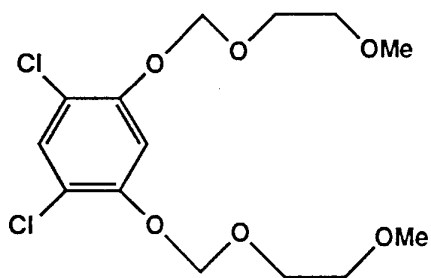
The ligands prepared in the course of this work were,



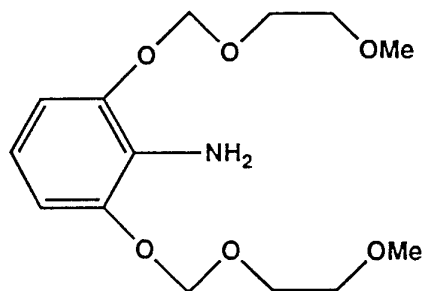
2-Chloro(1,3,6-trioxaheptyl)benzene (L1).



2-(1,3,6-trioxaheptyl)benzyl alcohol (L2).



4,6-Dichloro-1,3-bis(1,3,6-trioxaheptyl)benzene (L3).



1,3-bis(1,3,6-trioxaheptyl)-2-aminobenzene (L4).

Reactions involving 2-chloro(1,3,6-trioxaheptyl)benzene(L1).

Synthesis of L1.

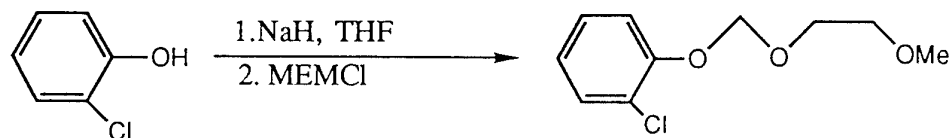


Fig.1.2 Preparation of L1

A two step procedure was used to synthesise the ligand. The first step involved the preparation of the phenoxide using NaH in thf, this was then followed by addition of MEMCl in a salt-elimination reaction to give the title compound in 76% yield. The ^1H nmr spectrum reveals a peak for each distinct type of proton. The coupling between the CH_2 groups of the ether side-chains is clearly resolved (*ca.* 5 Hz.) and the aromatics are resolved into three separate peaks. The ^{13}C nmr exhibits 10 non-equivalent C signals as expected.

Lithiation of L1 using nBuLi affords the lithium reagent in high yield.

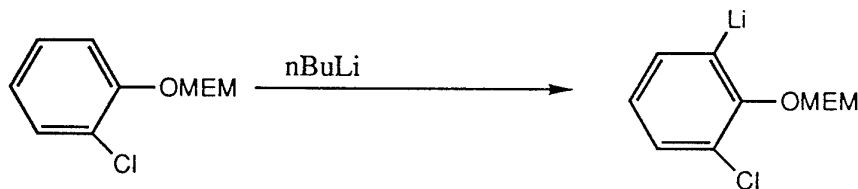


Fig.1.3 Lithiation of L1

The reagent is completely soluble in thf and can be handled freely inside the dry-box as a white powder. The lithiation of the 6 position was confirmed using a " D_2O shake" experiment.

1.1A Reaction of LnCl_3 with LiL1 ($\text{Ln}=\text{Nd, Ho}$).

The reaction of the lithium reagent with NdCl_3 and HoCl_3 produced an intractable brown solid in each case. Both products were found to contain lithium. The composition of the products from this reaction is not clear. They could contain a mix of polymeric materials containing the metal and the ligand. Significantly almost 1mmol of the ligand was recovered which suggests that the products have a metal:ligand ratio of 2:1. The i.r spectrum shows the expected peaks for the ligand and the metal analysis suggests that the metal:ligand ratio is also 2:1. The products both absorbed water when exposed to the atmosphere.

ligand is still visible in the spectrum. The product contains cyclopentadiene and thf as seen in the nmr and i.r. The phenyl protons were not located in the ^1H nmr. The metal analysis is correct for a metal:ligand ratio of 1:1 with one molecule of thf(Fig.1.7).

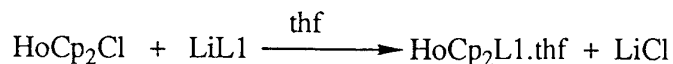


Fig.1.7

1.1D Reaction of $\text{SmI}_2(\text{thf})_2$ with LiL1.

$\text{SmI}_2(\text{thf})_2$ was prepared using the method described by Evans *et al.*⁽¹¹⁾ The synthesis is similar to that used to prepare SmCl_3 except that the samarium is kept in excess to prevent the Sm(III) product from forming (Fig. 1.8).

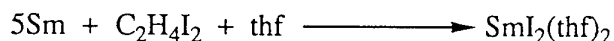


Fig. 1.8

$\text{SmI}_2(\text{thf})_2$ is a dark blue solid which must be used fresh for good results. The solid can be stored for short times under argon. Addition of the samarium to LiL1 gave a pale yellow solid. The product contained Sm(III) as shown from the uv/vis (401 nm). This indicates that oxidation of the metal occurred. This could be seen from the colour change in the reaction from dark blue to yellow. The ^1H nmr shows the presence of the ligand and thf in the product as does the i.r spectrum. The metal analysis suggests a ratio of 2:1 for ligand to metal however the fact that the Sm has been oxidised can not be explained with this data. The presence of hydroxide was not evident in the i.r. or the nmr.

Reactions involving 2-(1,3,6-trioxaheptyl)benzylalcohol (L2).

Synthesis of L2.

An increase in the oxygen functionality was achieved by the synthesis of L2. A two-step synthesis was used to produce the benzylic alcohol with the ether side-chain (MEM) in high yield(Fig.1.9). The product was purified by vacuum distillation to give a colourless viscous liquid. The benzylic alcohol is evident in the ^1H nmr as a broad singlet at $\delta 2.90\text{ppm}(\text{OH})$ and the singlet at $\delta 5.29(-\text{CH}_2\text{OH})$. The nmr spectrum exhibits coupling of the benzylic protons with the hydroxylic H-atom, ($^3J_{\text{HH}}$ 5.5 Hz.).

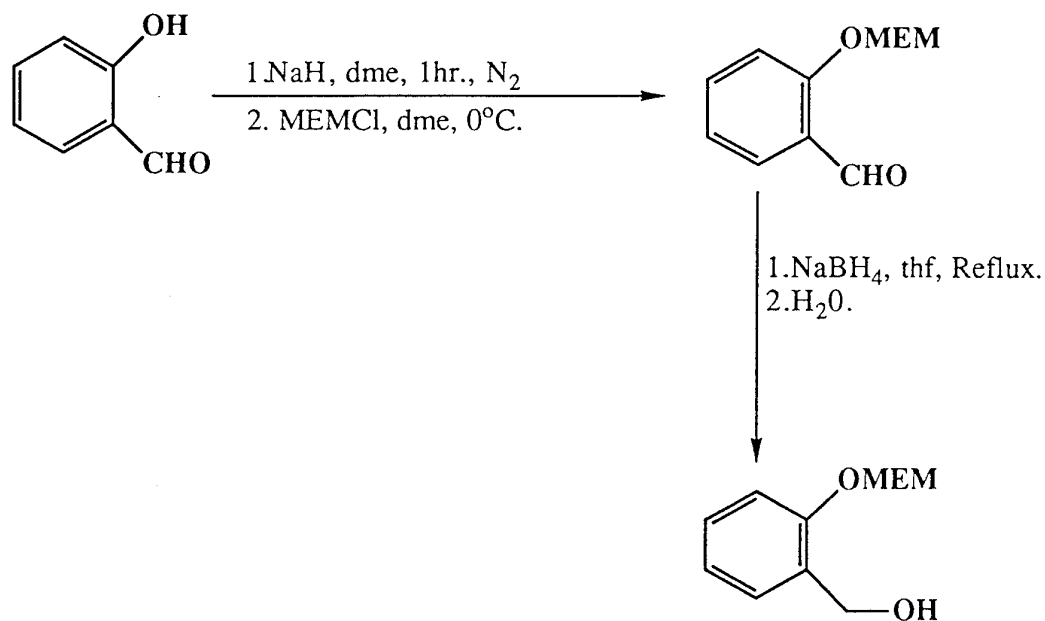


Fig.1.9 Synthesis of L2.

The sodium salt of the alcohol was made using NaH in thf (Fig.1.10), this was then used in a variety of salt-elimination reactions with lanthanide halides.

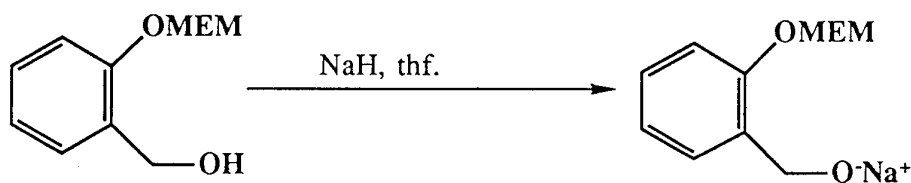


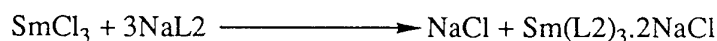
Fig.1.10 Synthesis of NaL2

1.2A Reaction of PrCl₃ with NaL2.

The reaction of PrCl₃ with the sodium salt of L2 produced a golden viscous oil which contained unreacted ligand. Almost 2mmol of L2 were recovered from the reaction which indicates that protonation occurred at some stage during the reaction. The reaction was carried out under the usual strict conditions to prevent H₂O and O₂ contamination. The final product (a red plastic material) contains Pr(III) and the ligand. This material was found to be insoluble in a wide range of solvents and only dissolved very slowly in warm HCl. The material darkens to a black/grey colour over a period of months. The product is probably a polymer of some sort. No accurate measurement of the metal content in the product was possible.

1.2B Reaction of $\text{SmCl}_3 \cdot (\text{thf})_2$ with NaL_2 .

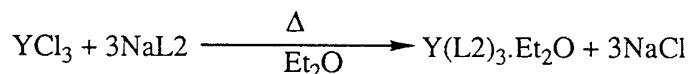
The reaction of SmCl_3 and the sodium salt of L2 gave a pale yellow powder which from the spectroscopic analysis consists of samarium with three equivalents of ligand. The expected metal analysis for this compound (23.7%) is 2.7% from the measured value (21%). This can be accounted for by the fact that the product also contains 2 equivalents of NaCl. Only 1 equivalent of NaCl was recovered from the reaction.



When this is taken into account the expected Sm analysis becomes 20%. The product was found to be sensitive to atmosphere.

1.2C Reaction of YCl_3 with NaL_2 .

The reaction of YCl_3 with three equivalents of NaL_2 produced a pale yellow powder which from the analysis is formulated to be $\text{Y}(\text{C}_{33}\text{H}_{45}\text{O}_{12}) \cdot \text{Et}_2\text{O}$. The reaction was carried out under reflux due to the low solubility of the Yttrium starting material. The yellow product was found to be soluble in a range of solvents.



Crystallisation was attempted from a toluene solution of the product. Repeated attempts produced a powder. The i.r spectrum shows the typical signals expected for the ligand and the ^1H nmr shows the expected peaks for the ligand and the absence of the hydroxyl proton. The data available suggest the formulation $\text{Y}(\text{L}_2)_3$.

1.2D Reaction of Yb metal with L2.

The reaction of alkali metals with alcohols to produce metal alkoxides and aryloxides has been known for some time. Lanthanide alkoxides/aryloxides are also known. The reactions attempted in this study up until now concentrated on the salt-elimination route to produce the alkoxide or aryloxide product (Fig.1.11).

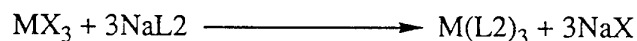


Fig.1.11 Salt-elimination route.

Another route is the direct reaction of the metal with the alcohol (Fig.1.12).



Fig.1.12 Direct route.

Activated ytterbium metal was found to react with L2 over a period of weeks to give a dark red oil. The reaction ratio was 1:1 to prevent the metal from oxidising fully (Fig. 1.13).

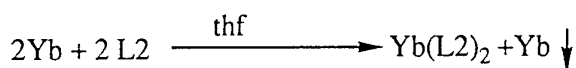


Fig.1.13.

After work-up of the red oil a yellow solid was isolated. This dissolved in a wide variety of solvents giving colours from pale yellow (thf) to purple (hexane/CHCl₃). Crystals of the compound were isolated from a hexane/CHCl₃ solution at -25 °C. The dark green crystals were found to be extremely sensitive to atmosphere and decomposed when removed from the solution. The orange decomposition product was shown to be an Yb(III) compound from vis/nir. The colours red, purple, yellow and green are the classic colours observed in Yb²⁺ compounds but not usually in the same compound. The visible spectra of the product in different solvents shows a blue shift associated with increasing co-ordinating ability of the solvent. A solution of the product was placed in a 1mm quartz cuvette and scanned from 800nm to 1100nm whilst the solution was exposed to the atmosphere. The appearance of an absorbance around 920nm with time indicated the oxidation of the Ytterbium from (II) to (III).

The ¹H nmr shows a significant upfield shift of the protons on C-4 from 5.29ppm to 4.76ppm.

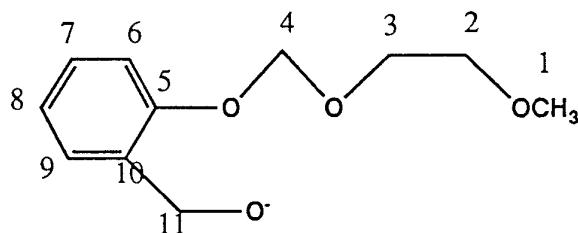


Fig.1.14. Numbering scheme for nmr analysis.

There is a small downfield shift associated with the protons on C-10 from 4.66ppm to 4.83ppm. The broad singlet at 2.90ppm associated with the hydroxyl proton in the ligand is not present. The individually resolved aromatic protons show a small upfield shift with some small broadening. One interesting feature noticeable in the spectrum is a weak broad signal at 5.69ppm ($\nu_{1/2}$ =66Hz). Magomedov⁽¹²⁾ assigns an almost

identical signal (6.65ppm, $\nu_{1/2}=80\text{Hz}$) to $^{171}\text{Yb}-^1\text{H}$ coupling in a similar system. This is unusual since coupling to ^{171}Yb which has a natural abundance of 14.3% has not previously been seen for a divalent Yb organometallic species. The lanthanide shift experiments which Bremont⁽¹³⁾ carried out on this ligand show that all the oxygen atoms in this ligand strongly co-ordinate to the metal. The most strongly co-ordinated oxygen atom was that in the hydroxyl position and it is interesting to note the appreciable shifts(1-2ppm) which were observed with the aromatic protons.

The ^{13}C spectrum of the product was recorded together with a DEPT experiment. All of the carbons with the exception of C-11 can be easily assigned. There is an appreciable upfield shift (7ppm) associated with C-10. The assignment of C-11 presents some difficulty. The signal occurs at 59ppm in the free ligand. No strong CH_2 signal is present at this position and could not be found within a 200ppm sweep. The weak signal at 61.80ppm has been assigned to this position. The other weak CH_2 signals can be assigned to thf.

The metal analysis is consistent with a formulation of $\text{Yb}(\text{L}2)_2$.

1.2E Reaction of NdCp_3 with L2.

NdCp_3 can be prepared using the classical NaCp and NdCl_3 route which gives reasonable yields but is difficult and time consuming. Deacon⁽¹⁴⁾ has utilised the thallium route which gives higher yields and avoids the difficult preparation of NaCp . In this synthesis (Fig.1.15) the thallium salt of cyclopentadiene is generated from TlOH and CpH . This then reacts with neodymium metal which displaces the thallium to give NdCp_3 in high yield. The NdCp_3 can appear as blue or pink crystals depending on the orientation of the crystal. When the NdCp_3 reacted with L2 the solution turned brown immediately.

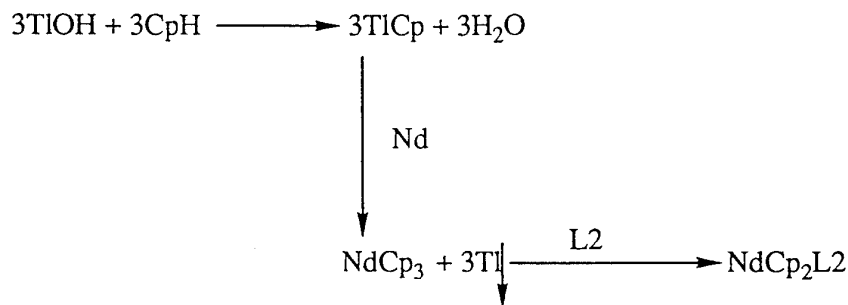


Fig.1.15

The product was dried under vacuum to give a pale brown powder. Infra-Red showed the presence of the ligand. ^1H nmr in D_6 -Acetone displayed the pattern for the ligand and also a signal at 5.8ppm which has been assigned to Cp. The nature of the paramagnetic $\text{Nd}(\text{III})$ prevents any further information from the ^1H nmr. The metal

analysis expected for $\text{NdCp}_2\text{L2}$ is 29% but the recorded values are higher especially the EDTA result of 35%. This might indicate that a bridged species is present in the product.

1.3 Reactions involving (L3)

4,6-dichloro-1,3-bis(1,3,6-trioxaheptyl)benzene.

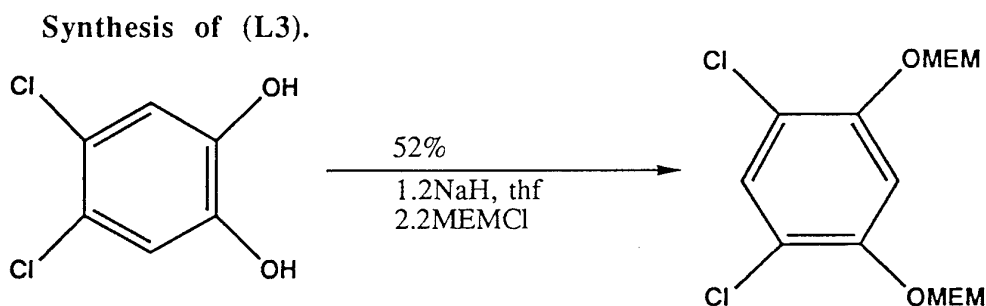


Fig. 1.16 Synthesis of L3.

This structure of this ligand arose out from two considerations. Firstly, the incorporation of a second ether side-arm will increase oxygen functionality. Secondly, having noted that 4-lithiated products can be obtained from the lithiation of 1,3-disubstituted aromatic ethers,⁽¹⁵⁾ the incorporation of two chlorine atoms in the 4 and 6 positions will prevent this as previous experience indicated that lithiation by metal/halogen exchange does not take place. Furthermore lithiation in the 5-position is not expected since the MEM groups are strongly ortho directing and the chloro substituent only weakly so.⁽¹⁶⁾

A two step synthesis afforded the ligand L3 as colourless crystals in reasonable yield. The i.r and nmr data all show the expected signals with the correct integrations. A crystal structure of the ligand was obtained by Cardin⁽¹⁷⁾ from material prepared by Bremont.⁽¹³⁾ The structure of the ligand is shown in Fig.1.16. There are two molecules in the asymmetric unit, which have their aromatic nuclei almost perpendicular to each other. The geometry of the two molecules is almost identical, differing slightly in the orientation adopted by the oxygen atoms of the two side-chains. In both cases, the second O-atoms from the ring are orientated such that a small rotation about the adjacent single bonds would bring them into an ideal conformation for interaction with a metal ion placed between the arms of the ligand. The oxygens at the end of the side-chains are not well positioned for complexation in the conformation of the crystal, although of course rotation will occur in solution allowing alternative conformations to be reached.

Since the ether side-chains are strongly ortho directing and the chloro-substituent only weakly so we would expect the lithiation of this compound to occur

mainly at the position ortho to both ether side-chains. Lithiation of L3 with Bu^nLi was found to occur at the ortho position in high yield (>90%) as opposed to the para position.

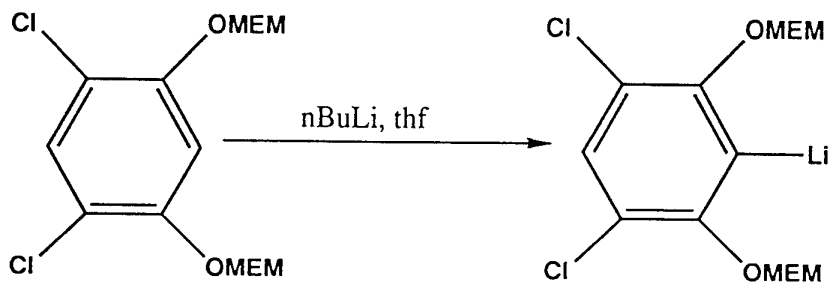


Fig. 1.17 Lithiation of L3.

1.3A Reaction of NdCl_3 with LiL3 .

The reaction of NdCl_3 with three equivalents of the lithium reagent of L3 produced an intractable brown solid which contained the ligand, neodymium and lithium. Protonation of the ligand was found to have occurred at some stage during the reaction which led to the regeneration of L3 from the lithium reagent. The brown intractable product reacted with the atmosphere slowly. The reaction was repeated with different stoichiometries but the same brown product was isolated each time. The product is most likely polymeric in nature containing some LiCl .

1.3B Reaction of YbI_2 with 2LiL3 .

YbI_2 can be made using a number of methods. The best known method involves the use of ytterbium powder and di-iodoethane ($\text{C}_2\text{H}_4\text{I}_2$) (Fig.1.18).⁽¹¹⁾ Another popular method involves the use of liquid ammonia and ammonium iodide.⁽¹⁸⁾ The success of this method requires the usual stringent measures when dealing with Ln^{2+} species and also the use of freshly recrystallised di-iodoethane. If the di-iodoethane is not fresh the yield is very small (<20%). Otherwise the method works well with high yield (>80%) to produce the product as a solvate. The thf can be removed under vacuum with gentle heating but this gives a much less stable product.



Fig.1.18 Synthesis of YbI_2

The reaction of $\text{YbI}_2 \cdot (\text{thf})_2$ with two equivalents of the lithium reagent of L3 produced on cooling a sensitive yellow microcrystalline powder. The i.r spectrum shows the presence of the ligand and metal analysis confirmed the presence of

ytterbium in the sample. A simple flame test demonstrated the presence of lithium in the product also. All attempts to obtain nmr data failed. The product decomposed in a range of dry degassed deuterated solvents.

1.4 Reactions involving L4 (1,3-bis(1,3,6-trioxaheptyl)2-aminobenzene).

Synthesis of L4.

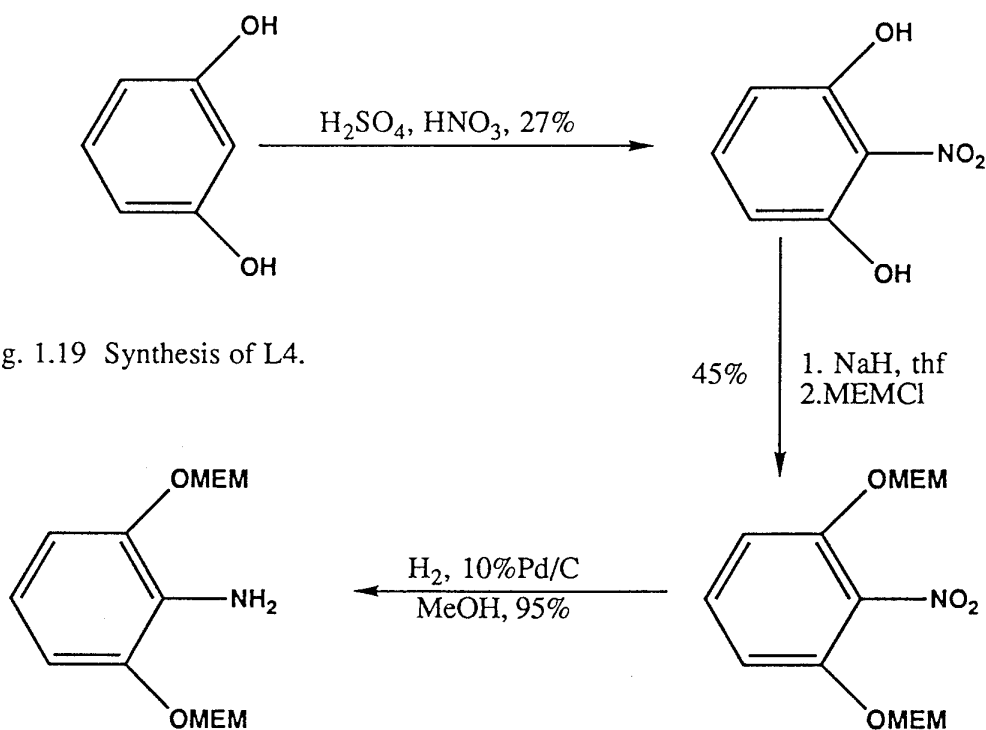


Fig. 1.19 Synthesis of L4.

L4 was synthesised using a lengthy three step procedure (Fig.1.19). Other approaches were attempted which included reducing the nitro group before attachment of the OMEM side-arms, but these failed. The over-all yield is approximately 11.5% and most of the loss is attributed to the purification procedure in the second step (silica column) and the low yield for the first step. The final product was obtained as a yellow liquid. This was found to be sensitive to the atmosphere turning dark brown on exposure. This new compound contains a reactive amino group which can be utilised to prepare metal derivatives. Schumann⁽¹⁹⁾ has used a simple route to produce lanthanide-phosphorous and lanthanide-arsenic bonds (Fig.1.20).



Fig.1.20

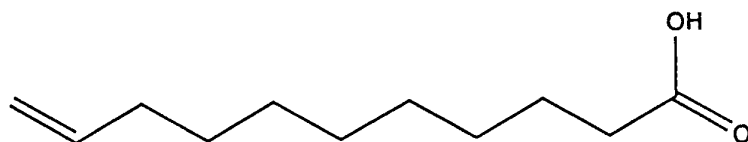
An analogous reaction using L4 can be envisaged where a labile proton on the amine is replaced by a species such as Cp₂Lu with the elimination of SiMe₄. Before a lanthanide synthesis was attempted the ligand was reacted with AlCl₂CH₃⁽²⁰⁾ in an attempt to synthesise the AlCl₂ derivative of L4.

1.4A Reaction of AlCl₂CH₃ with L4.

The reaction of AlCl₂CH₃ to L4 produced a blue/black solid immediately on addition. The product decomposes immediately on exposure to atmosphere to give a dark orange oil. The sensitivity of the product prevented a complete analysis however it is not clear if the desired reaction occurred as the i.r shows two signals in the region for N-H stretching. The ¹H nmr of the hydrolysed product shows the ligand clearly and also two signals at 9.74ppm and 10.64ppm which integrate as single protons. This is downfield from the region where amide protons are expected (5-8ppm) but the i.r shows a strong absorption at 1635cm⁻¹ which is attributed to a carbonyl stretch. The ¹³C spectrum displays a weak quaternary signal at 165ppm and the resonance at 133ppm which is assigned as the C-NH₂ has disappeared. This supports the idea that the orange decomposition product is an aromatic amide since we would expect this carbon to shift downfield on changing to an amide. In view of these results it was decided not to attempt the reaction of L4 with suitable lanthanide reagents.

1.4B Reaction of Samarium with Undecylenic acid.

The reaction of samarium with undecylenic acid produced a white powder which was shown to be samarium undecylenate (Fig.1.21). The reaction followed a straight-forward scheme whereby hydrogen was eliminated from the long-chain carboxylic acid and three moles of this reacted with the samarium to form the metal salt. The i.r and nmr data all support the formulation of the product as shown. The expected metal analysis for a solvent free product is 21.36% which fits well with the experimental results of 21% and 22%. The ¹H nmr of the product demonstrates why samarium is favoured in lanthanide chemistry. There are no shifts in the resonances and the broadening is minimal for a paramagnetic nucleus.



Undecylenic acid

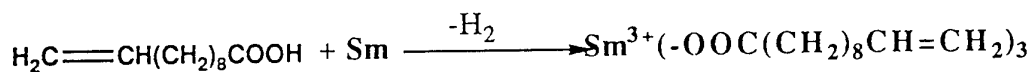


Fig.1.21 Reaction of samarium with undecylenic acid.

1.4C Attempted synthesis of 2-(1,3,6-trioxaheptyl)benzylic acid.

A variety of reaction schemes were attempted in order to produce the benzylic acid derivative of L2 (Fig.1.22). This product would be expected to react well with Lanthanide metals to produce the metal salts. The synthetic route taken when converting an aldehyde to an acid must take into account the nature of the aldehyde.

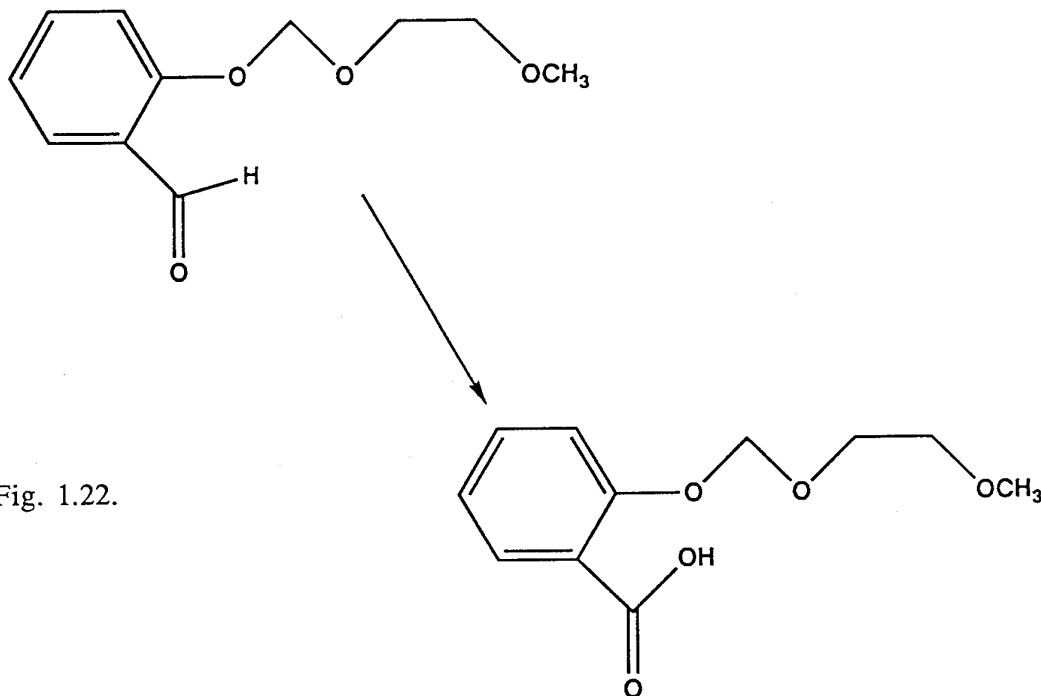


Fig. 1.22.

L2 has an ether side chain which we know is sensitive to acid because this cleaves the ether from the phenyl group. With this in mind a mild reagent was used. Pyridinium dichromate in dmf is a standard procedure for changing sensitive aldehydes to acids.⁽²⁰⁾ The reagent had no effect on the aldehyde under a variety of conditions. Less sensitive reagents (H_2O_2 , KMnO_4) were tried which cleaved the ether side-chain.

Conclusions.

The reaction of the lanthanide trichlorides (Nd, Ho) with L1 provided an intractable mixture. This was also seen for the reaction of the trichlorides with L2 and L3. The most likely explanation for this is the strong Lewis acidity of the lanthanide trihalides which could cleave the sensitive ether side groups producing a complex mix.

By softening the Lewis acidity of the lanthanide it was hoped to improve this situation. For this reason HOCp_2Cl and NdCp_3 were synthesised. Reaction of HOCp_2Cl with L1 produced a well defined product $\text{HoCp}_2\text{L1}$. NdCp_3 was reacted with L2 and although a clean product was isolated the analysis did not fit exactly the expected product. This was probably due to a bridged species. The use of smaller lanthanides than Nd and Pr produced better results also. SmCl_3 reacted cleanly with L1 and L2 to give $\text{Sm(L1)}_2\text{Cl}$ and SmL(2)_3 respectively. The use of lanthanides in the (II) oxidation state produced confusing results. SmI_2 and L1 reacted but the samarium was oxidised to (III) although the product analysis suggests Sm(L1)_2 . YbI_2 reacted with L3 but the product was uncharacterisable. YCl_3 reacted cleanly with L2 to give a product which has the formulation Y(L2)_3 . By adding a second ether side-arm to the benzene moiety it was hoped to isolate more stable lanthanide derivatives due to the increased chelating effect of three extra oxygen atoms. This however was not found due most probably to the increased steric bulk of the extra arm which prevented any Ln-C bond formation. Perhaps the most successful ligand is L2. This does not produce an organometallic lanthanide species but an aryloxo derivative. The best example of this is the reaction of Yb with the ligand to give a relatively (!) stable Yb(II) species.

EXPERIMENTAL CHAPTER 1

1.1 2-chloro(1,3,6-(trioxaheptyl)benzene (L1): A solution of 2-chlorophenol (24.5g, 190mmol) in dry dme (50cm³) was added dropwise to a cold suspension of NaH (6.84g, 228mmol) in dry dme (200cm³) and the mixture was stirred under nitrogen until the evolution of hydrogen had ceased. A solution of 2-methoxyethoxymethylchloride (28.4g, 228mmol) in dme (50cm³) was then added dropwise and the mixture was stirred at 0 °C for four hours. The reaction was followed by tlc on silica plate developed with ethyl acetate 45% and hexane 55%. Water (50cm³) was then added dropwise to destroy any remaining NaH. The organic phase was extracted with ether (3x150cm³), washed with brine, dried with MgSO₄ and concentrated under vacuum. This crude product was then purified by vacuum distillation (0.75mm, 90 °C) to afford 2-chloro(1,3,6-trioxaheptyl)benzene (L1) as a colourless viscous liquid (31.1g, 76%).

I.r (thin film, NaCl, cm⁻¹) 3070w, 3000-2821s(b), 1588m, 1478m, 1272s, 1199-974s(br), 750s

¹H nmr (300MHz, CDCl₃, TMS) δ3.364(s,3H), 3.557[t,2H,³J_{HH} 4.5Hz], 3.386[t,2H, ³J_{HH}4.5Hz], 5.337(s,2H), 6.911-9.946(m,1H), 7.186-7.213(m,2H), 7.366ppm[d,1H,³J_{HH}1.3Hz]

¹³C nmr (CDCl₃, TMS, 75.5MHz) δ58.94(CH₃), 71.56(CH₂), 60.05(CH₂) 94.23(CH₂), 152.94(1C, q), 116.65(CH arom), 130.29(CH arom), 122.72(CH arom), 127.75(CH arom), 123.68 (1C, q)ppm.

BuⁿLi: Chlorobutane (140g, 1.5mol) was added dropwise to a suspension of lithium wire (3%Na, 21g, 3mol) in dry degassed ether (500cm³) under an atmosphere of argon. Gentle reflux was maintained by dropwise addition of the chlorobutane over a period of 3 hours. When the reaction was completed the resulting BuⁿLi was assayed with 0.1M HCl and then stored at -25 °C until required.

2-chloro(1,3,6-trioxaheptyl)phenyllithium (LiL1): To a solution of BuⁿLi (3.5cm³, 10mmol) in ether (25cm³) was added dropwise (0 °C, 0.5h) a solution of L1 (2.16g, 10mmol) in ether (25cm³). The solution turned pale yellow and a white powder precipitated. After three hours the ether was removed on the vacuum line using a cannula and replaced with thf (50cm³) in which the lithium reagent was freely soluble. This enabled the lithium reagent to be assayed by hydrolysing a 1cm³ aliquot of the thf solution and titrating it with 0.1M HCl. The yield of the lithiated product

was 76%. The powdered lithium reagent could be handled with ease inside the dry-box.

1.1A Reaction of LnCl_3 with LiLi ($\text{Ln}=\text{Nd}, \text{Ho}$): A solution of LiLi (0.665g, 3mmol) in THF(50cm³) was added dropwise using a cannula into a Schlenk tube containing a stirring suspension of the lanthanide trichloride (NdCl_3 , 0.250g, 1mmol; HoCl_3 , 0.271g, 1mmol) in THF(75cm³) at -10°C. The reaction was stirred (3hrs) with gradual warming to room temperature. The resulting brown suspension was filtered through a grade 4 sintered filter to give a clear filtrate and an intractable brown solid(0.68g, Ho; 0.65g, Nd). The filtrate was hydrolysed and found to contain 0.85mmol of **L1**.

Brown solid m.p=192 °C(decomp.).

I.r (KBr disc, cm⁻¹) 3065w, 2985s, 2968s, 1497-1387m(br), 1172-985s(br), 824m, 799m, 501w, 462w.

Ho^{3+} metal analysis EDTA..22% UV/Vis 25%

Nd^{3+} metal analysis EDTA 21% UV/Vis 24%

Both products were found to contain lithium using a flame test.

The filtrate also contained lithium.

1.1B $\text{Sm}(\text{Li})_2\text{Cl}(\text{thf})_2$: Samarium trichloride was prepared using the method described by Deacon and Tuong⁽⁵⁾. HgCl_2 (0.542g, 2.00mmol) and samarium metal (0.451g, 3mmol) were allowed to react in the manner described to give the title compound as a white powder. Yield 0.240g (45%).

A solution of LiLi (0.665g, 3mmol) in thf (50cm³) was added dropwise to a stirring solution of $\text{SmCl}_3 \cdot 2\text{thf}$ (0.400g, 1mmol) in thf (50cm³) at -20 °C. The solution immediately turned dark red. After three hours stirring the solvent was slowly reduced under vacuum to 20cm³ and stored at -25 °C (8h). The red solution was filtered through a grade 4 filter to give a red filtrate and a pale yellow solid was collected on the filter (LiCl 0.118g). All of the solvent was removed from the red filtrate to give a dark red oil (1.20g) which was very sensitive to atmosphere. The oil slowly decomposed in the dry-box over a period of 2 days.

¹H nmr (80MHz, C₆D₆) δ1.9(d, br, THF), 3.3(d, OCH₃), 3.8ppm(m, 2CH₂&THF), 5.5(d, OCH₂O), 6.9-7.8(m, aromH)ppm.

Metal Analysis Sm^{3+} EDTA 20% UV/Vis 21%(22).

The product was shown to contain chlorine using the sodium fusion test.

1.1C HoCp₂(Li): HoCp₂Cl, an extremely air sensitive orange solid was prepared using the method of Dubeck *et al.*(6) from HoCl₃ and NaCp. A solution of HoCp₂Cl (0.330g, 1mmol) in thf (100cm³) was added slowly to a stirring solution of LiLi (0.22g, 1mmol) in thf (50cm³) at -10 °C. The reaction was allowed to warm up to room temperature with stirring over a period of 4 hours. Thf (150cm³) was removed on the vacuum line and the remaining solution was kept at -25 °C for ten hours. A yellow powder separated from the orange solution and this was isolated from the stock solution by removing the solvent with a cannula. The yellow powder (0.184g) was found to decompose quickly (minutes) when removed from the stock solution. The remaining orange solution yielded a mixture of the yellow solid and lithium chloride.

I.r (THF soln., NaCl) 3021w, 2985s, 2972s, 1642m, 1503m, 1462, 1422, 1269, 1209-994s(br), 932m, 870m, 704s cm⁻¹.

¹H nmr (C₆D₆ broadened significantly) δ18(m, br, 7H, CH₃OCH₂CH₂), 25.5(s, Cp), 32(s, br, 2H, OCH₂O).

Metal Analysis Ho³⁺ EDTA 29% UV/Vis 30%(32.1)

1.1D SmI₂(thf)₂ with LiLi: SmI₂ was prepared by the transmetallation reaction of Sm metal with HgI₂ in thf. Sm metal (0.750g, 5mmol) was added to a stirring solution of HgI₂ (1.817g, 4mmol) in thf (100cm³). The reaction was left stirring inside the dry-box for ten hours. The solution was then filtered to remove mercury and unreacted samarium. The solvent was then removed on the vacuum line to yield 1.58g of dark blue SmI₂.2thf.

A solution of LiLi (0.443g, 2mmol) in thf (50cm³) was added dropwise using a cannula to a stirring solution of SmI₂.2thf (0.548g, 1mmol) at -10 °C. The solution turned yellow as the reaction solution was gradually warmed to room temperature. thf (80cm³) was removed on the vacuum line and the remaining solution was stored for 10 hours at -25 °C. An off-white solid separated from the solution and this was removed by filtration. The solution was reduced to 40cm³ and stored for a further 10 hours. No further precipitation occurred. The solvent was removed to give a pale yellow solid (0.704g).

M.p=153 °C

I.r (KBr disc) 3070w, 2985m, 2897s, 1560m, 1445s, 1262s, 1183-908s(br) 804s, 768m, 662m cm⁻¹.

¹H nmr (C₆D₆) δ1.7(m, THF), 3.3-4.0(THF, Lig.), 5.2(d, CH₂), 6.8-7.6(m, arom H)ppm.

Metal Analysis Sm³⁺ EDTA 20% UV/Vis 19%.

2-(1,3,6-trioxaheptyl)benzylalcohol (L2): Salicylaldehyde (27g, 217mmol) in dme (50cm³) was added dropwise to a stirring suspension of NaH (6.84g, 228mmol) in dme (200cm³) over a period of 1 hour under an atmosphere of nitrogen. Stirring was continued until evolution of hydrogen ceased. The solution was then filtered to remove any unreacted NaH. MEMCl(27g,217mmol) in dme (50cm³) was added dropwise to the filtrate at 0 °C. The reaction was followed with TLC using a mixture of ethyl acetate 55% and hexane 45% and the crude product was purified by vacuum distillation(0.85mmHg, 135 °C) to afford 2-(1,3,6-trioxaheptyl)benzaldehyde as a colourless liquid (39g, 87%).

I.r (thin film) 3064w, 2955-2811s(b), 1749s, 1609m, 1584m, 1486m, 1178-1022s(b), 748s cm⁻¹.

¹H nmr (300MHz,CDCl₃,TMS) δ3.36(s, 3H), 3.55[t, 2H, ³J_{HH}4.6Hz], 3.81[t, 2H, ²J_{HH}, 4.6Hz], 5.35(s, 2H), 6.9-7.4(m, 4H), 10.4(s, 1H).

A solution of 2-(1,3,6-trioxaheptyl)benzaldehyde (25g,120mmol) in thf (100cm³) was added dropwise to a suspension of NaBH₄ (2g,52mmol) in thf (400cm³). The reaction was followed by tlc (55% ethylacetate,45%hexane). The mixture was refluxed for 18 hours and the resulting mixture was hydrolysed (H₂O,100cm³). The product was extracted into Et₂O (3x200cm³) washed with brine and dried with MgSO₄. The ether was evaporated to leave a yellow oil. This was distilled under vacuum (p=0.85mmHg, 144°C) to give 2-(1,3,6-trioxaheptyl)benzylalcohol (L2) as a colourless liquid (22g,85%).

I.r (thin film) 3400-3200s(b), 3043w, 3000s, 1602s, 1589s, 1484s, 1458m, 1366m, 1250s, 1150-1008s(b), 754s cm⁻¹.

¹H nmr (300MHz,CDCl₃,TMS,) δ3.332(3, 3H), 3.532[t, 2H, ³J_{HH}4.6Hz], 3.803[t, 2H, ³J_{HH}4.6Hz], 5.289(s, 2H), 6.981[t, 1H, ³J_{HH}7.4Hz], 7.227-7.4(m, 3H), 4.662[d, 2H, ³J_{HH}, 5.5Hz], 2.90(bs, 1H).

¹³C nmr 59.2ppm(CH₃), 72.8(CH₂), 69.0(CH₂), 94.6(CH₂), 155.2(qC), 115.0(CH), 128.5(CH), 122.6(CH), 129.0(CH),126.5(qC), 60.6(CH₂)

Sodium salt of L2 (NaL2): L2 (0.645g,3mmol) in thf (50cm³) was added to a suspension of NaH(0.200g,6mmol) in thf (50cm³). The suspension was refluxed for 10 hours under nitrogen and the resulting suspension was filtered through a grade 4 sinter to remove the excess NaH. The filtrate contained a quantitative yield of the sodium salt (0.704g).

1.2A Reaction of PrCl₃ with NaL₂: PrCl₃ (0.247g, 1mmol) was added to a solution of the sodium salt (0.711g, 3mmol) in Et₂O (100ml). The reaction suspension was refluxed (10h) under nitrogen. The resulting golden suspension was cooled (-10 °C), filtered through a grade 4 filter and the solvent removed on the vacuum line to give a golden viscous oil. L₂ (0.417g, 1.92mmol) was recovered from the oil after vacuum distillation (<0.1mm, 85 °C) of the golden oil. Further heating of the residue under vacuum resulted in a solid red film of material which was found to be insoluble in a wide range of solvents.

I.r golden oil (thin film) 3220s(br), 3052w, 2994s, 2890s, 2875s, 1489s, 1167-987s(br), 692s cm⁻¹.

Metal Analysis Red film contains Pr, no quantitative measurement.

1.2B Sm(L₂)₃.2NaCl: SmCl₃.2thf was prepared from Sm metal and HgCl₂ in thf as previously mentioned. A solution of SmCl₃.2thf (0.553g, 1mmol) in thf (40cm³) was added by cannula to a stirring solution of NaL₂ (0.711g, 3mmol) in thf (50cm³) at -10 °C. The reaction solution turned yellow over a period of three hours as it warmed up to room temperature. 45cm³ of thf was removed on the vacuum line and the reaction solution was kept at -25 °C (10 h). A fine white precipitate was separated from the yellow solution by filtration (NaCl, 0.06g). The yellow solution was evaporated to dryness to give an air sensitive pale yellow solid (0.858g). Repeated crystallisation attempts from toluene produced the yellow powder. The product decomposed inside a 10mm nmr tube for a ¹³C nmr. before the collection was completed.

M.p=169°C(decomp.)

I.r (KBr disc) 3070w, 2987s, 2950s, 1512m, 1470s, 1183-954s, 926m, 864m, 650s, 480s cm⁻¹.

¹H nmr (80MHz, CDCl₃) δ 3.3-3.8(m, br, OCH₃, OCH₂CH₂O), 4.6-5.4 (d, br, 2CH₂), 6.0-7.9(m, br, aromH)ppm.

Metal Analysis Sm³⁺ EDTA 21% UV/Vis 20%(20%)

1.2C Y(L₂)₃Et₂O : YCl₃ (0.195g, 1mmol) in Et₂O (75cm³) was added via a cannula to a stirring solution of NaL₂ (0.710g, 3mmol) in Et₂O (50cm³). The suspension was refluxed (9 h) under argon after the hot reaction mixture was filtered through a grade 4 sinter to give a pale yellow solution. The solvent was removed on the vacuum line to give a yellow/white solid. This yellow solid was dissolved in warm toluene (50cm³) and stored at -25 °C (10 h). This afforded 58mg of NaCl after filtration. The filtrate

was reduced to 20cm³ on the vacuum line and set aside for crystallisation at -25 °C. This procedure produced only a yellow powder (0.857g) but no crystals.

M.p=127 °C

I.r (KBr disc) 2987s, 2950s, 2874s, 1450s, 1390m, 1210-1009s(br), 794m, 702m cm⁻¹.

¹H nmr (80MHz,d₆-acetone) δ1.1ppm(t, Et₂O), 3.3(s, CH₃), 3.4-3.8 (m, CH₂, Et₂O), 4.68(s, br, CH₂), 5.3(s, CH₂), 6.98-7.5(m, aromH).

Metal Analysis Y³⁺ EDTA 12%

1.2D (*Bis(1,3,6-trioxaheptyl)benzylalkoxo*)ytterbium : A solution of L2 (0.424g,2mmol) in thf (20cm³) was added dropwise to a suspension of ytterbium metal powder (0.342,2mmol) which had been activated with mercury(II) chloride (10mg) in thf (20cm³). The solution immediately turned yellow and was left stirring (36 h). The Schlenk tube was removed from the dry-box and stored at -25 °C over a period of weeks whilst the colour changed from yellow to dark red. A red viscous oil was isolated after the red solution was filtered through a sinter and the solvent was removed on the vacuum line. The oil was transferred to a sublimation apparatus inside the dry-box. A bright yellow solid sublimed from the oil at approximately 43 °C (<1mm). The yield after sublimation was 0.17g. The yellow solid dissolved in hexane/chloroform to give a purple solution. Dark green crystals were isolated from this solution after storage at -25 °C. The crystals were extremely sensitive to atmosphere decomposing to give an orange solid.

I.r (Sol.Hexane,cm⁻¹) 3284w(br), 2980s, 2943s, 1484s, 1454s, 1116-1056s(br)
(Disc thf ppt.)3434w,3070w, 2931s,2890s,1482s,1437m,1262m,1096s(br) 669s, 595s, 529s cm⁻¹

UV/Vis Hexane λ_{max} 523nm, 263, CH₃Cl λ_{max} 504nm, C₆H₆ λ_{max} 495 Et₂O λ_{max} 360nm, CH₃CN λ_{max} 358nm, MeOH λ_{max} 355nm, THF λ_{max} 345nm.

¹H nmr (300MHz,CDCl₃,TMS) δ3.39(t, 3H,³J_{HH}), 3.56(q, 2H, ⁴J_{HH}9.21Hz), 3.72(q, 2H, ⁴J_{HH}9.21MHz), 4.76(s, 1H), 4.82(d, 2H, J_{HH}4.8Hz), 5.69(bs, ^ν_{1/2}66Hz), 6.86(t, 1H, ³J_{HH}, 16.9Hz), 7.02(d, 1H, ³J_{HH}9.54Hz), 7.17(t, 1H, ³J_{HH}, 16.9Hz), 7.30(d, 1H ³J_{HH}9.39Hz)ppm.

¹³C nmr and dept (CDCl₃,TMS,75.5MHz) δ58.7ppm(CH₃), 61.8(CH₂), 66.8(CH₂), 71.7(CH₂), 95.6(CH₂), 151.4(C), 116.3(CH), 129.1(CH), 121.3(CH), 128.4(CH), 119.8 (C).

Metal Analysis Yb³⁺ EDTA 31% UV/Vis 28%.

1.2E Thallium cyclopentadienide: $\text{NdCp}_3\cdot\text{thf}$ was prepared using the method described by Deacon *et al.*(11) as follows. Thallium hydroxide (3.315g, 15mmol) was added to a stirring solution of fresh cyclopentadiene(CpH, 1.00g, 15mmol) in thf (100cm³). The solution was evaporated to dryness after 1 hour to give a quantitative yield of TlCp (3.310g, 15mmol) as a white solid. The white solid was further dried on the vacuum line (<0.01mm) by warming at 50 °C for 1 hour to ensure no traces of water remained.

$\text{Nd}(\text{Cp})_3(\text{thf})$: A solution of TlCp (0.884g, 4mmol) in thf (50cm³) was added dropwise to a stirring suspension of neodymium metal (0.72g, 5mmol) in thf (25cm³) with 100mg of HgCl_2 . The mixture was refluxed (20 h) after which time it was filtered through a sinter to remove any unreacted neodymium and mercury. The product was obtained as blue crystals after storage at -25 °C for 48 hours and the solvent was removed to yield $\text{NdCp}_3\cdot\text{thf}$ (0.34g, 83%) as blue crystals.

$\text{NdCp}_2(\text{L}2)$: A solution of L2 (0.107g, 0.5mmol) in thf (40cm³) was added slowly using a cannula to a stirring solution of $\text{NdCp}_3\cdot\text{thf}$ (0.20g, 0.5mmol) in thf (25cm³). The colour of the solution changed from pale blue to light brown on addition of the alcohol. The reaction was refluxed for 2 hours inside the dry-box. The reaction was then evaporated to dryness on the vacuum line to give a pale brown powder(0.362g).

M.p=137 °C

I.r (KBr disc) 3097w, 2976vs, 2954s, 2894s, 1494m, 1262s, 1190-1010vs(br), 784s cm⁻¹.

¹H nmr (80MHz, d₆Acetone) The spectrum consisted of a series of resonances between δ22ppm and δ1.5ppm which were too broad to confidently assign any signal.

Metal Analysis Nd^{3+} EDTA 18% UV/Vis 19%(19.7)

1.3 4,6-dichloro-1,3-bis(1,3,6-trioxaheptyl) benzene (L3): A solution of 4,6-dichloro-1,3-dihydroxybenzene (1.8g, 10mmol) in thf (50cm³) was added dropwise to a suspension of NaH (2g) in thf (20cm³) and the mixture was stirred under argon until the evolution of H₂ had ceased. The mixture was then filtered to remove any unreacted NaH. The filtrate was cooled to 0 °C and a solution of MEMCl (2.5g, 20mmol) in thf (20cm³) was added dropwise with rapid stirring. The reaction was followed by tlc (silica, 50% ethylacetate, 50%hexane) for 2 hours after which time the MEMCl was no longer visible on TLC. Water(50cm³) was then added and the organic phase extracted with ether(3x50cm³), dried with MgSO_4 and concentrated. The crude product was purified by flash chromatography on a silica gel column to give 4,6-dichloro-1,2-bis(1,3,6-trioxaheptyl)benzene(1.84g, 52%). The product can be crystallised to give clear crystals (m.p 45 °C).

I.r (KBr disc) 3000-2800s(b), 1592s, 1484s, 1189-1007s(b), 873m, 844m 747m cm⁻¹.

^1H nmr (300MHz, CDCl_3 , TMS,) δ 3.362ppm(s, 6H), 3.558[t, 4H, $^3J_{\text{HH}}$ 4.7Hz], 3.962[t, 4H, $^3J_{\text{HH}}$ 4.7Hz], 5.292(s, 4H), 6.676-6.752(m, 2H), 7.139[t, 1H, $^3J_{\text{HH}}$, 8.2Hz].

^{13}C nmr (75.5MHz, CDCl_3 , TMS) δ 58.94ppm(CH_3), 71.56(CH_2), 60.05(CH_2), 94.23(CH_2), 152.94(w,C), 123(w,C), 106.46ppm(CH), 124.22(CH).

1.3A Reaction of 3LiL_3 with NdCl_3 : A solution of Bu^nLi (1.9M, 1.5cm³, 10mmol) in Et_2O (20cm³) was added dropwise to a rapidly stirring solution of L3 (1.43g, 5mmol) in Et_2O (50cm³) at -10 °C. The solution turned pale yellow and was left stirring (5 h) (Approximately 10 cm³ of thf was removed on the vacuum line and the reaction was cooled to -45 °C in an $\text{EtOH}/\text{liq. N}_2$ bath. This afforded the lithiated ligand as an off-white powder in 80% yield (1.164g). The remaining solvent was removed by cannula and the product washed with Et_2O (2x10cm³). The powder was quite stable inside the dry-box for long times but hydrolysed immediately on contact with air. The lithium reagent was readily soluble in thf.

A solution of the lithium reagent LiL_3 (0.88g, 3mmol) in thf (25cm³) was added dropwise to a stirring solution of NdCl_3 (0.25g, 1mmol) in thf (85cm³). The solution turned pale brown and stirring was continued (10 h) inside the dry-box. 50cm³ of thf were removed on the vacuum line and the reaction solution was stored at -25 °C for a further 10 hours during which time no precipitation occurred. All of the thf was removed on the vacuum line and replaced with 50cm³ of Et_2O . The suspension was filtered through a grade 4 filter to give a pale brown/pink filtrate. The collected solid contained LiCl and unreacted lithium reagent (flame test and UV/Vis). The filtrate was concentrated to 30cm³ and stored for 8 hours at -25 °C to give a brown oil (0.317g). Vacuum distillation (<0.01mm, 120 °C) of the oil resulted in an intractable brown solid (0.43g) and L3 (0.275g, 0.96mmol).

I.r (KBr disc, Brown solid) 3054vw, 2987s, 2873s, 1436s, 1511m, 1108-966s(b), 801m, 694s cm⁻¹.

Metal Analysis Nd^{3+} EDTA..35% UV/Vis 27%.

1.3.A Reaction of LiL_3 with NdCl_3 : The same procedure was followed here as for the previous reaction except that the ratio of metal to ligand was 1:1. As above an intractable brown solid was isolated which gave the same analysis.

1.3.B Reaction of YbI_2 with 2LiL_3 .

$\text{YbI}_2(\text{thf})_2$: A solution of freshly recrystallised di-iodoethane (0.843g, 3mmol) in thf (20cm^3) was added dropwise to a stirring suspension of activated ytterbium metal (1.04g, 6mmol, 100mg HgCl_2) in thf (50cm^3). The reaction immediately turned dark red and stirring was continued (3 h). The suspension was then filtered to give a dark red solution from which $\text{YbI}_2 \cdot 2\text{thf}$ (1.68g, 2.9mmol) was isolated after the solvent was removed on the vacuum line.

A solution of LiL_3 (0.58g, 2mmol) in thf (30cm^3) was added dropwise to a rapidly stirring solution of $\text{YbI}_2 \cdot 2\text{thf}$ (0.57g, 1mmol) in thf (50cm^3). The reaction solution turned yellow immediately and stirring was continued for 3 hours. Thf (20cm^3) was removed on the vacuum line and the solution was stored at $-25\text{ }^\circ\text{C}$ (10 h). No precipitation was apparent so the solution was cooled gradually in an $\text{EtOH}/\text{liq.N}_2$. LiI (0.108g, 0.8mmol) was isolated at approximately $-50\text{ }^\circ\text{C}$. Further cooling precipitated an extremely air sensitive yellow solid (0.88g). The remaining solvent was removed on the vacuum line to give 0.15g of yellow powder. The yellow product decomposed during several attempts to record a ^1H nmr.

M.p= $144\text{ }^\circ\text{C}$

I.r (KBr disc) 2977s, 2884s, 1458m, 1330m, 1262s, 1160-908s(br), 821s, 799m, 622s cm^{-1}

Metal Analysis Yb^{3+} EDTA 27% UV/Vis 25%.

1.4 Synthesis of *1,3-bis(1,3,6-trioxaheptyl)2-aminobenzene (L4)*

2-Nitroresorcinol:-Sulphuric acid (500cm^3 , 9.2mol) was added to a 2L round-bottomed flask containing resorcinol (110g, 1mol) and the mixture was rapidly stirred. A thick slurry of 4,6-disulphonic acid formed as the temperature of the mixture rose to $70\text{ }^\circ\text{C}$. The mixture was cooled ($-10\text{ }^\circ\text{C}$) and a cold mixture of nitric acid (70cm^3 , 1.2mol) and sulphuric acid (112cm^3 , 2.1mol) was added dropwise at a sufficient rate to maintain the temperature below $20\text{ }^\circ\text{C}$. The thick suspension became a yellow solution on addition of the acid mix. The yellow solution was then slowly diluted with ice (500g). The solution was steam distilled which afforded 2-nitroresorcinol as an orange red solid. The product was recrystallised from ethanol and dried on the vacuum line. (42.00g, 27%)

M.p= $84\text{ }^\circ\text{C}$

I.r (KBr disc) 3400-3100m(b), 3094w, 3068w, 1637s, 1583s, 1541s, 1372s, 1278m, 859w, 807s, 772w cm^{-1} .

^1H nmr (80MHz, CDCl_3 , TMS) δ 5.28ppm(s(b), 2, OH), 6.37(d, 2H), 7.12(t, 1H).

1,3-bis(1,3,6-trioxaheptyl)-2-nitrobenzene:-The method used in the synthesis of L3 was employed. The title compound was obtained as an orange liquid from the reaction of 2-nitroresorcinol (7g,45mmol) and 2-MEMCl (13.7g, 110mmol) followed by flash chromatography on a silica column (ethyl acetate 80%, hexane 20%). Yield=6.4g, 19mmol, 44%.

I.r (Thin film,NaCl,cm⁻¹) 3104w, 2932-2824s(b), 1614s, 1589s, 1373, 1165-1042s(b), 851s, 783s, 738s

¹H nmr (300MHz,CDCl₃,TMS) δ3.358ppm(s, 6H), 3.544[t, 4H, ³J_{HH}4.6Hz], 3.821[t, 4H, ³J_{HH}, 4.6Hz], 5.258(s, 4H), 6.785[d, 2H, ³J_{HH}, 7.7Hz], 6.59[t,1H, ³J_{HH}, 7.7Hz].

¹³C nmr (75.5MHz,CDCl₃) δ58.92(OCH₃), 67.79(CH₂), 71.62(CH₂), 94.35 CH₂), 109.21(C meta NO₂), 116.88(C-NO₂), 127.49(C para), 145.2(C ortho).

1,3-bis(1,3,6-trioxaheptyl)-2-aminobenzene(L4):-Palladium-on-charcoal (0.3g, 10%Pd/C) was added to a solution of 1,3-bis(1,3,6-trioxaheptyl)-2-nitrobenzene (2g, 6mmol) in methanol (200cm³). The mixture was then placed in a Parr hydrogenator (24h, P(H₂) 3atm) and the reaction was followed by i.r. and nmr until no further evolution of the NH₂ group could be detected. The solution was filtered, dried on MgSO₄ and the solvent was removed to give the title (L4) compound as an air sensitive yellow liquid.(1.71g. 95%).

I.r (Thin film, cm⁻¹) 3476m, 3373m, 3200-2800m(b), 1613m, 1501m, 1098-1027s(b), 874m, 750m, 724m .

¹H nmr (300MHz,CDCl₃,TMS) δ3.357ppm(s, 6H), 3.554[t, 4H, ³J_{HH}4.5Hz], 3.816[t, 4H, ³J_{HH}4.5Hz], 5.309(s, 4H), 6.94[d, 2H, ³J_{HH}8.5Hz], 7.296[t, 1H, ³J_{HH}8.5Hz], 7.93(s, br, 2H 23Hz)

¹³C nmr (75.5MHz,CDCl₃) δ58.92ppm(CH₃), 71.39(CH₂), 68.29(CH₂), 94.26(CH₂), 149.19(C), 108.92(CH), 130.99(CH), 133.87(C-NH₂ m).

1.4A Reaction of AlCl₂CH₃ with L4: A solution of AlCl₂CH₃ (0.23g,2mmol) in Et₂O (10cm³) was added dropwise to a rapidly stirring solution of L4 (0.394g,2mmol) in Et₂O (40cm³). A blue/black solid immediately precipitated from the solution. This solid was separated from solution by removing the solvent with a filter cannula. The product was then dried by removing any remaining solvent on the vacuum line. A KBr disc was prepared of the air-sensitive product but all attempts to prepare an nmr sample failed as chlorinated solvents resulted in degradation of the product. The compound decomposed quickly to give an orange oil.

I.r (KBr disc) 3552s, 3420s, 3244s, 3116m, 3097m, 2962s, 2929s, 1620s, 1531m, 1456m, 1262m, 1196-1049s, 803s, 611s, 489m, 401m cm^{-1} .

I.r (KBr disc orange decomp.) 3611m, 3526m, 3418m, 3010w, 2925s, 1630m, 1480m, 1264m, 1186-986m, 804m, 626w, 564w cm^{-1} .

UV/Vis (Orange decomp, toluene) $\lambda_{\text{max}}(\epsilon)$ 316nm(5000), $\lambda_{\text{max}}(\epsilon)$ 380nm(900).

^1H nmr (80MHz, CDCl_3 , TMS) δ 3.362ppm(s, 3H), 3.543(m, 2H), 3.83(t, 2H), 5.31(d, 2H), 6.53-7.42(m, 3H), 9.74(s, 1H), 10.64(s, 1H)

^{13}C nmr with DEPT (75.5MHz, CDCl_3 , TMS) δ = 58.2ppm(OCH_3), 68.3(CH_2) 72.5(CH_2), 93.8(d, CH_2), 108.3(CH), 130(CH), 139.5(CH), 148.8(q), 165(q).

1.4B Reaction of Samarium with Undecylenic acid.

Samarium tris(undecylenate): Undecylenic acid (0.550g, 3mmol) was dissolved in thf (40 cm^3) and added to a stirring suspension of samarium powder (0.150g, 1mmol) activated with 4 crystals of HgCl_2 in thf (40 cm^3). Evolution of hydrogen gas started immediately. The reaction was kept stirring (48h) after which all of the metal had been consumed and a small amount of a white precipitate was visible. The white product (0.754g) was isolated after storage at -25°C (10h) followed by filtration. M.p = 305°C (decomp.)

Undecylenic acid.

I.r (KBr disc) 3769-2663s(br), 2956s, 2877s, 1710s, 1622s, 1450s, 980s, 924m, 668m cm^{-1} .

^1H nmr (80MHz, CDCl_3) δ 1.27ppm(s, 8H), 1.96-2.40(m, 8H), 4.96(t, 2H), 5.45-6.04(m, 1H), 9.49(s, br, $\nu_{1/2}$ = 62Hz).

Product.

I.r (KBr disc) 2966s, 2897s, 1580m, 1410m, 1261w, 1036m, 976s, 900m, 710m, 684m cm^{-1} .

^1H nmr (80MHz, MeOD, CHCl_3) δ 1.5-2.6ppm(d, br), 5.17(t, br), 5.7-6.4(m, br).

Metal Analysis Sm^{3+} EDTA..22% UV/Vis 21%

1.4C Attempted synthesis of 2-(1,3,6-trioxaheptyl)benzylic acid: A solution of pyridinium dichromate (100mg) in dmf 40 cm^3 was added to a solution of 2-(1,3,6-trioxaheptyl)benzaldehyde (0.500g, 2.4mmol) in dmf (60 cm^3) and the solution was heated (50°C) with stirring (48h). Workup of the reaction produced only the starting materials. The reaction conditions were varied (conc., temp., time) but no reaction was observed.

Similar reactions involving H_2O_2 or KMnO_4 with the benzaldehyde resulted in the methoxyethoxymethyl moiety being cleaved from the phenyl ring.

References.

- 1 F.A. Hart, M.S. Saran, *Chem. Commun.*, 1968, 1614 also F.A Hart, A.G. Masey, M.S. Saran, *J. Organometal. Chem.*, 1970, **21**, 147.
- 2 L.E. Manzer, *J. Organometal. Chem.*, 1977, **C6**, 135.
- 3..G.K. Barker, M.F. Lappert, *J. Organometal. Chem.*, 1974, **C45**, 76.
- 4..M.F. Lappert, R. Pearce, *J. Chem. Soc., Chem. Commun.*, 1973, 126.
- 5 Advanced Inorganic Chemistry, F.A. Cotton and G. Wilkinson, 5th. Edit., 1988, Chpt. 20, Wiley-Interscience, N.Y.
- 6 J.M. Lehn, *Acc. Chem. Res.*, 1978, **11**, 49 and Organometallics of the f-Elements, Ed. T.J. Marks and R.D. Fischer, 1979, D. Reidel, Dordrecht, Holland.
- 7 L.E. Manzer, *J. Am. Chem. Soc.*, 1978, **100**, 8068.
- 8 E.J. Corey, J-L. Gras and P. Ulrich, *Tetrahedron Lett.*, 1976, 809.
- 9 G. Deacon, T.D. Tuong, D.L. Wilkinson, *Inorg. Synth.* **27**, 136 (Ed. A.P. Ginsberg, Wiley-Interscience).
- 10 R. Dubeck, M.Manastyrsky, *Inorg. Chem.*, 1963, **2**, 904.
- 11..W.J. Evans, J.W.Grate, H.W.Choi, I.Bloom, W.E Hunter, and J.L.Atwood, *J. Am. Chem. Soc.*, 1985, **107**, 941.
- 12 G.K.I. Magomedov, *Organomet. USSR (Metalloorg. Khim.)*, 1990, **3**, 706.
- 13 M. Bremont, MSc. Thesis, TCD, 1992.
- 14 (a) G. Deacon, A.J. Koplick and T.D. Tuong, *Polyhedron*, 1982, **1**, 423. (b) G. Deacon, A.J. Koplick and T.D. Tuong, *Aust. J. Chem.*, 1984, **37**, 517.

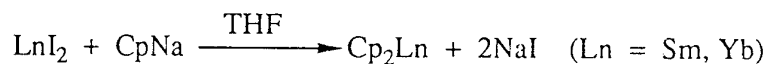
- 14 (c) G.Z. Suliemanov, L.F. Rybakova, Ya.A. Nuriev and I.P. Beletskaya, *J. Organomet. Chem.*, 1982, **235**, 254. (d) G. Wilkinson and T.S. Piper, *J. Inorg. Nucl. Chem.*, 1955, **2**, 32.
- 15 K.H. Boltze, H.D. Dell and H. Jansen, *Liebigs Ann. Chem.*, 1967, **709**, 63.
- 16 M.R. Winkle and R.C. Ronald, *J. Org. Chem.*, 1982, **47**, 2101.
- 17 D.J. Cardin, D.N. Weldon, M. Bremont and C.J. Cardin, (to be submitted).
- 18 T.D. Tilley, J.M. Boncella, D.J. Berg, C.J. Burns and R.A. Andersen, *Inorg. Synth.*, **27**, 146 and J.K. Howell and L.L. Pytlewski, *J. Less Common Met.*, 1969, **18**, 437
- 19 H. Schumann, E. Palamadis and J. Loebel, *J. Organomet. Chem.*, 1990, **384**, C49.
- 20 T. Mole and E.A. Jeffery, *Organoaluminium Compounds*, Elsevier, 1972.
- 21 R.T. Morrison and R.N. Boyd, *Organic Chemistry*, 4th. Edit., p504.

CHAPTER 2

Organometallic Lanthanide(II) Chemistry.

2.1 Introduction.

The recent synthesis of a new bridged cyclopentadienyl Yb(II) derivative by Recknagel and Edelmann⁽¹⁾ has prompted the study of its chemistry compared to other cyclopentadienyl Yb(II) derivatives. There are three well known cyclopentadienyl Yb(II) derivatives. Yb(Cp)₂ was first reported by Fisher *et al.*⁽²⁾ and subsequently by Calderazzo *et al.*⁽³⁾. Yb(Cp*)₂⁽⁴⁾ and Yb(CpSiMe₃)₂⁽⁵⁾ followed soon after and proved to be much more useful due to their increased solubility in non-polar solvents. The development of convenient synthetic methods for samarium and ytterbium dihalides made it possible to obtain the corresponding bis(cyclopentadienyl) derivatives by the following reaction.⁽⁶⁾



The reaction of metallic ytterbium with CpTl also constitutes a synthesis of YbCp₂⁽⁷⁾; the addition of metallic mercury accelerates the reaction. In dme the reaction leads to the formation of Cp₂Yb(dme), while in thf the product is Cp₂Yb(thf)₂. When the solvate Cp₂Yb(thf)₂ is heated in vacuo (140 °C-150 °C) and subsequently treated with benzene, solvent free YbCp₂ is obtained. Another method of synthesis of YbCp₂ involves the reduction of Yb(III) derivatives (Cp₂YbCl or Cp₃Yb) with metallic sodium or ytterbium⁽⁸⁾. The reductant can also be Bu^tLi⁽⁹⁾. Bis(cyclopentadienyl)samarium, Cp₂Sm(thf), has also been obtained by reducing Cp₃Sm with KC₁₀H₈⁽¹⁰⁾.

The bis(cyclopentadienyl) derivatives of the lanthanides are highly reactive unstable compounds which decompose instantly on contact with moisture or atmospheric oxygen. They are soluble only in polar solvents. The introduction of Me or SiMe₃ substituents into the cyclopentadienyl ring stabilises the lanthanocene without significantly altering the character of the Cp-Ln bond.

Cyclopentadienyl complexes of divalent lanthanides analogous to ferrocene should be unstable because of the co-ordinative unsaturation of the metal. Such complexes therefore form solvates, while the insoluble unsolvated complexes (C₅Me₅)₂Ln (Ln = Sm, Eu or Yb) form oligomers with increased co-ordination number of the metal.⁽¹¹⁾ The structure of a non-solvated organolanthanide complex, Cp*₂Sm, was first investigated by Evans.⁽¹²⁾ The structure showed that the ligands are at an angle (136.7°). This angle changes only slightly on passing from the non-solvated to the solvated complex.⁽¹³⁾

All of these compounds were made using the sodium or potassium salt of the cyclopentadienyl ligand and the ytterbium halide. This type of salt-elimination reaction has some disadvantages. Firstly the ligand may have to be made as most are not

available commercially, and secondly the product needs to be separated from the salt by-product of the reaction. The yields are not high for any of these schemes and the cost may be prohibitive. The preparation of these new cyclopentadienyl ytterbium and samarium compounds therefore offered an attractive one-pot, high yield, low cost alternative to the conventional preparations. A study was therefore undertaken to investigate the chemistry of this new compound and to improve the preparation (Fig. 2.2).

2.2 Synthesis and Reactions of $\text{Yb}(\text{CpCH}_2(\text{CH}_3)_2\text{CH}_2(\text{CH}_3)_2\text{Cp})$.

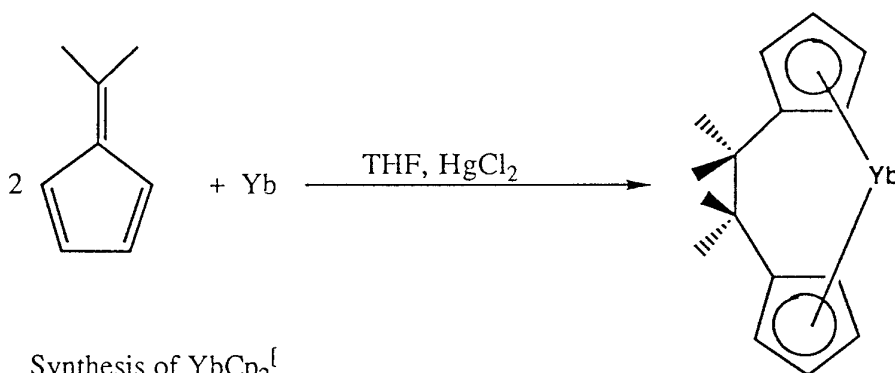


Fig.2.2 Synthesis of YbCp_2^{I}

Ytterbium metal is usually activated before a reaction using a small amount of mercury either as the chloride or as the metal. The preparation of Recknagel describes the use of mercuric chloride. This will obviously reduce the overall yield by a small amount and can sometimes destroy a reaction. Ytterbium dissolves in liquid ammonia to give the characteristic blue colour of the solvated electron. When the ammonia is removed under vacuum with rapid stirring a "mirror" of activated ytterbium is formed on the walls of the Schlenk-tube. This is a much cleaner method of activating ytterbium (and europium) and when this was used in the preparation of YbCp_2^{I} a 26% increase in yield was recorded. Also the product did not require any washing. The analysis of the product was as for Recknagel. It was found also that the commercially available 6,6-dimethylfulvene (Aldrich) should be distilled before use as all samples contained a white residue which accounted for up to 15% of the purchased product (the impurity could not be identified). Recknagel claims (based on mass spectrometric data) that the product is sterically unsaturated (the spectrum showed no evidence of coordinated thf). The metal analysis which I performed concurs with this claim.

2.3 Reaction of YbCp₂¹ with Co₂(CO)₈.

Divalent Yb and Sm organometallics are strong enough reducing agents to react with many transition metal carbonyl complexes to form anions.⁽¹³⁾ Although the simple unsubstituted cyclopentadienyl complexes like YbCp₂ will react with transition metal carbonyls, reaction with C₅Me₅ derivatives give products which are easier to characterise. The reactivity of Cp*₂YbOEt₂ has been extensively studied in this regard.⁽¹⁴⁾ Figure 2.3 shows a simple reduction scheme in which the metal-metal bond of Co₂(CO)₈ is cleaved to generate the anion [Co(CO)₄]⁻.

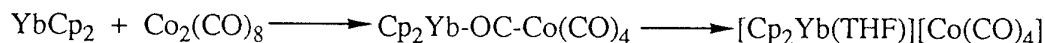


Fig.2.3 Reduction sequence.

This reactivity is typical in that the divalent lanthanide is oxidised and acquires an additional electronegative ligand. Iron pentacarbonyl reacts with Cp*₂YbOEt₂ to form an analogue of Na₂Fe(CO)₄⁽¹⁵⁾ as shown in Figure 2.4. However when Fe₃(CO)₁₂ reacted with Cp*₂YbOEt₂ an Fe-Fe bond was broken, a carbonyl ligand was lost and an Fe₃(CO)₁₁⁻ unit was formed which was attached to two [Cp*₂Yb]⁺ units via four isocarbonyl bonds.⁽¹⁶⁾

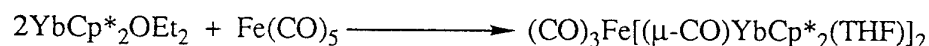


Fig.2.4 Isocarbonyl formation.

The isocarbonyl type of bond (Fig.2.5) is characteristic of heterobimetallic complexes of early transition elements and also of metal carbonyl salts of other oxophilic metals (Na, Mg, Al etc.).



Fig. 2.5 Isocarbonyl bond between two metals.

The unoccupied orbitals of the metal, which overlap with the orbital of the unshared electron pair of CO via the oxygen atom, participate in the formation of a donor-acceptor bond. As a result, the energy levels of the frontier orbitals are lowered and the carbon-oxygen triple bond is weakened still further. The stretching vibration frequency of such isocarbonyl groups are appreciably reduced in energy and appear at 1700cm⁻¹.

Recently Shore et al.⁽¹⁷⁾ reacted Fe₃(CO)₁₂ with Yb dissolved in liquid ammonia to give a polymeric compound that contains a definite Yb-Fe bond along with isocarbonyl linkages. Reductive formation of tight ion pairs containing isocarbonyl bonds has also been reported⁽¹⁸⁾ for Cp*₂YbOEt₂ with Cp*₂Fe(CO)₄, Cp₂Mo(CO)₆, and CpCo(CO)₂.

Similar reactions occur for the samarium analogues with the exception of the reaction of $\text{SmI}_2(\text{thf})_x$ with $\text{Co}_2(\text{CO})_8^{(19)}$ (Fig. 2.6) where the product does not have isocarbonyl linkages. The product has discrete $[\text{SmI}_2(\text{THF})_5]^+$ and $[\text{Co}(\text{CO})_4]^-$ units.



Fig. 2.6

When YbCp_2^1 was added to a solution of $\text{Co}_2(\text{CO})_8$ a red solid precipitated which was isolated by filtration. The red solid spontaneously ignited in air presumably due to the presence of very finely dispersed ytterbium powder. Analysis of the red precipitate was consistent with the formulation $\text{Cp}_2^1\text{Yb}(\text{OC})\text{Co}(\text{CO})_4$ (Fig.2.7). The product slowly decomposes when stored under N_2 but it is stable for much longer periods under Ar. The ^1H nmr spectrum exhibits the typical broadness associated with the paramagnetic Yb(III).

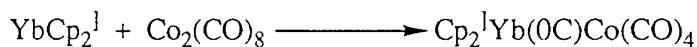


Fig.2.7 Reaction 2.1A

The product was studied by i.r as a solid (CsI sandwich, Nujol mull) and in solution (thf). The strong peaks at circa 1700cm^{-1} are indicative of isocarbonyl linkages in the product. There was no change in the spectra when they were recorded two weeks later demonstrating that the product is relatively stable when carefully stored under dry-box conditions.

The addition of YbCp_2 to $\text{Co}_2(\text{CO})_8$ affords initially a complex with an isocarbonyl ligand in high yield⁽¹⁸⁾, this compound is however thermodynamically unstable and gradually ionises (Fig. 2.8).



Fig. 2.8

When pentamethylcyclopentadienyl(Cp^*) is used as the ligand instead of Cp the compound $\text{Cp}_2^*\text{YbOCCo}(\text{CO})_4^{(14)}$ is formed, which becomes thermodynamically stable in solution in thf and does not ionise. This demonstrates the softening of the ytterbium as a Lewis acid in the sequence $\text{YbCp}_2 < \text{YbCp}_2^1 < \text{Cp}^*_2\text{Yb}$.

2.4 Reaction of YbCp_2^1 with $\text{Fe}_3(\text{CO})_{12}$.

The reaction of YbCp_2^1 with $\text{Fe}_3(\text{CO})_{12}$ did not follow the same route as that of YbCp^*_2 . Instead a species was detected in solution which had a very low symmetry

(23 terminal CO stretches) with some isocarbonyl bridging. All attempts at isolation of this species yielded only the starting materials.

2.5 Reaction of YbCp_2^1 with MeCN.

The compound YbCp_2^1 is believed to be sterically unsaturated and should therefore react with strongly coordinating solvents. YbCp_2^1 was added as a solid to acetonitrile and immediately gave a dark green solution. A similarly coloured solid was isolated from this solution on work-up. Small green crystals of poor quality were grown from a saturated solution of the product in MeCN at -27°C . The ^1H nmr, i.r and metal analysis are all consistent with an acetonitrile bridged dimer (Fig.2.9).

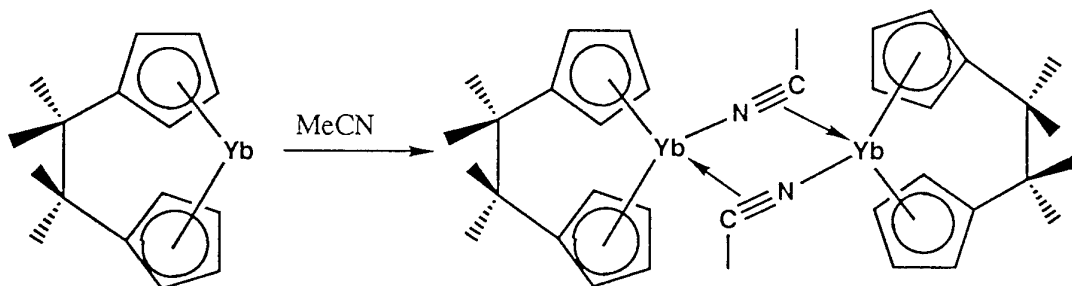
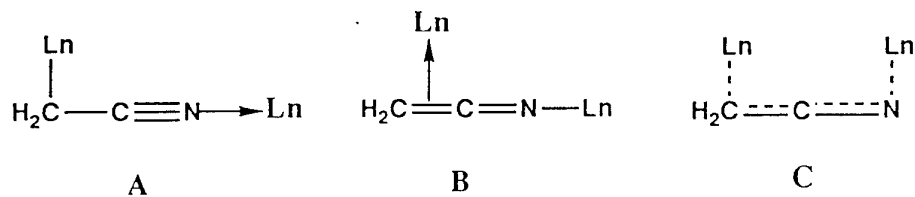


Fig. 2.9

The i.r spectrum for free MeCN shows C=N absorptions at 2293cm^{-1} and 2257cm^{-1} ⁽²⁰⁾. This frequency is lowered on co-ordination, for α -cyanomethyl complexes of Fe, Pt and Cu lie between 2210cm^{-1} and 2165cm^{-1} .⁽²¹⁾ The i.r spectrum of the green compound shows some free MeCN and co-ordinated MeCN with absorptions as low as 2041cm^{-1} . Teuben⁽²²⁾ has reported CH activation of MeCN by alkyl compounds of lanthanides, and Bercaw⁽²³⁾ reports the activation of the normally inert CH bonds of methane by complexes of the type Cp^*LnMe . This evidence suggests that the bonding in the MeCN bridges of this compound might be closer to those shown in Fig. 2.10.



- (A) C-metalated structure.
 (B) N-metalated ketenimine.
 (C) Intermediate of A and B⁰

Fig. 2.10

The dark green product was sensitive to air and moisture turning yellow even when stored under N₂. The yellow decomposition product Yb(III) was shown to contain no acetonitrile but co-ordinated OH from the i.r. Surprisingly the green acetonitrile dimer was converted to the monomeric form when dissolved in thf with the evolution of uncoordinated MeCN. This suggests either that the monomer does contain co-ordinated thf or that it oligomerises to increase the co-ordination number of the metal. The green dimeric form of the YbCp₂¹ compound can be synthesised using a more direct route. When MeCN was used instead of thf in the synthesis of YbCp₂¹ a green solid was isolated. The white precipitate which was isolated was shown to be ytterbium acetate presumably due to trace amounts of acetic acid in the MeCN despite rigorous drying.

2.5 Reactions involving Lanthanides and Transition metals.

Compounds having lanthanide to transition metal bonds have been proposed since 1973⁽²⁴⁾. The compounds were prepared by salt elimination methods⁽²⁴⁾ or by the reaction of finely divided lanthanide metals with organometallic compounds of transition metals (Fig.2.11).⁽²⁵⁾

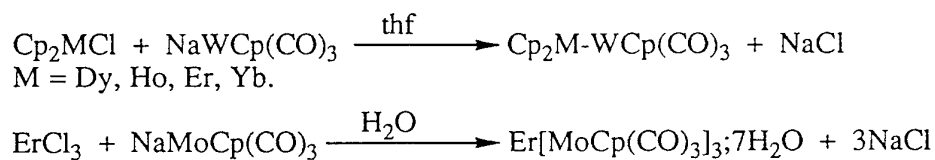


Fig.2.11 Proposed Ln-TM bonding.

The bonding in these compounds is not clear. The tungsten compounds have i.r spectra which imply the presence of isocarbonyl links and a polymeric structure has been suggested.⁽²⁵⁾ The reaction of Yb and other lanthanide metals with (CO)₅MnBr in thf produce air and water sensitive red solutions containing Grignard-like species

$[(CO)_5Mn]_xMBr_y$. The i.r spectra of these solutions do not however support the presence of isocarbonyl linkages.⁽²⁴⁾ An X-ray diffraction study was made on the complex $(EtOH)(H_2O)_4Er[CpMo(CO)_3]_3$ ⁽²⁶⁾ in which a weak Er-Mo interaction was detected according to the authors (the Er-Mo distance is 3.143 Å, while the sum of the atomic radii of the metals is 3.14 Å). This compound which was first synthesised by Crease and Legzdins⁽²⁵⁾ and its' proposed structure is in considerable doubt since water was used as a solvent. Also the structure determination by Suliemanov has not appeared in an international publication. A more recent publication by Magomedov *et al.* proposes a Lu-Ru interaction in the novel $(thf)(\eta^5-Cp)_2LuRu(CO)_2(\eta^5-Cp)$.⁽²⁷⁾ The complex was synthesised by the reaction of Cp_2LuCl with $CpRu(CO)_2Na$. The Lu-Ru distance is 2.955 Å (the sum of the atomic radii of the metals is 3.08 Å). The Lu atom is co-ordinated to two Cp ligands and the oxygen atom of thf, while the Ru atom is co-ordinated to one Cp and two CO ligands.

4.6 Reaction of Yb with $Fe_3(CO)_{12}$.

More recently Shore⁽¹⁷⁾ has synthesised a unique polymeric compound containing an ytterbium-iron bond. The compound was synthesised as shown in Figure 2.12.

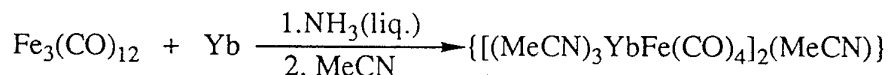


Fig.2.12 Synthesis of Yb-Fe polymer.

Shore has obtained an X-ray structure of the compound. A discrete Yb-Fe bond as well as isocarbonyl links exist. The complex has a ladder type structure (Fig.2.13)

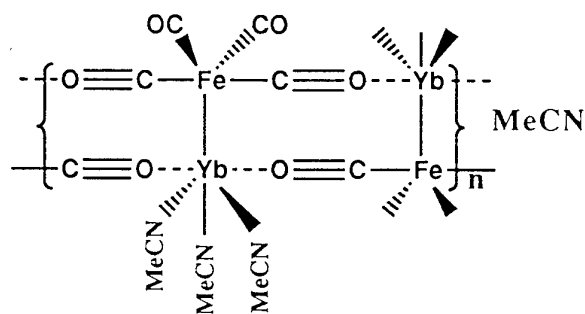


Fig. 2.13 'Ladder' polymer structure.

The reaction proceeds in two steps. The first generates the ammonia adduct $(NH_3)_xYbFe(CO)_4$, which on the addition of acetonitrile generates the title compound. The product decomposes on exposure to atmosphere. The decomposition material has been shown in this study to contain $Fe_3(CO)_{12}$.

$[(CO)_5Mn]_xMBr_y$. The i.r spectra of these solutions do not however support the presence of isocarbonyl linkages.⁽²⁴⁾ An X-ray diffraction study was made on the complex $(EtOH)(H_2O)_4Er[CpMo(CO)_3]_3$ ⁽²⁶⁾ in which a weak Er-Mo interaction was detected according to the authors (the Er-Mo distance is 3.143 Å, while the sum of the atomic radii of the metals is 3.14 Å). This compound which was first synthesised by Crease and Legzdins⁽²⁵⁾ and its' proposed structure is in considerable doubt since water was used as a solvent. Also the structure determination by Suliemanov has not appeared in an international publication. A more recent publication by Magomedov *et al.* proposes a Lu-Ru interaction in the novel $(thf)(\eta^5-Cp)_2LuRu(CO)_2(\eta^5-Cp)$.⁽²⁷⁾ The complex was synthesised by the reaction of Cp_2LuCl with $CpRu(CO)_2Na$. The Lu-Ru distance is 2.955 Å (the sum of the atomic radii of the metals is 3.08 Å). The Lu atom is co-ordinated to two Cp ligands and the oxygen atom of thf, while the Ru atom is co-ordinated to one Cp and two CO ligands.

4.6 Reaction of Yb with $Fe_3(CO)_{12}$.

More recently Shore⁽¹⁷⁾ has synthesised a unique polymeric compound containing an ytterbium-iron bond. The compound was synthesised as shown in Figure 2.12.

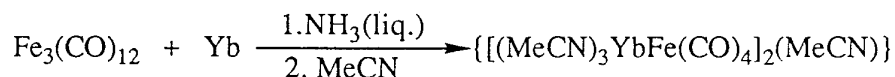


Fig.2.12 Synthesis of Yb-Fe polymer.

Shore has obtained an X-ray structure of the compound. A discrete Yb-Fe bond as well as isocarbonyl links exist. The complex has a ladder type structure (Fig.2.13)

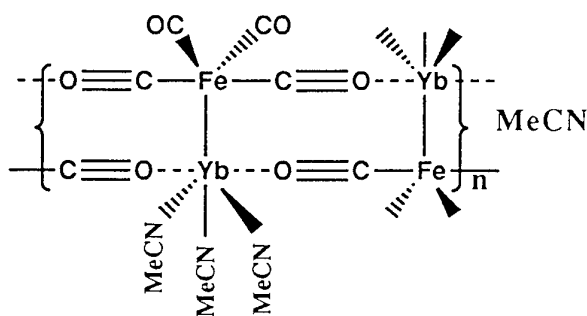


Fig. 2.13 'Ladder' polymer structure.

The reaction proceeds in two steps. The first generates the ammonia adduct $(NH_3)_xYbFe(CO)_4$, which on the addition of acetonitrile generates the title compound. The product decomposes on exposure to atmosphere. The decomposition material has been shown in this study to contain $Fe_3(CO)_{12}$.

It is possible to saturate some solvents with ammonia gas. Ether and acetonitrile can contain up to 15% NH_3 under the proper conditions. This was used in an effort to try and improve the yield and reduce the two steps necessary for the production of the yb-Fe polymer. Dried NH_3 was passed through an acetonitrile suspension of ytterbium and $\text{Fe}_3(\text{CO})_{12}$. The title product was generated but the yield (23%) was almost one third of that obtained using the original method.

2.7 Reaction of Eu with $\text{Fe}_3(\text{CO})_{12}$.

A similar reaction was attempted using europium instead of ytterbium. The reaction proceeded in the same manner as for ytterbium to give a red crystalline very air-sensitive product. Several attempts were made to mount the needle type crystals in a capillary but each time the compound decomposed. The metal analysis suggests an extra acetonitrile in the product compared to the ytterbium compound. The visible spectrum is almost identical to the Yb compound with λ_{max} at 538nm. The i.r spectra are identical. Without a crystal structure however it is impossible to speculate meaningfully on the presence of a europium-iron interaction. The synthesis was also attempted using the MeCN/ NH_3 technique tried for the ytterbium compound. Again this produced the same compound but the yield was reduced greatly from 36% to 7%.

2.8 EXPERIMENTAL CHAPTER 2

2.8A $YbCp_2^1$ using Hg activation:: Ytterbium powder (1.730g, 10mmol) was placed in a Schlenk tube with thf (50cm³) and mercuric chloride (100mg). After 2 hours stirring inside the dry-box a solution of 6,6-dimethylfulvene (1.06g, 10mmol) in thf (30cm³) was added dropwise to the activated ytterbium suspension. The solution was stirred (20 h) during which the colour changed from a pale green to a dark purple. This purple suspension was filtered through a grade 4 sintered filter and the solvent was removed to yield a sticky purple paste. This was washed with small amounts of cold Et₂O (4x10cm³) to finally yield the title compound in 37% yield (0.72g, 1.84mmol).

2.8B $YbCp_2^1$ using liq.NH₃ activation : Ammonia gas was dried by passing it through a series of NaOH filled tubes (Fig.2.14). The gas was then condensed in a Schlenk tube cooled to -70 °C in an EtOH/liq.N₂ bath.

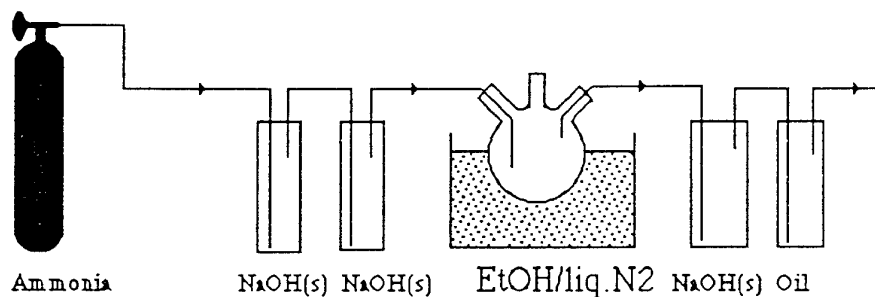


Fig. Apparatus for production of dry liq. Ammonia.

Using this procedure 40cm³ of liq.NH₃ was collected. Ytterbium powder (1.730g, 10mmol) was added to the Schlenk tube using a solid addition tube. The suspension was rapidly stirred whilst the colour turned dark blue. When all of the metal was dissolved in the ammonia the Schlenk was placed under vacuum and the ammonia was removed quickly to leave a metallic film of ytterbium on the sides of the Schlenk. The Schlenk was placed in the dry-box immediately and a solution of 6,6-dimethylfulvene (1.06g, 10mmol) in thf (80cm³) was added dropwise with stirring to the activated ytterbium. The reaction solution turned purple after a short time and was left stirring (20 h). The purple solution was filtered twice through a grade 4 sinter. The title product (1.21g, 63%) was obtained as a purple powder.

YbCp_2^1

M.p = 144 °C (142).

I.r (thf soln.) 3074w, 2988s, 2873m, 1533m cm^{-1}

^1H nmr (d_8 -thf, 80MHz) δ 4.9-6.0 (m, 8H, C_5H_4), δ 1.2 (s,br,12H,Me) ppm.

Metal analysis EDTA Yb^{3+} =42% NIR Yb^{3+} =44%(45%)

2.8C Reaction of YbCp^2_1 with $\text{Co}_2(\text{CO})_8$: $\text{Co}_2(\text{CO})_8$ (0.17 g, 0.5mmol) was dissolved in toluene (50cm^3) to give a red solution. YbCp_2^1 (0.38g, 1mmol) was dissolved in toluene (50cm^3) and added dropwise to a stirring solution of the cobalt carbonyl. The reaction suspension darkened immediately and after 1 hour a precipitate was separated from the reaction solution by filtration. This material ignited in air upon removal of solvent presumably due to the presence of finely divided ytterbium. The precipitate was therefore redissolved in an excess of thf and filtered twice through celite and a grade 4 sinter. This gave the product as a red powder. It decomposed slowly under N_2 to a brown/green solid but was stored for long periods under argon.

I.r (thf soln.) 2099w, 1975s(br), 1785w(sh), 1745w, 1736w cm^{-1} .

(Nujol mull) 2005s, 1963s, 1936s, 1794s, 1756s cm^{-1} .

(CsI sandwich). 1938s, 1910m, 1871s, 1757m, 1738w, 1714m, 1703m 1687m cm^{-1} .

^1H nmr(d_8 -thf, 300MHz) δ 5.24(s(br), 8H, $\nu_{1/2}$ =15Hz, C_5H_4), δ 3.34(s(br), 12H, $\nu_{1/2}$ =30Hz, 4 CH_3)ppm.

The carbonyls could not be located in the ^{13}C nmr.

2.8D Reaction of YbCp^2_1 with $\text{Fe}_3(\text{CO})_{12}$: YbCp_2^1 (0.38g, 1mmol) was dissolved in thf(40cm^3) in a three-necked 150ml round-bottomed flask equipped with a micro-syringe adaptor for sampling of the reaction solution. $\text{Fe}_3(\text{CO})_{12}$ (0.100g, 0.2mmol) dissolved in thf (40cm^3) was added dropwise to the lanthanide solution. The reaction solution turned orange immediately. This orange solution was stirred (6 h) during which samples were withdrawn using the syringe for liquid i.r analysis. After this time the solvent was removed to yield a dark orange oil. Addition of small amounts of hexane to the oil in an attempt to induce crystallisation washed out the $\text{Fe}_3(\text{CO})_{12}$ and left the ytterbium starting material as a powder.

I.r. analyses $\text{Fe}_3(\text{CO})_{12}$ in Hexane 2049s, 2028w cm^{-1} ., reaction solution 2049-1846(23 peaks all strong), 1826s, 1779s, 1752s cm^{-1} , hexane wash(green) 2049s, 2025w cm^{-1}

2.8E Reaction of YbCp_2^1 with acetonitrile: YbCp_2^1 (0.50g, 1.4mmol) was dissolved in acetonitrile (75cm^3) to give a dark green solution. Removal of the solvent on the vacuum line after 1 hour stirring gave a dark green solid which was dried by gentle heating under vacuum to yield the product (0.59g). Small green crystals of poor quality were grown from a saturated solution of the product in MeCN at -27°C . See text for details of formulation.

I.r (CsI sandwich) 3076w, 2985s, 2973s, 2938s, 2300m, 2269m, 2195m, 2145s, 2103w, 2098m, 2041m, 1688-1590s, 901s, 394w cm^{-1} .

^1H nmr (80MHz, CD_3CN) δ 6.10(m,br,8H), 2.00(q, CH_3CN), 1.6-1.0(m, br, 17H)ppm.

Metal Analysis EDTA Yb^{3+} 43%(40.6) NIR Yb^{3+} 42%

The dark green product is sensitive to air and moisture turning yellow even when stored under N_2 . It was stored under Ar inside the dry-box. The yellow decomposition product was shown to contain no co-ordinated MeCN and to contain bound -OH from the i.r.

2.8F Reaction of Yb with 6,6-dimethylfulvene in MeCN: Ytterbium metal (0.346g, 2mmol) was activated using liq. NH_3 as described previously in 2.1. A solution of dmfu (0.206g, 2mmol) in MeCN (100cm^3) was added dropwise to the activated ytterbium with fast stirring. As the metal was consumed the solution turned blue/green and a white precipitate formed. After 2 hours stirring the suspension was filtered through a grade 4 sinter to yield a very unstable blue/green solution. The solvent was removed on the vacuum line to yield a green solid (0.100g) that analysed the same as the product in 2.1C.(yield 24%).

2.8G $\{[(\text{MeCN})_3\text{YbFe}(\text{CO})_4]_2(\text{MeCN})\}$ via liq. NH_3 : The title product was synthesised in a method similar to that described by Shore *et al.*⁽¹⁷⁾ Ytterbium(0.519g, 3mmol) was dissolved in liq. NH_3 (50cm^3) at -60°C . $\text{Fe}_3(\text{CO})_{12}$ (0.504g, 1mmol) was added to the solution using a solid addition tube. The mixture immediately turned a tan/red colour. After stirring (30m) the liquid ammonia was removed to give a quantitative yield of the ammonia adduct $(\text{NH}_3)_x\text{YbFe}(\text{CO})_4$ as a tan/yellow solid. MeCN(40cm^3) was then added to the ammonia adduct using a cannula. The product dissolved in the acetonitrile to give a burgundy coloured solution after 30 minutes stirring as the temperature was slowly raised to 20°C . A brown solid material was noticed in the reaction solution and this was removed by filtering through a grade 4 sinter to give a clear red solution of the title compound. Removal of the solvent

yielded the product as a red solid (0.637g, 1.89mmol, 62%). The brown decomposition material was shown to contain $\text{Fe}_3(\text{CO})_{12}$.

M.p=165-168 °C(168 °C)

UV/VIS λ_{max} 540nm(br 477-672nm)

I.r (Nujol) $\nu(\text{CO})$ 1890w, 1781m, 1720s cm^{-1}

(KBr sandwich)2963m, 2927s, 2854m, 2078-1832s(br), 1736s, 1712s, 695s, 581s cm^{-1} .

Metal analysis n.i.r: Yb(III) 34% (34).

2.8H Synthesis of Yb-Fe polymer via MeCN/NH₃: ytterbium metal powder (0.520g, 3mmol) and $\text{Fe}_3(\text{CO})_{12}$ (0.504g, 1mmol) were added to MeCN (100 cm^3) in a Schlenk tube. Dried NH₃ was bubbled through the stirring suspension using a gas inlet fitted with a small sinter to disperse the ammonia. The ytterbium metal slowly dissolved on stirring to give first a bronze coloured reagent and then a blue colour before reacting with the iron carbonyl to give a red solution (3 h). The reaction was filtered to give a clear red solution of the product. Work-up of the solution gave the title compound in a yield of 23%. Analysis of the product was consistent with $\{[(\text{MeCN})_3\text{YbFe}(\text{CO})_4]\text{MeCN}\}$.

2.8I Reaction of Eu metal with $\text{Fe}_3(\text{CO})_{12}$ via liq.NH₃: europium metal (0.456g, 3mmol) was dissolved in liq.NH₃ (60 cm^3) at -65 °C to give the typical blue solution. $\text{Fe}_3(\text{CO})_3$ (0.504g, 1mmol) was added to the solution using a solid addition tube attached to the Schlenk.

The reaction mixture immediately turned brown/red and after stirring (45min.) the liq.NH₃ was removed under vacuum to give a tan/yellow solid. MeCN(70 cm^3) was added to the powder with stirring and the solution was warmed to 20 °C. The red solution was filtered (a brown residue was collected on the sinter) and the solvent removed to give 0.522g of product.(Yield=36%). Crystals of the product were grown in a Schlenk tube from MeCN at -27 °C. Several attempts were made to mount the needle type crystals in a capillary but the crystal decomposed inside the sealed capillary.

UV/VIS λ_{max} 538nm(broad 460-672nm).

I.r (CsI sandwich) 2988m, 2873m, 2088s-1822s, 1740s, 1712m, 1699s, 1639m, 617s, 581s cm^{-1} .

Metal analysis UV/VIS Eu³⁺ 28.5%(31.3).

2.8J Reaction of Europium and $Fe_3(CO)_{12}$ via MeCN/ NH_3 : The same procedure for this reaction was used as in the ytterbium analog. Europium metal powder (1.455g, 3mmol) and $Fe_3(CO)_{12}$ (0.504g, 1mmol) were added to a Schlenk containing MeCN (100cm³) and dried NH_3 was bubbled through. A bronzing effect was noticed on the surface of the europium before the typical blue colour appeared. A brown precipitate formed and the reaction was filtered through a grade 4 sinter to give a red solution of the Eu-Fe compound. Work-up of the solution yielded the product (107mg, 6.89%). Analysis as for 2.2C.

2.8K Reaction of Ytterbium with $Co_2(CO)_8$: ytterbium metal powder (0.348g, 2mmol) was dissolved in liq. NH_3 (40cm³) at -55 °C. The temperature was maintained using an EtOH/liq. N_2 bath. $Co_2(CO)_8$ (0.349, 1mmol) was added to the ytterbium solution using a solid addition tube. After stirring (40 min.) the reaction turned orange/brown. The ammonia was removed on the vacuum line to leave a brown solid. MeCN(30cm³) was added dropwise to the brown solid at 20 °C. The resulting brown suspension was stirred (12h). The resulting red solution was filtered leaving a brown/grey powder. The red solution was pumped to dryness on the vacuum line to give a red/orange material. Hexane(20cm³) was added to the material and this washed out unreacted $Co_2(CO)_8$ leaving a very air-sensitive red solid (0.358g). The brown/grey decomposition material exploded on contact with air.

M.p = 107 °C

I.r 2988s, 2943, 2886m, 2267m, 2195s, 2020s, 1920s, 1807s cm⁻¹.

Metal analysis n.i.r: Yb(III) 24.5%

References.

- 1 A. Recknagel, F.T. Edelman, *Angew. Chem. Intl. Ed. Eng.*, 1991, **30**, No.6, 693.
- 2 E.O. Fisher, H. Fisher, *Angew. Chem.*, 1964, **76**, 52.
- 3.F. Calderazzo, R. Pappalardo, S. Losi, *J. Inorg. Nucl. Chem.*, 1966, **28**, 987.
- 4 T.D. Tilley, R.A. Andersen, B. Spencer, H. Rubin, A. Zalkin and D.H. Templeton, *Inorg. Chem.*, 1980, **19**, 2999.
- 5 (a)W.J. Evans, R.A. Keyer and J.W. Ziller, *J. Organomet. Chem.*, 1990, **394**, 87 (b) M.F. Lappert, P.I. Yarrow, J.L. Atwood, R. Shakir and J. Holton, *J. Chem. Soc., Chem. Comm.*, 1980, 810.
- 6 P. Girard, I.L. Namy, H.G. Kagan, *J. Am. Chem. Soc.*, 1980, **102**, 2693.
- 7 G.B. Deacon, A.I. Koplík, T.D. Tuong, *Polyhedron*, 1983, **1**, 423.
- 8 W.J. Evans, A.L. Wayda, W.E. Hunter, J.L. Atwood, *J. Chem. Soc., Chem. Comm.*, 1981, 205.
- 9 R. Kopuec, F. Macasek, V. Mikulaj and P. Drinnovsky, *Radiochim. Rad. Lett.*, 1969, **1**, 177.
- 10 M. Strohmeier, V.W.H. Landsfeld, F. Gernert, W. Langhauser, *Z. Anorg. Chem.*, 1960, **307**, 120.
- 11 W.J. Evans, L.A. Hughes, T.P. Hanusa, *J. Am. Chem. Soc.*, 1984, **106**, 4270.
- 12 W.J. Evans, I. Bloom, W.E. Hunter, J.L. Atwood, *J. Am. Chem. Soc.*, 1981, **103**, 6507.
- 13 W.J. Evans *et al.*, *Polyhedron*, 1987, **6**, 5.

- 14 R. Andersen, D. Tilley, *J. Chem. Soc., Chem. Commun.*, 1981, 985.
- 15 J.M. Boncella, R.A. Andersen, *Inorg. Chem.*, 1984, **24**, 432.
- 16 D. Tilley, R. Andersen, *J. Am. Chem. Soc.*, 1982, **104**, 1772.
- 17 H. Deng, S. Shore, *J. Am. Chem. Soc.*, 1991, **113**, 8538.
- 18 W.J. Evans, *Inorg. Chem.*, 1985, **24**, 4620.
- 19 R.E. Dessy, *J. Am. Chem. Soc.*, 1966, **88**, 5112.
- 20 M.R.M Bruce, D.R. Tyler, *Organometallics*, 1985, **4**, 528.
- 21 S.D. Ittel, C.A. Tolman, A.D. English, J.P. Jesson, *J. Am. Chem. Soc.*, 1978, **100**, 7577.
- 22 J.H. Teuben, H.J. Heeres, A. Meetsua, *Angew. Chem. Intl. Ed.*, 1990, **29**, 420.
- 23 (a) J.E. Bercaw, M.E. Thompson, *Pure & Appl. Chem.*, 1984, **56**, 1 (b) P.L. Watson, *J. Am. Chem. Soc.*, 1983, **105**, 6491.
- 24 A.E. Crease and P. Legzdins, *J. Chem. Soc. Chem. Comm.*, 1973, 775.
- 25 A.E. Crease and P. Legzdins, *J. Chem. Soc., Dalton Trans.*, 1973, 1501.
- 26 G.Z. Suleimanov, R.Y. Mechdiev, T.Kh. Kurbanov, V.G. Trunov, I.P. Beletskaja, *I International Rare Earth Conference, Zurich*, 1985, J6.

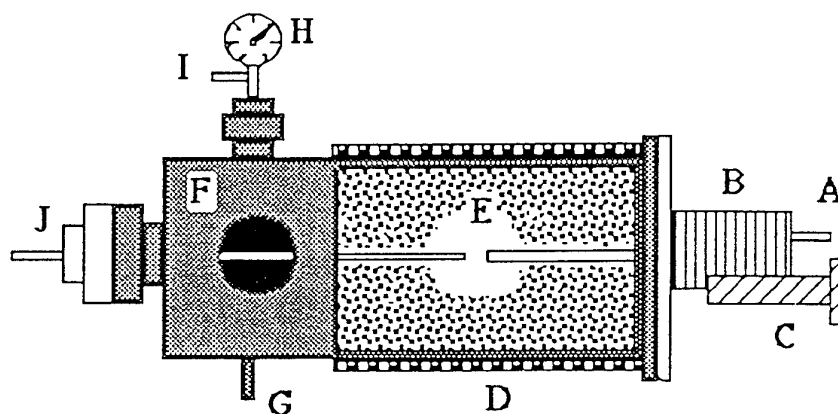
CHAPTER 3.

Synthesis and Purification of Fullerenes and the Organometallic chemistry of C₆₀.

3.1 Production of C₆₀ and C₇₀.

Two different fullerene generators were used in this study to produce fullerenes. Both were based on the Krätschmer-Huffman method of vapourising graphite in a helium atmosphere using the arc/plasma generated by passing a high current through the electrodes. The optimum yield from the stainless steel reactor (Fig.3.1) was approximately 4%(weight of total fullerene/weight of soot). This relatively low yield can be attributed to the poor cooling in the reactor, the inability to view directly the arc gap and the static pressure in the reactor. However the machine was capable of using graphite electrodes of any diameter between 2mm and 10mm. The time taken to consume a 200mm long rod depended on the diameter. An 8mm wide rod took almost 100 minutes to consume whereas a 5mm wide rod took 30-40 minutes. The optimal burning rate was assumed to be occurring when the plasma was at its brightest. The pressure of helium in the reactor was a crucial factor. The optimum pressure according to Krätschmer⁽¹⁾ and others⁽²⁾ was approximately 150 Torr. We discovered a new pressure window at 450 Torr for the production of fullerenes. This led to increased yields of material(6.5%). The ratio C₆₀/C₇₀ changes with pressure. At 150 Torr it is approximately 3:1 but as the pressure increases to 450 Torr the ratio becomes almost 1.5:1. The current we used was set at a maximum of 130A with a voltage of 20V. The welding supply unit used with the steel generator did not allow these values to be changed. Despite all of the limitations of the steel generator it still produced approximately 500mg of C₆₀ and C₇₀ per day. The water flow through the cooling jacket was 6.5L/min. The carbon vapour inside the generator was condensed on the collection can which could be removed after burning and the soot generated was removed by scraping the inside of the can.

Fullerene generator

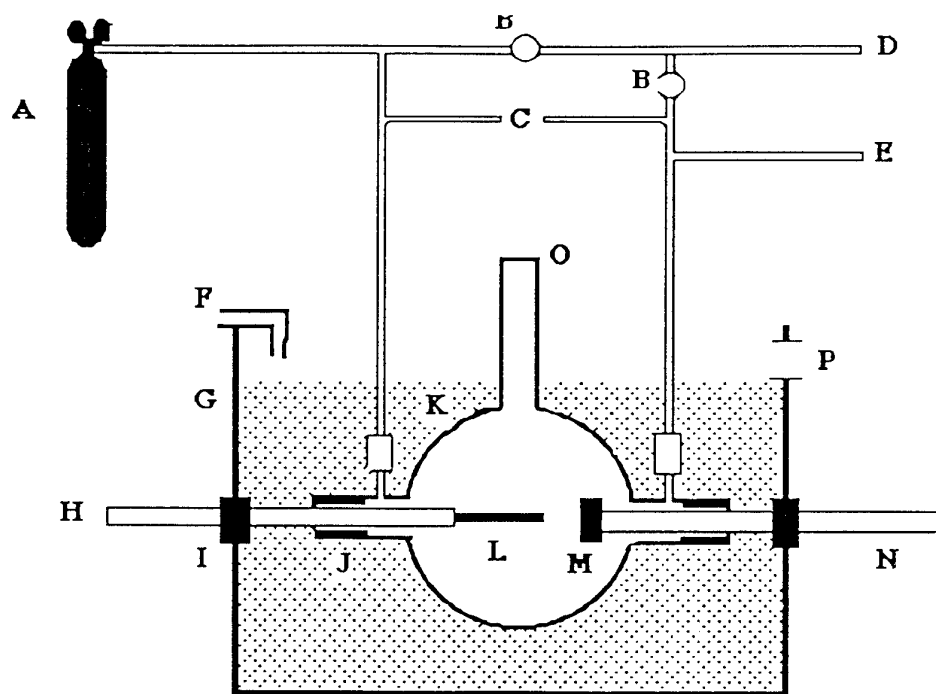


- A : Negative electrode
- B : Steel bellows
- C : Screw mechanism for bellows
- D : Water cooling jacket
- E : Cut-away view of inside showing the collection can
- F : Stainless steel generator
- G : Helium inlet
- H : Pressure gauge
- I : To vacuum
- J : Steel rod holding positive electrode

Fig. 11 Stainless steel fullerene generator.

The operation of the machine could be hazardous due to the high electrical current, the high temperature of the plasma (3000 K), circulating water and the soot itself which is very probably carcinogenic. Face masks and rubber-soled footwear along with heat-resistant gloves were used at all times.

The low yields obtained from the Krätschmer type generator prompted a design which would enable the control of the four main parameters which control the yield. An all-glass generator submerged in a tank of water was built along the same type of design proposed by Tour *et al.*(Fig.3.2).⁽³⁾ The yields from this machine were a significant improvement on the steel generator. Using 8mm graphite (99.99%) rods an average yield of 450mg of fullerene mix was obtained (18%). This contains approximately 57% C₆₀, 40% C₇₀ and 3% higher fullerenes. The time taken to consume a rod did not change significantly.

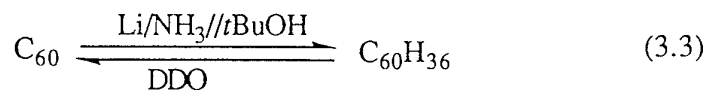


- A : Helium supply
- B : Flow control valve
- C : Silicon oil manometer
- D : Vac. pump
- E : Mercury manometer
- F : Water in
- G : Plastic storage vessel
- H : Positive copper electrode(to welder)
- I : Copper flange seal
- J : Copper mount for graphite electrode attached to B24 male
- K : 1L pyrex flask
- L : Positive graphite electrode
- M : Negative graphite block electrode
- N : Negative copper electrode (to welder)
- O : Viewing port
- P : Water out.

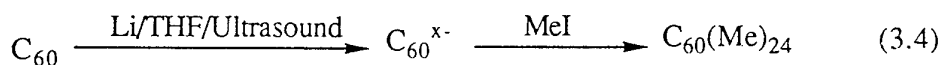
The original yield of 1% extractable material has been increased substantially:(a) 8% Taylor *et al.*⁽⁴⁾, (b) 10% Haufler *et al.*⁽⁵⁾, (c) 14% Ajie *et al.*, (d) 25-35% Diederich *et al.*, (e) 44% Parker *et al.*⁽⁶⁾ The methods of Diederich and Parker involve the use of up to five different solvents in the extraction stage and as a result they are time consuming and costly. Our method is the most cost effective to date. A new synthetic procedure conducted at significantly lower temperatures by the evaporation of carbon in a high frequency furnace has been described by Peters and Jansen.⁽⁷⁾

3.2 Chemistry of C₆₀.

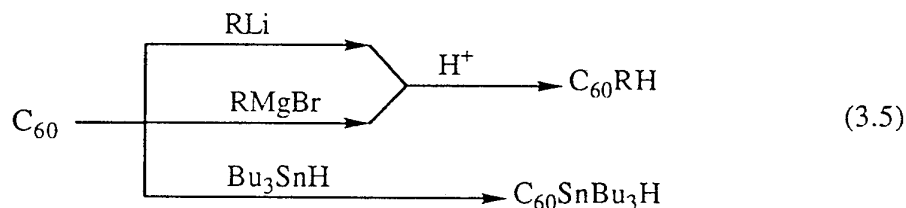
The isolation of macroscopic amounts of C₆₀ enabled its structure and chemistry to be investigated. One of the first derivatizations of C₆₀ was achieved with the Birch reduction⁽⁵⁾, which produced colourless C₆₀H₃₆. Because oxidation of this hydrogenation product with dichlorodicyanoquinone(DDQ) regenerates C₆₀, the reduction is assumed to proceed without structural changes in the C₆₀ cluster (Fig.3.3).



The reduction of C₆₀ with Li/thf/ultrasound provides diamagnetic polyanions whose ¹³C nmr signals are shifted 14ppm downfield which is unusual for carbanions.⁽⁸⁾ Methylation of the C₆₀ polyanions with an excess of MeI gave polymethylated C₆₀ containing up to 24 methyl groups (Fig.3.4), and higher degrees of methylation have been reported.⁰

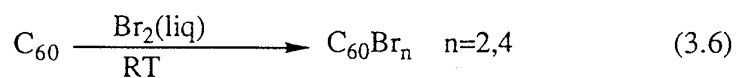


Hirsch *et al.*⁽⁹⁾ have shown how controlled two-step nucleophilic hydroalkylations, hydroarylations as well as hydrostannylations of C₆₀ lead to defined organofullerenes C₆₀HR (Fig.3.5). In all cases the addition takes place at a double bond between two six-membered rings of the fullerene.



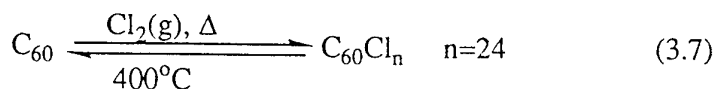
R = methyl, t-butyl, ethyl, i-propyl, octyl, phenyl.

The chlorination and bromination of fullerenes combined with the nucleophilic methoxylation and an AlCl₃-mediated Friedel-Crafts reaction of the polychlorofullerenes were described by Olah.⁽¹⁰⁾ The reaction of C₆₀ with Br₂ at intermediate temperatures gives C₆₀Br₂ and C₆₀Br₄, which both lose the halogen quantitatively at 150 °C (Fig.3.6).

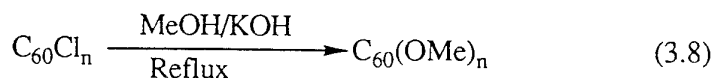


Chlorination affords fullerenes containing an average of 24 chlorine atoms. Complete

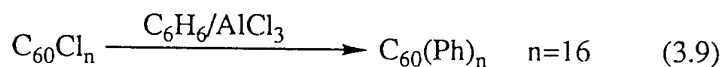
dehalogenation of these products could be achieved at temperatures greater than 400 °C (Fig.3.7).



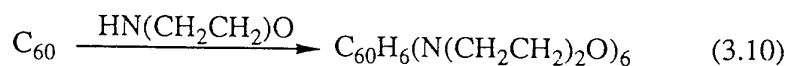
In the reaction of polychlorofullerenes C_{60}Cl_n with $\text{MeOH/KOH}(\text{xs})$ at reflux, all of the chlorine atoms were replaced by methoxy groups. According to the FAB mass spectrum, the product mixture contains compounds with up to 26 MeO groups(Fig.3.8).



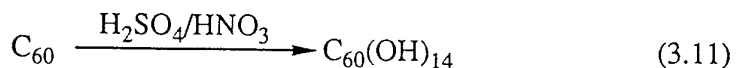
Because ethoxy groups do not add to C_{60} under the same conditions⁽¹¹⁾, it appears that this Cl--OMe exchange occurs by a front-side substitution on the surface of the cluster. Polychlorofullerenes also undergo Friedel-Crafts reactions. Thus C_{60}Cl_n reacts with benzene or toluene in the presence of trace amounts of AlCl_3 providing polyarylfullerenes. In the presence of AlCl_3 , C_{60} reacts with benzene to give $\text{C}_{60}(\text{HC}_6\text{H}_5)_{12}$ ⁽¹²⁾ as the major product(Fig.3.9) and with toluene to give the para-substituted $\text{C}_{60}(\text{HC}_6\text{H}_4\text{CH}_3)_{12}$ -fullerene.



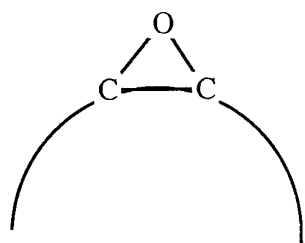
The addition of some nucleophiles to C_{60} provides water-soluble fullerenes. For example morpholine (Fig.3.10) leads to the product $\text{C}_{60}\text{H}_6(\text{N}(\text{CH}_2\text{CH}_2)_2\text{O})_6$.⁽¹³⁾ Proton nmr of the product suggested that there was rapid H-migration, but this has been queried.



Chiang⁽¹⁴⁾ has described an efficient aqueous acid chemistry for the preparation of fullerols, consisting of 14-15 hydroxy moieties on C_{60} (Fig.3.11).

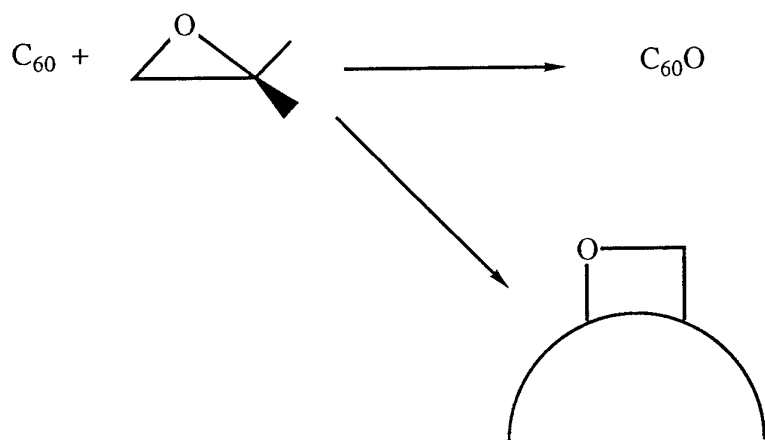


Kroll *et al.*⁽¹⁵⁾ observed photon-induced oxidation of C_{60} . A more recent paper by Taliani *et al.*⁽¹⁶⁾ describes the light induced opening of the fullerene cage due to the reaction with excited molecular oxygen ($^1\text{O}_2$) generated via C_{60} triplet energy transfer with $^3\text{O}_2$. The reaction produces the epoxide structure over a 6:6 ring fusion(Fig.3.12). Elmes *et al.*⁽¹⁷⁾ reacted C_{60} with dimethyldioxirane to get two products; one was C_{60}O and the other a 1,3-dioxolane derivative of C_{60} (Fig.3.13). Hawkins⁽¹⁸⁾ produced the first crystal structure of a C_{60} derivative which showed

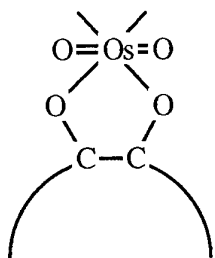


C₆₀ "epoxide"

3.12



3.13



C₆₀ osmolate

3.14

clearly the spherical nature of C_{60} . The reaction produced the first metal containing derivative (Fig. 3.14). The osmate ester was shown by X-ray crystallography to add across a 6:6 fusion. It is not yet clear why multiple addition of this adduct to C_{60} has not been observed. X-ray structures of a benzene solvated C_{60} and a co-crystallised ferrocene/ C_{60} compound provided unique molecular pictures of the unreacted C_{60} molecule (Fig. 3.15).

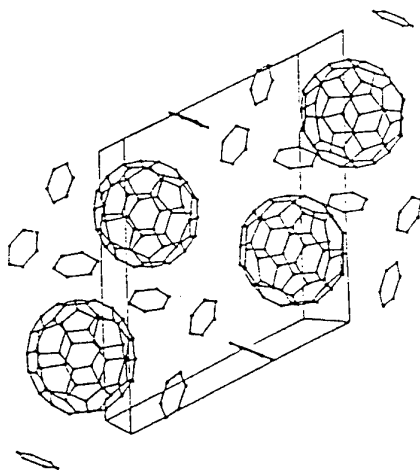
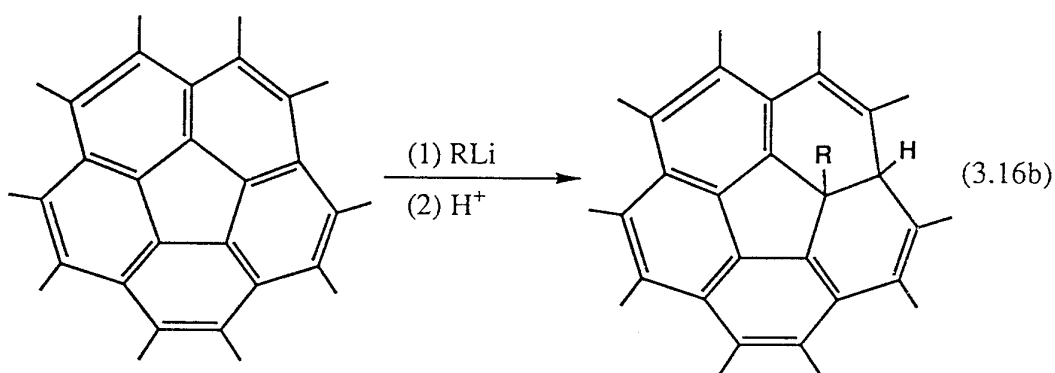
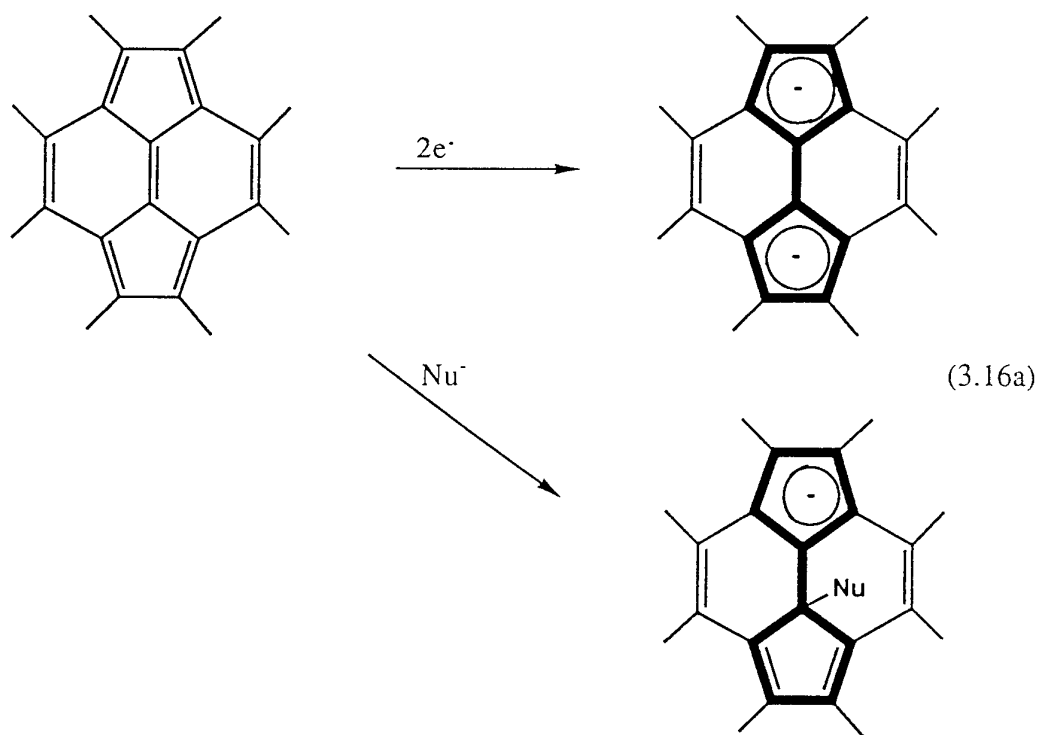
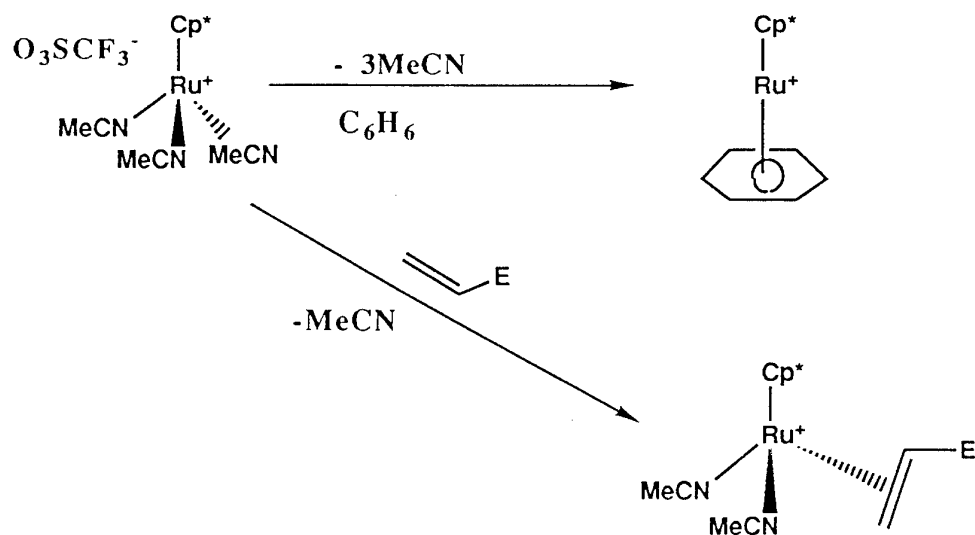


Fig. 3.15

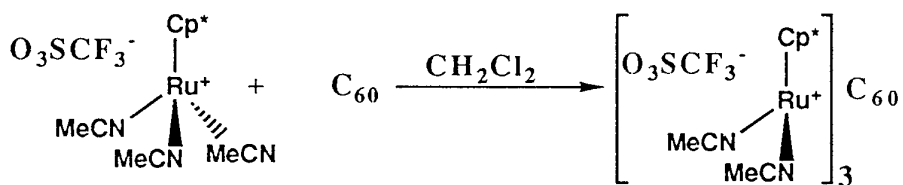
These studies completed the structural characterisation of the molecule. The three dimensional cage structure comprises 12 pentagons and 20 hexagons. There are 60 π -orbitals, 30 bonding and 30 antibonding. There are 30 C-C double bonds and 60 C-C single bonds which leads to a possible 12,500 Kekule structures, of which only one is a good approximation to the true structure. C_{60} is the lowest fullerene to have isolated pentagons in its structure. It is now generally accepted that the double bonds in C_{60} are all inter-pentagonal i.e. there are no double bonds in the pentagons.⁽¹⁹⁾ Taylor considers the structure of C_{60} to contain six pyracyclene units (Fig. 3.16a) and the addition of a nucleophile to this unit converts one of the pentagonal rings into a 6π aromatic system. Likewise the addition of two electrons will give two aromatic pentagonal rings.⁽²⁰⁾ This then accounts for the observed formation of polyanions⁽²¹⁾ up to 6^- . Hirsch considers the structure to consist of fused [5]-radialene and cyclohexatriene units like corannulene (Fig 3.16b). This structure is used to explain the fact that all additions occur over 6:6 fusion, these represent various possible views of the overall fullerene structure.



The first indication that C_{60} was not chemically similar to an electron rich arene or alkene but more like an electron deficient alkene(or arene) was provided by Fagan⁰ by the reaction of C_{60} with $\{\eta^5\text{-Cp}^*\text{Ru}(\text{MeCN})_3^+(\text{CF}_3\text{SO}_3^-)_3\}$. When this reagent reacts with relatively electron-rich planar arenes, the three coordinated acetonitrile ligands are displaced, resulting in strong η^6 -bonding of ruthenium to the six-membered rings of the arene. In the presence of electron-poor alkenes, one of the acetonitrile ligands is displaced, and an olefin complex is formed(Fig.3.17).

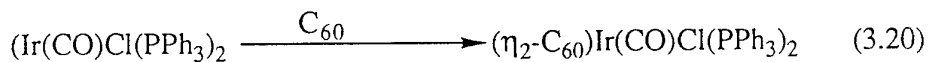
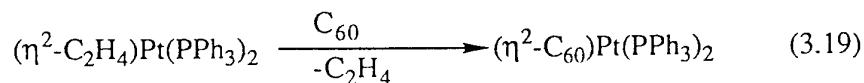


C₆₀ reacted with the Ru compound in the manner of an electron deficient alkene(Fig.3.18).

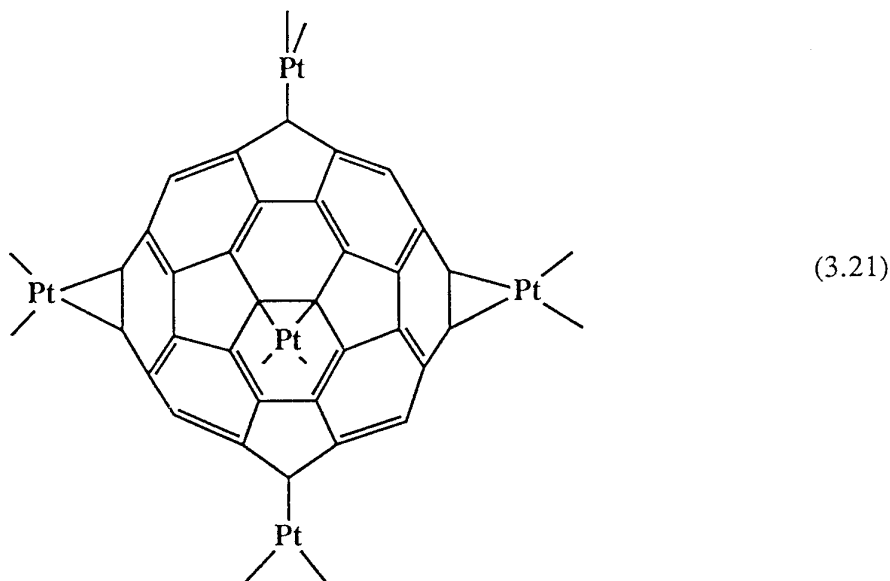


The result is not that surprising since C₆₀ was determined to have a high electron affinity in the gas phase⁽²⁴⁾ and was easily reduced electrochemically in solution.⁽²⁵⁾

This finding was followed quickly by four publications. Fagan *et al.*⁽²⁶⁾ treated the zero valent (η^2 -C₂H₄)Pt(PPh₃)₂ with C₆₀ to give an organometallic compound with the metal atom bound in an η^2 -fashion to the fullerene (Fig.3.19). Fagan obtained a crystal structure of the compound which shows the two carbon atoms bound to the metal drawn slightly out of the frame of the parent fullerene. The metal is bound over a 6:6 ring fusion. Balch *et al.*⁽²⁷⁾ studied the reaction of C₆₀ with Ir(CO)Cl(PPh₃)₂. The Ir complex added to the fullerene over a 6:6 junction in an η^2 fashion also(Fig.3.20). Koefod *et al.*⁽²⁸⁾ synthesised (η^5 -C₉H₇)Ir(CO)(η^2 -C₆₀) (Fig.3.20) in a similar manner. Fagan *et al.*⁽²⁹⁾ then synthesised the novel (η^2 -C₆₀){Pt(PEt₃)₂}₆ and obtained a crystal structure of the compound (Fig.3.21). Six η^2 -bound platinum atoms were found in an octahedral array on the C₆₀ sphere. These findings prompted a study of organometallic C₆₀ derivatives described in this chapter. The compounds synthesised in this chapter were then subject to a nonlinear optics study described in Chapter 5.



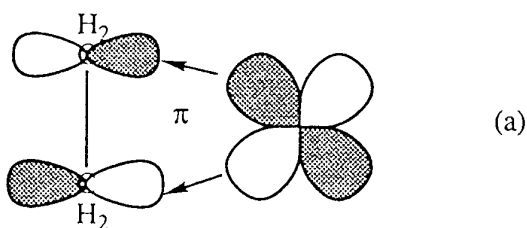
Octahedral array of Pt on C₆₀. One Pt is hidden at the rear of the C₆₀.



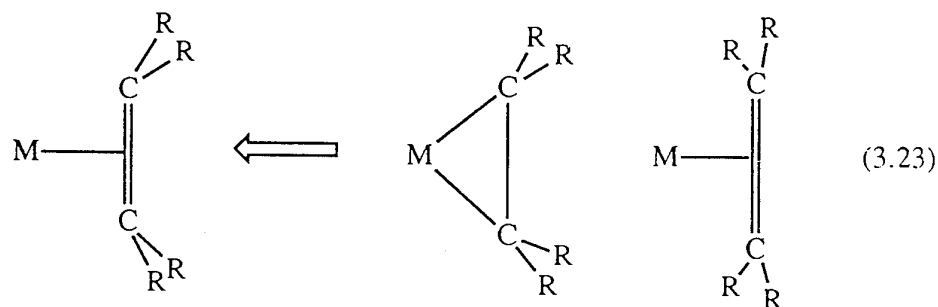
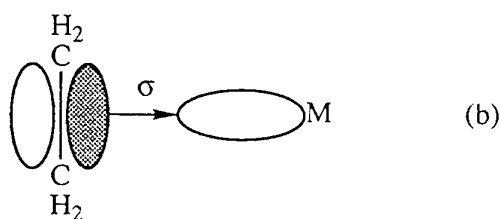
3.3 Metal alkene bonding.

The bonding in alkene complexes was first suggested to involve electron donation from the π bond of the alkene into a vacant metal orbital of σ symmetry. This idea was later modified by Chatt and Duncanson to form the basis of the Dewar-Chatt-Duncanson theory.⁽³⁰⁾ The bonding is considered to arise from two interdependent components as shown in Fig.3.22. In the first part (a), σ overlap between the filled π -orbital of ethene and a suitably directed vacant hybrid metal orbital forms the electron-pair donor bond. This is reinforced by the second component (b) which arises from overlap of a filled metal d-orbital with the vacant antibonding orbital of ethene; these orbitals have π symmetry with respect to the bonding axis and allow M-C₂ π back bonding to strengthen the σ C₂-M bond synergically as for CO. The interplay of these two components allows a wide variety of experimental observations to be rationalised: in particular the theory convincingly interprets the orientation of the alkene with respect to the metal and the observed lengthening of the C-C bond. However, the details of the

distortion of the alkene from planarity are less easy to quantify on the model and evidence is accumulated which suggests that the extent of π backbonding may have been over-emphasised for some systems in the past. At the other extreme back donation may become so dominant that the C-C distances approach values to be expected for a single bond and the interaction would be described as oxidative addition to give a metallocyclopropane ring involving two 2-electron 2-centre M-C bonds (Fig.3.23).

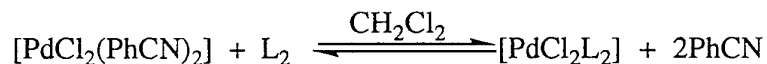


(3.22)



For example, tetracyanoethylene has a formal C=C double bond (1.339 Å) in the free ligand but in the complex $[\text{Pt}\{\text{C}_2(\text{CN})_4\}(\text{PPh}_3)_2]$ the C-C distance (1.52 Å) is that of a single bond and the CN groups are bent away from the Pt and 2P atoms; moreover, the 2P and 2C that are bonded to Pt are nearly coplanar as expected for Pt(II) but not as in tetrahedral 4-coordinate Pt⁰ complexes. The tendency to form a metallocyclopropane-type complex is seen also in the complex $[\text{Rh}(\text{C}_2\text{F}_4)\text{Cl}(\text{PPh}_3)_2]$ where the C-C distance is 1.41 Å with pseudo-5-coordinate Rh(III) rather than a pseudo-4-coordinate η^2 -alkene complex of Rh(I). The two descriptions are not mutually exclusive and in principle there can be a continuous gradation between them. A variety of spectroscopic techniques has been applied to the problem of metal-olefin bonding. The binding

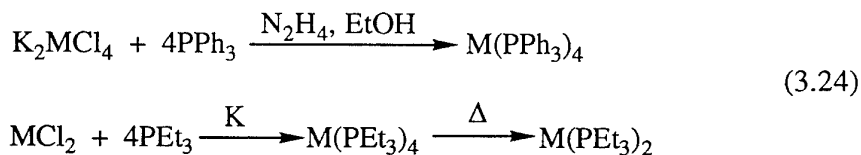
energies of the Pt $4f_{5/2}$ and the $4f_{7/2}$ electrons in complexes of the general formulae $[\text{Pt}(\text{olefin})(\text{PPh}_3)_2]$, olefin = C_2H_4 , C_2H_4 , C_2F_4 or *tcne*, as measured by ESCA are independent of the olefin, suggesting that the Lewis basicity of the $\text{Pt}(\text{PPh}_3)_2$ moiety completely outweighs any effect arising from the substituents on the olefin in determining the extent of the back-donation.⁽³¹⁾ The same may be true for $\text{RhCl}(\text{PPh}_3)_3$ group but not for the $\text{IrCl}(\text{CO})(\text{PPh}_3)_2$ moiety. The application of ^{13}C nmr spectroscopy to metal-olefin and acetylene complexes has provided a more sensitive probe of the bonding situation. Thus the marked shielding of the olefinic carbon atoms on coordination in the order $[\text{Pt}(\text{C}_2\text{H}_4)(\text{PPh}_3)_2] > [\text{PtCl}_3(\text{C}_2\text{H}_4)]^- > \textit{trans} [\text{PtMe}(\text{C}_2\text{H}_4)(\text{PMe}_2\text{Ph})_2]^+ > [\text{PtMe}_2(1,5\text{-COD})] > [\text{Pt}(\text{CF}_3)_2(1,5\text{-COD})]$ has been correlated with metal-olefin $d\text{-}\pi^*$ backbonding, and the values of $^1J(^{195}\text{Pt}, ^{13}\text{C})$ have been interpreted to show that there is no sharp boundary between the two descriptions of metal-olefin bonding as shown in Fig.3.23. The upfield shift in $[\text{Ag}(\text{C}_2\text{H}_4)_n]\text{BF}_4$ has been interpreted in terms of small changes of excitation energy due to increasing p-orbital energy on coordination; an alkyl substituent on the olefinic carbon atom induces a marked paramagnetic (deshielding) effect as a result of electronic interactions with the olefinic system⁽³²⁾. ^{13}C nmr experiments suggest that back-donation is unimportant in $[\text{Ag}(\text{propene})_2]\text{BF}_4$ but is significant in the complexes $\text{Rh}(\text{acac})(\text{propene})_2$ and $[\text{Fe}(\text{Cp})(\text{CO})_2\text{propene}]^+$.⁽³³⁾ The correlation between ^{13}C shieldings and backbonding in platinum complexes has been disputed, and the upfield shifts have been ascribed principally to a non-bonding, paramagnetic effect arising from partly filled metal d-orbitals; this presumably does not operate for metal ions with a d^{10} configuration such as Pt^0 and Ag^1 . Silver mono-olefins are unique in that the olefinic proton resonances are deshielded on coordination, whereas the same protons in the analogous $\text{Cu}(\text{I})$ and $\text{Au}(\text{I})$ complexes are shielded; the shielding order is $\text{Cu}(\text{I}) > \text{Au}(\text{I}) > \text{Ag}(\text{I})$, and since this is also the order of the first ionization of the metals it is plausible to relate the effect with decreasing $d\pi\text{-}\pi^*$ bonding.⁽³⁴⁾ The value of the equilibrium constant for the reaction



falls in the order $\text{Ni} \gg \text{Pt} > \text{Pd}$: $\text{L} = (\text{p-MeC}_6\text{H}_4)_3\text{P} > \text{PPh}_3 > (\text{m-MeC}_6\text{H}_4)_3\text{P}$.⁽³⁵⁾ It is likely that these trends are primarily a reflection of changes in the metal-olefin bond strength and that these in turn are governed largely by $d\pi\text{-}\pi^*$ back-bonding (the ionization potentials in this triad are in the order $\text{Ni}^0 \gg \text{Pt}^0 > \text{Pd}^0$).

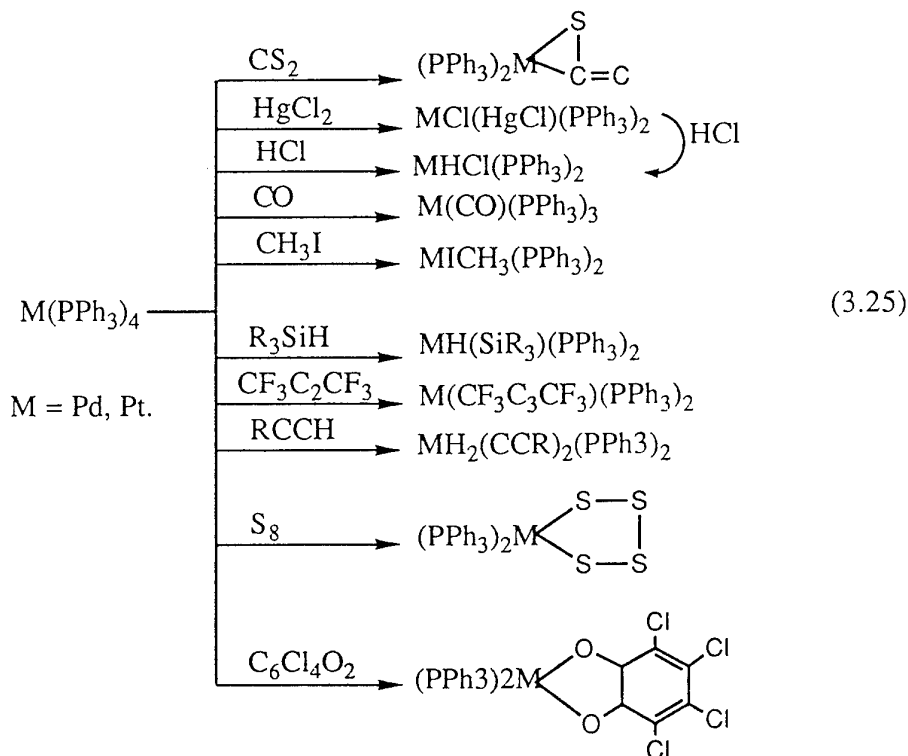
3.4 Palladium(0) and Platinum(0) chemistry.

Phosphine complexes of palladium and platinum in the zero-oxidation state have been studied extensively, especially the triphenylphosphine complexes. They undergo a wide variety of oxidative addition reactions and have found many applications in catalysis. Unlike Ni the heavier two members of the Group 10 metals do not form binary carbonyl compounds probably owing to a poorer tendency to π -bonding associated with the greater ionization enthalpies of Pd and Pt. In the presence of triphenylphosphine however, the carbonyl compounds $\text{Pd}(\text{CO})(\text{PPh}_3)_3$ and $\text{Pt}(\text{CO})_2(\text{PPh}_3)_2$ are relatively stable (triphenylphosphine is a better σ -donor but a poorer π -acceptor). The Pd^0 and Pt^0 compounds all contain tertiary phosphines. Some involve ligands that are extremely strong π -acids e.g. $\text{Pt}(\text{PF}_3)_4$ and $\text{Pt}[\text{P}(\text{CF}_3)_2\text{F}]_4$. These compounds are volatile liquids, stable at 25 °C; $\text{Pd}(\text{PF}_3)_4$ decomposes above -20 °C. The triaryl- and trialkyl-phosphine derivatives are usually made by the interaction of the dihalides, or $[\text{MX}_4]^{2-}$ complexes, with the phosphines in the presence of strong reducing agents(Fig.3.24).



010 All the compounds have broadly similar chemical properties centering around their tendency to lose PR_3 and to undergo oxidative addition reactions whereby $\text{Pd}(\text{II})$ and $\text{Pt}(\text{II})$ are formed. The $\text{Pt}(\text{PPh}_3)_4$ compound has been the most extensively studied.⁽³⁶⁾ The tendency of the $\text{Pt}(\text{PR}_3)_4$ molecules to lose PR_3 giving $\text{Pt}(\text{PR}_3)_3$ and $\text{Pt}(\text{PR}_3)_2$ appears to depend considerably on the size of the phosphine. For triaryl and alkyldiaryl phosphines the dissociation of $\text{Pt}(\text{PR}_3)_4$ to $\text{Pt}(\text{PR}_3)_2$ is extensive, whereas for the trialkyl and dialkylarylphosphines dissociation does not occur. With $\text{P}(\text{cyclohexyl})_3$ the $\text{Pt}(\text{PR}_3)_2$ compound can be isolated. Substantial dissociation of $\text{Pt}(\text{PPh}_3)_4$ to give $\text{Pt}(\text{PPh}_3)_2$ occurs in solution at 25 °C but the extent of dissociation of $\text{Pt}(\text{PPh}_3)_3$ or $\text{Pt}(\text{C}_2\text{H}_4)(\text{PPh}_3)_2$ to give $\text{Pt}(\text{PPh}_3)_2$ is too slight to allow detection of the latter by nmr.⁽³⁵⁾ However $\text{Pt}(\text{PPh}_3)_2$ has been shown kinetically to play a significant role in some reactions.⁽³⁷⁾ The oxidative addition reactions of $\text{M}(\text{PR}_3)_4$ molecules in which PR_3 ligands are lost are numerous. A few are illustrated in Fig.3.25. The description of the reactions in this figure as oxidative additions is not entirely correct since the degree of net charge transfer to the ligand is not always sufficient to warrant this classification. Clearly when HCl , RI , etc. are added with bond breaking the reaction

can be described as an oxidative addition. However for $\text{Pt}(\text{PR}_3)_2(\text{C}_2\text{H}_4)$, calculations suggest that it is essentially a π complex of Pt^0 .



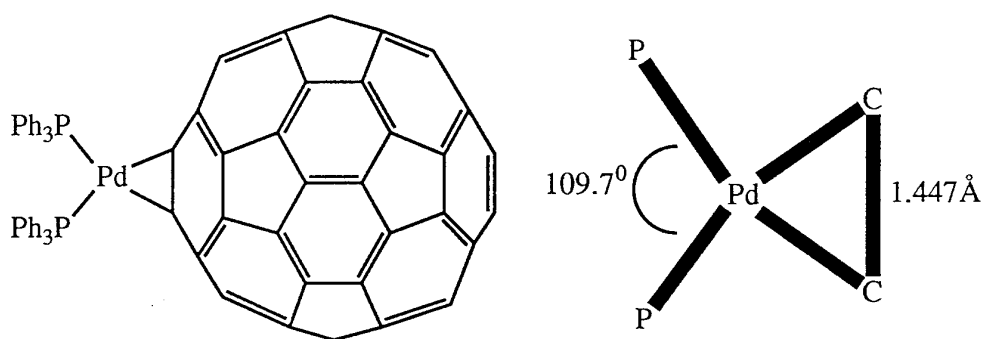
Compounds containing $\text{M}-\eta^2$ -alkene bonds are generally prepared by direct replacement of a less strongly bound ligand such as a halide ion (e.g., Zeise's salt), a carbonyl, or another alkene. Chelating dialkene complexes can be made similarly, e.g., with *cis-cis*-cycloocta-1,5-diene (COD). For many metals it has been found that increasing alkyl substitution of the alkene lowers the stability of the complex and that *trans*-substituted alkenes give less stable complexes than do *cis*-substituted alkenes. Alkenes are better σ -donors than CO and may stabilise higher positive oxidation states on the metal. Thus, many alkene complexes are known with metals in relatively high (II) oxidation states, whereas such complexes are unknown for CO (e.g. $[\text{Fe}(\text{CO})_6]^{2+}$ does not exist). Alkenes prefer the perpendicular bonding mode in square planar complexes due to steric factors (there is less steric interaction with other ligands when the alkene is perpendicular to the square plane). Rotation of the alkene about the midpoint of C=C is possible. The activation energy for this process is usually not high (30kJ/mol.) which suggests that the energy difference between the two configurations is small.

3.5 Reaction of Pd(PPh₃)₄ with C₆₀.

The addition of Pd(PPh₃)₄ to C₆₀ in toluene produced initially a deep green solution from which a black powder precipitated. The product was soluble in a range of solvents including, thf, CH₂Cl₂, CH₃Cl and CS₂. Analysis of the black powder showed it to be the palladium analogue of the platinum compound prepared by Fagan *et al.* Excluding possible solid-state effects, there are 174 vibrational modes for a C₆₀ atom molecule(3N-6), but under I_h symmetry only 4 vibrations are allowed in the i.r spectrum and 10 in the Raman spectrum. The four infrared active modes have T_{1u} symmetry (triply degenerate). The Raman active modes consists of two singly degenerate A_{1g} modes and eight 5-fold degenerate H_g modes. The i.r srectrum recorded as a CsI disc showed the expected signals for C₆₀ at 1430cm⁻¹, 1180cm⁻¹, 575cm⁻¹ and 525cm⁻¹. The region from 700cm⁻¹ to 400cm⁻¹ contains a number of signals in all of the C₆₀ derivatives, most noticeably at 743, 722, 695 and 544 wavenumbers, possibly due to a lowering in the symmetry of the C₆₀ molecule. The Raman spectrum was recorded using an exciting line at 514nm and exhibited a number of interesting features. The phosphine ligand modes at 1460cm⁻¹ and 1000cm⁻¹ are weak in comparison to the C₆₀ modes. The A_{1g} modes do not split but are found at lower frequencies than in the parent C₆₀ molecule. These and other features of the Raman spectra of metal derivatives of C₆₀ will be discussed at the end of this chapter. The visible spectrum was recorded in toluene and exhibited absorbances at 395nm, 435nm and a weaker absorbance from 510nm to 700nm with maxima at 615nm and 660nm. These absorbances are weak compared to the uv absorbance by two orders of magnitude. The absorbance at 435nm is attributed to a ligand-to-metal charge transfer. This feature is visible in most organic and inorganic derivatives of C₆₀. The ³¹P nmr contains a resonance at 25ppm which corresponds to PPh₃ coordinated to a metal. The resonance at -4.96ppm is indicative of free PPh₃. This could be an impurity from the reaction (PPh₃ is a by-product) or it could arise from the product itself due to an equilibrium between coordinated PPh₃ and free PPh₃. The ¹H nmr is equally featureless exhibiting a multiplet at 7.2ppm due to the aromatic protons on the PPh₃. The ¹³C nmr provides limited information due to the fact that the resonances of the aromatic carbons in PPh₃ occur in the same region as those for C₆₀. This is exacerbated by the fact that the best solvents for these compounds are benzene and toluene which even with the best deuterated samples still have residual resonances in the region. Despite this some information is still available. There are 17 different carbon environments in a molecule of C₆₀ with a metal coordinated over a 6:6 fusion. Thus we would expect to observe 17 resonances in the ¹³C nmr. A weak resonance at 882ppm corresponds to the two carbons attached to the palladium. The resonances at 8142ppm-8145ppm are fullerene derived. The phenyl moiety on the phosphine occurs

at $\delta 128\text{ppm}$ - $\delta 137\text{ppm}$ and a similar resonance to the one at $\delta 158\text{ppm}$ has been assigned by Fagan as the M-C-C feature in the molecule. On the basis of this analysis the compound was taken to be $(\eta^2\text{-C}_{60})\text{Pd}(\text{PPh}_3)_2$.

During the course of this work two papers were published which confirmed the findings of this experiment. Chase⁽³⁸⁾ published a paper on the Raman spectroscopy of a range of organometallic compounds prepared by Fagan *et al.* A Raman spectrum was shown for a compound taken to be $(\eta^2\text{-C}_{60})\text{Pd}(\text{PPh}_3)_2$. No other analysis of this compound was provided. Following this Bashilov *et al.*⁽³⁹⁾ produced a crystal structure of this compound. The nmr and electronic spectra they reported, agree with those presented here. The structure obtained (Fig.3.26) by Bashilov *et al.* is almost identical to that obtained by Fagan for the platinum analogue.⁽³⁹⁾



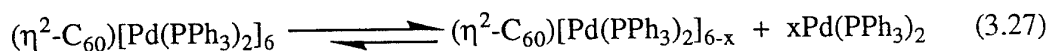
3.26 $(\eta^2\text{-C}_{60})\text{Pd}(\text{PPh}_3)_2$

They report that the elongation of the C1-C2 bond is expectedly less than in its platinum analogue (1.447 vs 1.502Å compared with 1.39Å for an unperturbed 6:6 fusion). This fact reflects less strong C₆₀-metal bonding for the palladium as compared with platinum.

3.6 Reaction of excess Pd(PPh₃)₂ with C₆₀.

A solution of Pd(PPh₃)₄ was added dropwise to a solution of C₆₀. On the addition of the sixth equivalent of metal the solution changed from dark green to dark red. A red microcrystalline powder was isolated from after workup of the reaction. This product was found to be soluble in a range of solvents. However in coordinating solvents like thf and CS₂ the compound changed colour from dark red to green over relatively short periods of time (hrs). The visible spectrum of this compound exhibited a strong absorption at 475nm with another weaker absorption extending from 570nm out to 850nm. The ¹H nmr spectrum was obtained and this showed a multiplet between $\delta 7.14\text{ppm}$ and $\delta 7.78\text{ppm}$ indicative of aromatic protons. The ¹³C nmr spectrum revealed three resonances apart from the arylphosphine and solvent at $\delta 153.99\text{ppm}$, $\delta 143.18\text{ppm}$ and $\delta 89.8\text{ppm}$. These are very similar to those reported for the

hexaplatinum- C_{60} compound found by Fagan *et al.*⁽²⁹⁾($\delta 79.2$ ppm Pt-C, 142.1ppm Pt-C-C-C, 152.8ppm Pt-C-C-C.). The ^{31}P nmr is the same as that seen for the mono-substituted palladium compound with one strong resonance at 25ppm indicative of triphenylphosphine bound to a metal. The i.r spectrum of the product was recorded as a CsI disc. Apart from the expected signals for the triphenylphosphine the spectrum contains peaks at 1430cm^{-1} and 1180cm^{-1} as for C_{60} . There are also the peaks between 750cm^{-1} and 500cm^{-1} which are common to all the metal derivatives of C_{60} . The Raman spectrum of the product was recorded at 514nm and this shows the slight downward shift in frequency for the A_{1g} modes along with enhancement of the H_g modes (this will be discussed in more detail at the end of this chapter). The Raman spectrum recorded by Chase and Fagan⁽³⁸⁾ for the compound which they claim is $(\text{Et}_3\text{P})_2\text{PdC}_{60}$ exhibits the main features found in this spectrum. This analysis of the product leads to the assumption that it is $(\eta^2\text{-C}_{60})[\text{Pd}(\text{PPh}_3)_2]_6$. It is similar to the novel structure obtained by Fagan *et al.* of $(\eta^2\text{-C}_{60})[\text{Pt}(\text{PEt}_3)_2]_6$ ⁽²⁹⁾ which shows the metals distributed around the C_{60} surface in an octahedral fashion(Fig 3.21). The compound dissociates quickly in most solvents to give green solutions which are assumed to be mixtures of C_{60} molecules with between 1 and 5 $\text{Pd}(\text{PPh}_3)_2$ moieties bound according to the equilibrium in Fig.3.27 which lies towards the RHS:



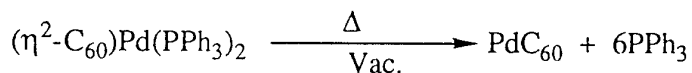
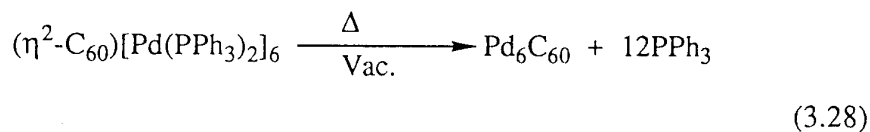
The electron affinity of C_{60} decreases each time a metal adduct is added to the molecule which makes it harder for the next metal to attach itself and at the same time increases the possibility that a metal fragment will detach. The maximum number of six metal phosphines is reached due to steric and electronic factors. From Fagan's crystal structure it is clear how each metal phosphine bonded over a 6:6 fusion sterically protects four of the neighbouring 6:6 fusions.

A mass spectrum of the product was obtained using Fast Atom Bombardment(FAB). The result showed an abundance of peaks up to 4650m/z. The expected parent ion is at 4500m/z. It proved impossible to unscramble the multitude of peaks to obtain any meaningful result. The most abundant (%) peaks are listed in the experimental. This problem was assumed due to the technique which involves dissolving the compound in a benzyl alcohol. Owing to the sensitive nature of the product the result was not that surprising. The technique performed better on other less sensitive compounds.

3.7 Synthesis of an 'Organometallic polymer' : $C_{60}\text{Pd}_x$.

During the work-up of the previous two compounds a new material was isolated. The first attempt to remove excess triphenylphosphine from the products involved a sublimation procedure. The impure product $(\eta^2\text{-C}_{60})\text{Pd}(\text{PPh}_3)_2$ was heated gently

under vacuum. The sublimate which formed was removed and weighed. The amount of sublimate corresponded to four equivalents of PPh₃ i.e. the excess PPh₃ and the metal-bound PPh₃. This left a residue containing C₆₀ and palladium. A similar procedure was attempted with (η²-C₆₀)[Pd(PPh₃)₂]₆ and this gave a product which can be formulated as Pd₆C₆₀(Fig.3.28).



Large amounts of this material were obtained (obviously this procedure failed to purify the materials, this was achieved by an ethanol wash). The i.r spectrum of the material demonstrates the absence of any PPh₃ and the presence of derivatised C₆₀. The Raman spectrum is almost identical to that for (η²-C₆₀)[Pd(PPh₃)₂]₆. A clue to the structure of these compounds was provided by Nagashima *et al.*⁽⁴⁰⁾ By the reaction of Pd₂(dba)₃.CHCl₃ (dba=dibenzylideneacetone) with C₆₀. This immediately gave an insoluble black material containing only palladium and C₆₀. The authors were able to alter the ratio Pd:C₆₀ by refluxing Pd₁C₆₀ in toluene to produce Pd₃C₆₀. This suggests that thermal recombination of C₆₀ and Palladium induced the conversion of kinetically produced Pd₁C₆₀ to a thermodynamically more stable Pd₃C₆₀. Nagashima *et al.* suggest that the palladium atoms act as a binder of C₆₀ by coordination to the π-electrons on the 'aromatic' surface of C₆₀. They also discovered that heterogenous hydrogenation of diphenylacetylene occurred with a catalytic amount of Pd_{3.5}C₆₀ in cyclohexane whereas the catalytic activity was not observed with Pd_nC₆₀(n<3). This suggests that surface palladium species exist when the ratio of Pd:C₆₀ exceeds 3:1 The Raman result obtained here concurs with the idea that the palladium atoms are bound chemically to the C₆₀ surface. This neutral, amorphous and air-stable material requires more intensive analysis e.g. powder diffraction, to explain its structure. Schogl has synthesised a range of naked metal complexes of C₆₀. By reacting metal carbonyls with C₆₀ and then irradiating the samples he has obtained Fe⁰C₆₀ and Pd⁰C₆₀ materials. He reports that there is no chemical interaction between the metal atoms and the fullerene.⁽⁴¹⁾

3.9 Raman studies on palladium C₆₀ organometallics.

The vibrational modes of C₆₀ have been calculated by many groups.⁽⁴²⁾ The total of 174 (3N-6) modes are distributed as,

$$\Gamma = 2A_g(R) + 3T_{1g} + 4T_{2g} + 6G_g + 8H_g(R) + A_u + 4T_{1u}(i.r) + 5T_{2u} + 6G_u + 7H_u.$$

Only the two A_g (singly degenerate) modes and the 8H_g (five-fold degenerate) modes are Raman active. The two A_g modes are expected around 1500cm⁻¹ and 450cm⁻¹ and are known as the pinch mode (reduction of pentagon) and the breathing mode (deformation mode), respectively. If the symmetry of the molecular structure could be reduced without a significant perturbation of the normal mode structure of the fullerene the degeneracy of some or all of these modes might be observed. Surface enhanced Raman spectra of C₆₀ adsorbed onto a gold surface show a dramatic increase in the number of vibrational modes in the Raman spectra and the additional features have been attributed to the distortion of the molecular geometry, a reduction in symmetry and electronic effects or a combination of all three.⁽⁴³⁾

From the crystal structures of organometallic derivatives of C₆₀ obtained by Fagan and Hawkins we know that there is no significant distortion of the C₆₀ structure when a metal is bound in an η² fashion over a 6:6 fusion. Addition of the metal reduces the symmetry of the system i.e. C₁ for Pd(PPh₃)₂C₆₀ and O_h for the [6Pd(PPh₃)₂]C₆₀ molecule. For C₁ the degeneracy of all the possible modes is lifted. The normal modes of vibration are a function of geometry, mass and force constant. Any change due to mass effects should be small since there is only a slight perturbation of the C₆₀ sphere. Electronic effects however may affect the force constants of the vibrations because the bonding of the palladium will disrupt the electronic distribution in the σ and π systems. This should provide information on the bonding situation between palladium and C₆₀ in these compounds.

The Raman spectra of the three compounds (η²-C₆₀)Pd(PPh₃)₂, (η²-C₆₀)[Pd(PPh₃)₂]₆ and Pd₆C₆₀ were recorded at 514.5nm. Since these compounds absorb in this region of the visible spectrum the Raman shifts will have a resonant enhancement. The phosphine ligand modes are weak relative to the C₆₀ modes and were not visible in the spectra. Fig.3.29 shows the Raman spectra of C₆₀ and (η²-C₆₀)[Pd(PPh₃)₂]₆. The A_g and H_g modes are indicated on the C₆₀ spectrum. Note the relative intensities of the two types of modes. In the palladium compound we can see three immediate effects (a) some of the H_g modes have been split (b) there is a general lowering in the frequency of the modes and (c) the greater intensities in the palladium compound.

Fig.3.30a to 3.30c show the Raman spectra of the three compounds in three different regions. The lowering in frequency is especially noticeable in the region shown in 3.30b. This signal corresponds to the second A_g mode.

Ramanspectra of C_{60} and Pd_6C_{60} measured with 514.5 nm

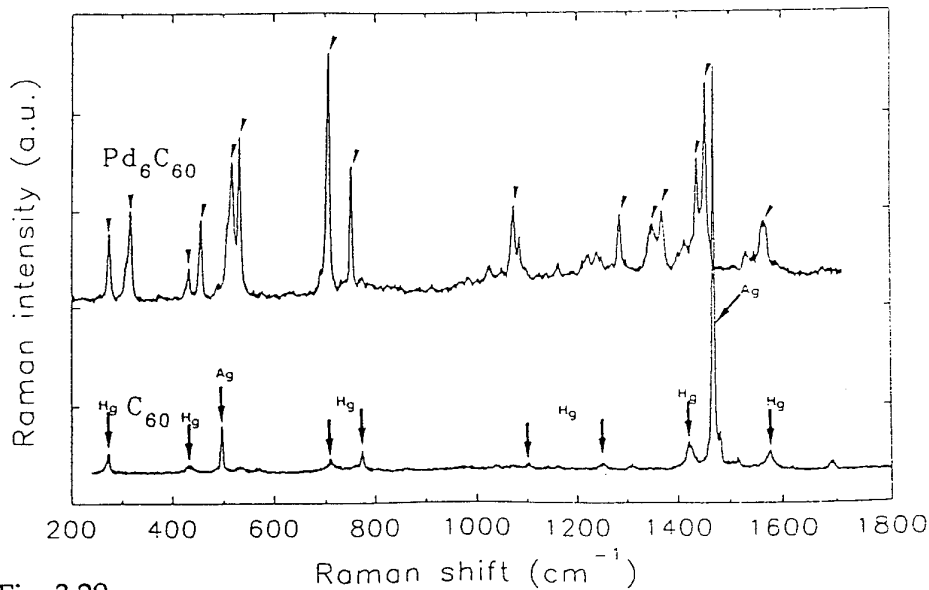


Fig. 3.29

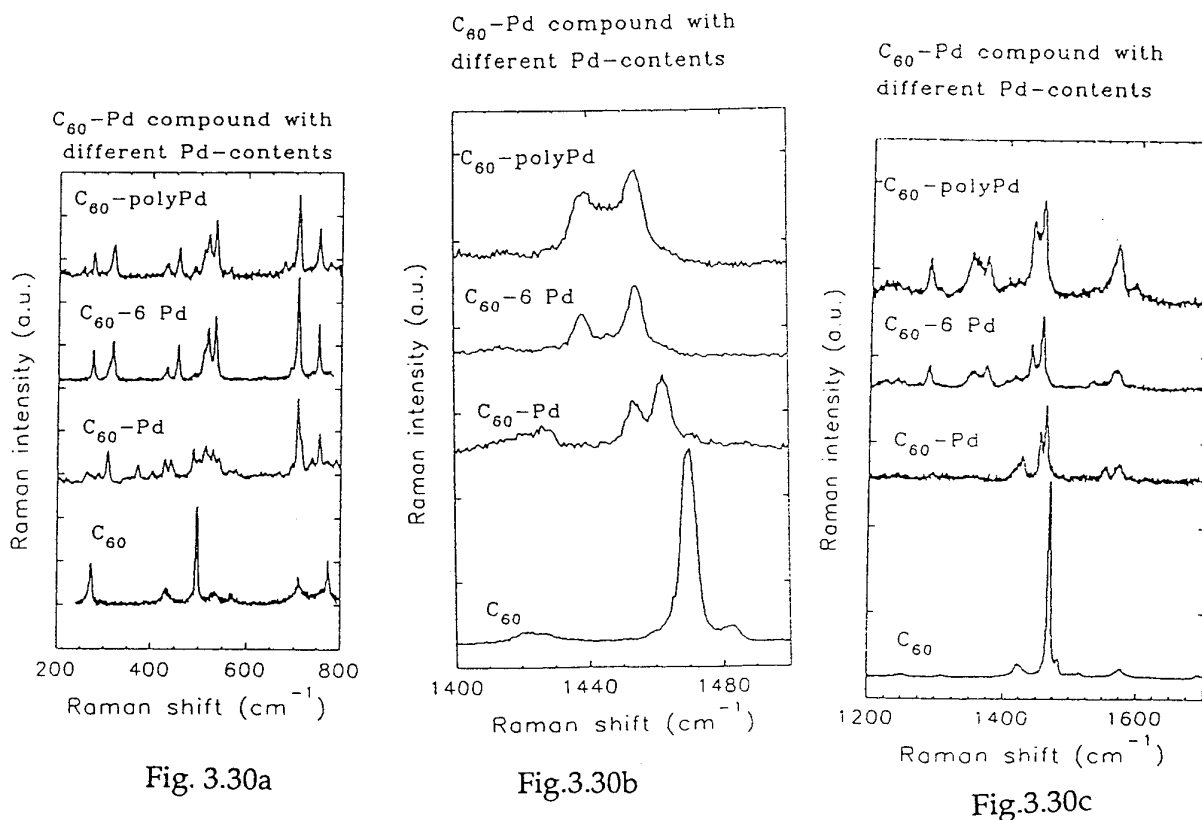
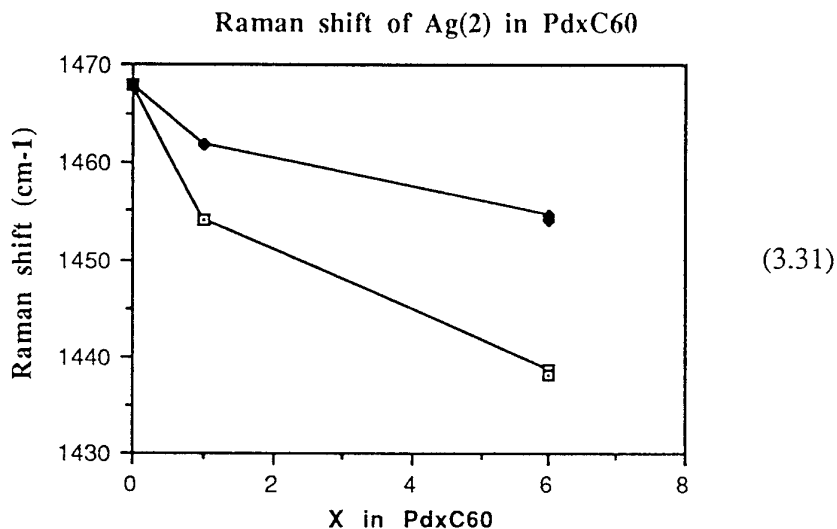


Fig. 3.30a

Fig.3.30b

Fig.3.30c

Fig.3.31 summarises this lowering in frequency for the second A_g (pentagonal pinch) mode for the three different compounds.

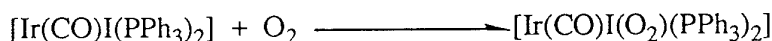


This lowering of frequency upon complexation is indicative of a loss of electron density from the C_{60} due to donation of π electron density to the metal or metal to C_{60} backbonding to the π^* orbitals as suggested by the SERS (Surface Enhanced Raman Spectroscopy) study by Zhang *et al.*⁽⁴⁴⁾ The backbonding hypothesis is the most strongly favoured from both electrochemical studies⁽⁴⁵⁾ and x-ray crystal structures.⁽¹⁾ Using this argument we would expect a further lowering in frequency with increased metal content and this is what is evident from the graph in Fig.3.31. As the extent of backbonding increases the frequency of the A_g mode decreases. The Raman spectrum of the "polymer" suggests that the all six palladium atoms are chemically bound to the C_{60} sphere as opposed to the view of Nagashima that only three are chemically bound and the rest lie on the surface.

3.10 Addition reactions of Ir(I) compounds.

$IrCl(CO)(PPh_3)_2$, known as Vaska's compound after its discoverer⁽⁴⁶⁾, can be prepared by the reaction of triphenylphosphine and $IrCl_3$ in a solvent such as 2-methoxyethanol which acts both as a reducing agent and as a source of CO. It has been widely studied in oxidative addition reactions since the products are generally stable and readily characterised. It is the most thoroughly investigated Ir(I) compound. Oxidation states lower than (II) require the stabilising effect of π -acceptor ligands and this compound is no exception with two triphenyl phosphines. Complexes of Ir(I) are predominantly square planar although 5-coordination does also occur. It forms octahedral Ir(III) complexes in oxidative addition reactions with H_2 , Cl_2 , HX , MeI and RCO_2H . In each of these cases the phosphine ligands are *trans* to each other. Addition

reactions such as those with CO or SO₂ differ in that no oxidation occurs, and 5-coordinate 18-electron Ir(I) products are formed. The facile absorption of O₂ by a solution of Vaska's compound is accompanied by a change in colour from yellow to orange which may be reversed by flushing with N₂. There has been much discussion over the method of bonding of the O₂ in this complex. It is generally accepted that the O₂ acts as a neutral unidentate ligand giving rise to a 5-coordinate Ir(I) product. If the chlorine atom in Vaska's compound is replaced with iodine this oxygen carrying capability vanishes as the oxygenation becomes irreversible (Fig. 3.32).



This has been rationalised using the argument that the lower electronegativity of the iodine allows a greater electron density on the metal, thus facilitating metal to oxygen p-donation: this increases the strength of the M-O₂ bond and by placing charge in antibonding orbitals of the O₂, causes an increase in the O-O distance from 1.30 Å to 1.51 Å. This formally univalent d⁸ complex is somewhat unusual in that it contains a single coordinated carbon monoxide, the stretching frequency (ν_{CO}) of which responds sensitively to any changes in the environment of the central atom.⁽⁴⁷⁾ Since the reaction of neutral covalent molecules with the compound is a simple addition reaction, any difference between the ν_{CO} of the starting material and the product must originate from the added molecule. Table 3.33 displays the ν_{CO}s of a series of complexes. Note that all of the stretching frequencies are higher than that of the starting complex and this has been interpreted as an indication that the iridium carries a higher positive charge than in the starting material. (cf. transition-metal carbonyl complexes, where electron withdrawing groups shift the ν_{CO} to a higher frequency as a result of diminished back-donation from the metal to the antibonding (π*) orbitals of the CO and from a synergic decrease in the σ-donation from the CO to the central atom.

Adduct stability	Added molecule	ν (CO) cm ⁻¹ in CHCl ₃
'Easily reversible'	O ₂	2015
"	SO ₂	2021
"	D-D	2034
Stable reversible	H-Cl	2046
"	CH ₃ I	2047
"	C ₂ F ₄	2052
"	C ₂ (CN) ₄	2057
"	BF ₃	2067

Table 3.33

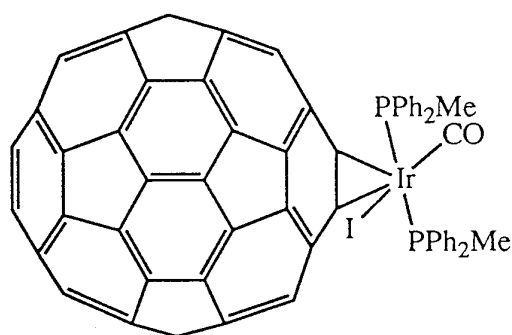
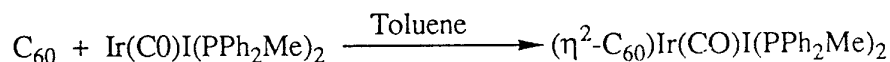
"	BF ₃	2067
Stable irreversible	I-I	2067
"	Br-Br	2072
"	Cl-I	2074
"	Cl-Cl	2075
Ir(CO)Cl(PPh ₃) ₂		1967

From this table we can see that the CO stretching frequency increases continuously from O₂ to Cl-Cl. Vaska uses this information to assign a series of fractional oxidation states for the iridium extending from 1.89 for the O₂ complex to 3.00 for the Cl-Cl complex on the assumption that the ν_{CO} is a linear function of the electron density on the metal. These fractional oxidation states are then a rough measure of the relevant extent of electron loss by the central atom and electron gain by the added molecule, furthermore the stability of the products appears to parallel the extent of electron transfer from the metal to the added molecule. The ν_{CO} is dependent not only on the nature of the other ligands present but also on the total stereochemistry of the complex (*trans* effects *etc.*). Vaska noted that the uptake of O₂ and ethylene is considerably slower than that of other molecules but that some highly electronegative substituted ethylenes react instantly with the iridium precursor.

3.11 Reaction of C₆₀ with IrI(CO)(PMePh₂)₂.

The compound IrI(CO)(PMePh₂)₂ was made in a similar manner to the production of Vaska's compound. A solution of IrI₃.H₂O in 2-methoxyethanol was treated with the phosphine PPh₂Me to give the title compound as yellow crystals in good yield. The ν_{CO} of this starting material occurs at 1908cm⁻¹ (thin film on NaCl). When equimolar solutions of C₆₀ and the Ir(I) compound in toluene were added the reaction darkened immediately. A dark green/black solid separated from the solution and this was isolated by filtration. Residual phosphine was removed from the product under vacuum. The product dissolved in thf or CH₂Cl₂ to give green solutions similar to the palladium compounds. The i.r. spectrum of the product displays peaks at 3030cm⁻¹ (aromatic protons), 2964cm⁻¹ aliphatic protons, the expected four C₆₀ peaks with the usual peaks at 507cm⁻¹, 692cm⁻¹ and 740cm⁻¹ seen for derivatised C₆₀. Significantly ν_{CO} has shifted to 2001cm⁻¹. Substitution of iodine for chlorine in the iridium compound was chosen because it is known that for the O₂ adduct the reverse reaction whereby the O₂ detaches from the iridium centre does not occur with iodine (see above). The same should also be true for ethylene and indeed C₆₀ adducts. This has been shown to be true in this account as the product is more stable than the similar one reported by *Batch?*

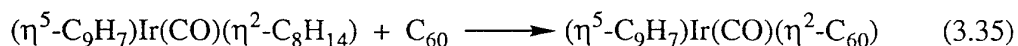
for a period of days. The visible spectrum of the compound contains two strong absorbances at 300nm and 374nm with another at 480nm which tails off at 720nm. The ^1H nmr displays the expected resonances for the PPh_2Me moiety, there is also some residual thf visible. The ^{13}C nmr was recorded in d^8 -thf. The resonance at $\delta 15\text{ppm}$ is attributable to the methyl group. The phenyl resonances appear at $\delta 128\text{ppm}$ and as a doublet at $\delta 136\text{ppm}$. Not all of the 17 expected resonances for C_{60} were detectable however though the ones that were visible are important. The weak resonances at $\delta 158.9\text{ppm}$ and $\delta 73.4\text{ppm}$ are very similar to those observed for the η^2 -coordinated C_{60} palladium and platinum species. Other resonances at $\delta 143.2\text{ppm}$ - $\delta 150\text{ppm}$ support this. The ^{31}P nmr supports the structural assignment of the product as shown in 3.34. There is a single resonance at $\delta 36\text{ppm}$ which is the same as starting material and is indicative of metal coordinated PPh_2Me . There is also a strong resonance centered at $-\delta 6.67\text{ppm}$ which would seem to indicate that some free phosphine was present in the solution. The origin of this could be due to an equilibrium between the product and free phosphine *via* a dissociation mechanism or more probably it is due to a residue from the reaction (Fig.3.34). A FAB mass spectrum was obtained of the compound. The parent molecular ion 1468m/z is not visible but a peak at 1063m/z corresponds to the fragment $\text{C}_{60}\text{Ir}(\text{CO})\text{I}$. This is followed by a peak at 719m/z (C_{60}). Lower peaks correspond to fractions contaminated with the matrix.



(3.34)

There are two examples of similar compounds in the literature. Balch⁽²⁷⁾ reacted C_{60} with Vaska's compound to obtain a very similar product and a crystal structure of the product confirmed the bonding of the iridium as η^2 over a 6:6 ring fusion in C_{60} . He found that the product quickly dissociates in dichloromethane. The shift in ν_{CO} between the product and the starting material is 50 cm^{-1} . Balch argues that the electron withdrawing capability of C_{60} is the same as that of O_2 on the basis of their similar shift in ν_{CO} . The product isolated in this study exhibits a shift of 93 cm^{-1} which is

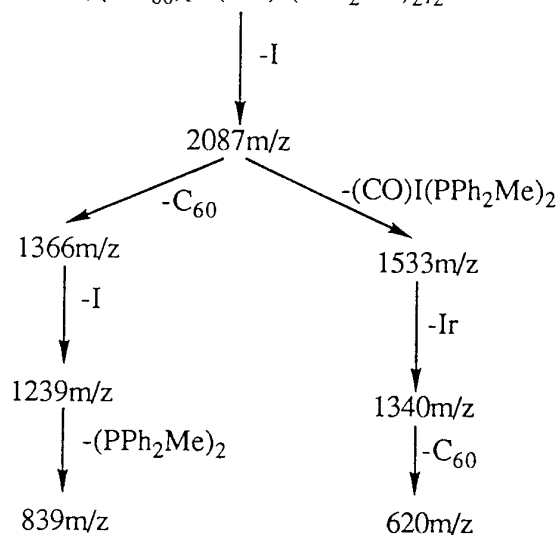
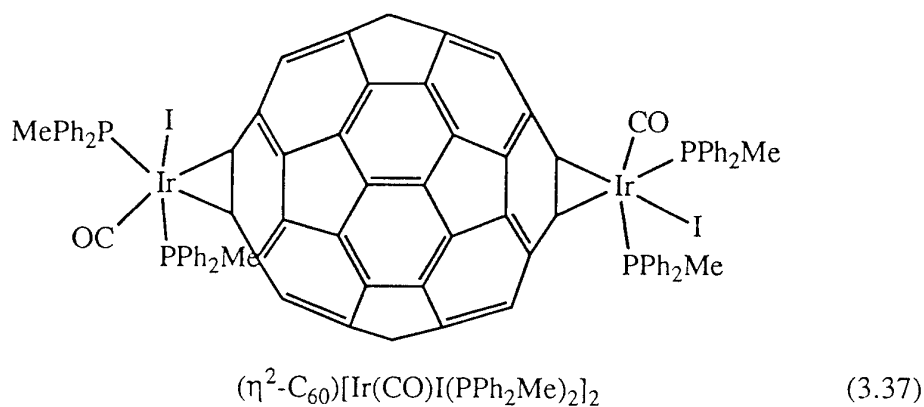
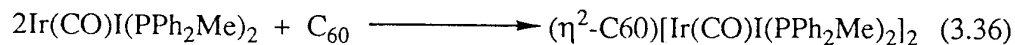
in ν_{CO} . The product isolated in this study exhibits a shift of 93cm^{-1} which is presumably indicative of the fact that iodine is used instead of chlorine. Shapley *et al.*⁽⁴⁸⁾ reacted $(\eta^5\text{-C}_9\text{H}_7)\text{Ir}(\text{CO})(\eta^2\text{-C}_8\text{H}_{14})$ with C_{60} to obtain $(\eta^5\text{-C}_9\text{H}_7)\text{Ir}(\text{CO})(\eta^2\text{-C}_{60})$ (Fig.3.35). The carbonyl shift of 54cm^{-1} is similar to that of Balch. Exposure of a solution of this compound to an excess of CO, $\text{P}(\text{OMe})_3$ or PPh_3 led to a rapid change from green to the characteristic purple colour of C_{60} . They found that the product also dissociates in CH_2Cl_2 .



Shapley *et al.*⁽⁴⁸⁾ interpret these results in which smaller and/or more nucleophilic ligands are favoured, to indicate an associative path for the substitution reaction. This has been seen for other reactions involving indenyl complexes. *Ref*

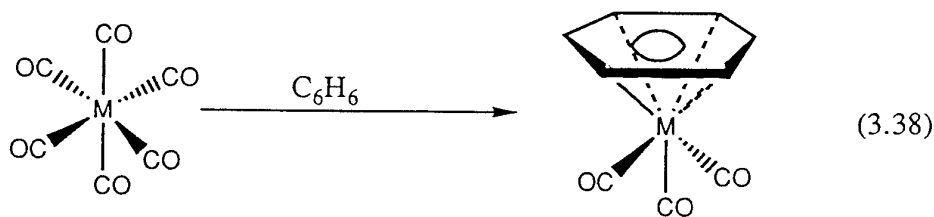
3.12 Reaction of excess $\text{Ir}(\text{CO})\text{I}(\text{PPh}_2\text{Me})_2$ with C_{60} .

There is only one example in the literature of a reaction in which more than one organometallic fragment added to C_{60} , that of Fagan's hexapalladium substituted C_{60} .⁽²⁹⁾ Other researchers report attempts to synthesise a range of multisubstituted organometallic C_{60} molecules which have failed. C_{60} has thirty 6:6 ring fusions and therefore there are thirty possible addition sites. It has been made clear from this study and others that the electron affinity of the C_{60} molecule decreases as the number of metal fragments increases. Fagan has suggested that the C_{60} molecule becomes more "aromatic" with increasing addition. To date there has been no reports of di-, tri-, tetra-, or penta-substitution of metal fragments onto C_{60} (there is a di-substituted C_{70} -Ir compound, see next chapter). In this reaction a two-fold molar excess of the Ir compound was added to a solution of C_{60} in toluene. From this reaction a black solid very similar to that obtained from the previous reaction was isolated. The i.r. of this compound was similar with the exception that the ν_{CO} lies at 2016cm^{-1} which is 15cm^{-1} higher than the monosubstituted Ir-C_{60} . The ^1H and ^{31}P nmr were identical to the mono compound also. The visible spectrum displayed a small shift in the absorbance centered at 475nm . The main evidence however comes from the FAB mass spec. A molecule of the formula $(\eta^2\text{-C}_{60})[\text{Ir}(\text{CO})\text{I}(\text{PPh}_2\text{Me})_2]_2$ (Fig.3.36) would have a molecular weight of 2216amu (^{193}Ir). The compound would be expected to be labile similar to the polysubstituted palladium and platinum compounds. The molecular ion at 2087m/z corresponds to the loss of iodine from the parent. Fragmentation leading to loss of C_{60} (1366m/z), $(\text{CO})\text{I}(\text{PPh}_2\text{Me})_2$ (1533m/z , C_{60}I (1238m/z), $\text{Ir}(\text{CO})\text{I}(\text{PPh}_2\text{Me})_2$ (1340m/z) is very clear from the results (Fig.3.37). There is also a strong molecular ion at 721m/z corresponding to C_{60} .



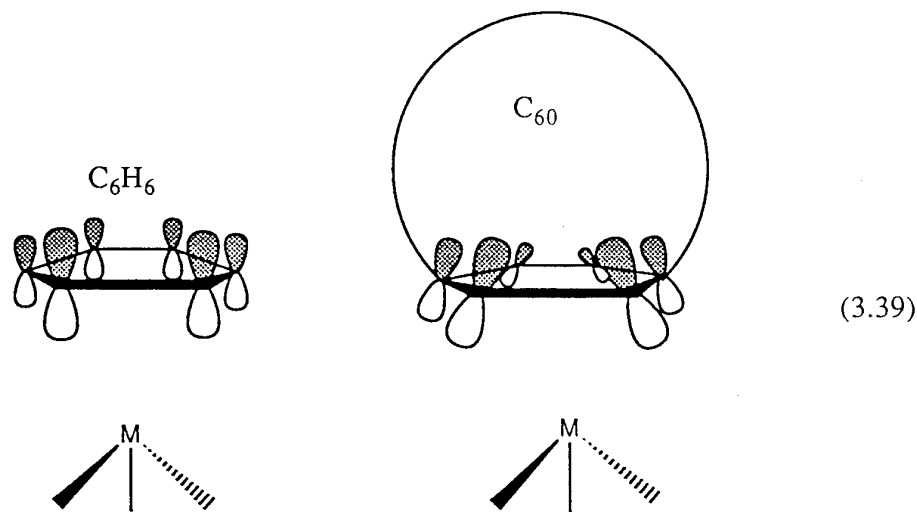
3.12 Reaction of C_{60} with $\text{Mo}(\text{MeCN})_3(\text{CO})_3$.

The η^2 -bonding mode that C_{60} adopts with electron-rich metal centres is well documented. Fagan *et al.* initially reacted C_{60} with a ruthenium reagent (see 3.) to investigate the chemistry of the C_{60} molecule. The ruthenium reagent reacts with electron rich arenes and alkenes in an η^6 -fashion. There are numerous examples of η^6 -bonding especially from the Cr, Mo and W triad. These include the so called "piano-stool" complexes shown in Fig.3.38.



The i.r. absorptions of the $M(\text{CO})_3$ groups are sensitive to the electronic effects of the substituent on the arene ligand transmitted through the metal to the carbonyls.⁽⁴⁹⁾ The frequency and the force constants calculated using the approach proposed by Cotton are found to decrease slightly with the electron donating power of the substituents within the ring. Good correlations are also found between the force constants of the carbonyls (or the stretching frequency) and the different Hammett constants of the substituents.⁽⁴⁹⁾ This indicates that an increase in π -electron density enables the metal atom to transfer electrons into the antibonding orbitals of the carbonyl groups, thus decreasing the carbonyl bond order. A decrease in the ν_{CO} is also observed when one of the carbonyls is replaced by a phosphine, an imine, or an olefin. Phosphines, imines, and olefins are electron-releasing substituents which increase electron density on the metal atom. Back donation from the metal atom occurs into the antibonding orbitals of the two remaining carbonyls and thus decreases the carbonyl bond order. Empty d-orbitals of the phosphine as well as π -antibonding orbitals of the imines and olefins are less available than those of the carbonyl for such backbonding. According to i.r. results, numerous studies of the inductive effect of the $M(\text{CO})_3$ group and theoretical data, it is well accepted that in $M-(\text{CO})_3$ complexes there is a transfer of electrons from the arene ligand through the metal to the carbonyl groups.⁽⁴⁹⁾

A paper by Rogers and Marynick described from a theoretical study,⁽⁵⁰⁾ the η^6 bonding capability of C_{60} in transition metal complexes. They argue that the reason no η^6 transition metal complexes of C_{60} have been synthesised to date is that owing to the curvature of C_{60} , the hybrid π -orbitals are not perpendicular to the hexagonal faces, but point away from the metal centre. As a result, overlap between the metal valence orbitals is reduced and the bonding interaction is weakened (Fig.3.39).

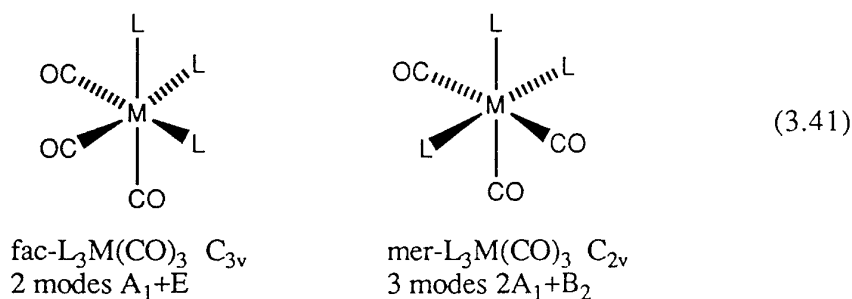


Their calculations yield an estimated tilt angle of 22°. The calculation were based on the reaction(theoretical) of C₆₀ with (η⁶-C₆H₆)Cr(CO)₃ (Fig.3.40).



The authors found the energetics of the exchange prohibitive and advanced two proposals. By modification of the exchanging ligand and/or the use of a larger metal than chromium the reaction should proceed to produce an η⁶-C₆₀ adduct.

The compound (MeCN)₃Mo(CO)₃ is a well known precursor to systems of the type (η⁶-Arene)Mo(CO)₃ through the replacement of the three labile acetonitrile groups. The synthesis of the compound is straightforward but the product needs to be stored in the absence of O₂ and light. The i.r. spectrum of the product displays the expected carbonyl stretches at 1915cm⁻¹ and 1785cm⁻¹ for the C_{3v} symmetry (there are two possible isomers for the formula shown in Fig.3.41).



Since there are only two carbonyl stretches in the i.r the product can be assumed to be the fac-L₃M(CO)₃ isomer.).

In view of this we decided to study the reaction of (MeCN)₃Mo(CO)₃ with C₆₀. When (MeCN)₃Mo(CO)₃ was added to a solution of C₆₀ the reaction immediately darkened and a black precipitate was formed. This black product was found to redissolve in a number of aromatic and chlorinated solvents to give an intensely purple solution. This was stable in CH₂Cl₂ inside the dry-box for up to three days. The purple solutions were found to be extremely sensitive to O₂ and light. If they are exposed to atmosphere an insoluble black precipitate forms. An intermediate in this process is a green solution which is much more stable than the purple solution although still sensitive. I.r. spectra were recorded of the purple solution and the black solid and are shown in table 3.42. The i.r. spectra also revealed the presence of the four C₆₀ bands and those of the

solvent but there were no MeCN vibrations visible in any of the spectra indicating that the three labile acetonitrile groups had been displaced.

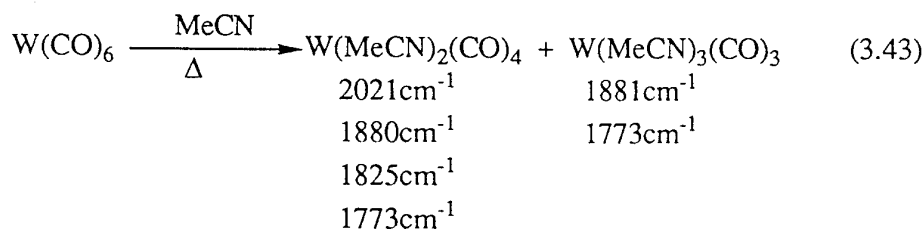
ν_{CO} Black solid.	ν_{CO} Purple soln.	ν_{CO} Black solid(*)	
2083cm ⁻¹ sh	2080cm ⁻¹ w	2083cm ⁻¹ w	
2026cm ⁻¹ vs	2024cm ⁻¹ m	1955cm ⁻¹ s	
1886cm ⁻¹	1944cm ⁻¹ s	1888cm ⁻¹ sh	Table 3.42
1834cm ⁻¹	1920cm ⁻¹ s	1842 cm ⁻¹ sh	
	1864cm ⁻¹ m		
	1807cm ⁻¹ m		
	1739 cm ⁻¹ w		

(*) this solid gives rise to the green solution.

The presence of four carbonyl stretches might indicate the C_{2v} symmetry type of compound seen for cis-L₂M(CO)₄ but a structure of this type would require carbonyl migration and rearrangement. The visible spectrum of the green solution displays a strong absorbance at 374nm with a broad absorbance from 448nm to 808 nm.(two weak absorbances were detected at 876nm and 892nm but these were variable and the spectrometer was performing at its limits). This is very similar to the visible spectra of the η²-coordinated palladium, iridium and platinum compounds. A FAB mass spectrum was attempted for the black solid but because of the sensitivity of the product this failed. The compound did not survive several attempts at nmr spectroscopy. From these results we know that C₆₀ will react with this type of reagent and the preliminary data indicates that the bonding mode is η², though the presence of only two strong ν_{CO} bands in the sensitive purple specimen might indicate the initial formation of an η⁶-species (cf. no ν_{CN} detected) which is too unstable to be obtained completely pure.

3.13 Reaction of C₆₀ with W(MeCN)_x(CO)_{6-x}. (x=3,2)

It was then decided to attempt the same reaction except with the tungsten analogue. The synthesis of the starting material W(MeCN)₃(CO)₃ is not as straightforward as for the Mo analogue owing to the fact that the product is always contaminated with W(MeCN)₂(CO)₄ even after 100 hours of refluxing in MeCN. The presence of this intermediate is evident from the i.r.(see Fig.3.43)



The addition of a solution of the tungsten starting material to a solution of C₆₀ gave immediately a green solution. This was found to be less susceptible to O₂ and light than the molybdenum analogue. The visible spectrum was identical to that of the green molybdenum compound. The i.r. analysis of the dark green/black powder which was isolated from the solution contained the usual four C₆₀ stretches and no peaks that correspond to acetonitrile (notably the strong C-H stretch at ca.2900cm⁻¹). There are five distinct carbonyl stretches, 2043cm⁻¹, 1970cm⁻¹, 1903cm⁻¹, 1847cm⁻¹ and 1775cm⁻¹. This result is possibly the signature of the η²-bonded C₆₀-W(CO)₄ compound. There was no purple intermediate in this reaction. A possible scheme for the reaction is shown in Fig.3.44



The shift of the ν_{CO} to higher wavenumbers can be expected from the approach proposed by Cotton.⁽⁴⁹⁾ The addition of an "electron poor" reagent such as C₆₀ to the metal centre would increase the carbonyl bond order (increase frequency) by not allowing the metal atom to transfer electrons into the antibonding orbitals of the carbonyl groups. To compare the reactivity of the acetonitrile derivatives with the hexacarbonyl species two experiments were carried out whereby the metal (Mo, W) hexacarbonyl was refluxed with C₆₀ (up to 5 days). As expected no reaction took place and all of the reagents were recovered.

A series of ¹³C nmr experiments are under way at present to elucidate more information on the structure of these compounds. The analogous experiments were carried out with C₇₀, the results of which are discussed in Chapter 4.

3.14 Reaction of C₆₀ with activated Ytterbium.

The discovery of superconductivity in potassium doped C₆₀⁽⁵¹⁾ has given rise to intense work in this area. The superconducting transition temperature (T_c) of alkali-metal-doped C₆₀ was raised from 18 K for K₃C₆₀⁽⁵¹⁾ to 33 K for RbCs₂C₆₀.⁽⁵²⁾ The superconducting phase of alkali-metal-doped C₆₀ (M_xC₆₀) where M is the alkali-metal, has been confirmed to be M₃C₆₀ with face-centered cubic (fcc) structure.⁽⁵³⁾ In addition, body-centered tetragonal (bct) M₄C₆₀⁽⁵⁴⁾(insulating) and body-centered cubic(bcc) M₆C₆₀⁽⁵⁵⁾(insulating) phases have also been confirmed. The cubic symmetry of the M₃C₆₀ compounds confirms the three dimensional nature of the superconducting materials. It is known that between x=1 and x=3 a phase separation occurs for some intercalants and M₁C₆₀ and M₂C₆₀ disproportionate to neutral C₆₀ and M₃C₆₀. This new group of superconductors is molecular (C₆₀) and therefore should show some properties different from those of copper oxide high T_c superconductors.

The high electron affinity of C_{60} together with the large interstitial lattice sites make the solid forms of this molecule ideal candidates for metallic doping.⁽⁵⁶⁾ C_{60} forms a variety of intercalation compounds with alkali and alkaline earth metals and these compositions include insulators, conductors and superconductors.⁽⁵⁶⁾ Photoemission studies indicate that C_{60} films lead to a metallic state on exposure to some of the alkaline earth metals.⁽⁵⁷⁾ It has been shown that calcium intercalates into the C_{60} fcc lattice to form a solid solution and that a phase transformation occurs near a Ca: C_{60} ratio of 5:1 to produce a simple cubic structure which is a superconductor with $T_c=8.4K$.⁽⁵⁸⁾

Recent work by Haddon *et al.*⁽⁵⁸⁾ suggests that the conductivities observed in M_xC_{60} films ($M=Ca, Sr, Ba$) between $0 < x < 3$ are associated with the population of bands derived from the t_{1u} LUMO levels of C_{60} whereas the most conducting phases have the composition $x=5$ and involve energy bands derived from the t_{1g} LUMO+1 levels of C_{60} .

Ruoff *et al.*⁽⁵⁹⁾ have suggested that lanthanide and actinide based fullerite compounds are potential M_xC_{60} superconductors. Their calculations indicate that the M_3C_{60} structure which is isomorphic to K_3C_{60} , is the most stable phase for all the rare earth compounds. In the case of the trivalent intercalants, by analogy with the half-filled first LUMO of K_3C_{60} they expect the Ln_3C_{60} solids to be metallic and possibly superconducting since the second lowest unoccupied molecular orbital of C_{60} with t_{1g} symmetry would be half filled. They also suggest that the Ln_2C_{60} phase for the $Ln(II)$ species (Sm, Eu, Yb) is another candidate for superconductivity although the phase is found to be thermodynamically metastable.

The synthetic method employed to produce these intercalates has varied since their discovery. The first experiments designed to produce alkali-metal fullerenes were based on the electrocrystallisation technique which had previously given rise to superconducting charge-transfer salts. Using this technique the conduction is realized only with p-type doped molecules and since all of the theory suggested that it would be best to attempt n-type doping of C_{60} this technique gave very limited results. Wudl *et al.*⁽⁶⁰⁾ did succeed in isolating a charge transfer salt containing reduced C_{60} . This material utilised a bulky counterion and was also found to contain supporting electrolyte in the lattice, which serves to inhibit contact between the C_{60} molecules and to decrease conductivity. Chemical reduction of C_{60} has worked successfully though, as illustrated by the synthesis of the TDAE- C_{60} {TDAE = [tetrakis (dimethylamino)] ethylene} compound by Wang *et al.*⁽⁶¹⁾ This compound is an organic ferromagnet.⁽⁶²⁾ Despite this the preferred method of preparation now avoids the use of solvents. The most common technique used is the doping of C_{60} films by the evaporation of the metal onto the film. Haddon *et al.* have devised an apparatus for this.⁽⁶³⁾ The process involves evaporating an excess of the metal onto the C_{60} film (usually to produce a phase

M_6C_{60}) and then the dilution of this phase by adding the required amount of C_{60} to obtain, usually M_3C_{60} . The process produces small amounts of material in sometimes poorly defined phases. Because of this and the work of Ruoff *et al.* it was decided to try and synthesise a lanthanide fullerite utilising a novel method.

The synthesis of activated ytterbium films using liquid ammonia has been described in Chapter 2. These highly reactive films are made on the walls of a Schlenk tube and when a solution of C_{60} was added to such a film and the system heated with stirring a dense black precipitate formed. The reaction was allowed to continue until the solution was colourless and the metallic film had been consumed. The product was then heated for an extended time (hrs) under a vacuum to remove any traces of the solvent (toluene). After this it was stored inside a Schlenk tube inside the dry-box. The percentage ytterbium metal in the sample was determined by the two techniques described in Chapters 1 and 2 and the technical annex. This was found to be 37%. A percentage of 41.88 would be expected for a compound of the formula Yb_3C_{60} . A FAB mass spec. was attempted but as expected the NOBA matrix reacted with the compound. The fullerene molecular ion is the strongest peak (a peak at 1067m/z may correspond to $C_{60}Yb_2$). At present there is no more data on the product but a series of Raman and superconductivity tests are planned.

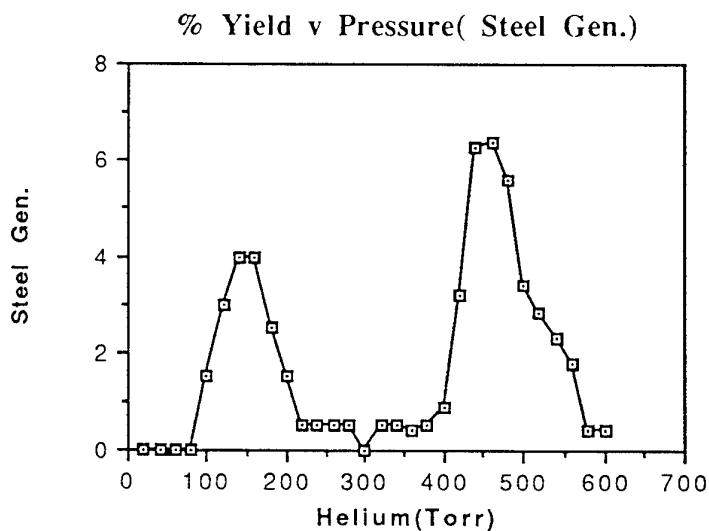
The compound $(\eta^2-C_{60})Pt(PPh_3)_2$ was prepared according to the process described by Fagan *et al.*⁽²⁶⁾ This was used in the non-linear study in chapter 5. The synthesis of the C_{70} analogue is described in chapter 4.

3.15 EXPERIMENTAL

3.15A Production of Fullerenes.

C_{60} and C_{70} were produced using the general technique of vapourising high purity graphite rods (99.99%) under specific conditions. The general conditions were (a) Helium atmosphere 150T-450T, (b) D.C.20V, 130A, (c) Arc gap 4mm. Two machines were used for the production of fullerenes. The first was a simple Kratschmer-Huffman design which was then replaced with a machine based on a design proposed by Tour. This was an all-glass machine which allowed better control over the four parameters which determine the yield of fullerenes.

During the course of this study we uncovered a pressure window which gave improved yields on the previous specification. When the pressure of Helium was increased to 450T the overall yield of fullerenes was more than doubled and the ratio of $C_{60}:C_{70}$ changed from 3:1 to 1.5:1.



The soot generated from the experiments was assumed to be carcinogenic and was handled accordingly.

3.15B Separation and purification of C₆₀ and C₇₀: The separation of fullerenes can be accomplished using various types of columns and mixtures of solvents. For the separation of gram quantities of C₆₀ and C₇₀ I developed a system which gives the optimum yield in the minimum time.

The soot generated from the consumption of a 8mm graphite rod was placed in a 250cm³ Erlenmeyer flask. Carbon disulphide(100cm³) was added to the soot and the suspension was sonicated for 5minutes. The resulting solution/suspension was filtered using a Buchner flask. The solid residue was washed with CS₂(100cm³) in the sonic bath and filtered again. The two filtrates were combined and the CS₂ was removed on a rotary evaporator to give 450mg of C₆₀/C₇₀ mix. The fullerene mix was dissolved in toluene(200cm³), sonication was sometimes used to assist the process. Decolourizing charcoal(16g) was added to toluene(100cm³) to make a slurry. This was then poured into a 4.25cm diameter column fitted with a grade 3 sinter. The charcoal was packed with toluene. The fullerene solution was added to the packed column and a positive pressure of N₂ used to give a flow rate of approx 20cm³/min. More toluene was added to the column as needed. Within 1min. C₆₀ begins to elute from the column. When the C₆₀ colour faded the next 50cm³ approx. was set aside as it contained C₇₀ with small amounts of C₆₀.(this was added to the next toluene solution for separation). C₇₀ was eluted from the column next, approximately 85% elutes in the first 10.minutes, the remaining C₇₀ can be removed from the column by adding CS₂ to the toluene eluent. This C₇₀ contains trace amounts of higher fullerenes and again was set aside for the next separation. The separated solutions of C₆₀ and C₇₀ were worked up by removing the toluene on a rotary evaporator to give the fullerenes as black powders. The powder was then placed in a Schlenk tube and warmed to 90 °C under a vacuum(<0.01mm) for 1 hour. This 'out-heating' procedure was necessary to completely remove all traces of solvent. The total time taken for this procedure was approximately 2.5 hours which is a significant improvement on previous schemes. The fullerenes produced by this procedure had purities of 99.9% . 237mg of C₆₀ and 140mg of C₇₀ were recovered from 400mg of soot. The procedure has been scaled up to separate 1.00g of fullerene mix with similar yields.

The fullerene powders were stored in Schlenk tubes under argon. All solvents used in the handling of fullerenes were dried and degassed using conventional methods. The fullerenes produced were characterised using i.r, uv/vis, ¹³C nmr, ¹H nmr and FAB Mass Spec.

C₆₀:

I.r (CsI disc) 1429s, 1183m, 577s, 526m cm^{-1} .

Uv/vis (Hexane) $\lambda_{\text{max}}(\epsilon)$ 213(135,000), 257(175,000), 329(50,000), 404w, 440-680w(br)nm.

^{13}C nmr (300MHz, C_6D_6) δ 142.7ppm.

FAB ms 720m/z(100%)

C₇₀:

I.r (CsI disc) 1429s, 1183m, 795w, 673m, 577s, 526m cm^{-1}

Uv/vis (Hexane) $\lambda_{\text{max}}(\epsilon)$ 215(140,000), 236(142,000), 313w, 331-378(3400), 469-650(br)nm.

^{13}C nmr (300MHz, C_6D_6) δ 131(10C), 144.95(20C), 146.90(10C), 147.65(20C), 150.20(10C)ppm.

FAB ms 840m/z(100%).

3.16 ($\eta^2\text{-C}_{60}$)Pd(PPh₃)₂: C_{60} (36mg, 5×10^{-2} mmol) was dissolved in toluene(20 cm^3) in a Schlenk tube with a magnetic stirrer. Pd(PPh₃)₄(57mg, 5E-2 mmol) was dissolved in toluene(40 cm^3) in another Schlenk. The palladium solution was added to the C_{60} solution dropwise using a cannula. The reaction solution darkened initially and then turned emerald green. The reaction was left stirring (1 hr) after which time the toluene was removed on the vacuum line to give a dark green solid. The product was washed with cold ethanol (2x10 cm^3) to remove residual triphenylphosphine. The yield of product was quantitative(67mg, 5E-2mmol). The product was sensitive to oxygen and was stored under argon.

M.p = 274 °C (dec)

I.r (CsI disc.) 3061w, 2966s, 2931s, 2861m, 1485w, 1462m, 1438m, 1262s, 1187w, 1097s, 803s, 743m, 722m, 695m, 579w, 544s, 524m, 398w cm^{-1} .

Uv/vis (Toluene) $\lambda_{\text{max}}(\epsilon)$ 395(sh), 435(6486), 615(3108), 660(2702)nm.

Raman (514.5nm, pellet) 310m, 440 doublet, 500-550 multiplet, 705s, 755m, 1425w, 1454s, 1462s cm^{-1} .

^1H nmr (CDCl_3 , 300MHz) δ 7.39-7.736(m, arom H)ppm.

^{13}C nmr (75.5 MHz, CD_2Cl_2) δ 82, δ 128d, δ 137d, δ 142.8, δ 143.7, δ 144.2, δ 144.6, δ 145.3, d158ppm.

^{31}P nmr (124.44MHz, H_3PO_4 , C_6D_6) δ 27.5, -4.86ppm

3.17 (η^2 -C₆₀)[Pd(PPh₃)₂]₆: C₆₀(72mg, 0.1mmol) was dissolved in benzene(25cm³) in a Schlenk tube under argon. Pd(PPh₃)₄(0.922, 0.8mmol) was dissolved in benzene(50cm³) and added dropwise to a stirring solution of C₆₀. Initially the reaction mixture turned dark green, but turned red on the addition of the last 10cm³ of the palladium solution. The solvent was removed on the vacuum line to give a dark red powder. The product was dissolved in a minimum amount of thf and stored at -27 °C (72 h). A red microcrystalline powder separated from the solution. The solvent was removed using a filter-cannula and the red powder dried on the vacuum line. The air-sensitive red solid(600mg) was stored under argon. The product quickly dissociates in solution to give a green solution if the solvent is not properly degassed or is strongly co-ordinating (*e.g.* CS₂).

I.r (CsI disc) 3061m, 1482w, 1437s, 1361w, 1192s, 1122s, 803s, 752s, 722s, 696s, 541s, 507s cm⁻¹.

Raman (514.5nm, pellet) 274m, 315m, 431w, 455m, 515s, 532s, 706s, 752s, 1073m, 1286m, 1352m, 1438s, 1454s cm⁻¹.

Uv/vis (Toluene) λ_{max} 475(sh), 550-850(br, 620, 660)nm.

¹H nmr (300MHz, CD₂Cl₂) δ 7.14-7.78(arom. H)ppm.

¹³C nmr(75.5MHz, C₆D₆) δ 153.9, 143.18, 128(d), 132(d), 134w(s), 89.8ppm.

³¹P nmr(124.44MHz, THF, H₃PO₄) δ 25.3, -4.5ppm.

FAB ms Complex m/z(%) 1134(64), 1369(62), 2448(65), 3211(37), 4409(20), 4535(13), 4643(17).

3.18 Decomposition of (η^2 -C₆₀)Pd(PPh₃)₂: A sample of (C₆₀)Pd(PPh₃)₂ (135mg, 0.1mmol) was placed in a small, preweighed sublimation apparatus. The flask was evacuated (<0.001mmHg) and slowly heated to 200°C. A white sublimate collected on the cold-finger and after 30 minutes of further heating the process was stopped. The sublimate was found to be Triphenylphosphine from m.p, i.r and nmr.(0.44mg, 0.1mmol). The black powder which remained was found to be insoluble in a wide range of solvents.

I.r (CsI disc) 1436s, 1415m, 1262s, 1187m, 746s, 721s, 689s, 525vs, 393m, 250w, 224w cm⁻¹.

The same procedure was used with a sample of (C₆₀)₆(Pd(PPh₃)₂). Similarly all of the Phosphine was recovered as a sublimate. The residue gave an identical i.r.

Raman (514nm, pellet) 1565m, 1454.5s, 1438m, 751s, 704vs, 532s, 515s, 450m, 310m, 262m cm⁻¹. See text for details.

3.19 (η^2 -C₆₀)Ir(CO)I(PPh₂Me)₂: C₆₀(36mg, 0.05mmol) was dissolved in toluene(20cm³) in a Schlenk under argon. A solution of Ir(CO)I(PPh₂Me)₂(37mg, 0.05mmol) in warm toluene(50cm³) was added to the C₆₀ dropwise using a cannula. The mixture darkened immediately. After 2 hours the reaction was completed.(It was followed by solution i.r). The starting material has $\nu_{(\text{CO})}$ 1908cm⁻¹, the product shows $\nu_{(\text{CO})}$ 2001cm⁻¹.) The product was isolated from the solution after the solvent was removed on the vacuum line. The dark green/black product was warmed gently, 35°C, under vacuum(<0.001mmHg) to remove residual phosphine. The product was sensitive to oxygen and was stored in a Schlenk under argon. It was soluble in a range of solvents, giving dark green solutions.

I.r (CsI disc) 3032w, 2964s, 2931s, 2857m, 2001s(2064sh), 1436s, 1362m, 1263s, 1183m, 801s, 740s, 692s, 578w, 528m, 507s, 399m cm⁻¹.

Uv/vis (Toluene) $\lambda_{\text{max}}(\epsilon)$ 330(35,710), 375(sh, 14,000), 480(br, 6,000) nm.

¹H nmr (80MHz, CDCl₃) δ 1.94(s, br, 3H), 7.00-7.70(m, br, 10H) ppm.

¹³C nmr (75.5MHz, d₈thf) δ 15, δ 73.4, δ 128d, δ 136d, δ 143.2, δ 144.5, δ 144.8, δ 145.2, δ 145.5, δ 145.9, δ 146.1, δ 147.3, δ 149.8, δ 158.9ppm.

³¹P nmr (124.44MHz, H₃PO₄, PPh₃) δ 36.6ppm, δ -6.67ppm.

FAB ms m/z (%) 1063(14), 719(10), 702(38), 561(63), 322(40).

3.20 (η^2 -C₆₀)[Ir(CO)I(PPh₂Me)₂]₂: C₆₀(36mg, 0.05mmol) was dissolved in toluene(20cm³) in a Schlenk tube. A solution of Ir(CO)I(PPh₂Me)₂(74mg, 1mmol) in toluene(70cm³) was added dropwise to the stirring fullerene solution. When addition was completed a black solid precipitated which was isolated by removing the solution with a filter cannula. The black product was dried by warming (35 °C) under a vacuum(<0.001mm Hg).

I.r(CsI disc) 3058w, 2967s, 2825s, 2857w, 2016s(2065sh), 1680s, 1628s, 1461m, 1436s, 1395m, 1262s, 1160m, 802s, 741m, 693s, 579w, 562m, 527m, 506m, 401w cm⁻¹.

Vis (Toluene) $\lambda_{\text{max}}=475(\text{br})$.

¹H nmr (80MHz, CDCl₃) δ 7.13-7.60(m, 10H), 2.9(s, w), 2.09(s, 3H), 1.19(s, 15H) ppm.

³¹P nmr (40MHz, C₆D₆) δ 36.83, -1.24, -6.64, -8.36, -15.70, -17.10, -34.49, -37.36ppm.

FAB ms m/z(%) = 2087(7), 1533(27), 1366(35), 1016(23), 720(97).

3.21 Reaction of C₆₀ with Mo(MeCN)₃(CO)₃: Mo(CO)₆(0.264g, 1mmol) was added to MeCN(100cm³) in a 100ml 3-necked round bottomed flask fitted with a reflux condenser. The mixture was refluxed under argon (6 h) during which time the solution turned bright yellow. After the solution had cooled down the solvent was removed on the vacuum line to give a yellow solid.(300mg,100%).

I.r (CsI disc) 2965s, 2940s, 2873m, 2305w, 2278m, 1915s, 1785m, 1455m, 938w cm⁻¹.

C₆₀(50mg, 0.07mmol) was dissolved in toluene(50cm³) in a Schlenk tube. Mo(MeCN)₃(CO)₃(20mg, 0.07mmol) was dissolved in MeCN(5cm³) to give a saturated solution. The carbonyl solution was added dropwise to the fullerene using a pipette inside the dry-Box. The solution darkened immediately. After addition was completed the dark solution was stirred for 30 minutes. A black solid precipitated when the stirring stopped. The product was dried on the vacuum line to give a very air-sensitive black solid (60mg). Small amounts of the product were removed inside the dry-box and added to a range of solvents. The product gives a bright purple solution when dissolved in aromatic and chlorinated solvents. The purple solutions are extremely sensitive to oxygen, light and moisture. Strongly co-ordinating solvents give a green solution when added to the black powder. Due to the sensitivity of the product complete analysis proved difficult.

I.r (CsI disc) See Table 3.42

Uv/vis (Toluene) λ_{max}374, 448-808 br with λ_{max}518, 876, 892 nm

FAB ms m/z(%) 923(15), 795(5), 673(98), 554(20), 492(80), 462(77), 410(55), 364(99), 267(92).

3.22 Reaction of C₆₀ with W(MeCN)_n(CO)_{6-n}.(n=3,4): W(CO)₆(0.351g, 1mmol) added to MeCN(50cm³) and reflux under argon (72 hr) to give a yellow solution of W(MeCN)₃(CO)₃ which contained a small amount of W(MeCN)₂(CO)₄ which using this method is unavoidable. The solid was isolated after the solvent was removed on the vacuum line. The total yield was 0.380g.

I.r (CsI disc.) 2018w, 1881s, 1825w, 1773s cm⁻¹.

C₆₀(72mg, 0.1mmol) was dissolved in toluene(40cm³) to give the characteristic mauve coloured solution. A saturated solution of W(MeCN)₃(CO)₃ (39mg, 0.1mmol) in MeCN(8cm³) was added to the stirring solution of the fullerene inside the dry-box. The solution immediately turned dark green. After 30 minutes the reaction was stopped and 20cm³ of the solvent was removed on the vacuum line. The remaining solution was stored at -27 °C (48 hr). A black microcrystalline solid was isolated from this

solution. This solid was separated from the stock solution and dried under vacuum to give a dark green solid. Yield 71mg.

I.r (CsI disc) 2043m, 1970s, 1903s, 1847s, 1775s, 1458w, 1354w, 1182m, 1025s, 729m, 702m, 576m, 527s, 416m cm^{-1} .

Visible spectrum as for Molybdenum adduct.

The reactions of $\text{W}(\text{CO})_6$ and $\text{Mo}(\text{CO})_6$ with $\text{C}_{70}/\text{C}_{60}$ gave no products and the starting materials were recovered in each case. The reactions involved dissolving the metal carbonyl in boiling toluene and adding the fullerene. The mixture was then refluxed under argon for up to five days.

3.23 Reaction of C_{60} with activated ytterbium: Ytterbium metal powder (0.519g, 3mmol) was dissolved in liq.NH_3 (80 cm^3) at $-55\text{ }^\circ\text{C}$ in a Schlenk. When all of the metal was dissolved the NH_3 was removed slowly under vacuum with rapid stirring to leave a film of activated ytterbium metal on the sides of the Schlenk. A solution of C_{60} (0.72g, 1mmol) in toluene (150 cm^3) was added to the ytterbium metal with stirring. The Schlenk was heated to $100\text{ }^\circ\text{C}$ for five hours. After this time the metal was totally consumed and a black suspension was visible in the colourless solution. The solvent was removed on the vacuum line to leave a black solid.

The black air-sensitive product has been sent for Raman and superconductivity analysis.

Metal analysis EDTA 38% UV/VIS Yb^{3+} 38%.

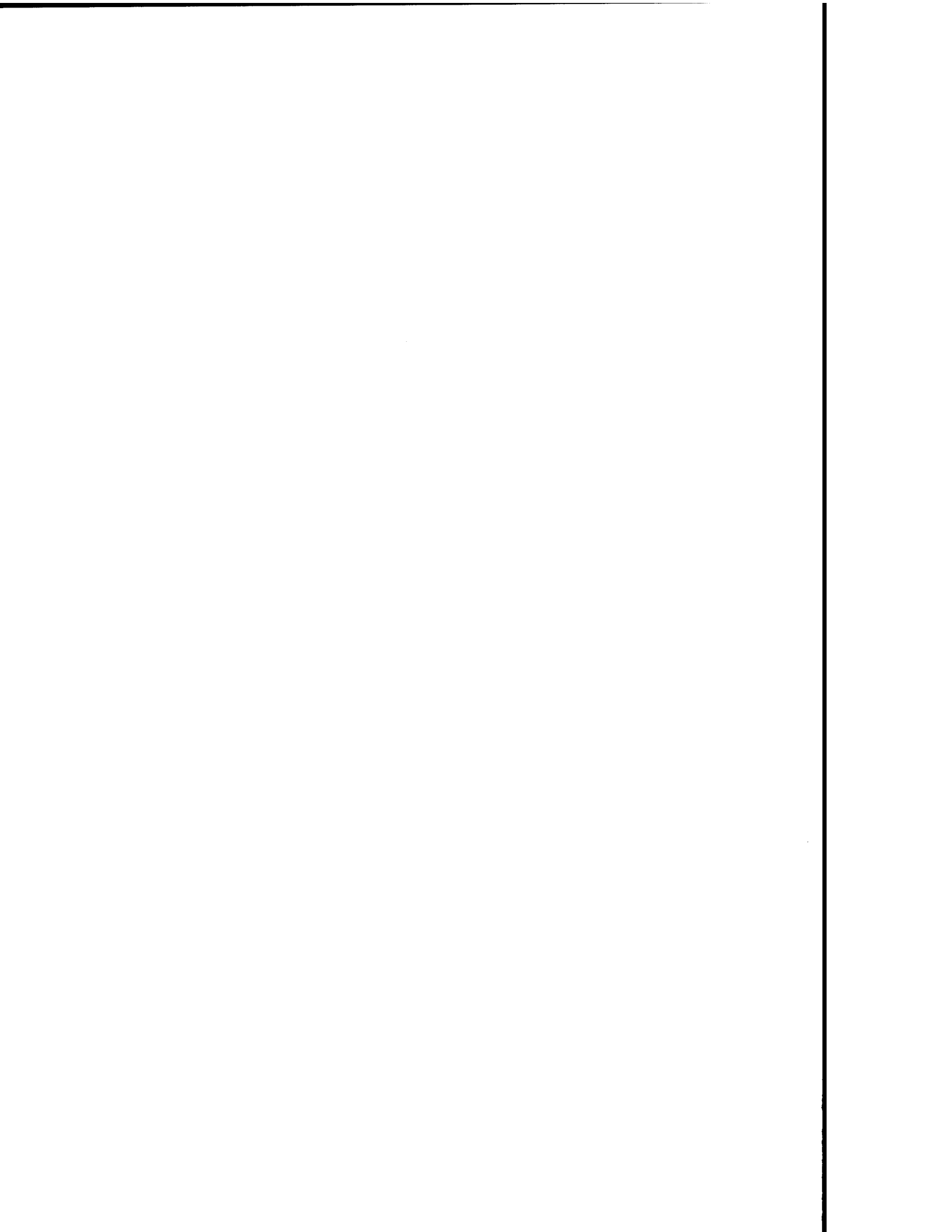
References.

- 1 W. Kratschmer, L.D. Lamb, K. Foristopoulos, D.R. Huffman, *Nature*, 1990, **347**, 354.
- 2 F.W. McLafferty, Ed., *Acc. Chem. Res.*, 1992, **25**, 97 and H.W. Kroto, *Angew. Chem. Intl. Ed. Engl.*, 1992, **57**, 6932.
- 3 W.A. Scrivens, J.M. Tour, *J. Org. Chem.*, 1992, **57**, 6932.
- 4 R. Taylor, J.P. Hare, A. Abdul-Sada and H. Kroto, *J. Chem. Soc., Chem. Commun.*, 1990, 1423.
- 5 R.E. Haufler, J. Conceicao, L.P.F. Chibante, Y. Chai, N.E. Byrne, S. Flanagan, M.M. Haley, S.C. O'Brien, C. Pan, Z. Xiao, W.E. Billups, M.A. Ciufolini, R.H. Hauge, J.L. Margrave, L.J. Wilson, R.F. Curl and R.E. Smalley, *J. Phys. Chem.*, 1990, **94**, 8634.
- 6 D.H. Parker, P. Wurz, K. Chatterjee, K. Lykke, J. Hunt, M.J. Pellin, J.C. Hemminger, D.M. Gruen, L.M. Stock, *J. Am. Chem. Soc.*, 1991, **113**, 7499.
- 7 G. Peters, M. Jansen, *Angew. Chem. Intl. Ed. Engl.*, 1992, **31**, 223.
- 8 T.E. Hogan-Esch and J. Smid, *J. Am. Chem. Soc.*, 1967, **89**, 2764.
- 9 F. Wudl, A. Hirsch, K.C. Khemani, T. Suzuki, P-M Allemand, A. Koch, H. Eckert, G. Srdanov and H.M. Webb, *Fullerenes*, ACS symposium, Series 481, Eds. G.S. Hammond and V.J. Kuck, Chap. 11, ACS., Washington D.C. 1992.
- 10 C.S. Yannon, P.P. Bernier, D.S. Bethune, G. Meijer and J.R. Salem, *J. Am. Chem. Soc.*, 1991, **113**, 3190.
- 11 G.A. Olah, I. Bucsi, C. Lambert, R. Aniszfeld, N.J. Trivedi, D.K. Sensharma and G.K.S. Prakash, *J. Am. Chem. Soc.*, 1991, **113**, 9385.
- 12 *ibid.* *J. Am. Chem. Soc.*, 1991, **113**, 9387.
- 13 A. Hirsh, Q. Li and F. Wudl, *Angew. Chem. Intl. Ed. Engl.*, 1991, **30**, 1309.
- 14 L.Y. Chiang, J.W. Swirczewski, C.S. Hsu, S.K. Chowdhury, S. Cameron, K. Creegan, *J. Chem. Soc., Chem. Commun.*, 1992, 1791.
- 15 G.H. Kroll, P.J. Benning, Y. Chen, T.R. Ohno, J.H. Weaver, L.P.F. Chibante and R.E. Smalley, *Chem. Phys. Lett.*, 1991, **181**, 112.

- 16 C. Taliani, G. Ruani, R. Zamboni, R. Danieli, V.N. Denisov, V.M. Burlakov, F. Negri, G. Orlandi and F. Zerbetto, *J. Chem. Soc., Chem. Commun.*, 1993, 220.
- 17 Y. Elemen, S.K. Silverman, C. Shev, M. Kao, C.S. Foote, M.M. Alvarez and R.L. Whetten, *Angew. Chem. Intl. Ed. Engl.*, 1992, **31**, 351.
- 18 J.M. Hawkins, T.A. Lewis, S.D. Loren, A. Meyer, J.R. Heath, Y. Shibato, R.J. Saykally, *J. Org. Chem.*, 1990, **55**, 6250 and J.M. Hawkins, A. Meyer, T.A. Lewis, S.D. Loren, F.J. Hollander, *Science*, 1991, **252**, 312.
- 19 N. Matsuzawa, D. Dixon and P. Krusic, *J. Phys. Chem*, 1992, **96**, 8317.
- 20 R. Taylor, A postbuckminsterfullerene view of the chemistry, physics and astrophysics of carbon, *Phil. Trans. Royal. Soc.*, Eds. H.W. Kroto, A.L. Mackay, G. Turner and D.R.M Walton, 1992, 87.
- 21 F. Wudl, *Acc. Chem. Res.*, 1992, **25**, 106.
- 22 J.W. Bausch, *J. Am. Chem. Soc.*, 1991, **113**, 3205.
- 23 P.J. Fagan, J.C. Calabrese and B. Malone, *Science*, 1991, **252**, 1160.
- 24 R.F. Curl and R.E. Smalley, *Science*, 1988, **242**, 1017.
- 25 P.M. Allemand, A. Koch, F. Wudl, Y. Rubin, F. Diederich, M.M. Alvarez, S.J. Anz and R.L. Whetten, *J. Am. Chem. Soc.*, 1991, **113**, 1050.
- 26 P.J. Fagan, J.C. Calabrese, B. Malone, *Science*, 1991, **252**, 1160.
- 27 A.L. Balch, V.J. Catalano and J.W. Lee, *Inorg. Chem.*, 1991, **30**, 3980.
- 28 R.S. Koefod, M.F. Hudgens, J.R. Shapley, *J. Am. Chem. Soc.*, 1991, **113**, 8957.
- 29 P.J. Fagan, J.C. Calabrese, B. Malone, *J. Am. Chem. Soc.*, 1991, **113**, 9408.
- 30 G.E. Coates, M.L.H. Green, P. Powell, K. Wade, *Principles of Organometallic Chemistry*, Methuen, London, 1968, 259 pp.
- 31 R. Mason, D.M.P. Mingos, G. Rucci and J.A. Connor, *J.C.S. Dalton*, 1972, 1729.
- 32 C.D.M. Beverwijk and J.P.C.M van Dongen, *Tetrahedron Lett*, 1972, 4291.
- 33 K.R. Aris, V. Aris, J.M. Brown, *J. Organomet. Chem.*, 1972, **42**, C67.

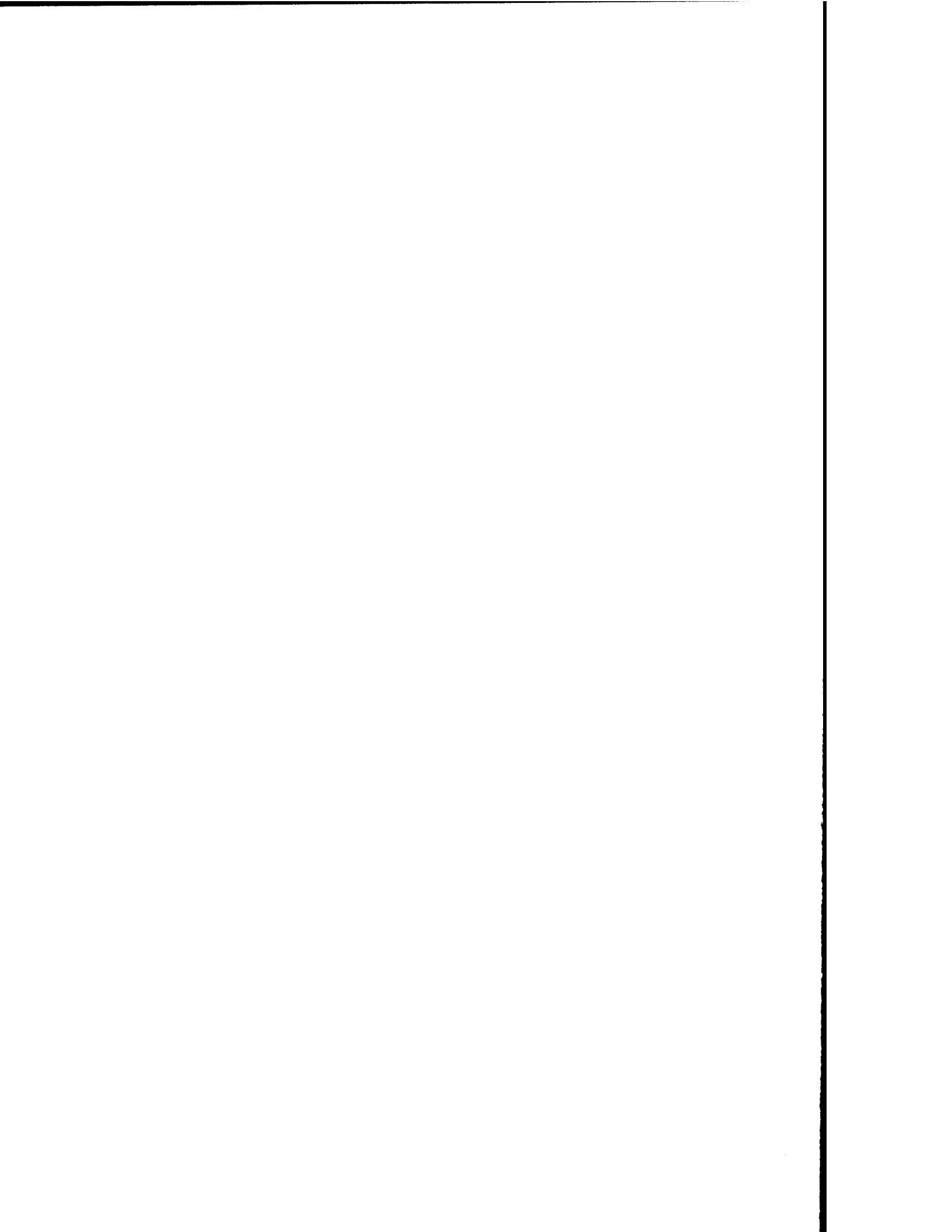
- 34 R.G. Salomon and J.K. Kochi, *J. Organomet. Chem.*, 1972, **43**, C7.
- 35 C.A. Tolman, W.C. Seidel, D.H. Gerlach, *J. Am. Chem. Soc.*, 1972, **94**, 2669.
- 36 V.I. Solokov and O.A. Reutov, *Coord. Chem. Rev.*, 1978, **27**, 89.
- 37 J. Halpern and T.A. Weil, *J. Chem. Soc. Chem. Commun.*, 1973, 631.
- 38 B. Chase and P.J. Fagan, *J. Am. Chem. Soc.*, 1992, **114**, 2252.
- 39 V.V. Bashilov, P.V. Petrovskii, V.I. Sokolov, S.V. Lindeman, I.A. Guzey, Y.T. Struchkov, *Organometallics*, 1993, **12**, 991.
- 40 H. Nagashima, A. Nakaoka, Y. Saito, M. Kato, T. Kawanishi, *J. Chem. Soc., Chem. Commun.*, 1992, 377.
- 41 M. Shlogl private communication.
- 42 B. Chase, N. Herron and E. Holler, *J. Phys. Chem.*, 1992, **96**, 4262 and D.S. Bethune, G. Meijer, W.C. Tang, H.J. Rosen, *Chem. Phys. Lett.*, 1991, **179**, 181.
- 43 R.L. Garrell, T.M. Herne, C.A. Szafranski, F. Diederich, F. Ettl, R.L. Whetten, *J. Am. Chem. Soc.*, 1991, **113**, 6302.
- 44 Y. Zhang, Y. Du, J. Shapley, M.J. Weaver, *Chem. Phys. Lett.*, 1993, **205**, 508.
- 45 S. A. Lerke, D. Evans, P.J. Fagan, B. Parkinson, *J. Am. Chem. Soc.*, **114** in press.
- 46 L. Vaska and J.W. Di Luzio, *J. Am. Chem. Soc.*, 1961, **83**, 2784.
- 47 L. Vaska, *Acc. Chem. Res.*, 1968, **1**, 335.
- 48 R.S. Koefod, M.F. Hudgens, J.R. Shapley, *J. Am. Chem. Soc.*, 1991, **113**, 8957.
- 49..A. Solladie-Cavallo, *Polyhedron*, 1985, **4**, 901 and references therein.
- 50 J.R. Rogers and D.S. Marynick, *Chem. Phys. Lett.*, 1993, **205**, 197.
- 51 A.F. Hebard, M.J. Rosseinsky, R.C. Haddon, D.W. Murphy, S.H. Glarum, T.T.M. Palstra, A.P. Ramirez, A.R. Kortan, *Nature*, 1991, **350**, 600.
- 52 K. Holczer, O. Klien, S.M. Huang, R.B. Kaner, K.J. Fu, R.L. Whetten, F. Diederich, *Science*, 1991, **252**, 1154.
- 53 R.M. Fleming, R.C. Haddon *et al.*, *Mater. Res. Soc. Symp. Proc.*, 1991, **206**, 691.
- 54 O. Zhou *et al.*, *Nature*, 1991, **351**, 462.
- 55 R.M. Fleming R.C. Haddon *et al.*, *Nature*, 1991 **352**, 701.

- 56 R.C. Haddon, *Acc. Chem. Res.*, 1992, **25**, 127.
- 57 A.R. Kortan and R.C. Haddon *et al.*, *Nature*, 1992, **355**, 529.
- 58 R.C. Haddon, G.P. Kochanski, A.F. Hebard, A.T. Fiory, R.C. Morris, *Science*, 1992, 1636.
- 59 R.S. Ruoff, Y. Wang, D. Tomanek, *Chem. Phys. Lett.*, 1993, **203**, 438.
- 60 P.M. Allemand, F. Wudl, Y. Rubin, F. Diederich, R.L. Whetten, *J. Am. Chem. Soc.*, 1991, **113**, 2780.
- 61 H.H. Wang *et al.*, *Inorg. Chem.*, 1991, **30**, 2838.
- 62 P.M. Allemand, K.C. Khemani, A. Koch, F. Wudl, K. Holczer, S. Donovan, *Science*, 1991, **252**, 301.
- 63 R.C. Haddon *et al.*, *Nature*, 1991, **350**, 320.



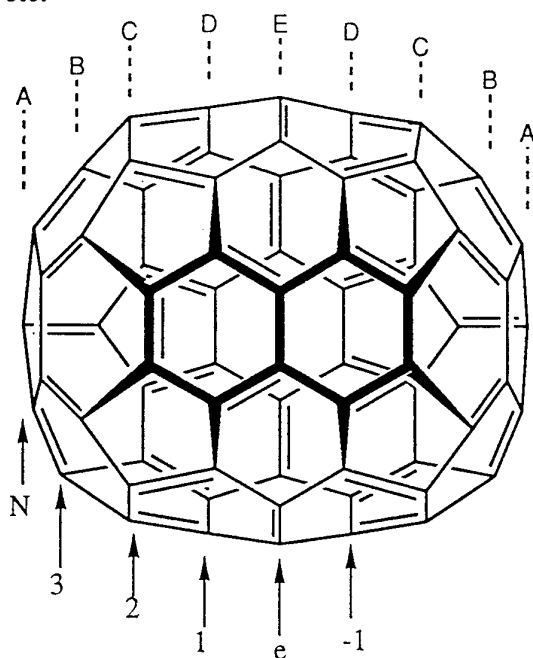
CHAPTER 4.

Organometallic Chemistry of C₇₀.



4.1 Introduction.

The chemistry of the C_{70} molecule has yet to be explored to the same extent as that of C_{60} despite the fact that it should display a greater variety of reactions. For C_{70} , spectroscopy and theoretical considerations have focussed on the D_{5h} structure (Fig.4.1), which consists of 12 pentagonal faces fused to 25 hexagonal faces. In this structure there five different types of carbon atom and eight distinct types of C-C bonds. Four of these types are formed at fusions of two six membered rings and the other four at fusions of five and six membered rings. We have seen in Chapter 3 how the reactivity noted so far is exclusively at a 6:6 fusion. Hirsch *et al.*⁽¹⁾ have proposed a numbering scheme for C_{70} where the 5 different sets of C-atoms are assigned as N, 3, 2, 1, e, -1 etc.



(4.1)

The closest geometrical similarity to C_{60} is given at the pole areas of C_{70} . Although the regiochemistry for additions to the fullerene core seems to be more complicated in the case of C_{70} , predictions on nucleophilic additions indicate, that among the large number of possible isomers only a few are energetically favoured.⁽¹⁾ Hirsch has calculated the most energetically favoured isomers which result from a nucleophilic addition followed by protonation(Fig.4.2).

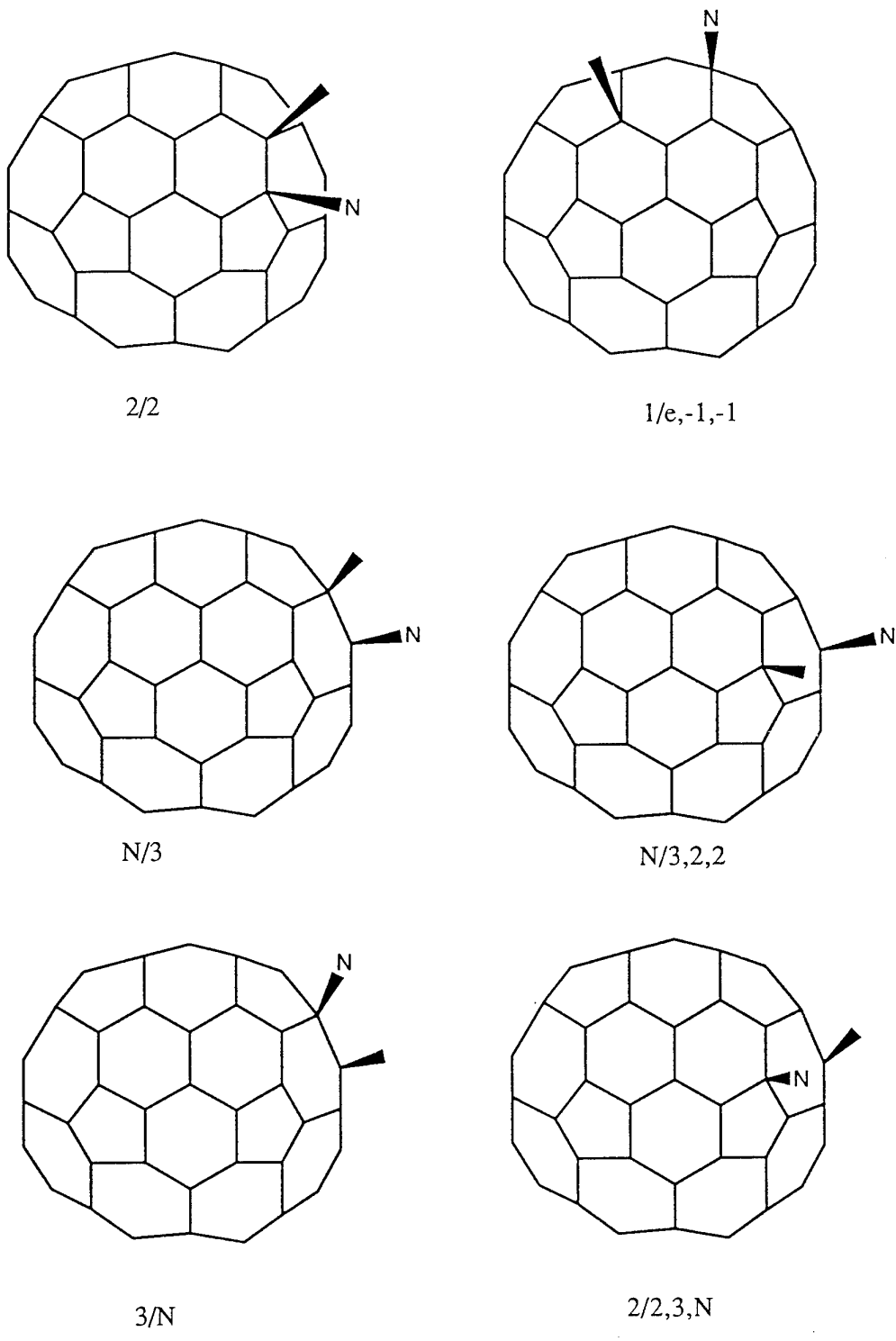
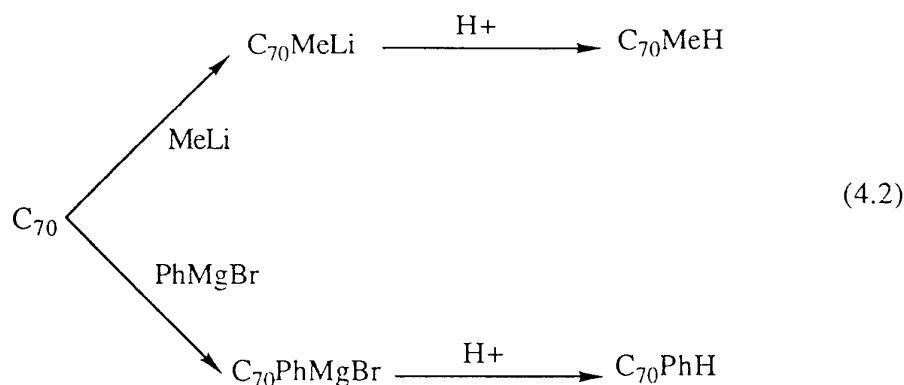
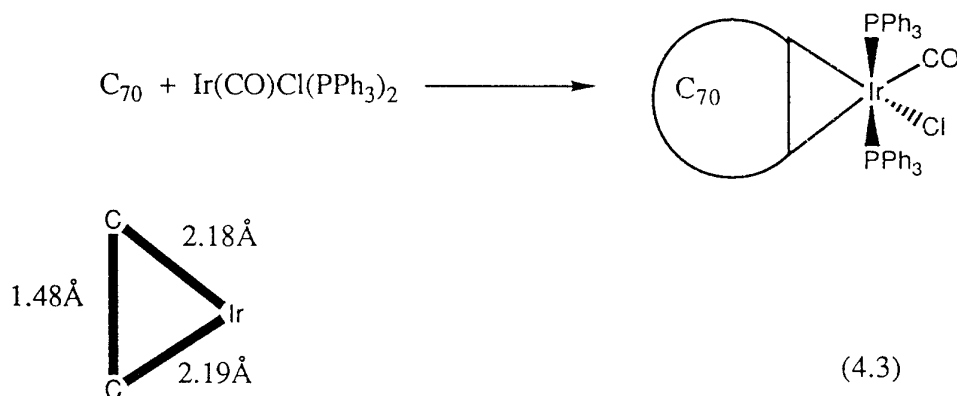


Fig.4.2 The six most energetically favoured isomers of $C_{70}NuH$ as calculated by Hirsch. For η^2 -addition of a metal the isomers $3/N$ and $N/3$ are identical as are $N/3,2,2$ and $2/2,3,N$.

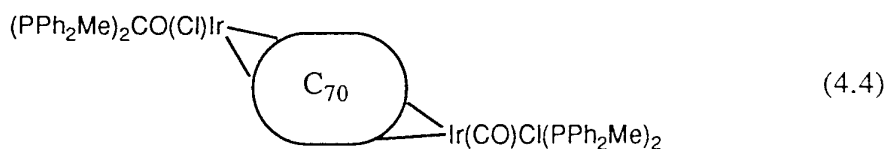


Out of the thousands of possible isomers six energetically favoured arrangements were found. The isomers have the notation (a) 2/2, (b) 1/e,-1,-1, (c) N/3, (d) N/3,2,2, (e) 3/N (f) 2/2,3,N. The position of the nucleophile is given by the character before the dash, followed by the path to the position of the added proton. Hirsch followed these calculations with a series of elegant experiments which showed that the nucleophilic addition reactions proceeded at the N/3 position exclusively. Earlier Balch *et al.*⁽²⁾ had synthesised the first organometallic derivative of C₇₀ through the addition of Vaska's compound. The addition of the metal centre was shown with a crystallographic structure to occur on the N/3(6:6) fusion position. The bond lengthening of the C=C is identical to that seen for the C₆₀ analogues with the subsequent formation of metallocyclopropane structure (Fig.4.3).



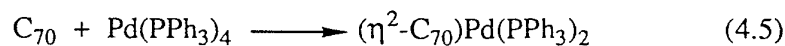
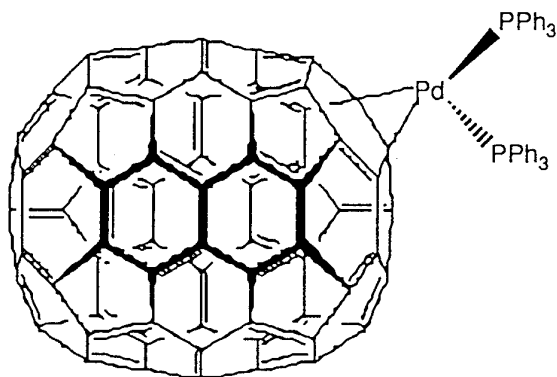
The measured bond lengths agree with the theoretical calculations of Negri *et al.*⁽³⁾, which predict the equatorial bonds to be the longest (1.46 Å) and the 2/2 and N/3 bonds to be the shortest (1.38 Å and 1.37 Å respectively). Simple geometric considerations show that the N/3 addition is the most favoured as the other 6:6 fusions all have a more flattened local structure which would require much larger distortion to accommodate metal co-ordination. Balch *et al.*⁽²⁾ suggest that Vaska's compound will be a useful reagent for obtaining crystalline samples of the higher fullerenes whose structures

remain to be crystallographically determined. Other workers have produced the remarkable compound (Fig.4.4) by the addition of two equivalents of the Vaska's analogue. The crystal structure reveals that both metal centers are added over two 6:6 fusions at the N/3 and N/-3 positions.



4.2 Reaction of C₇₀ with Pd(PPh₃)₄.

The reaction of C₇₀ with Pd(PPh₃)₄ (Fig.4.5) in toluene produced a black precipitate. After work-up the fine black/green powder was found to be soluble in a range of chlorinated and aromatic solvents. The product produces green solutions in these solvents similar to the C₆₀ compounds. The product produces green solutions in these solvents similar to the C₆₀ compounds. The visible spectrum of the compound is again similar to the C₆₀ analogue. The ligand to metal charge transfer band at 435nm is stronger but the red-shift of the absorptions centered at 550nm is not as pronounced as in the C₆₀ product. Due to the lower symmetry of C₇₀ in comparison to C₆₀ there are many more infrared and Raman active modes in C₇₀. Group theoretical analysis ⁽⁴⁾ indicates that C₇₀ has 53 Raman active modes and 31 infrared active modes. The metal adducts would therefore be expected to have even more modes due to a further reduction in the symmetry. Many of these modes in the infrared are however very weak and are not observed. The i.r. of the product recorded as a solid on CsI displays the expected peaks for the phenyl groups (C-H str. at 3054cm⁻¹) and a number of peaks which can be attributed to the C₇₀ molecule around 1436cm⁻¹ and a series of peaks from 800cm⁻¹ to 400cm⁻¹.



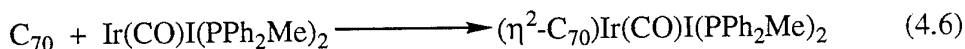
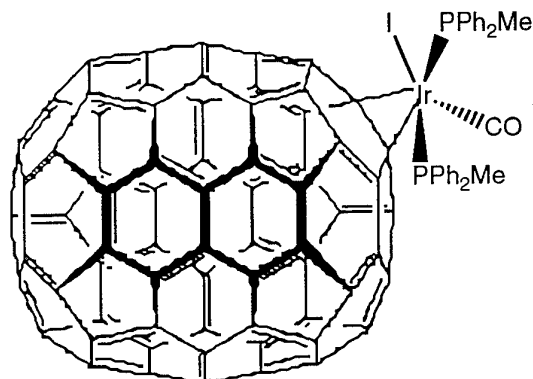
The Raman spectrum was obtained using excitation at 514nm. The strongest Raman peaks for C_{70} occur at 1565cm^{-1} , 1447cm^{-1} , 1227cm^{-1} and 1182cm^{-1} . The pattern between 1570cm^{-1} and 1420cm^{-1} is clearly visible in the Raman of the product and there is also a slight decrease in the frequency of the major peaks. The strong peak at 1227cm^{-1} has not shifted, but is slightly broader in the product. The feature at 1062cm^{-1} appears to be shifted to 1034cm^{-1} which is the largest noticeable shift in the spectrum. In the lower end of the spectrum the most noticeable feature is the strong sharp peak at 564cm^{-1} which is not present in the C_{70} spectrum. As yet this peak is unassigned. Other small Raman signals are visible which correspond to positions in the C_{70} spectrum but the signals are weak and broad. As there is still discussion on the correct assignment of the Raman modes it is difficult to explain these changes. The ^{31}P nmr contains a single resonance at 26ppm as in the starting material, there was no evidence of free triphenyl phosphine. The ^1H nmr is also simple containing a single multiplet between $\delta 7.02$ and $\delta 7.78$ indicative of the phenyl protons. The ^{13}C nmr is complicated. A total of 35 different carbon environments exist for a η^2 -bonded C_{70} molecule. Many of the resonances are visible including the ones attributable to the phenyl moiety at $\delta 128\text{ppm}$ and $\delta 135\text{ppm}$ however to determine the precise geometry of the product it is necessary to observe the exact number of quaternary carbons. The FAB mass spectrum of the product contains several ions corresponding to fragments of the product (eg. $557\text{m/z}=\text{Pd}(\text{PPh}_3)(\text{PPh})^+$, $630\text{m/z}=\text{Pd}(\text{PPh}_3)_2^+$). There is an unusual couple of strong peaks at 1577m/z and 1762m/z , these could correspond to a disubstituted C_{70} product ($1577\text{m/z} = \text{PdC}_{70}\text{Pd}(\text{PPh}_3)_2^+$ and $1762\text{m/z} = \text{C}_{70}(\text{Pd}(\text{PPh}_3)_2\text{Pd}(\text{PPh}_2))^+$).

4.3 Reaction of C_{70} with $\text{Pt}(\text{PPh}_3)_2$.

The slow addition of $\text{Pt}(\text{PPh}_3)_4$ to a solution of C_{70} in toluene produced an emerald green solution. Work-up of this solution gave a dark green solid. The infrared spectrum of the solid is almost identical to the palladium analogue although more bands are visible in this spectrum around 1435cm^{-1} . The visible spectrum is identical also. The main features in the Raman spectrum between 1200cm^{-1} and 1700cm^{-1} are very similar to C_{70} . There is a small decrease in frequency (10cm^{-1}) in the bands centered around 1450cm^{-1} . The ^1H nmr displays the expected phenyl proton resonances between $\delta 7.12\text{ppm}$ and $\delta 7.85\text{ppm}$. The FAB mass spectrum shows signs of decomposition of the product in the matrix although some significant fragments are visible: $1220\text{m/z } C_{70}\text{Pt}(\text{PPh}_2)^+$, $1035\text{m/z } C_{70}\text{Pt}^+$ and $719\text{m/z } \text{Pt}(\text{PPh}_3)_2^+$.

4.4 Reaction of C₇₀ with Ir(CO)I(PPh₂Me)₂.

The reaction of the Vaska's analogue Ir(CO)I(PPh₂Me)₂ with C₇₀ did not proceed when the molar ratio was 1:1. However when an excess of the metal compound was added the reaction occurred immediately. As usual a black solid was isolated which was carefully analysed.



The infrared spectrum of the product clearly shows that the reaction has occurred with the increase in frequency of the carbonyl stretch to 2004cm^{-1} . This effect has been discussed in detail in Chapter 3. It is indicative of the electron withdrawing nature of the fullerene. The rest of the infrared spectrum displays the typical bands for the methyl and aryl moieties and for the C₇₀ molecule. The visible spectrum is noticeably different from the others in that the absorptions have lower extinction coefficients. This is probably due to the low solubility of the product which made such measurements difficult due to precipitation. This also led to difficulties in recording the ¹³C nmr. Usually very long collection times (days) are necessary ($\tau > 20\text{s}$) for a ¹³C spectrum of these compounds. The low solubility of this product was such that it was impossible to obtain reasonable spectra. The ³¹P nmr can be obtained in seconds and the single resonance at $\delta 37\text{ppm}$ in the spectrum was the same as the starting material. The Raman spectrum of the product exhibits the characteristic features expected. The strong signal at 1560cm^{-1} has been down-shifted by 5cm^{-1} from the parent fullerene as have the peaks at 1445cm^{-1} and 1465cm^{-1} . The strong peak at 1227cm^{-1} in the parent fullerene does not shift substantially for the iridium derivative. The lower frequency signals do not yield much information owing to their multiplicity and intensity. The frequency lowering observed for these materials is similar to that observed for the C₆₀

derivatives and has been explained in Chapter 3. The mass spectrum of the product again demonstrates the difficulty with these materials. The molecular ion is not observed but fragmentation is evident from the strong ion peaks at 591m/z $\text{Ir}(\text{PPh}_2\text{Me})_2^+$, 621m/z $\text{IrI}(\text{PPh}_2\text{Me})^+$ and 721m/z $\text{IrI}(\text{PPh}_2\text{Me})_2^+$. As in other examples their are peaks which are higher (2055m/z) than the expected molecular ion which suggests that the compound has reacted with the matrix or that a recombination occurs in the beam.

4.5 Reaction of C_{70} with $\text{Mo}(\text{CO})_3(\text{MeCN})_3$.

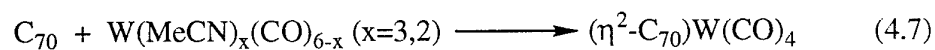
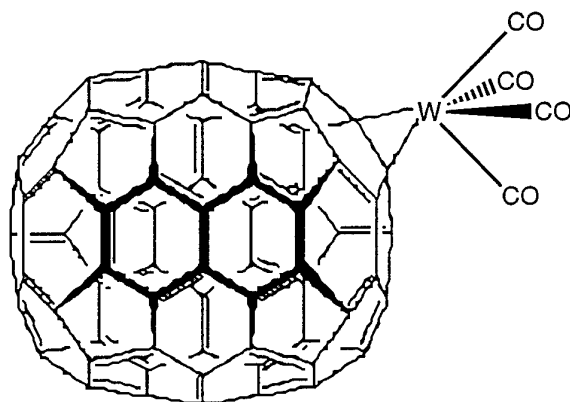
The attempts to obtain an η^6 -bonded C_{60} compound have been outlined in Chapter 3. The failure is attributable to the tilt of the available p-orbitals on the surface of the fullerene away from the centre of the hexagon. This effect is quite pronounced for C_{60} with calculations estimating the outward tilt to be in the region of 22° away from a parallel orientation. The use of large metals (Mo, W) did not overcome this problem. However with C_{70} the situation should be different. From spectroscopic(5) and crystallographic studies(2) the structure of C_{70} has been solved. The poles of C_{70} are very similar physically and chemically to the surface of C_{60} . The difference lies in the structure around the equator of C_{70} . Here the surface is flatter than at the poles and one would expect therefor the p-orbitals to tilt significantly less than at the poles. Hirsch has identified an equatorial bond which is an energetically favoured position for additions, the 1/e,-1,-1 bond. This would seem to favour the possibility of η^6 -bonding.

C_{70} was added to a solution of $\text{Mo}(\text{CO})_3(\text{MeCN})_3$ to give a purple solution from which was isolated a black solid. This black solid when redissolved gives a green solution. The product was worked-up from the green solution. The infrared spectrum of this product displays an almost identical carbonyl stretching region with four peaks: 2083cm^{-1} , 2026cm^{-1} , 1882cm^{-1} and 1834cm^{-1} . There are also the expected peaks for C_{70} in the spectrum. The visible spectrum is identical to the C_{60} analogue. The Raman spectrum of the product exhibits the usual broadening of the lower frequencies but the shifts are very small in the higher frequency modes compared to the other metal derivatives. Although this is inconclusive it was decided to study the tungsten analogue.

4.6 Reaction of C_{70} with $\text{W}(\text{CO})_x(\text{MeCN})_{6-x}$ ($x=3,2$).

The reaction with the tungsten compound was then attempted. This proceeded in exactly the same way as the C_{60} reaction. A green solution was obtained immediately on addition of the metal to the C_{70} solution. A black solid was extracted from this green solution. The infrared spectrum exhibits four carbonyl frequencies: 2043cm^{-1} , 1970cm^{-1} , 1900cm^{-1} and 1847cm^{-1} . There were no peaks attributable to acetonitrile and the C_{70} peaks were observed as previously. As discussed in Chapter 3 the four

carbonyl stretching frequencies are indicative of an $L_2M(CO)_4$ formula and this concurs with the hypothesis that the C_{70} is adding in an η^2 -fashion (Fig. 4.7).



The fact that no acetonitrile is present in the product tends to support this view. This formula is difficult to explain for the molybdenum compound. However the hypothesis that C_{70} may be more likely to give η^6 co-ordination remains to be proven.

4.7 Experimental.

4.7A Reaction of C₇₀ with Pd(PPh₃)₄: C₇₀(210mg, 0.25mmol) was dissolved in toluene(150cm³) to give the characteristic orange brown solution. A solution of Pd(PPh₃)₄ (280mg, 0.25mmol) in toluene(100cm³) was added dropwise to the stirring C₇₀ solution. The colour immediately darkened to give a black solution. The reaction ceased after 2 hours and the product stored at -25°C (8 h). A black precipitate separated and was isolated from the solution using a filter cannula. The dark green solid was dried on the vacuum line.(Yield 0.255g, 69%).

I.r (Thin film, NaCl) 3061w, 2967s, 1434s, 1262s, 1184w, 1091s, 797s, 741m, 692s, 674m, 665s cm⁻¹.

I.r (KBr disc) 3054w, 2970s, 2930m, 1438m, 1264s, 1190m, 1190s, 800s, 752m, 722m, 694w, 542m, 510w, 452m, 392m cm⁻¹.

Uv/vis (Toluene) λ(ε) = 435(12941), 555(6176), 600(6170), 650(4117) nm.

Raman (514nm) 494w, 521w, 564s, 680m, 957m, 706m, 790m, 1034m, 1065s, 1230m, 1356w, 1421m, 1452m, 1464s, 1552m, 1570m cm⁻¹.

¹H nmr (80MHz, CDCl₃) δ7.02-7.76(m, Arom H)ppm.

¹³C nmr (300MHz, C₆D₆) δ78.7(s), 102.6(s), 116.4(s), 125(m), 128(m),134.3(d), 137.5(m), 141.2(s), 142.4(s), 143.4(s), 143.7(s), 144.3(s), 145.2(s), 163.1(s) ppm.

³¹P nmr () δ26.017ppm.

FAB MS m/z(%) 1762(15), 1744(55), 1735(83), 1577(35), 1168(15), 1060(7), 907(10), 858(13), 802(42), 769(37), 630(20), 557(52), 279(100).

4.7B Reaction of C₇₀ with Ir(CO)I(PPh₂Me)₂: A solution of Ir(CO)I(PPh₂Me)₂(37mg, 0.05mmol) in warm toluene(40cm³) was added dropwise using a cannula to a solution of C₇₀(42mg, 0.05mmol) in toluene(30cm³). No immediate colour change after 3 hours was noticed. A further 0.05mmol of the iridium starting material in solution was added. After 10 minutes the solution had darkened and a black solid began to precipitate. The reaction was stopped after a further 30 minutes and the black precipitate was isolated by removing the solution with a filter cannula. The product was dried by gently heating under vacuum (35 °C, <0.001mm Hg). Yield 72mg.

I.r (CsI disc) 3055w, 2967s, 2928s, 2853m, 2004s, 1433s, 1263s, 1183m, 1099s, 887m, 801s, 738m, 692m, 577s, 527w, 507w, 454w, 394w, 350w cm⁻¹.

Uv/vis (Toluene) λ(ε) = 404w(6349, 460(4761), 550(3015), 600(2222) nm.

Raman (514nm) 410m, 455m, 496s, 575s, 702s, 740s, 782s, 1060vs, 1230s, 1330m, 1445s, 1465s, 1525w, 1560vs cm^{-1} .

^1H nmr (80MHz, CDCl_3) δ 1.92(s,br,3H), 7.03-7.76(m,11H) ppm.

^{31}P nmr δ 37ppm.

FAB MS $m/z(\%)$ 2055(7), 1567(5), 1269(7), 980(10), 903(7), 849(25), 821(100), 721(32), 647(33), 621(25), 591(37), 413(29).

4.8C Reaction of C_{70} with $\text{Pt}(\text{PPh}_3)_4$.

Synthesis of $\text{Pt}(\text{PPh}_3)_4$: A saturated aqueous solution of K_2PtCl_4 (2.2g, 1mmol) was slowly added with vigorous stirring to a warm(65 $^\circ\text{C}$) saturated ethanolic solution of PPh_3 (6.5g, 5mmol) containing KOH (2.5mmol). A yellow precipitate formed immediately. The reaction was stirred for a further 5 minutes on a warm hot-plate. The resulting suspension was filtered on a Buchner funnel to give a bright yellow solid. This was washed with warm ethanol, cold water and finally with ethanol before being dried under vacuum

A solution of $\text{Pt}(\text{PPh}_3)_4$ (43mg, 0.03mmol) in toluene(40 cm^3) was added dropwise to a solution of C_{70} (26mg, 0.03mmol) in Toluene(40 cm^3). The solution immediately turned emerald green. After stirring (8 h) the solvent was removed on the vacuum line to give an impure dark green solid. The product was washed with cold ethanol (3x10 cm^3) to remove any residual PPh_3 affording the adduct (43mg, quantitative)

I.r (KBr disc) 3058w, 1481m, 1451w, 1435s, 1262s, 1198m, 1169m, 1095s, 799s, 742s, 720s, 692s, 618w, 581w, 539s, 508s, 452m, 396w cm^{-1} .

Raman (514nm) 1220w, 1240w, 1300m, 1340m, 1435s, 1450s, 1510w, 1560s, 1580w cm^{-1} .

^1H nmr (80MHz, CDCl_3) δ 7.12-7.85(m, Arom H) ppm.

FAB MS $m/z(\%)$ 2189(7), 2174(15), 2031(15), 1981(10), 1908(13), 1631(15), 1583(13), 1463(7), 1257(45), 1220(16), 1155(37), 1035(25), 898(20), 834(13), 675(20), 633(35), 398(100).

4.8D Reaction of C_{70} with $\text{Mo}(\text{MeCN})_3(\text{CO})_3$: $\text{Mo}(\text{MeCN})_3(\text{CO})_3$ (20mg, 0.07mmol) was dissolved in MeCN (5 cm^3) and added dropwise to C_{70} (59mg, 0.07mmol) in toluene(50 cm^3). The solution turned dark purple immediately and was left stirring (72 h). The purple colour faded and a black precipitate separated from the reaction. The precipitate was separated from the solution by filtering off the solvent using a filter cannula. The black air sensitive solid was dried on the vacuum line. When the product was dissolved in thf or toluene it gave green solutions. Work-up of these solutions gave dark green solids. The green solid was air and light-sensitive.

Analysis of the product proved difficult as the compound started to decompose as soon as the beam(i.r or uv/vis) passed through the solution.

I.r (CsI disc sandwich) 2953w, 2324w, 2083m, 2026s, 1882s(br), 1834s, 1436m, 1366w, 1189w, 1034m, 775m, 743m, 644w, 610m, 577m, 561w, 505m, 471m, 361w cm^{-1} .

Uv/vis (Toluene) λ_{max} 368, 440-900w nm.

Raman (514nm) 1568s, 1516w, 1470s, 1451w, 1365w, 1340m, 1236s, 1082s, 700-800triplet w, 572w, 400-500multiplet w cm^{-1} .

4.8E Reaction of C_{70} with $\text{W}(\text{MeCN})_3(\text{CO})_3$: A yellow saturated solution of $\text{W}(\text{MeCN})_3(\text{CO})_3$ (39mg, 0.1mmol) in $\text{MeCN}(8\text{cm}^3)$ was added dropwise with stirring to a solution of C_{70} (84mg, 0.1mmol) in toluene(45cm^3). The solution darkened immediately and after 1 minute had turned green. toluene(20cm^3) and $\text{MeCN}(8\text{cm}^3)$ were removed on the vacuum line and the remaining solution was stored at $-27\text{ }^\circ\text{C}$ (24 h).

The dark green precipitate which separated was dried on the vacuum line to give an air and light sensitive solid(78 mg). The product was less sensitive to air and light than the molybdenum adduct but the analysis still proved difficult.

I.r (CsI disc sandwich) 2043m, 1970s, 1900s, 1847s, 1775s, 1455w, 1354w, 1182m, 1022s, 778m, 729m, 716s, 702m, 655m, 577m, 525s, 416m cm^{-1} .

References.

1. H. R. Karfunkel, A. Hirsch, *Angew. Chem. Intl. Ed.*, 1992, **31**, (1), 1468.
2. A.L. Balch, V.J. Catalano, J.W. Lee, M.M. Olmstead, S.R. Parkin. *J. Am. Chem. Soc.*, 1991, **113**, 8953.
3. F. Negri, G. Orlandi, F. Zerbetto, *J. Am. Chem. Soc.*, 1991, **113**, 6037.
4. D.S. Bethune, G. Meijer, W.C. Tang, H.J. Rosen, W.G. Golden. H. Seki, C.A. Brown, M.S. de Vries, *Chem. Phys. Lett.*, 1991, **179**, 181.

CHAPTER 5.

Non-Linear Optics of Fullerenes

and

Metallofullerenes.

5.1 Introduction.

The field of nonlinear optics draws on a wide variety of materials from organic through organometallic to inorganic systems. The organic systems which have been studied are great in number and reflect the low cost, and ease of synthesis of these materials. There are two main groups, those displaying a high second-order hyperpolarizability ($\chi^{(2)}$) and those investigated for third order non-linearity ($\chi^{(3)}$). Only the latter will be considered here. The nature of nonlinear optical phenomena, and their interpretations and applications are covered elsewhere. A general discussion of principles and applications is given by Prasad and Williams.⁽¹⁾

Investigations in the field of third order non linearity and also in the field of conducting and semiconducting materials have been directed towards conjugated organic and organometallic polymers because of the limitations imposed by inorganic systems. The most important of the organic materials is polydiacetylene.

Wegner⁽²⁾ synthesised (poly(2,4-hexadiyne-1,6-diyl-di-*p*-toluene sulphonate)) by irradiation of crystals of the monomer. This method permitted the synthesis of many other polydiacetylenes. Soluble polydiacetylenes such as poly[4,6-decadiyne-1,10-diolbis(3-butoxycarbonylmethylurethane)](p3.B.C.M.U). which were first synthesised by Patel⁽³⁾ have a much improved third order response over the earlier polydiacetylenes. The reason is that the new form of the polymer called the "exitonic" form confines the electron excitation to one direction. There are some drawbacks to these materials in their synthesis and stability. Such studies prompted investigations into other conjugated polymers such as polythiophene, polybenzothiophene, polyphenylene and polyaniline.

The inorganic materials investigated are relatively simple molecules. Certain forms of semiconducting gallium arsenide and indium antimonide have been shown to display large optical non-linearities. Multilayer semiconducting materials which have been synthesised using new crystal growth techniques⁽⁴⁾, exhibit special optical properties not apparent in the bulk material. This has been shown to be due to quantum size effects. Semiconducting materials have some aptitude in optical devices due to the properties which arise due from the limitation of the length of electron-hole correlation to the order of the exciton Bohr radius (*ca.*100Å). The semiconductors have two major disadvantages (a) high cost due to the complexity of production and (b) strong absorption in the visible region which eliminates them from many applications.

Crystalline lithium niobate (LiNbO₃) and lithium tantalate (LiTaO₃) were the first such materials to demonstrate optical nonlinearities⁽⁵⁾. A photoinduced change in refractive

index and later a photorefraction were observed in crystals of other inorganic complexes such as $\text{Bi}_{12}\text{SiO}_{20}$ ⁽⁶⁾, KNbO_3 ⁽⁷⁾ and BaTiO_3 . The first application of this group of materials was in holographic storage and it was only later that their usefulness in non-linear optics was exploited. A change in polarisation due to photoinduced charge transfer within the crystal⁽⁸⁾ is proposed to be the cause of the change in refractive index with low intensity incident visible or near infrared laser beams.

In recent years there has been a growing interest in organometallic materials and their applications in the field of nonlinear optics. These materials which have a large diversity of oxidation states and ligand environments potentially offer a far greater range than either organic or inorganic materials. Polarizable d-electrons (even f electrons!) present in organometallic systems may induce larger values of non-linearity than other systems. The third order optical nonlinearity of some metallocene systems such as ferrocene, hafnocene, ruthenocene, and zirconocene have been investigated by Winter *et al.*⁽⁹⁾ These materials have quite large second order molecular hyperpolarizabilities of the order of $10^{-45}\text{m}^5\text{V}^{-2}$ in the molten phase. Third order properties of platinum phenylacetylide polymers have been carried out by Frazier *et al.*⁽¹⁰⁾ and have shown a large non-linearity similar to the yellow form of p3.B.C.M.U. Prasad *et al.*⁽¹¹⁾ have investigated a range of polymeric ferrocene derivatives but with poor results attributed to the ineffective transfer of charge across the ferrocene moiety. Davey *et al.*⁽¹²⁾ conducted an extensive study of group 10 (Ni, Pd, Pt) polyacetylides. These well characterised polymers exhibit reasonably large third order non-linearities and a hyperpolarizability dependence on the type of metal and metal ligand was clearly demonstrated (*e.g.* Ni > Pt > Pd). Because of the small range of these types of materials available the studies are still in their infancy. Group 10 metal containing polymeric acetylides have received much of the attention because of their extended conjugated system consisting of a regular arrangement of square planar metals with acetylenic carbons in the polymeric chain. The extensive delocalised π -system resulting from the overlap of the metal π -orbitals with the alkyne π -orbitals in these polymers has shown interesting physical properties such as liquid crystalline behaviour⁽¹³⁾ and nonlinear optical effects.⁽¹⁴⁾

The majority of the nonlinear optical (NLO) measurements reported to date have been carried out in the near-infrared spectral region, away from any one photon resonance⁽¹⁵⁾. Meth *et al.*⁽¹⁶⁾ measured the dispersion of the third-order NLO response of a C_{60} film by third harmonic generation (THG) over the fundamental wavelength range .1-2.4 μm . Their study showed a three-photon resonance centered at 1.32 μm . The first degenerate four wave mixing (DFWM) study of C_{60} was reported by Blau *et al.*⁽¹⁷⁾. A predominantly pulse-limited NLO response was measured using 35ps pulses at 1.064 μm . The third order optical susceptibility $\chi^{(3)} = 7 \text{ E-12 esu}$, compares well with the value of 4 E-12 esu determined by THG, away from the three photon

resonance. Kafafi *et al.* have investigated the NLO properties of C₆₀ and C₇₀ films by time-resolved DFWM, at 597nm and 675nm.⁽¹⁵⁾ Their figures agree with previous studies. Tutt and Kost⁽¹⁸⁾ first reported the phenomenon of "optical limiting" in solutions of C₆₀. For optical limiting to occur at a particular wavelength, the material must possess a weak but non-zero absorption at that wavelength. However at the given wavelength there must be a higher energy transition with a large excited-state absorption cross-section from the state that is populated from the residual ground state absorption. Hence a material can act as a saturable absorber for wavelengths of light within a strong absorption band and as an optical limiter at wavelengths that are in a relatively transparent region. The large triplet excited state absorption makes C₆₀ an ideal molecule for optical limiting. The optical limiting threshold for C₆₀ is very low due to the extended lifetime of the triplet state (up to 100μsec).

The absorption co-efficient of a molecule may be written as

$$\alpha = \alpha_0 + \Delta\alpha \quad (5.9)$$

where $\Delta\alpha = \beta I$. Thus if $\beta > 0$ the absorption will grow with increasing intensity. β is called the "two photon co-efficient". Two photon absorbance (TPA) arises from the simultaneous absorption of 2 photons of frequency ω by an electron and its promotion to an excited real state is *via* a virtual level (Fig.5.9). (Theory shows ⁽¹⁹⁾ that the strength of the nonresonant third order nonlinear optical response of conjugated materials is strongly affected by an electron-electron repulsion which arises mainly from a previously undiscovered energetically high lying two-photon state that has a large excited-state absorption cross-section.) However what is believed to be happening in C₆₀ is different. Under resonant excitation the ground state of the molecule, S₀, becomes depleted, electrons being promoted to S₁ and/or S_n. In S₁ the molecule may relax radiatively into S₀(fluorescence) or *via* an intersystem crossing end up in T₁. Radiative decay from T₁ to S₀ is forbidden and so T₁ has a long lifetime. Reported values for the intersystem crossing time are very fast in the order of picoseconds⁽²⁰⁾ hence electrons in S₁ have little chance to fluoresce. This results in a highly efficient population of T₁.

The term given to this phenomenon is "excited-state absorption" or "reverse saturable absorption" and the origin of the optical limiting in C₆₀ is agreed to be an RSA process. This a nonlinear process and is specifically related to the imaginary component of $\chi^{(3)}$.

5.2 Aims.

The availability of a range of organometallic C₆₀ derivatives prompted the study of their nonlinearity using the Z-scan technique. To our knowledge there have been no studies of any C₆₀ (let alone C₇₀) derivatives in the literature. The aims of the study were (1) to measure the Im($\chi^{(3)}$) component of the third order nonlinear response of a range of fullerene organometallics and to compare their magnitudes with the parent fullerenes,

and (2) to identify and explain any trends present between the different metals Pd, Pt and Ir.

5.3 Z-scan technique.

There are numerous techniques for the measurement of nonlinear effects in materials. Nonlinear interferometry⁽²¹⁾, degenerate four-wave mixing⁽²²⁾, nearly degenerate three-wave mixing⁽²²⁾, ellipse rotation⁽²³⁾ and beam distortion methods⁽²⁴⁾ are among the most common. The first three techniques are sensitive but require a complex experimental set-up. Beam distortion methods require precise beam scans followed by complex wave propagation analysis. In 1990 a paper by Sheik-bahae *et al.*⁽²⁵⁾ described a new technique which was called Z-scan. This single beam technique was developed for measuring the sign and magnitude of refractive nonlinearities. Using a Gaussian laser beam in a tight focus they measure the transmittance of a nonlinear medium through a finite aperture as a function of the sample position (Z) measured with respect to the focal plane (Fig.5.1)

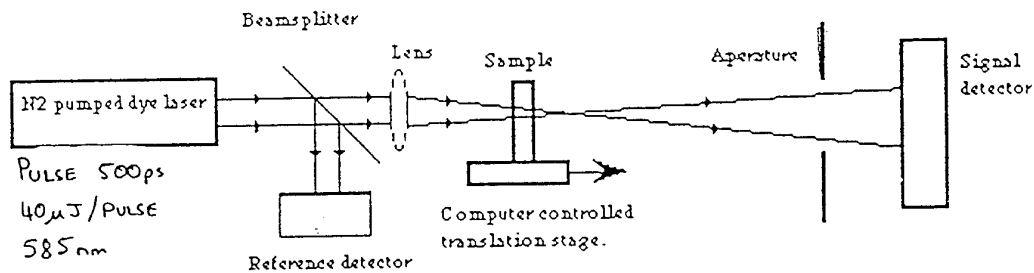


Fig.5.1

Starting the scan from a distance far away from the focus (-Z), the beam irradiance is low and negligible nonlinear refraction occurs, hence the transmittance remains relatively constant. As the sample is brought close to the focus the beam irradiance increases, leading to self-lensing in the sample. A negative self-lensing prior to focus will tend to collimate the beam, causing a beam narrowing at the aperture which results in an increase in the measured transmittance. As the scan in Z continues the sample passes the focal plane to the right (+Z), the same self-defocussing increases the beam divergence, leading to a beam broadening at the aperture and hence a decrease in the transmittance. This suggests that there is a null as the sample passes the focal plane. This is analogous to placing a thin lens at or near the focus, resulting in a minimal change in the far-field pattern of the beam. The power of the beam is measured and using this a range of intensities for the beam position (Z) can be calculated. The data gathered is displayed as a plot of transmittance vs intensity. The Z-scan is completed as

the sample moves away from the focus such that the transmittance becomes linear since the irradiance is again low (this describes the negative nonlinearity i.e peak and then valley. The opposite may be observed (valley then peak) for a positive refractive nonlinearity). Multiphoton absorption suppresses the peak and enhances the valley, whilst saturation effects produce the opposite effects. Large refractive nonlinearities in materials are commonly associated with a resonant transition which may be of single or multiphoton nature. The nonlinear absorption in such materials from either direct multiphoton absorption or saturation of the single photon absorption have strong effects on the measurement of nonlinear refraction using the Z-scan technique. Z-scan traces with no aperture allow the co-efficients of nonlinear absorption to be easily calculated. Z-scan has been shown to compare very favourably with other methods.⁽²⁵⁾ For a three-level mode for which two absorption cross-sections are involved (Fig.5.8) the change in the absorption co-efficient α is related to the saturation intensity which is related to the total absorption α_{tot} of the system(5.2)

$$\alpha_{tot} = \sigma_0 n_1 - \sigma_0 n_3 + \sigma_{ex} n_5 \quad (5.2)$$

where n is the total number density of molecules. Using the Beer-Lambert law a saturation transmittance is found

$$T_{sat} = (T_o \cdot T_{ex})^{1/2} \quad (5.3)$$

where T_o and T_{ex} are the low and high-level transmissions respectively. To simplify the model the following assumptions can be made,

- (1) relaxation from the triplet state T_1 to the ground state S_o will take place on a time scale much longer than the pulse width and thus can be neglected
- (2) The propagation of the higher excited states (S_n, T_n) are very small and can be neglected due to their short relaxation times.

On solving the simplified rate equations for the three level system we can obtain the ground state absorption cross-section (5.4)

$$\sigma_o = \frac{-\ln T_o}{CNal} \quad (5.4)$$

and then the excited state absorption cross-section (5.5)

$$\sigma_{ex} = \sigma_o \frac{\ln T_{ex}}{\ln T_o} \quad (5.5)$$

If $\sigma_{ex} < \sigma_o$ then saturable absorption is observed *i.e.* an increase in transmittance with increasing intensity. Inverse saturable absorption is observed when $\sigma_o < \sigma_{ex}$.

The absorption co-efficient is directly related to the imaginary part of the third order nonlinear susceptibility $\text{Im}(\chi(3))$ by (5.6)

$$\text{Im}(\chi(3)) = \frac{\epsilon_0 c n_0 \lambda \Delta \alpha}{4 \pi I} \quad (5.6)$$

where ϵ_0 is the permittivity of free space, c is the velocity of light, n_0 is the linear refractive index and λ is the wavelength of the laser. This can be modified⁽²⁶⁾ to give (5.7)

$$\text{Im}(\chi(3)) = \frac{\epsilon_0 c n_0 N_a C (\sigma_{\text{ex}} - 2 \sigma_0)}{16 \pi I_{\text{sat}}} \quad (5.7)$$

where N_a is Avogadro's number and C is a molar concentration.

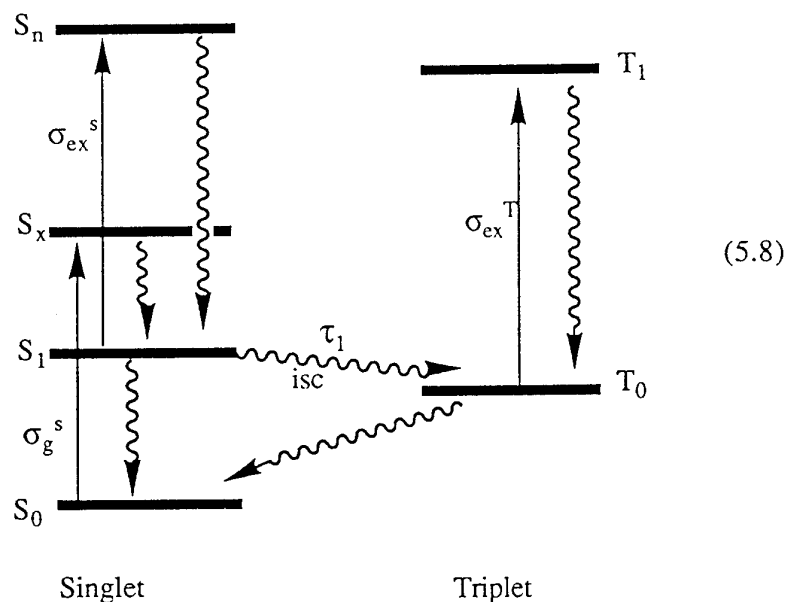


Fig.5.8 Energy level diagram. The absorption cross sections are given by σ_g^S , σ_{ex}^S and σ_{ex}^T , where g denotes the ground state, ex denotes excited state.

5.4 Absorption spectra.

The absorption spectrum of C_{60} exhibits a broad band centered around 550nm. The spectrum of C_{70} is different in that there is a band centered at 450nm which extends out to 700nm also because of the reduced symmetry of C_{70} relative to C_{60} the S_0 - S_1^* transition is not as strongly forbidden and the visible maxima are much stronger. The homo(H_u)-lumo(T_{1u}) excitation for C_{60} consists of fifteen transitions, all of which are optically forbidden and are predicted to lie to the red of the first optically allowed transition. Absorption bands observed between 410nm and 620nm have been assigned to these forbidden transitions from the singlet A_g ground state to excited states with triple (T_{1g} , T_{2g}), quadruple (G_g) or quintuple (H_g) degeneracy⁽²⁷⁾. The optical

forbiddenness is partially lifted by Herzberg-Teller interactions in which excitation of a vibration of a suitable symmetry results in symmetry borrowing from an allowed transition. The degeneracy of the upper states may be removed by Jahn-Teller distortions. In solution, the bands in the 560-620nm region have been assigned to vibronically allowed transitions between the A_g and the quasi-degenerate T_{1g} and T_{2g} states. The broad absorption band measured for solid C_{60} between 550nm and 650nm appears to be associated with these transitions. A series of very weak bands between 640nm and 700nm for C_{60} in solution has been assigned to the spin and orbitally forbidden 1A_g - $^3T_{1g}$ transition, one of the lowest singlet-triplet transitions. It is possible that the observed absorptions in the solid are due to similar transitions. A detailed spectral assignment for C_{70} has not yet been reported. The absorption spectra of the metal derivatives of C_{60} display a red shift in the absorptions between 450nm-650nm out to 550nm to 800nm. These absorptions are much stronger than in the parent fullerene. A large ligand to metal charge transfer band is visible in all the samples between 430nm and 500nm. The C_{70} metal complexes exhibit similar effects. The charge transfer bands appear stronger than the C_{60} derivatives but C_{70} has a strong absorption in the same region. The absorptions between 500nm-650nm are not red-shifted to the same extent as in the C_{60} derivatives

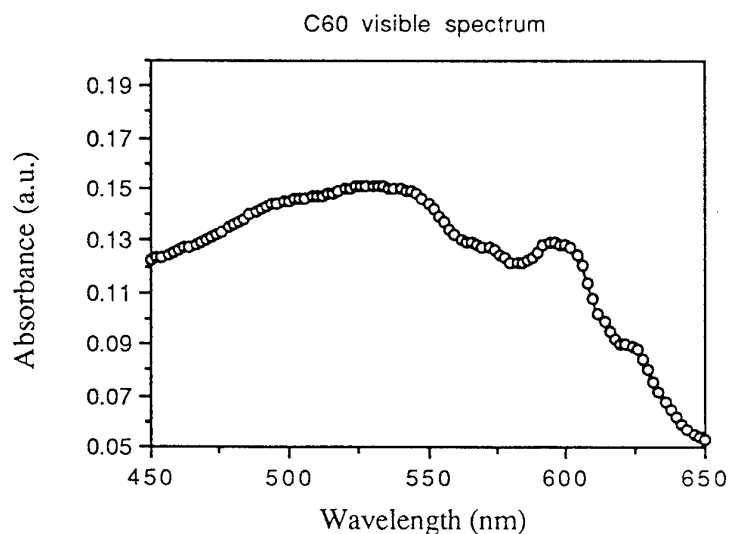


Fig. 5.9

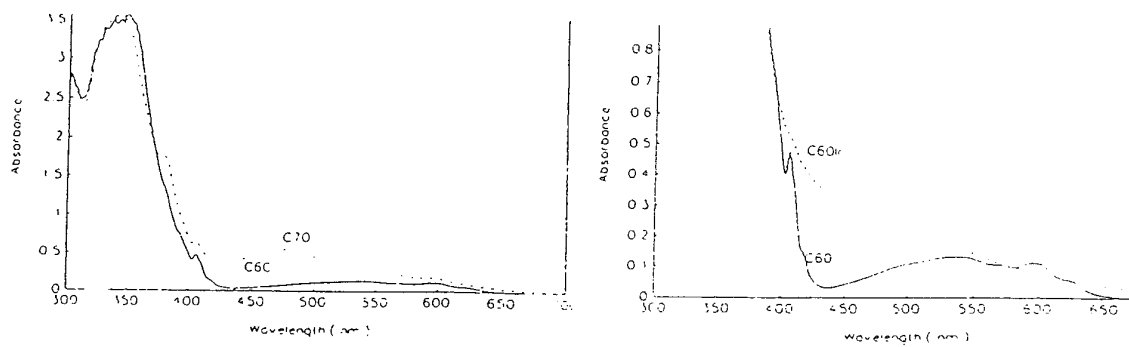


Fig. 5.10 Visible spectra of C₆₀ and C₇₀.

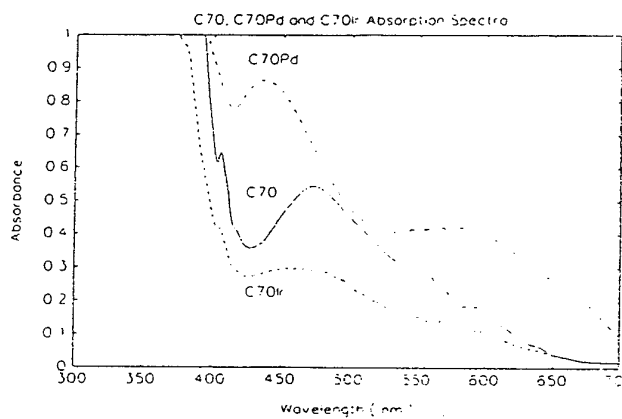
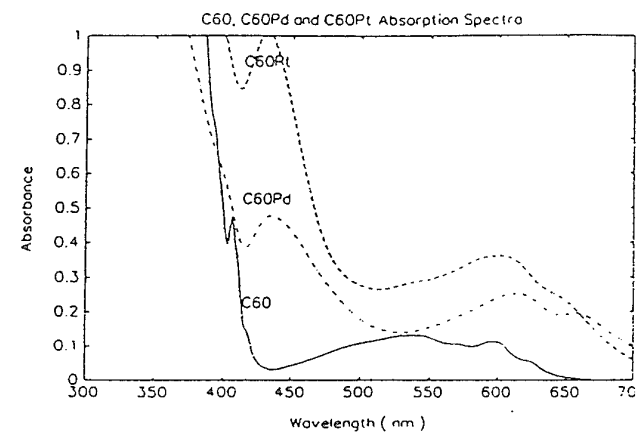


Fig. 5.11 Visible spectra of metal derivatives.

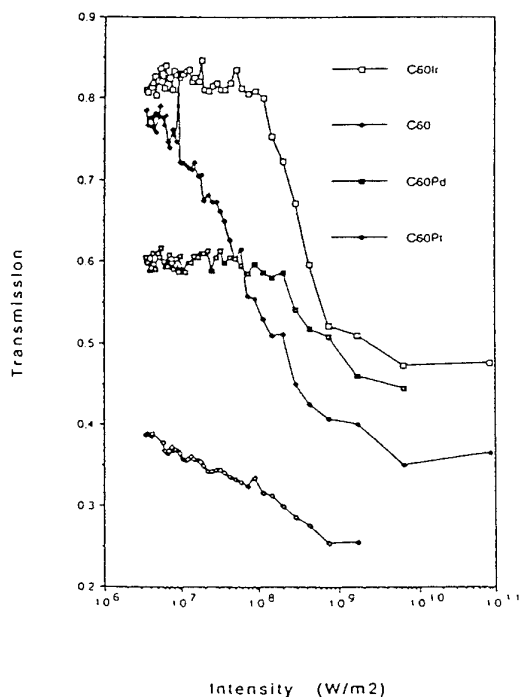
5.5 Experimental.

The nonlinear absorption measurements were performed using a PRA LN100 nitrogen pumped dye laser with rhodamine 6G as the lasing dye. This laser has a pulsewidth of 500ps and lasing at 588nm gave a typical energy output of 40μJ/pulse. Samples under investigation were contained in a 1mm quartz cuvette and placed on a linear translation stage which permits the sample to be moved through the focal plane of a 5cm lens. Variations of the transmitted fluence with incident intensity were measured using wide array photodiodes and a digital storage oscilloscope interfaced to a PC. The maximum incident intensity was 100GW/m², which occurred at focus. Data points were averaged over 20 laser shots with a repetition rate of 1Hz.

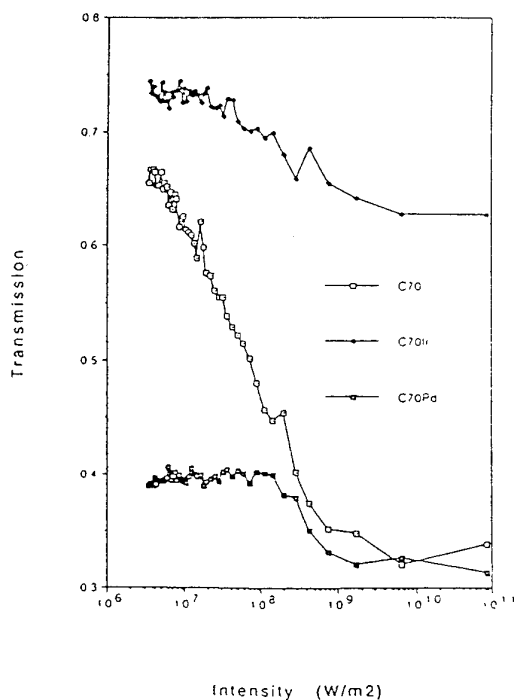
5.6 Results.

Figures 5.12 and 5.13 show the transmission vs intensity plots for the C₆₀ and C₇₀ derivatives respectively.

Transmission vs Intensity of C60 and Derivatives



Transmission vs Intensity of C70 and Derivatives



From these plots we can calculate the absorption cross sections which allows us to calculate the $\text{Im}(\chi^{(3)})$ component. The calculated values are shown in Table 5.14.

Sample	σ_0 (cm ²)	σ_{ex} (cm ²)	$\text{Im}\chi^{(3)}$ (m ² /V ²)
C ₆₀	1.45 E-18	6.03 E-18	1.78 E-16
C ₆₀ Pd	5.61 E-18	9.08 E-18	1.55 E-17
C ₆₀ Pt	1.14 E-17	1.64 E-18	1.32 E-16 (5.14)
C ₆₀ Ir	2.56 E-18	7.14 E-17	4.14 E-17
C ₇₀	1.16 E-17	8.05 E-18	7.55 E-17
C ₇₀ Pd	1.16 E-17	1.42 E-17	5.78 E-17
C ₇₀ Ir	3.46 E-18	8.91 E-18	2.64 E-17

5.7 Discussion.

The first result obvious from these measurement is that the size of $\text{Im}(\chi^{(3)})$ for the derivatives is lower (except for Pt C₆₀) than the parent fullerene although the difference is small. It is known that when organic materials are co-ordinated with heavy metals (or atoms) that any fluorescence may be quenched due to the increased spin-orbit coupling promoted by the heavy atom. This occurs *via* an intersystem crossing, whereby one electron in a paired molecular system may change it's spin so both are aligned parallel leading to the formation of a triplet state in turn causing a higher intersystem crossing yield. If the presence of a heavy atom leads to increased triplet population then in the case of the organometallic fullerene it might be expected that any optical limiting behaviour would be enhanced due to the increased number of carriers available for excited state absorption. This is not evident from these measurements at 588nm. We have observed the significantly decreased fluorescence of the metal containing fullerenes at room temperature which is evidence *for* the presence of a heavy atom effect. However there is another effect which a metal has on the parent fullerene. We know from the crystallographic data of analogues that the η^2 -coordination mode results in a double bond in the fullerene being broken which reduces the π delocalisation on the surface of the fullerene. This would reduce the magnitude of the non-linear effect. It is obvious from these measurements that this effect outweighs the heavy atom effect in this system and leads to a lowering of the nonlinearity. For the C₆₀Pt compound we notice that the $\text{Im}(\chi^{(3)})$ value is slightly larger than the parent fullerene. This can be explained by the fact that (a) platinum is heavier than the other metals and hence has a larger heavy atom effect and (b) platinum is the transition metal that exhibits the strongest π -bonding feature⁽²⁹⁾ which suggest that this kind of

interaction is smaller for lighter metals and hence the delocalisation on the surface of the parent fullerene is disrupted to a lesser extent.

Two important points must be noted. First the visible spectra of the compounds, although very similar are not exactly the same. Therefore the relative enhancements of the nonlinearities due to thermal effects are different. Secondly all of the measurements are on-resonance.

Since none of the compounds absorb in the near infrared a series of experiments is underway to measure the third-order nonlinear susceptibilities of these compounds using the technique of degenerate four wave mixing at 1064nm. Any possible contributions from two-photon effects are discernable with this technique and do not pose a problem. The fluorescence yield of each compound is being measured to quantify the heavy atom effect in these materials.

5.8 $\text{Im}(\chi^{(3)})$ determination for $\{[(\text{MeCN})_3\text{YbFe}(\text{CO})_4]_2(\text{MeCN})\}$

The title compound was first prepared by Shore⁽³⁰⁾ and is described in detail in Chapter 2. The crystal structure of the compound displays a ladder polymer structure with Fe-Yb bonds and isocarbonyl links between the ytterbium atoms and the carbonyls on the iron atoms. Due to its unique structure and the fact that there is intense interest in organic ladder polymers for optical devices I decided to measure the imaginary component of $\chi^{(3)}$ for this compound.

The Yb-Fe polymer is extremely sensitive to atmosphere so the solution for measurement was prepared in the dry-box and placed into a 1mm cuvette attached to a Young's tap. The compound was then sealed in the cuvette and placed on the translation stage.

The value of $\text{Im}(\chi^{(3)})$ which was measured is of the order(averaged) of $10^{-19}\text{m}^2/\text{V}^2$ which is a large response for such a system. Several metalloporphyrins (PtTPP, ZnTPP, NiTPP and CuTPP) measured by Peuch⁽³¹⁾ give a response of the order of $10^{-20}\text{m}^2/\text{V}^2$ to $10^{-21}\text{m}^2/\text{V}^2$. These systems contain the π -conjugated porphyrin structure. The result seems to indicate that there is delocalisation along the polymer although resonance effects will need to be accounted for before a full explanation can be given. All of the measurements were obtained on-resonance. This is the first example of a third order nonlinear measurement on a lanthanide organometallic.

References

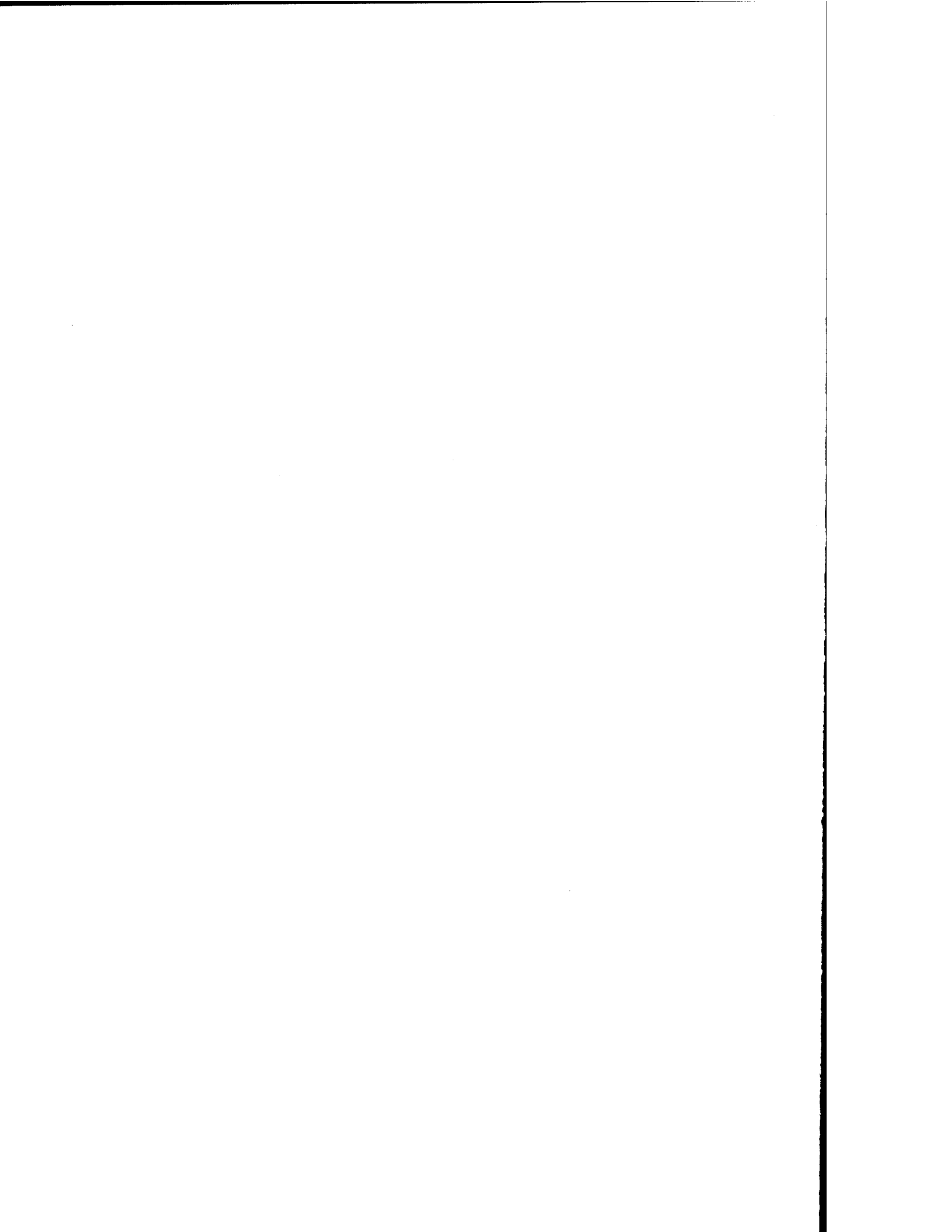
- 1 P.N. Prasad, D.J. Williams, *Introduction to Nonlinear Optical Effects in Molecules and Polymers*, Wiley, New, York, 1991.
- 2 G. Wegner, *Naturforsch.*, 1969, **24B**, 824.
- 3 G.N. Patel, *J. Polymer Sci., Polymer Lett.*, 1978, **16**, 609.
- 4 A. Ashkin, G.D. Boyd, J.M. Dizezik, R.G. Smith, A.A. Ballman, K. Nassau, *Appl. Phys. Lett.*, 1966, **9**, 72.
- 5 R. Dingle (Ed.), *Device and Circuit Applications of III-V Semiconductor Superlattice and Modulation Doping*, 1985, Academic, New York.
- 6 A.M. Glass, *Opt. Eng.*, 1978, **17**, 470.
- 7 D.L. Staebler, In *Holographic Recording Materials*, 1977, Ed. H.M. Smith, Springer Verlag, 101pp.
- 8 J.P. Huignard, G. Roosen, In *Nonlinear Optics, Materials and Devices*, 1986, Eds. C. Flytzanis and J.L. Oudar, Springer Verlag.
- 9 C.S. Winter, S.N. Oliver, J.D. Rush, *Organic Materials for Nonlinear Optics*, R.S.C., 1988, 232.
- 10 C.C. Frazier et al., *Materials for Optical Switches, Isolators and Limiters*, 1989, **14**, 1105.
- 11 S. Ghoshal, M. Samoc, P.N. Prasad, J.J. Tufariello, *J. Phys. Chem.*, 1990, **94**, 2847.
- 12 A.P. Davey, H.J. Byrne, H. Page, W. Blau, D.J. Cardin, *Synthetic Metals*, in press.
- 13 A. Carpita, A. Lessi, R. Rossi, *Synth. Commun.*, 1984, 571.

- 14 X. Lou, Ph D Thesis, TCD, 1993 and L. Odie, MSc Thesis, 1992.
- 15 S.R. Flom, R.G.S. Pong, F.J. Bartoli, Z.H. Kafafi, in press.
- 16 J.S. Meth, H. Vanherzeele, Y. Wang, *Phys. Rev. Lett.*, Submitted.
- 17 W.J. Blau, H.J. Byrne, D.J. Cardin, T.J. Dennis, J.P. Hare, H.W. Kroto, R. Taylor, D.R.M. Walton, *Phys. Rev. Lett.*, 1992, **68**, 2705.
- 18 L.W. Tutt, A. Kost, *Nature*, 1992, **356**, 225.
- 19 J. Messier *et al.*, (Eds) *Nonlinear Optical Effects in Organic Polymers*, Kluwer Academic, Boston, 1989.
- 20 R.A. Cheville, N.J. Halas, *Phys. Rev.* 1992, **B45**, 4548.
- 21 M.J. Weber, D. Milam, W.L. Smith, *Opt. Eng.*, 1978, **17**, 463.
- 22 S.R. Friberg, P.W. Smith, *IEEE J. Quantum. Elect.*, 1975, **QE-11**, 259.
- 23 A. Owyong, *IEEE J. Quantum. Elect.*, 1973, **QE-9**, 1064.
- 24 W.E. Williams, M.J. Soileau, E.W. Van Stryland, *Opt. Commun.*, 1984, **50**, 256.
- 25 M. Sheik-Bahae, A.A. Said, T-H. Wei, D.J. Hagan, E.W. Van Stryland, *IEEE J. Quantum Elect.*, 1990, **26**, 4.
- 26 F. Henari, J. Callaghan, H. Stiel, W. Blau, D.J. Cardin, *Chem. Phys. Lett.*, 1992, **199**, 144.
- 27 *Chem. Phys. Lett.*, 1993, **205**, 204.

CHAPTER 6

NANOPARTICLES

MORPHOLOGY AND SPECTROSCOPY.



6.0 Introduction.

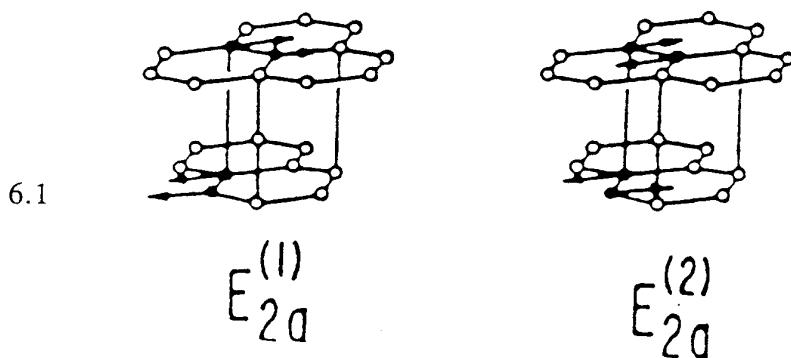
The discovery of nanoparticles in a carbonaceous deposit formed by evaporating graphite using the arc/plasma technique^(1,1a) has opened a new line of research which has applications in a wide variety of fields^(2,3) including composites, catalysts, and molecular wires^(30,31). Their applications as molecular solenoids, generators and electromagnets have been proposed.⁽³²⁾ Ebessen *et al.*⁽⁴⁾ demonstrated that the yield of nanoparticles is dependant on the pressure at which the graphite is consumed. The presence of heptagons in these structures has been a matter of controversy since negative curvature was first noticed.⁽⁵⁾ The presence or absense of heptagons to explain novel curved nanotubes is studied in this chapter. No other study of nanotubes has revealed these curved structures and their occurence is explained in this chapter. Bundles of nanotubes (called 'Buckybundles') have been observed by various workers^(6,7). This study shows unique micrographs of these bundles and discusses their structure. Ugarte recently⁽⁸⁾ reported his observations that the structure of nanoparticles change under electron irradiation in the microscope. The resultant 'Spheroids' seem to be more stable than their precursors. This irradiation process has been studied in detail and the experiments on nanotubes and polyhedra were recorded on video. Electron diffraction of the spheroids on the microscope has shown some interesting effects that are discussed here. The methods by which nanotubes are capped have been discussed in detail⁽⁹⁾. Observations made in this study conflict with some of the results obtained by Iijima^(1,1a). The stacking of concentric tubes is studied in this chapter using micrographs which show for the first time stacking patterns with exceptional resolution.

Raman spectroscopy has been used only once⁽¹⁰⁾ in the study of nanotubes. A series of experiments using first and second order Raman spectroscopy have shown some interesting results. A study with different Raman laser lines was also carried out which demonstrates a unique dispersive effect. Results from an i.r study will also be discussed.

RESULTS AND DISCUSSION.

6.1 Raman Spectroscopy of Nanoparticles.

Graphite consists of stacked sheets with the carbons within the layers arranged in a two dimensional network of hexagons. Two modifications of graphite exist, differing in the ordering of the layers. In no case do all the carbon atoms of one layer lie directly over those in the next layer but in one form carbon atoms in every other layer are superimposed (ABAB stacking.). This is the more stable form and exists in the commonly occurring hexagonal form of graphite. There is also a rhombohedral form, frequently present in naturally occurring graphite, in which the stacking order is (ABCABC,), every third layer is superimposed. Local areas of rhombohedral structure can be formed by mechanical deformation of hexagonal crystals and can be removed by heat treatment. The many forms of "amorphous" carbon, such as charcoals, soot and lampblack, are all actually microcrystalline forms of graphite. In some soots the microcrystals are so small that they contain only a few unit cells of the graphite structure. The aromatic character of the hexagons is reflected in the short carbon-carbon distances, 142pm, within the hexagonal sheets compared to 335.4pm between the layers. In the hexagonal form the space group is $P6_3/mmc$ with 4 carbons in the primitive hexagonal cell. For graphite in this form two Raman active modes are predicted, both vibrating in the plane of the sheets(Fig.6.1).

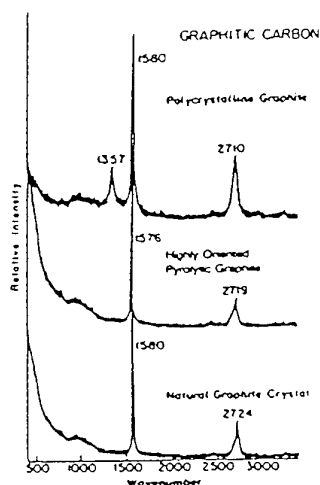


One is a stretching of the individual sheets and the other is a shear mode of the two adjacent sheets in the unit cell. The stretching mode should occur at high wavenumbers and be largely independent of the stacking sequence. The shear mode has been observed at low wavenumbers but is broadened and lost by disorder in the stacking sequence. Because of the weak interlayer bonding, graphite crystals are subject to disorder along the C axis while at the same time the strong interlayer carbon-carbon bonding maintains a high degree of order within the individual carbon sheets. At the limit is a condition known as turbostratic stacking in which there is random relative

orientation of successive layers. These crystallographic characteristics strongly influence the features seen in the vibrational spectrum.

The Raman spectrum of natural single crystal graphite shows the main features(Fig.6.2).

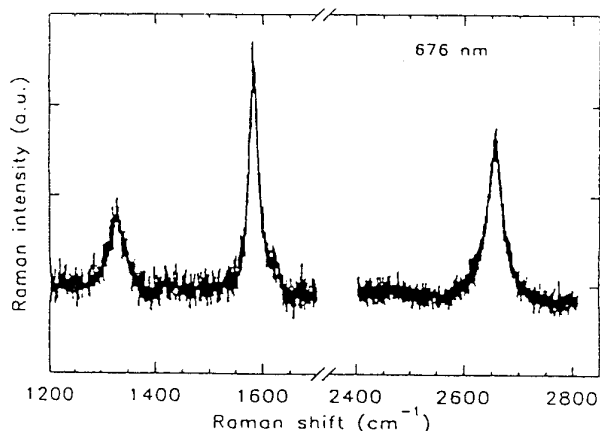
6.2



There is a sharp intense band at 1580cm^{-1} which has been assigned to the predicted E_{2g} C-C stretching mode⁽¹¹⁾. The feature at $2710\text{-}2724\text{cm}^{-1}$ is a two phonon band taken to be 2×1357 the band that appears in polycrystalline graphite. The 1357cm^{-1} band has generated considerable debate in the literature. It does not appear in large grain single crystals but does appear in well crystallised graphites with small particle size.

The Raman spectrum(514nm) of a sample of nanoparticles is shown in Fig.6.3.

6.3



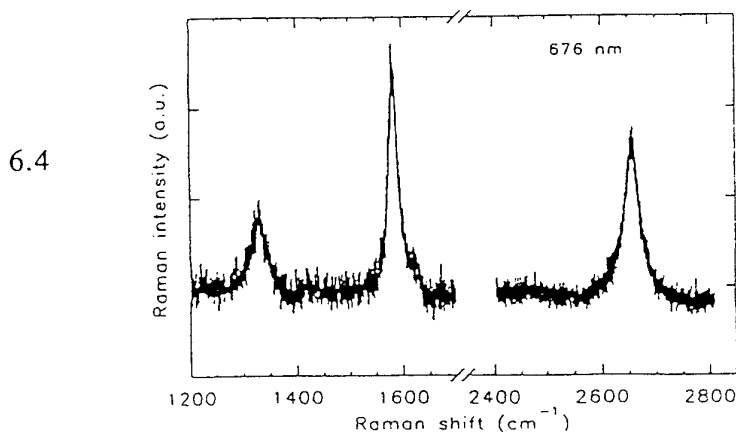
The results are similar to that for crystalline graphite. The strongest line at 1583cm^{-1} ($\nu_{1,2}21\text{cm}^{-1}$) is well known in graphitic materials and is designated the G-line. It is the broadened E_{2g} mode of monocrystalline graphite(vibrational mode corresponding to the movement in opposite directions of two neighbouring carbon atoms in a graphitic sheet)⁽¹¹⁾. The width of the G line is only slightly bigger than that of monocrystalline graphite and hence the nanotubes show a high degree of crystallinity. The second mode in the low frequency range has its maximum at 1350cm^{-1} . This is usually called

the D line because it is disorder induced. This occurs because the selection rules break down at grain boundaries and defects. The intensity of the D line depends on the degree of disorder. The ratio of the integrated intensity of the D line to the G line $R(=I_D/I_G)$ depends inversely on the in-plane crystallite size L . This dependence is well known from Raman studies on ordered and disordered graphite^(11,12). It could theoretically be used to estimate the length of nanotubes. The nanotubes consist of closed and sometimes curved graphitic carbon layers where the ends are closed using pentagons. The measured length can be considered to be an "effective" length, where the graphitic planes are not interrupted by defects or pentagons/heptagons. When this was calculated for a sample a figure of 30nm was found. The usefulness of this figure is uncertain since the samples contain polyhedra which are much smaller than nanotubes and hence will reduce the observed "effective" length.

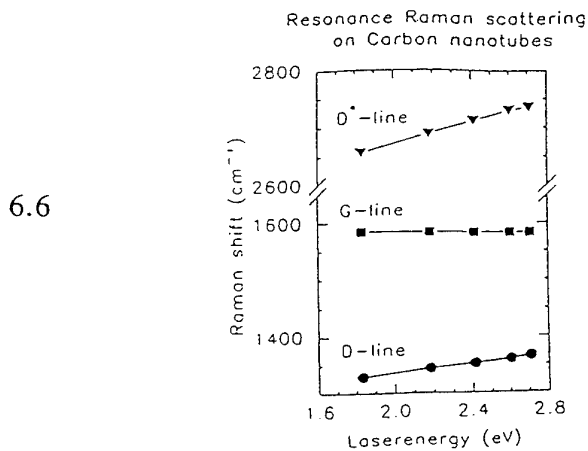
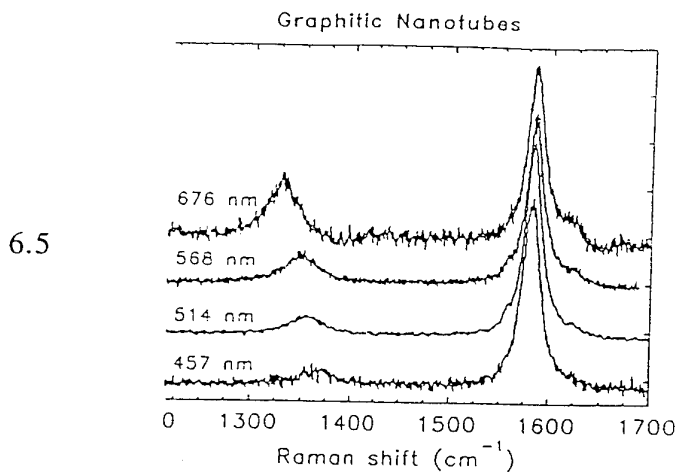
In the second order Raman spectrum there is a weak line at 2450cm^{-1} and a stronger one at 2700cm^{-1} . The latter is the D* line (ie. the second order of the D line). In addition to these intrinsic lines a very narrow line at 2330cm^{-1} (Fig.6.2) appeared in almost all of the spectra. Its intensity varies from measurement to measurement but its width and position stay the same. The origin of this line is probably a contamination but it is too high for C=O stretching and too low for C-H. The Raman spectra of samples from 400T and 500T are similar, the only difference is that the intensity of the D line is slightly stronger for the 400T sample. Results agreeing with these have been published⁽¹⁰⁾.

6.2 Resonance Raman Spectroscopy of Nanoparticles.

In this section all of the measurements were carried out on a sample prepared at 500T. The spectrum at 676nm is shown in Fig 6.4.



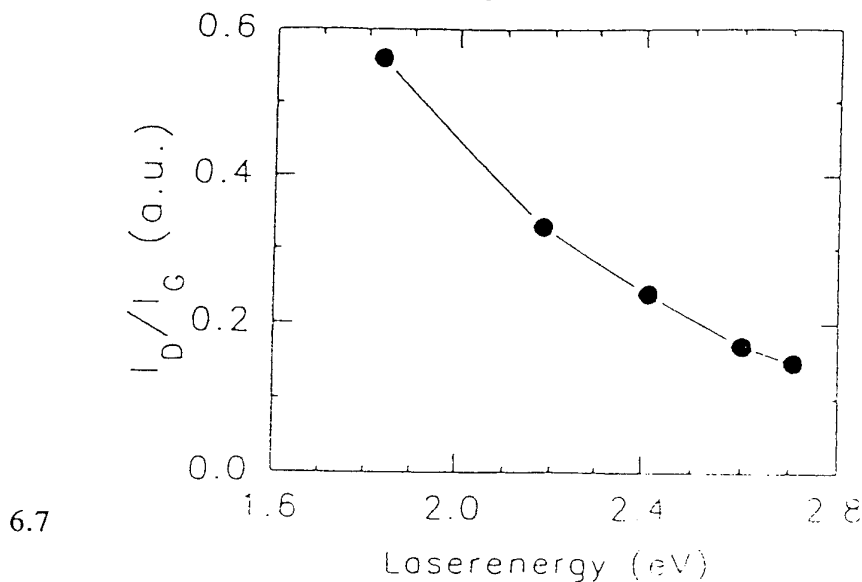
The D line has shifted to lower frequency. In addition there is a new line at 1620cm^{-1} . This line has also been observed in disordered graphite and is supposed to be disorder induced. The first order Raman spectra of nanoparticles after excitation with different laser energies is shown in Fig.6.5. The D line shifts to higher frequency with increasing laser energy. Fig.6.6 shows this behaviour on graph.



The maxima of the D and D* lines shift to higher frequencies with increasing laser energy, whereas the G line remains static. The shift of the D* line is approximately twice that of the D line which supports the explanation that it is the second order of the D line.

In addition to the shift of the Raman lines, the intensities are also influenced. The D line is much stronger compared with the G line after excitation with the red laser than after excitation with the blue or green lasers(Fig.6.6).

Resonance Raman scattering on Carbon nanotubes



The intensity ratio of the D/G lines is plotted against the energy of the laser in Fig.6.7. Clearly the ratio decreases with increasing laser energy. The dependence of the Raman spectrum on the energy of the exciting laser is called the dispersion effect. It has also been observed for graphitic systems. There are several explanations for this effect:

1. The line shifting might be related to probing the sample at different depths below the surface. This is a similar explanation to that proposed for inorganic semiconductors. Since the refractive index and extinction coefficient of graphite are constant over the visible frequency range this explanation is improbable.

2. The effect might be attributed (as in conjugated polymers) to a photoselective process of nanotubes with different sizes. Force constants, frequencies and electronic transitions depend on the size of the nanoparticles. The blue laser (3-4 eV) has similar energy to the π - π^* transition in graphitic layers. The red laser is out of resonance with this transition and the Raman spectrum shows more contributions from defects, grain boundaries and caps (pentagons). Thus the disorder induced lines are stronger and shift to lower frequencies.

Detailed measurements on particles of well defined size are planned and the results of this study should help to understand this dispersion effect.

6.3 Infra Red Spectroscopy of Nanoparticles.

Graphite has two i.r. active vibrations. The A_{2u} mode(E_{1c}) and the E_{1u} mode(E_{1c}). The irreducible representation for the zone centre optic modes of graphite have been determined to be^(13,19): $\tau_{opt} = 2E_{2g} + E_{1u} + 2B_{2g} + A_{2u}$.

The E modes are solely concerned with motions in the plane layers while the A and B modes represent displacements normal to the plane(Fig.6.8).

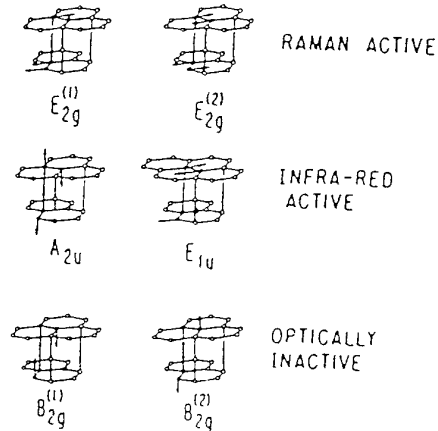


Fig.6.8

The E_{1u} line at 1587cm^{-1} is generated from the Raman active E_{2g} mode. The A_{2u} line is seen at 868cm^{-1} .(Fig 6.8).

The i.r. spectrum of nanoparticles shows a line at 1620cm^{-1} which we interpret as an upshifted E_{1u} mode. This upshift is probably due to fact that the nanoparticles have curved surfaces. The second line of graphite, the A_{2u} mode at 868cm^{-1} which is due to displacements between layers is not visible in the nanoparticle spectrum(Fig6.9).

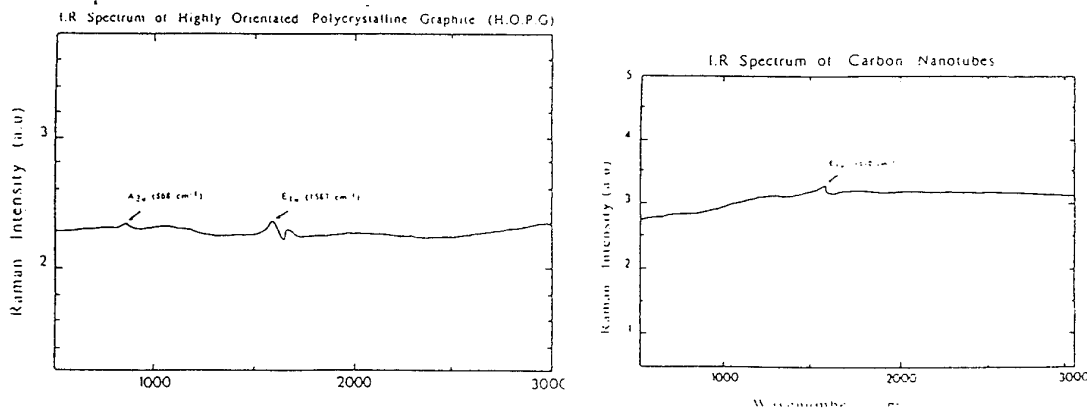


Fig.6.9

One possible explanation for this is the fact that the A_{2u} mode is generated as we look at the Ellz plane where it is possible to see the modal shifts between the graphite sheets, in nanoparticles the inward curvature of the hexagonal network causes the direction of the z plane to change for every hexagon. This has the effect of reducing or cancelling the A_{2u} mode.

6.4 Conclusions.

Carbon nanoparticles have a Raman spectrum which resembles graphite closely. In the first order spectrum there are two main lines (1350cm^{-1} D line, 1583cm^{-1} G line). The disorder induced D line is weak compared to the G line which indicates that the nanotubes are highly crystalline materials. This suggests that other physical properties such as mechanical strength and conductivity should reflect features of pure single crystals. The position and intensity of the D line was found to depend strongly on the energy of the exciting laser. This dispersive effect was also observed for graphitic particles and can possibly be explained by a photoselective resonance process of nanoparticles with different sizes.

The i.r. spectroscopy of nanoparticles raises some interesting possibilities. The two i.r active modes for graphite are weak and especially the A_{2u} mode is difficult to distinguish from the background. No trace of this A_{2u} mode was found in a sample of nanoparticles after repeated attempts. The absence of this mode could be used as a method for characterising nanoparticles. The width of the E_{1u} mode is indicative of the size dispersion of the nanoparticles, thus a sharp peak would indicate a homogeneously sized sample and this will be useful when a process for separating nanoparticles is available. Electron microscopy of these samples shows very little amorphous carbon and no crystalline graphite.

6.4 Microscopy of Nanoparticles.

Transmission electron microscopy was performed using two microscopes. A description of these is given at the end of this chapter along with the sample preparation. The main impurity visible in the samples of nanoparticles is a fused mixture of tubes and polyhedra(M4.2) which originates in the hard grey outer shell. Amorphous carbon was sometimes visible(M4.1) but was not common. M4.3 shows a low resolution image of graphite scraped from a graphite electrode. The planar sheet structure of graphite is clearly visible. The thin film of carbon which was evaporated onto the samples was found to break on occasion. This gives structures which can be mistaken for nanotubes under low resolution as shown in M4.4. Also visible in this micrograph is an example of a nanobundle with a curved structure and some spherical

structures which are polyhedra. Some of these polyhedra are attached to the nanotubes (which presumably act as nucleation sites). Micrographs 4.5 and 4.8 show samples rich in nanotubes and polyhedra and also curved tubes. All of these micrographs were taken on thin copper discs on the 200KV microscope (resolution approx. 2nm). The Holey carbon grids used with the 300KV microscope are clearly visible in M.6 and M.7. Also visible in M.6 is a series of nanotubes aligned along their length. The longest single nanotube in the micrograph is 4 μ m long.

6.5 Curved Nanotubes.

During the course of this microscopy study a number of unusual features was noticed. The first was the occurrence of curved nanotubes in the samples. The relative abundance of these curved tubes was found to be very low ($<0.5\%$). M5.1 shows an unusual collection of these curved tubes at one site. Four curved tubes are visible and M5.1,1 shows two of these in better detail. The darkening of the R.H.S tube arises due to the fact that the tube is bending towards the viewer. The sequence of pictures M5.2 - 5.2,2 shows one tube with several curved regions. The dark region in M5.2,2 is due to the tube bending towards the viewer. The micrographs M5.3 to M5.6 show several examples of curved tubes. The structure of the carbon network at these bends can not be easily explained from these micrographs. The majority of the curved tubes do not exhibit dislocations or breaks in the structure which could explain the phenomenon. M5.7 and M5.10 show tubes which appear to contain dislocations or "breaks" at the bend but these structures are in the minority of curved tubes. Some tubes exhibited a darkened structure at the bend (M5.9) or were at junctions of tubes forming bundles of tubes (M5.3, M5.8). One unusual curve contained a folded or rippled structure on the inside of the bend. These findings initiated a high resolution study (HREM) of these curved structures.

The presence of pentagons in a hexagonal sheet has the effect of bending the sheet inwards (positive surface disclinations ($+60^\circ$)). Ajayan⁽⁹⁾ showed that nanotubes are capped using 6 pentagons in various arrangements. Phillips *et al.*⁽¹⁴⁾ and Dunlap⁽¹⁵⁾ discussed the effect of including heptagon/pentagon pairs in the hexagonal structures. Heptagons induce negative surface disclination (-60°). Negative curvature analogues of fullerenes were found by Phillips *et al.* to be energetically favourable and Dunlap showed how they could be used to connect tubes. Later Iijima⁽⁵⁾ showed how the use of heptagons could explain some of the structures which he had observed. At the same time a paper by Shen ⁽¹⁶⁾ demonstrated how [7]circulene (a 7 membered ring surrounded by benzene rings) can convert easily between the planar D_{7h} structure to the C_2 geometry with a barrier of only 8.5kcal/mol. The C_2 equilibrium geometry resembles a saddle with the heptagon at the saddle-point. This remarkably floppy structure demonstrates the versatility that the heptagon can introduce into a hexagonal network and strengthens the evidence for the existence of heptagons. Ugarte⁽¹⁷⁾ published a structure which he claims must contain a heptagon to explain the negative curvature. The concept of heptagon inclusion could also be used to explain the curved tubes which were found in this study. The use of a heptagon/pentagon pair on opposite sides of a tube would cause that tube to bend by 60° . Further combinations of these pairs would induce bending with angles that are multiples of 60° . Several of the curved tubes seen on the 200KV microscope displayed angles which appeared to be multiples of 60° (mainly 180°).

6.7 "Buckybundles".

A common feature apparent in all samples studied was the occurrence of bundles of nanotubes several tens of microns in diameter and up to one centimeter in length. Wang *et al.*⁽⁶⁾ have argued that the only interaction between the tubes in these bundles is Van der Waals in nature since the valence requirements of all atoms in a closed tube are satisfied and it is "therefor energetically favourable for buckytubes packed closely together to form a buckybundle". This is a rather simplistic view of the phenomenon given the data available on their structure and does not attempt to explain the growth mechanism by which the bundles arise. The buckybundles which were observed in this study consisted of nanotubes which were not evenly spaced but were staggered along their length (M7.1). Not all samples were alligned parallel to each other either, some had a structure which was described as "Eiffel Towering"(M5.3, M6.7, M7.1). The bundles often had a coating of amorphous material and polyhedra (M5.3, M6.7, M4.8, M7.4, M7.5). These observations contradict the findings of Ebbesen, Hiura *et al.*⁽²⁰⁾ who claim that the bundles occur separately from nanoparticles. They also dismiss the hypothesis that cavities created by other nanotubes could act as seeding sites for more tubes(thereby forming a bundle) by claiming that such a process would result occasionally in two or more tubes being wrapped by a sheet of graphene giving two or more tubes inside a larger nanotube and such structures have not been observed by the authors. Although the hypothesis is probably not correct their observations are peculiar. There is no reason why such a process should result in a graphene wrapped bundle and structures similar to these have been observed in this study frequently (M6.7). The amorphous carbon which is visible on bundles which have not been sonicated (buckybundles can be separated into smaller bundles by sonicating a suspension in methanol or acetone) could be nanotube precursor which forms tubes at higher temperature. This undefined material could also act as a "glue" holding nanotubes together. Such a scheme is supported by theoretical predictions according to Ebbesen and Hiura, where calculations show that small carbon ribbons will spontaneously close at high temperature⁽²¹⁾ and that nanotubes are favoured energetically over open flat graphite sheets of width equal to the nanotube circumference⁽²²⁾. The observation that the tubes are staggered along their length in a bundle is explained by the fluctuating nature of the arc. The intensity and duration of the arc currents fluctuate in time⁽⁶⁾ thus the evaporation and condensation of the carbon is not a continuous process at one position. This movement of the arc across the surface of the anode results in tubes of various lengths and diameters.

6.8 Electron Irradiation of Nanoparticles.

During the course of the HREM studies on nanoparticles an intriguing effect was noticed that on further examination formed the basis for an understanding of the growth mechanism of nanotubes. Ugarte⁽⁸⁾ was the first to notice the effect that electron irradiation had on nanoparticles. This observation was followed with a report⁽¹⁷⁾ on the formation of "quasi-spherical" carbon particles by electron beam irradiation on the microscope. Ugarte had subjected a sample of nanoparticles to intense electron irradiation by focussing the electron beam and removing the apertures. Over a period of minutes the angular polyhedra were transformed into spheroids and the nanotubes were curved and smoothed at their tips. Two publications followed; Saito et al.⁽²³⁾ showed how a finely focussed(2nm) electron beam was used to open a polyhedron which contained YC_2 and Ugarte⁽²⁶⁾ showed that by irradiating the whole of a gold-filled polyhedron the metal could be extracted when the polyhedron underwent the transformation to a spheroid. Both of these publications demonstrated the usefulness of the irradiation procedure.

To explain the morphology of nanotubes in terms of their growth pattern it is necessary to consider that the tube growth must involve the addition of carbon radicals and atoms to the tip of the tube while all the layers of the concentric tubes are open with highly reactive dangling bonds surrounding the edge of each layer. This is necessary to explain the presence of complete tubes within tubes and the existence of tubes with high length to diameter ratios, since if lengthening occurred by addition to the closed, pentagon rich, end of a tube⁽²⁴⁾ then most tubes would grow sideways quicker (dangling bonds) than lengthways. This is the same as proposed by Iijima⁽¹⁾. The interesting point to note is that at such high temperatures (3000-4000K) one would expect the tips to anneal by closing. The only factor present which can prevent this is the presence of the very high electric field. The importance of this can be seen in the parallel alignment of all tubes with the electric field. If the field is high enough then it could stabilise the open ended tubes and the highly reactive double bonds. Although the voltage drop is only 300V/cm between the electrodes the ion density is so high in a carbon arc at 0.5 atm.pressure that the resultant screening length is of the order of 10-100nm⁽²⁵⁾ which gives rise to an electric field of approx. 10^6 V/cm on a smooth cathode. This can increase by orders of magnitude on the tips of open tubes giving an electric field which could stabilise the open form of nanotubes. The movement of the field from point to point on the surface of the cathode results in the capping-off of nanotubes since immediately the electric field moves from an open tube it would quickly anneal at the very high temperatures.

Samples of nanoparticles are subjected to electron irradiation in a vacuum of $>10^{-7}$ for electron microscopy. The current density can be as high as $150\text{A}/\text{cm}^2$ during the process. Small changes were noticed in our samples over relatively long times on the microscope (15min). When the intensity was increased these changes were dramatic and resulted in the process first noticed by Ugarte⁽⁸⁾. The series of micrographs M8.1 to M8.3 show the effect of electron irradiation on a tube tip over a short period of time (4min) under normal conditions. There are many examples in the literature of micrographs of nanoparticles which have deteriorated under irradiation without the knowledge of the researcher. This is an important point for future work, the intensity of the beam and the exposure time should be kept at a minimum to avoid this effect. The series M8.4 to M8.10 show the effect of irradiation on a tube tip and a polyhedra. The rounding effect on the tip is noticeable as is the collapse of the centre of the tube during irradiation. The diameter of the smallest sphere at the centre of the spheroid is approximately 8\AA ($C_{60}=7\text{\AA}$). M8.11 shows the disorder present at the centre of the tube while the outside is less disordered. A polyhedron was singled out (M8.12) for irradiation and the beam focussed carefully on it. The surrounding material was not irradiated and the process was completed (M8.13) in approximately 3 minutes. An electron diffraction pattern was recorded of the polyhedron before and after the event and will be discussed later. Perhaps the most dramatic example is seen in M8.14 and M8.15. Several different structures are visible which change dramatically upon irradiation. Note the nested spheres on the left hand side of M8.15. A series of irradiations were carried out which were recorded on video tape. The process was studied from this recording at slow speed and frame to frame. It is possible, on the video, to follow "defects" move (fluidlike) from site to site until they are accommodated into the structure. Some generalisations can be made about the transformations;

1. The pentagon-rich areas (bends) of a tube tip are the first to undergo change as are the "edges" of a polyhedron.

2. The outer layers are the first to complete the process with the centre taking much longer.

3. Initially the structures become more compact and as the centre starts to become ordered it forces the outer layers to change by passing a dangling bond defect to the surface where it is accommodated with the subsequent growth of the outer layers.

4. The speed of transformation is directly proportional to the intensity of the beam.

Ugarte⁽¹⁷⁾ calls an irradiated polyhedron a "quasi-spherical onion-like particle". Obviously the structure of these spheroids is not well understood. It has been shown earlier that the inclusion of a pentagon into a hexagonal sheet bends that sheet through a positive disclination of 60° . This bending is obvious in the tips of nanotubes and the

corners of polyhedra. From the video and the micrographs it can be seen that the first sites affected by the irradiation and those involving the most intense rearranging are pentagon-rich bends or corners. The resulting structures have eliminated all sharp bends and straight surfaces in favour of the spherical structure. There is no apparent loss or gain of carbon atoms during this process but yet the particle undergoes a process similar to melting where the structure assumes a minimum surface area because of surface tension. An electron diffraction study was carried out in an attempt to elucidate some structural information on the spheroids.

An electron diffraction pattern from a single particle(M8.12) is shown in M8.12+. The $00.l$ reflections are strong in intensity and form discrete spots(especially the $d_{00.2}$ which is the spacing between the graphitic sheets), while the $hk.0$ are weak and distributed on annular rings. The strong $00.l$ spots are due to Bragg reflections from graphitic layers parallel to the incident electron beam. The character of the $hk.0$ reflections (the intensity distributed on rings) indicates that the stacking of graphitic sheets is disordered (turbostratic packing). The electron diffraction pattern of the spheroid is devoid of $00.l$ reflections and the $hk.0$ reflections have become more intense and equally distributed on the annular rings. The absence of the $00.l$ reflections indicates that the structure is spherical since in a sphere the graphitic layers will not be parallel to the incident beam. Because of the lack of resolution on the annular rings we can conclude that the individual spheres are spinning very rapidly, this may be a clue to the unusual stability of this form of carbon. The particles remain intact even after 30 minutes of further electron bombardment, the electron flux is very high($150A/cm^2$) and one would expect the particles to disintegrate but most of this energy may be spent spinning the individual spheres. The particle must be an almost perfect sphere since there are no individual reflections visible. Electron diffraction was carried out on another polyhedron with similar results (M16 and M17). The molecular structure of these spheres is not well understood. To this end samples of these spheroids are being prepared for a series of spectroscopic studies and scanning electron microscopy.

6.9 Capping and Helicity.

According to Iijima *et al.*⁽¹⁾ the method by which a tube is capped determines whether that tube has a helical structure or not. The asymmetric and symmetric caps (Fig.6.11) described by Ajayan *et al.*⁽⁹⁾ have been seen in all HREM studies on nanotubes. The 3-dimensional geometries of the tips shown in Fig.11 are difficult to visualise from the micrographs and indeed may not be valid as other arrangements (Fig.6.12) can be constructed which fit the patterns observed. Iijima⁽⁵⁾ states that helicity can only arise from asymmetrically capped tubes and that "the extremely rare occurrence of these structures with symmetric tips suggests that helicity does play a role in aiding tube growth. We have no evidence yet to suggest the direct role of helicity in growth". From this study we have noticed that symmetric caps appear to be just as prevalent as asymmetric ones. M9.4 shows such a symmetric tip at the bottom and near the top an unusual curved tip is visible. M9.2 shows a collapsed or deformed cap but the interesting point is the tube inside the tip which is symmetrically capped. The cap in M9.3 is symmetric but is curved on the left hand side and the darker contrast of this curve suggests that it is a bulge or deformation of some nature. The inner tubes in M9.4 all contain symmetric caps and this feature is common to all inner tubes seen. The only exceptions to this are at the very end of a complete tube where the inner tubes are capped in the same manner as the outer tubes (M9.5) (this is more evidence for the open-ended growth scheme). This micrograph (M9.5) contains some unusual features. The innermost tube (left hand side) is capped asymmetrically and this pattern is then followed for each successive layer. Gaps appear in the layered structure on the bottom LHS of the tube. The gaps could have arisen from the fact that the tube seems to have been diverging from left to right as the internal diameter increases until the first inward turn. This turn (closed triangle) is followed by an area of negative curvature (open triangle) which is due to either a dislocation or heptagons. Both are possible since there is an amount of amorphous material surrounding the bend but at the same time some of the layers are continuous. M9.6 shows a typical asymmetrically capped tube but towards the bottom of the micrograph there is a symmetrically capped tube inside this. Note also the single capped tube inside. M9.8 and M9.7 show two more asymmetrically capped tubes. M9.7 contains almost 70 concentric tubes and unusual gaps are visible in the layers on the top side as in M9.5. M9.8 shows signs of irradiation damage.

Iijima's suspicions that helicity aids the growth of tubes may well be correct since it is easier to visualise the addition of a single atom at a time to a helix to enable growth than the addition of a number of atoms at the same time to each layer to achieve growth. However because here we have seen an almost equal distribution of both types of caps the matter is under doubt. Perhaps one solution for this (serendipitously) is in a paper by Li, Fagan and Liang⁽²⁷⁾. They show a micrograph of an asymmetric

tube (Fig.6.13) at two different viewing angles, -20° and $+30^\circ$. At the $+30^\circ$ angle the asymmetry is clearly visible but at -20° the cap appears to be almost symmetric. A HREM study of samples of nanotubes viewed at different tilt angles will resolve this problem and one is currently under way.

We have already seen how the stacking of graphitic sheets in polyhedra is disordered (turbostratic) from the electron diffraction studies. From this result the same is expected in nanotubes due to the similarity in their structures. However a series of micrographs here reveals patterns from the stacked layers. If the packing was truly turbostratic no pattern would be visible from the hexagonal sheets. There are two types of cylindrical pattern, rational and irrational. In rational lattices further lattice points lie exactly above others with a displacement parallel to the axis of the cylinder. With irrational lattices a second lattice point never occurs directly above the first. Iijima⁽¹⁾ used electron diffraction to show a 3-8 irrational lattice for very small tubes. With such an irrational lattice it would be impossible to view regular stacking patterns let alone individual hexagons on the nanotube due to the random allocation of the sheets and hexagons. M9.9 shows a nanotube with diagonal and straight lines spanning the tube across its width (bottom arrow). The lines are more visible over the centre of the tubes as there are no strong 00.2 reflections at this position. Individual hexagons are visible at the top of the tube (top arrow). The diameter of these hexagons is less than 0.3 nm. M9.4 and M9.5 both show these features across the centres of the tubes. In M9.5 the pattern is very regular on the left hand side of the tube and runs diagonally across the tube as would be expected for a helical arrangement. This is also visible in M9.10 but in greater detail, diagonal orthogonal patterns are clearly visible and this could not be described as turbostratic. M9.11 does display turbostratic (random) orientations. This series of micrographs shows that the rational and irrational lattices are possible and the helical nature of some nanotubes can be seen using HREM.

6.10 Conclusions.

This microscopy study of nanoparticles has revealed many properties of these structures not seen to date. The phenomenon of curved tubes has been studied in detail and their occurrence explained. The presence of heptagons has been discounted in these curved structures although their existence has been confirmed in this and other studies. There are some obvious sources of mechanical stress which would explain the curvature in most examples. Scraping, grinding and sonication are some. The carbonaceous deposits visible around most bundles of tubes can act as a glue to contain tubes in a tight packed configuration. These bundles can be broken into individual tubes by sonication. The various capping mechanisms possible have been studied as has the helicity which should be inherent in asymmetric capped tubes. HREM has revealed the stacking patterns of the layered nanotube structures and the helicity is clearly visible in some. The remarkable resolution possible with the technique enabled individual hexagons on the surface of a nanotube to be seen. Electron irradiation of nanoparticles has produced another form of closed carbon cages that are more stable than their precursors. The video recording provides a unique possibility to view on an atomic scale how the process occurs and concurs with the proposals⁽²⁸⁾ of a fluid-like nature for these carbon structures under concentrated ion bombardment. The presence and possible distribution of pentagons in spheroids produced as a result of electron irradiation of polyhedra is currently being studied. These spheres may be the source of the 217.5 nm interstellar absorption feature⁽²⁹⁾. It was the search for the origin of this feature that realised the discovery of fullerenes. It is fitting therefore to finish on that point.

EXPERIMENTAL CHAPTER 6

6.1 Preparation of Nanotubes.

The steel fullerene generator described in Chapter 3 was used to make samples of nanotubes for this study. An 8mm graphite rod was used as the positive electrode. A plug of graphite was used as the negative electrode. The generator was flushed with helium three times before evacuating to 400 Torr. The burning sequence was exactly the same as for the synthesis of fullerenes. After the positive electrode was consumed a grey/black cylinder was found on the negative electrode. This cylinder consisted of a grey metallic outer layer and a black inner core. The cylinder was placed in methanol (100cm^3) and sonicated for 10 minutes. This removed some of the inner black material from the cylinder to give a fine black suspension. This suspension was evaporated to yield a fine black powder which contains nanotubes, polyhedra (onions) and amorphous carbon. Alternatively the inner black core can be scraped out to give a black powder which is rich in nanoparticles. The outer grey material contains very few nanoparticles.

6.2 Electron Microscopy of Nanoparticles.

Low resolution Transmission Electron Microscopy (TEM) was performed using a Hitachi H-7000 machine with an acceleration voltage of 200kV. The samples were ground in a mortar before being placed on thin copper discs. A thin carbon film was then evaporated onto the disc. This enhanced the stability of the samples on the disc by preventing the samples from moving due to charging or evaporation of small amounts of solvent. This technique gave a resolution of approximately 2nm.

High Resolution Electron Microscopy (HREM) was performed using a Philips CM30ST field emission microscope with an acceleration voltage of 300kV. This microscope has a point-to-point resolution of 0.20nm. The minimum spot size of the electron beam is 3nm in diameter. The samples for HREM were mounted on holey-carbon discs which were prepared *in situ*.

6.3 Preparation of 'Holey-carbon' grids.

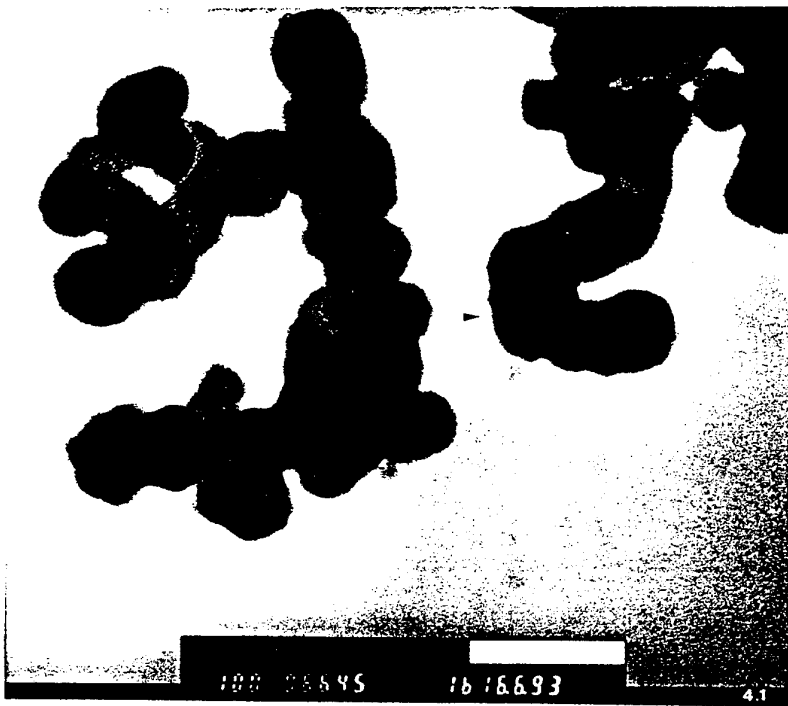
Two drops of glycerol were added to a rapidly stirring solution of Triafol (a commercially available polymer). Glycerol and Triafol are immiscible and very vigorous stirring is necessary to ensure an even distribution of the polymer in the glycerol. After 30 minutes the stirring was stopped and a glass slide was dipped into the cloudy suspension. The slide was then set aside to dry in a dust free environment. After the chloroform had evaporated the edges of the slide were scratched to loosen the carbon film. The slide was then introduced to a beaker of deionised water at an angle of approximately 45° . This allows the thin film to slide off of the glass and float on the surface. The slide was dropped to the bottom of the beaker. The thin film of holey-carbon was just visible on the water surface. Copper grids (3mm diameter) were then dropped onto the film. A filter paper was used to remove the coated grids and these were allowed to dry dust free. A thin layer of carbon was then evaporated onto the grids. The nanoparticle sample was suspended in methanol and drops of the suspension were dropped onto the holey-carbon grids on absorbant paper using a pipette. The grid was then mounted for microscopy. Any particle which rested across a hole in the carbon grid could be resolved to an information limit of 0.14 nm.

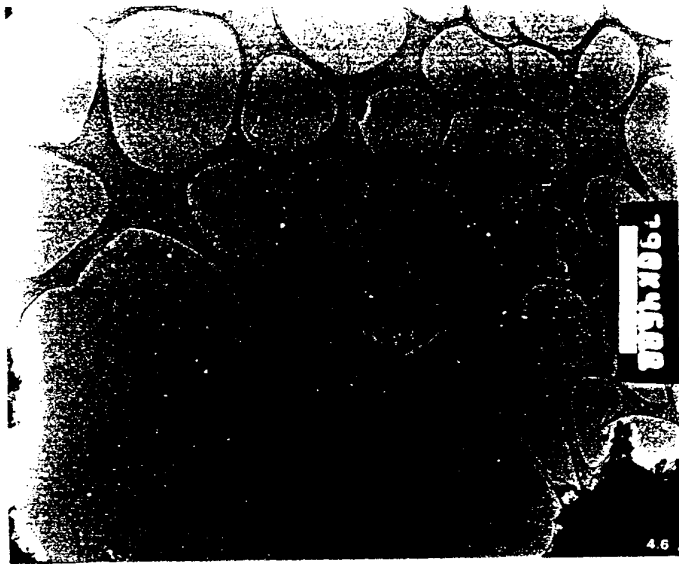
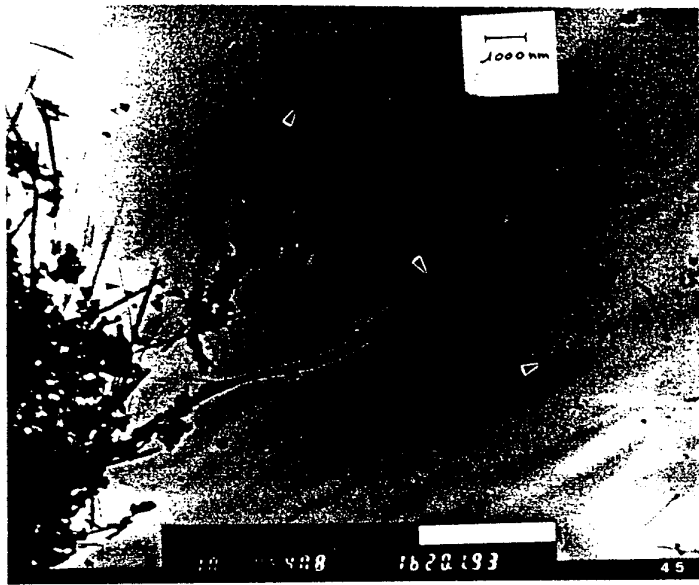
6.4 Spectroscopy of Nanoparticles.

Powder samples of carbon nanotubes were characterised by Raman spectroscopy using a Dilor XY spectrometer after excitation with laser lines ranging from 457 nm to 676 nm. I.r spectroscopy was performed using pellets of monocrystalline graphite and nanoparticles made with KBr (1:100). The spectra were recorded on a Bruker IFS 66V spectrometer.

REFERENCES.

1. S. Iijima, *Nature*, 1991, **354**, 56.
2. M.R. Pederson & J.Q. Broughton, *Phys.Rev.Lett.*, 1992, **60**, 2689.
3. H.W. Kroto, *Nature*, 1992, **539**, 670
4. T.W. Ebbesen & P.M. Ajayan, *Nature*, 1992, **358**, 220 .
5. S. Iijima *et al.*, *Phys. Rev. Lett.*, 1992, **69**, 21,3100.
6. X.K. Wang *et al.*, *Appl. Phys. Lett.*, 1993, **63**, 1881.
7. T.W. Ebbesen, H. Hiura *et al.*, *Chem. Phys. Lett.*, 1993, **209**, 83.
8. D. Ugarte, *Nature*, 1992, **359**, 707.
9. P.M. Ajayan & S. Iijima, *Chem. Phys. Lett.*, 1993, **202**, 384.
10. H. Hiura *et al.*, *Chem. Phys. Lett.*, 1993, **202**, 509.
11. R.J. Nemanich & S.A. Solin, *Phys. Rev.*, 1979, **B20**, 392.
12. D.S. Knight & W.B. White, *J.Mater Res.*, 1984, **4**, 385.
13. R. Zallen, *Phys. Rev.*, 1968, **173**, 824.
14. B.I. Dunlap *Phys. Rev.*, 1992, **B 46**, 1933.
15. R. Phillips *et al.*, *Phys. Rev*, 1992, **B 46**, 1941.
16. Mingzuo Shen *et al.*, *J. Phys. Chem.*, 1993, **97**, 3212.
17. D. Ugarte, *Chem. Phys. Lett.*, 1993, **207**, 473.
18. D. Ugarte, *Ibid.*, 1992, **198**, 596.
19. R.J. Nemanich & G. Lucovsky, *Solid State Commun.*, 1993, **23**, 112.
20. T.W. Ebbesen, H.Hiura *et al.*, *Chem. Phys. Lett.*, 1993, **209**, 83.
21. D.H. Robertson *et al.*, *Phys. Rev.*, 1992, **B45**, 12592.
22. S. Sawada & N. Hamada, *Solid State Commun.*, 1992, **83**, 917.
23. Y. Saito *et al.*, *Chem. Phys. Lett.*, 1993, **209**, 72.
24. M. Endo & H.W. Kroto, *J.Phys.Chem.*, 1992, **96**, 6941.
25. R.E. Smalley, Abstract from *4th NEC Symp. on Phys. and Chem...*, 1992.
26. D. Ugarte, *Chem. Phys. Lett.*, 1993, **209**, 99.
27. Z.G. Li, P.J. Fagan & L. Liang, *Chem. Phys. Lett.*, 1993, **207**, 148.
28. Y. Saito *et al.*, *Chem. Phys. Lett.*, 1993, **204**, 277.
29. W.A. deHeer & D. Ugarte, *Chem. Phys. Lett.*, 1993, **207**, 480.
30. P. Ross, *Sci. Am.*, 1991, **265**, No.6, 16.
31. P. Calvert, *Nature*, 1992, **357**, 365.
32. K. Tanaka, private commun.(in press).



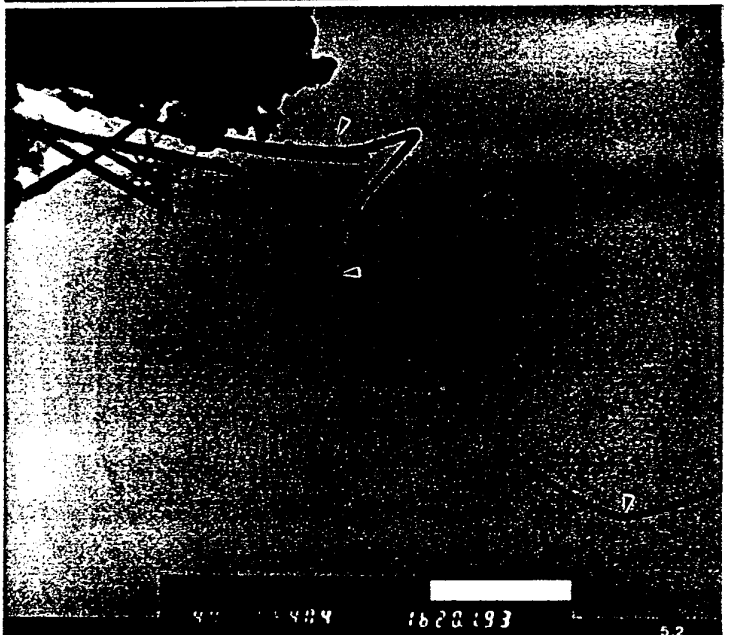


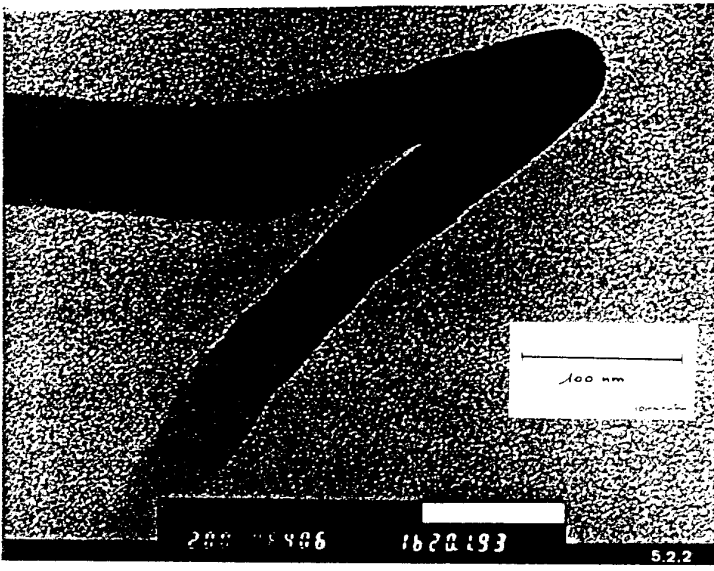
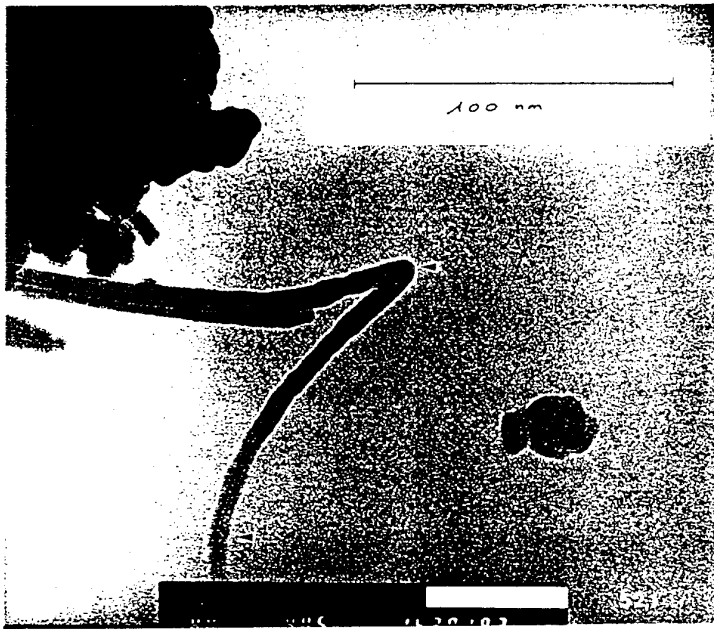


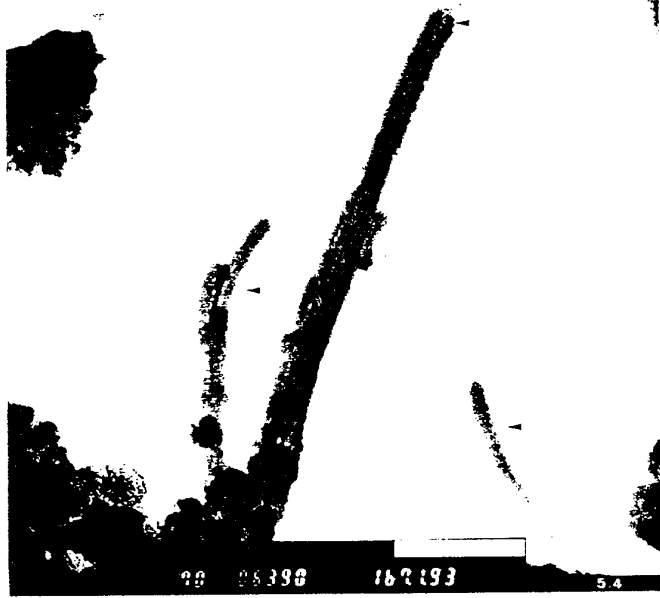
4.1

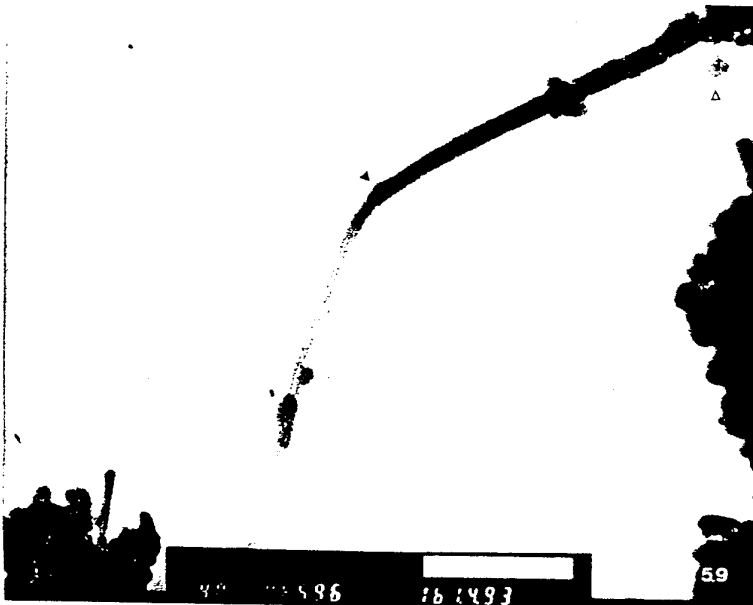
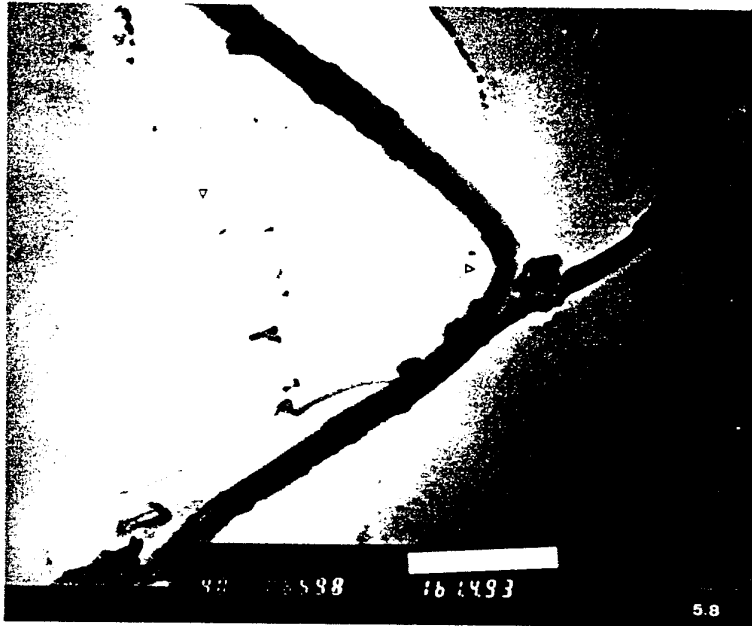


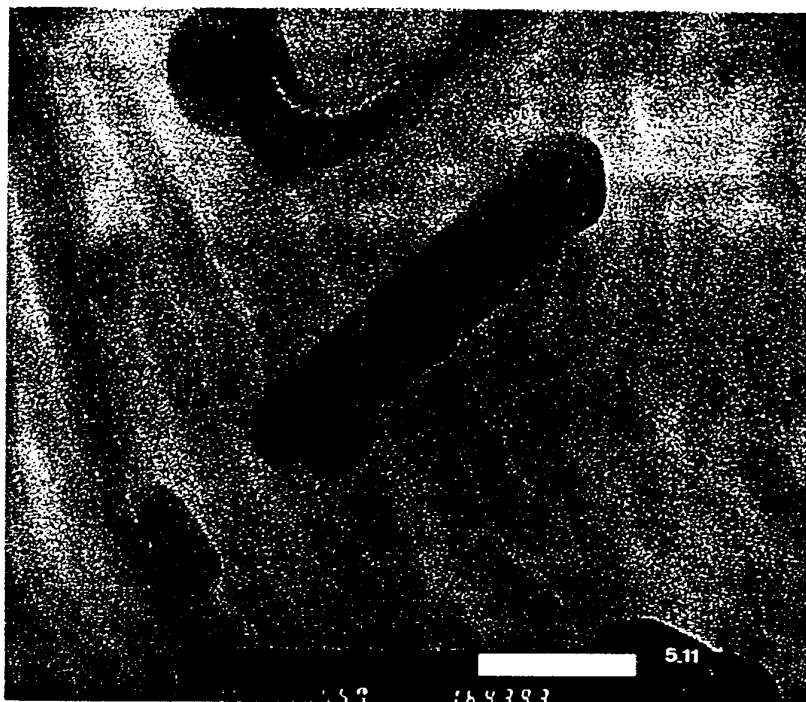
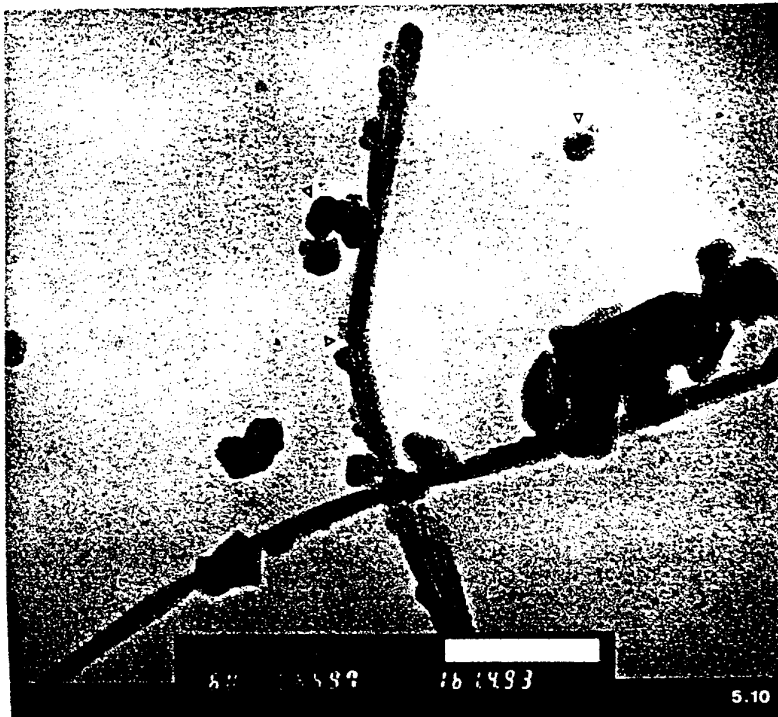
6.2



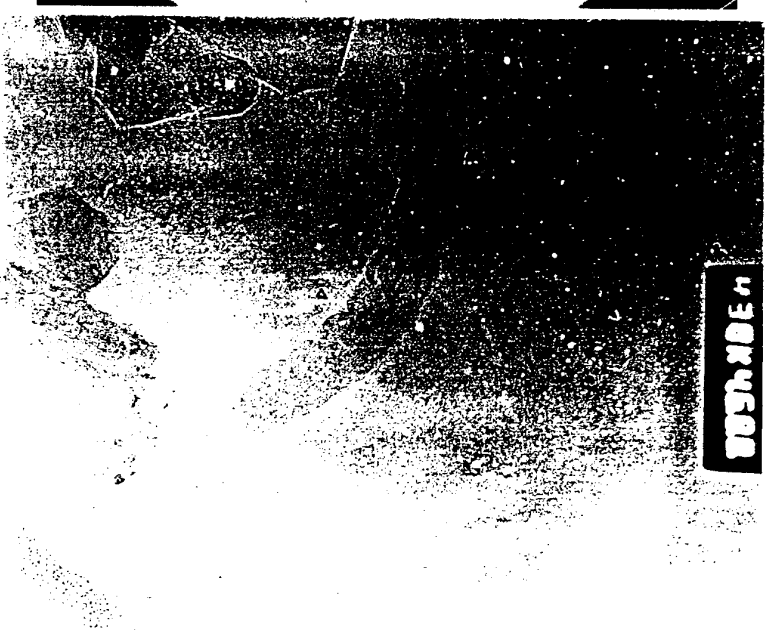
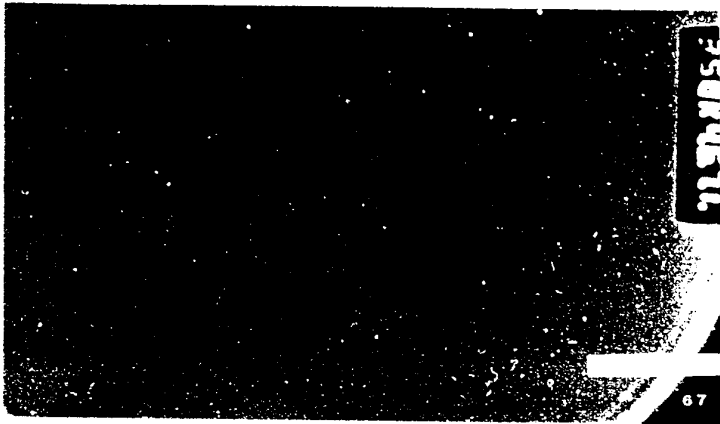






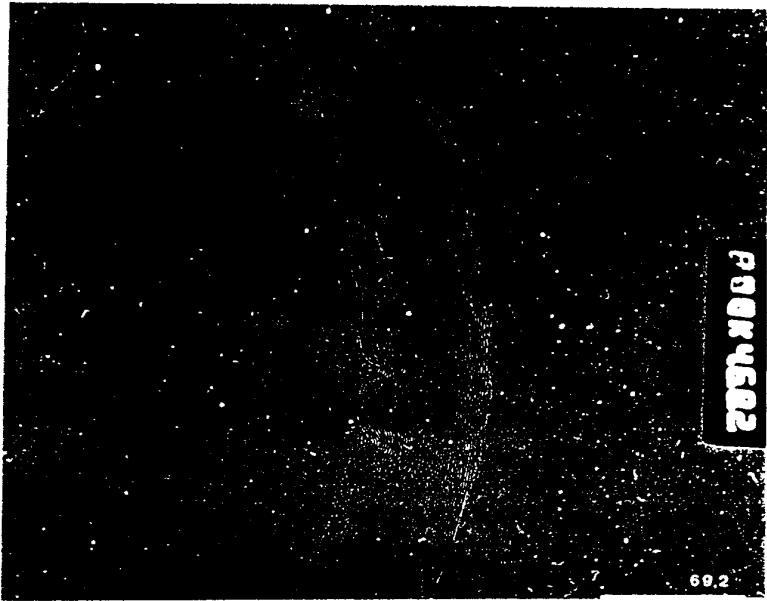


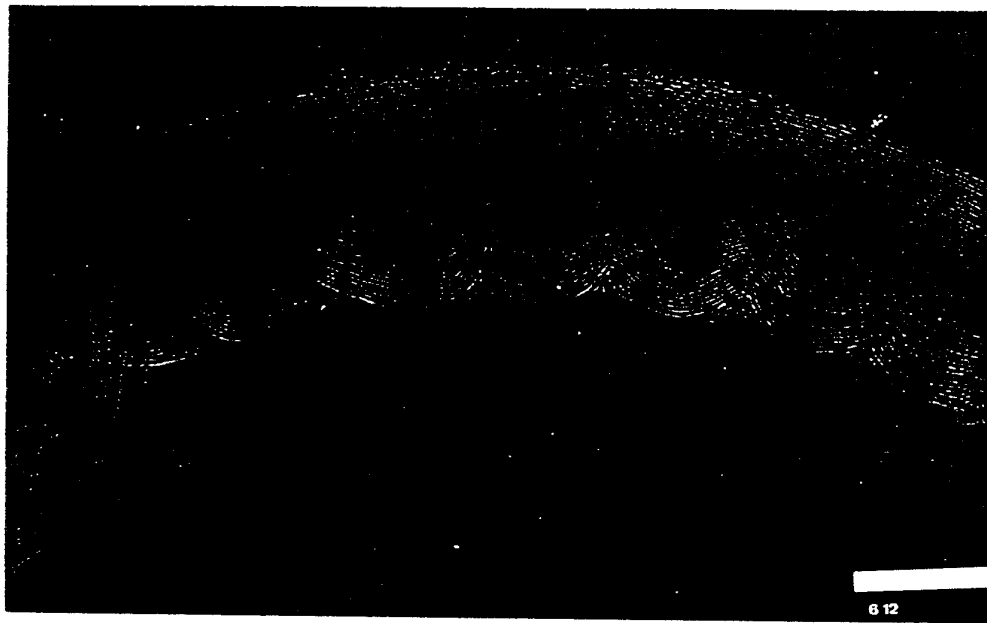
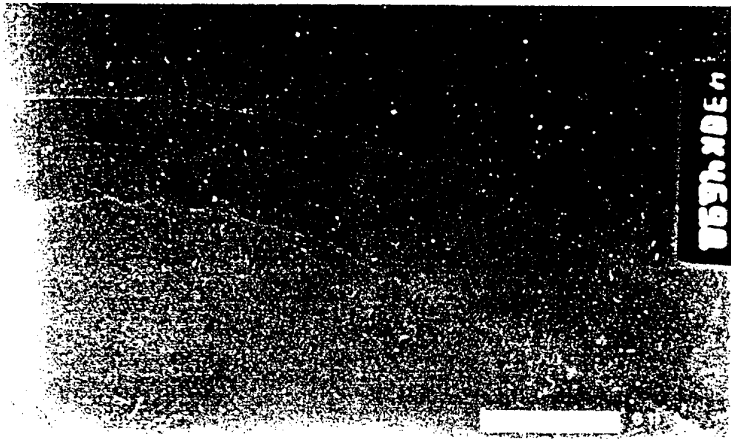


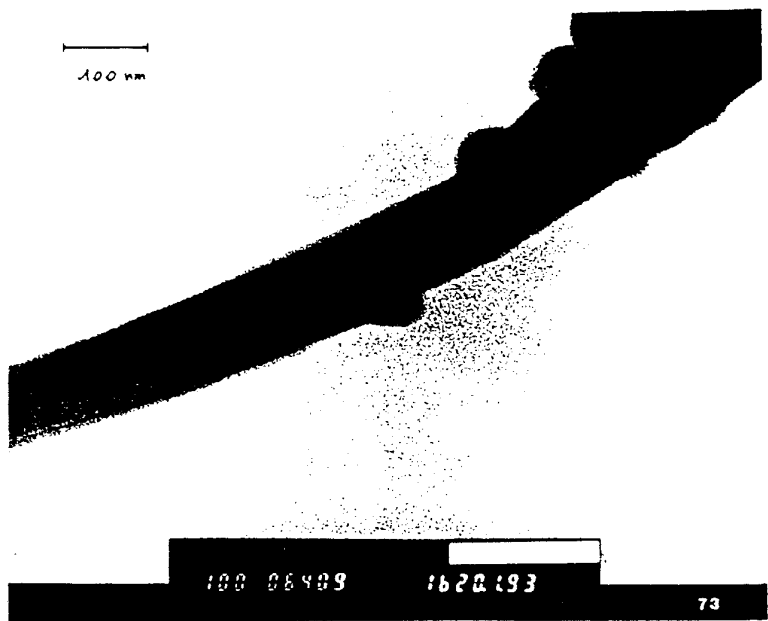
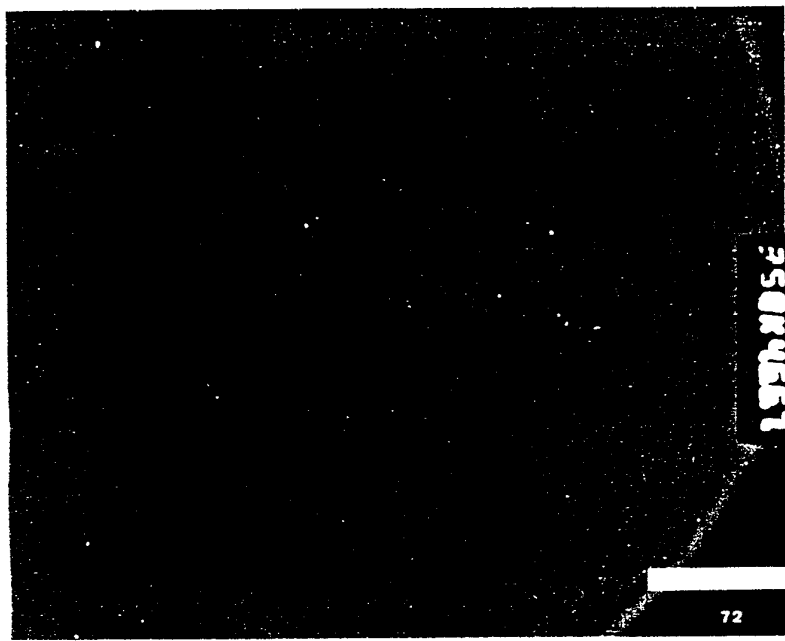
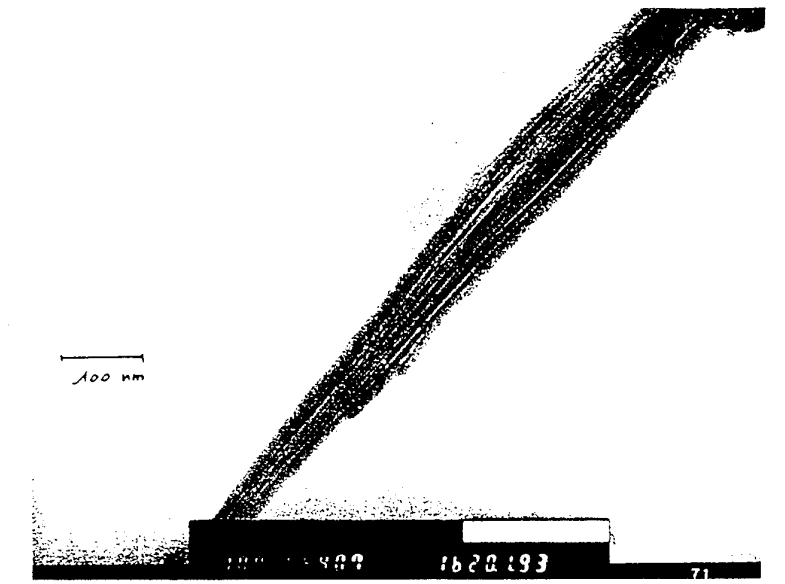


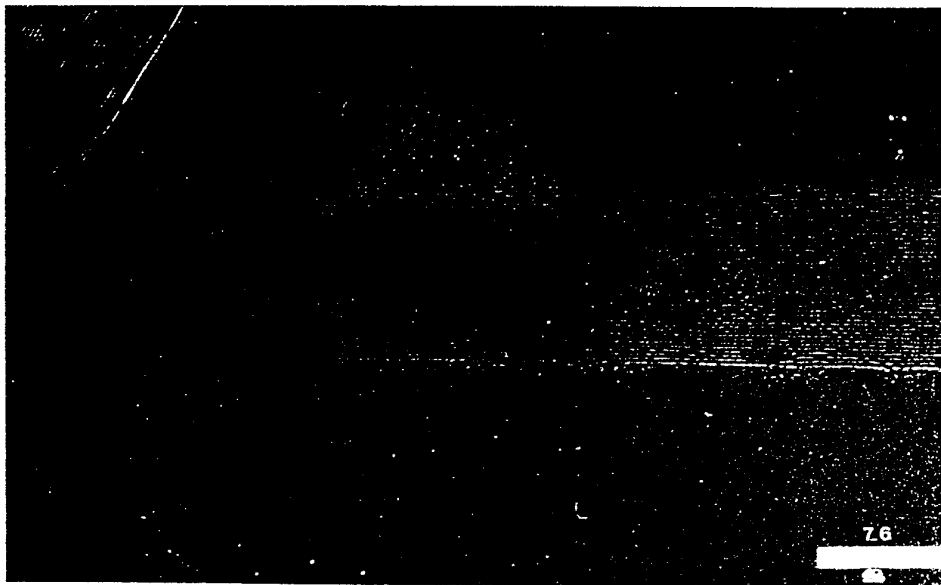
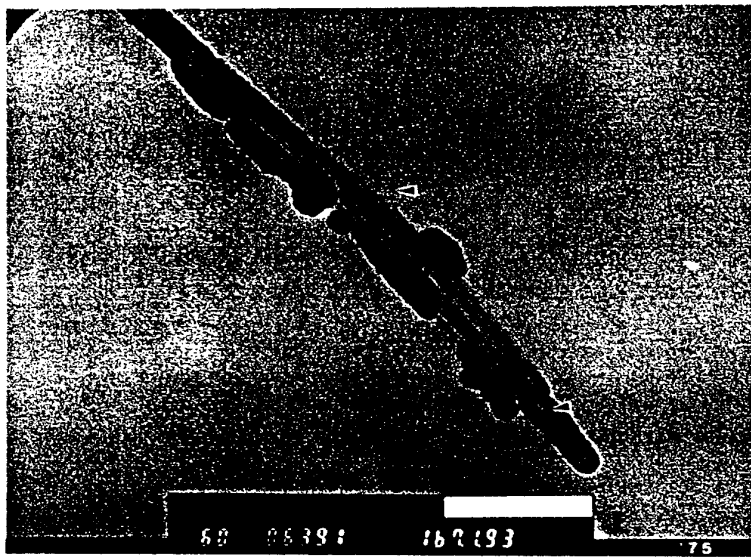
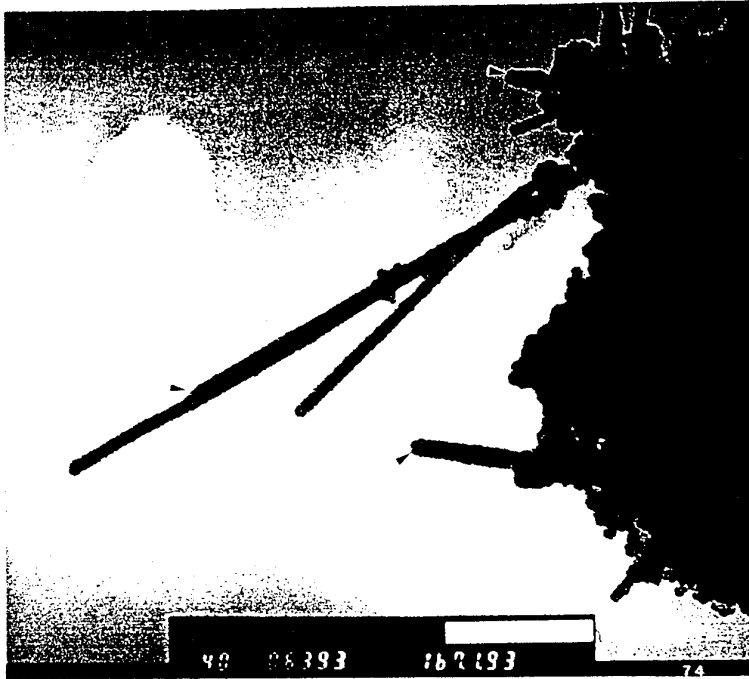
VI

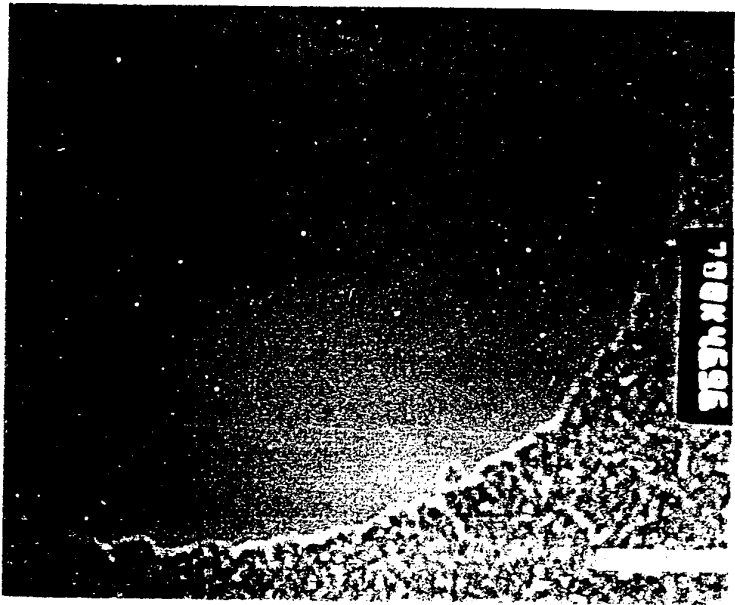
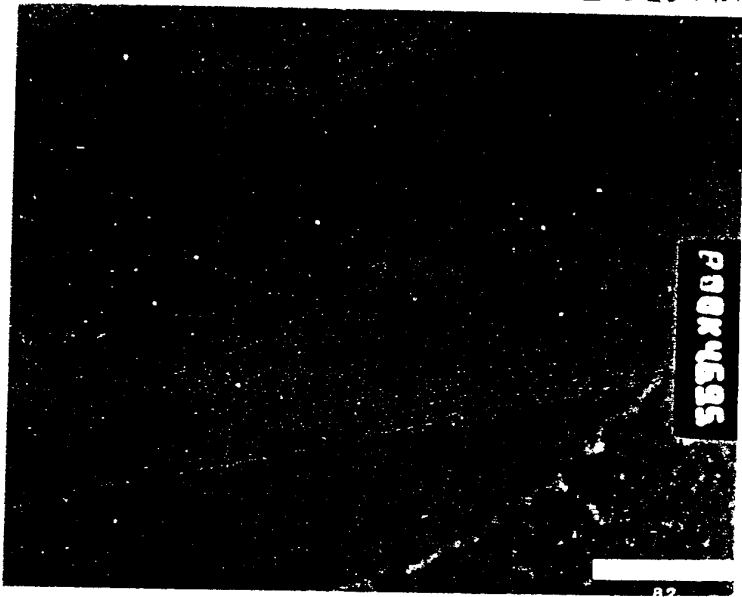
VI

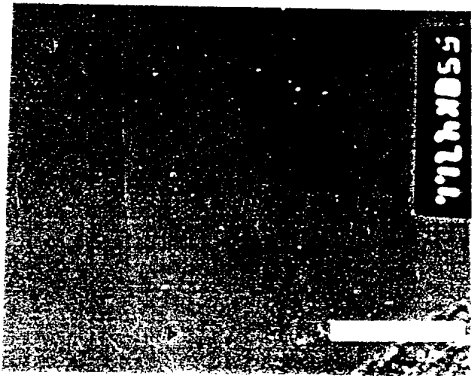
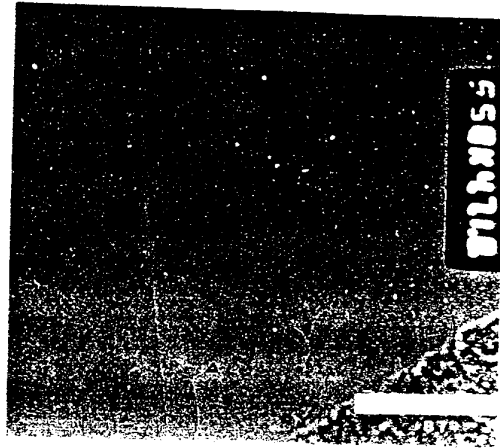
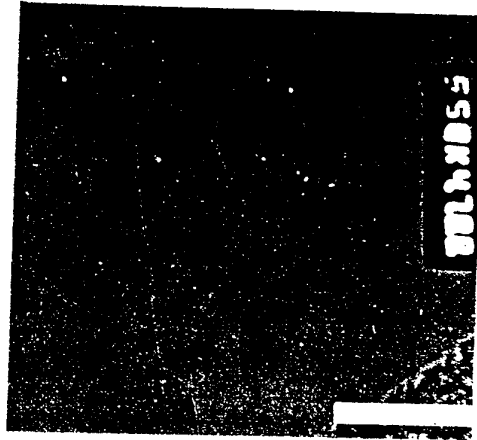
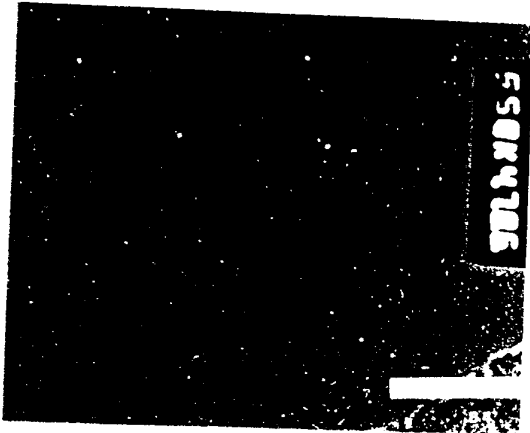


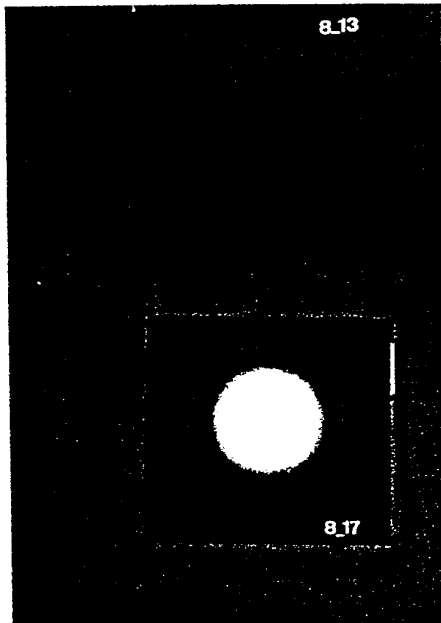
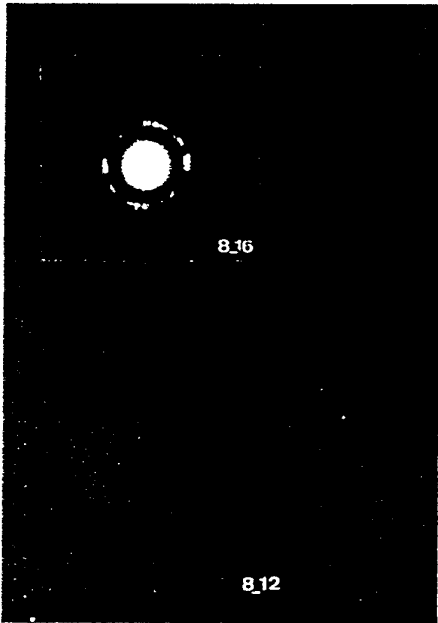
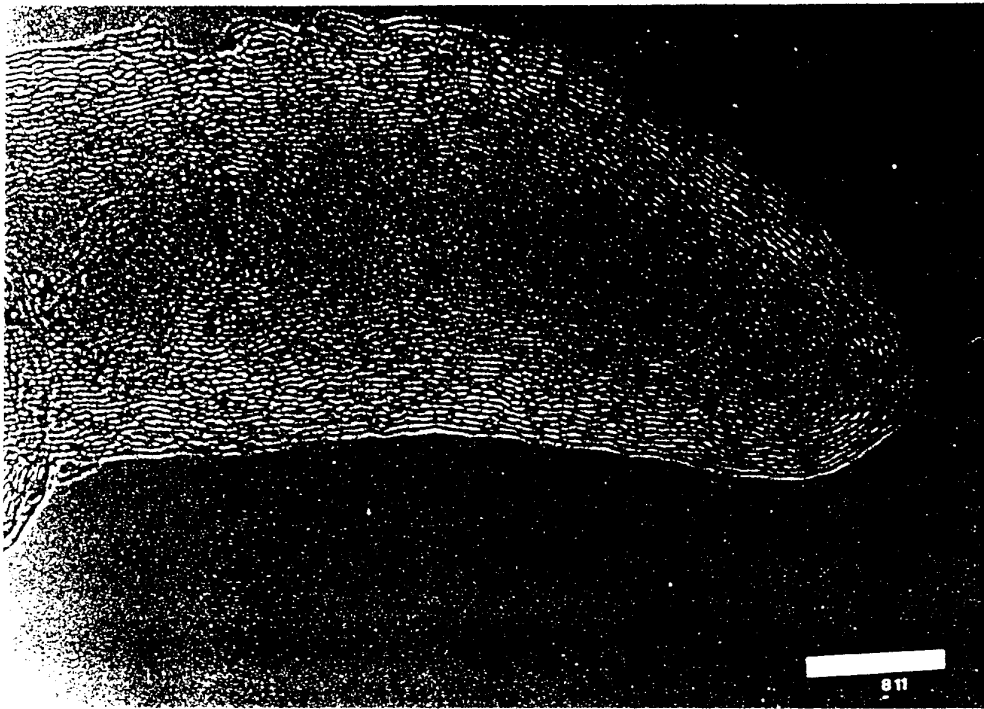










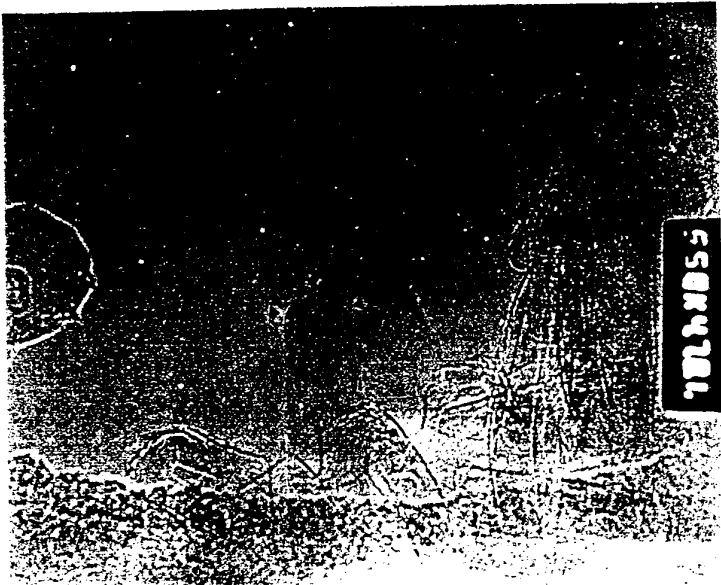
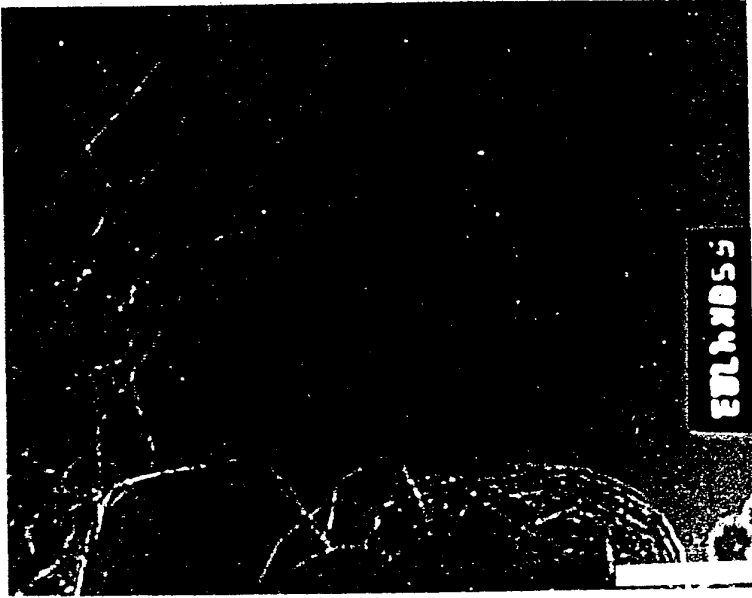
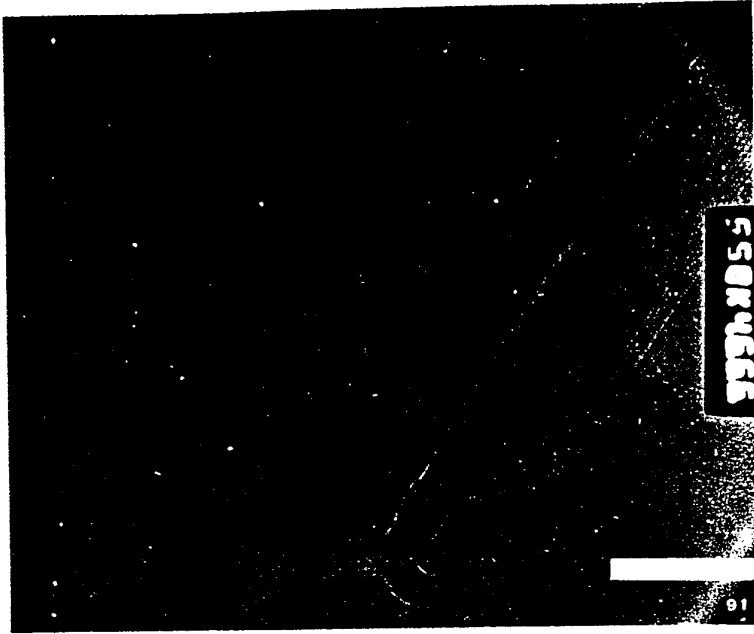




8 14

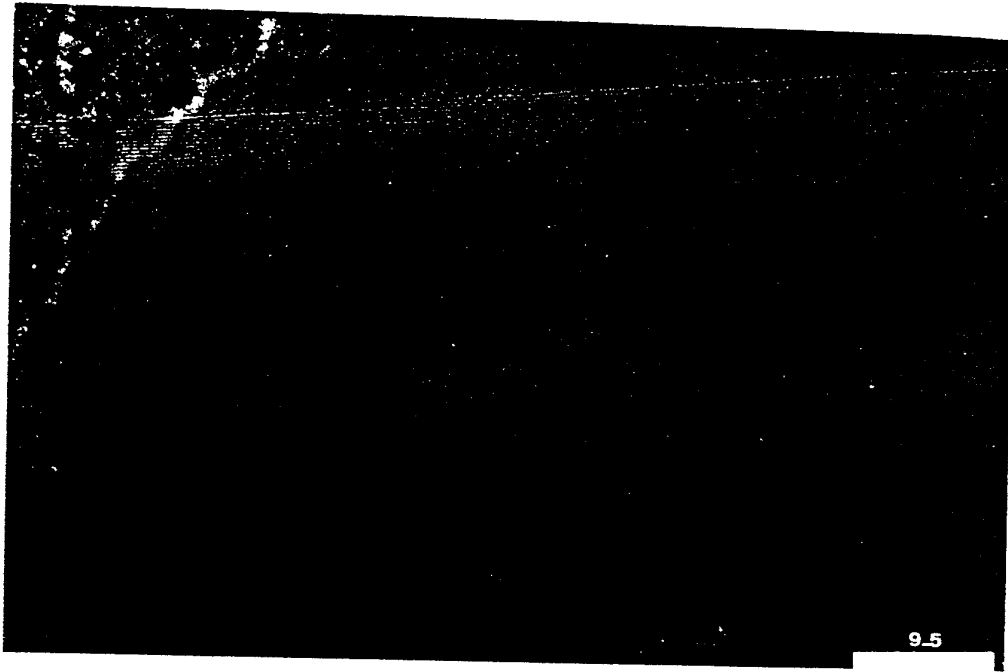


8 8

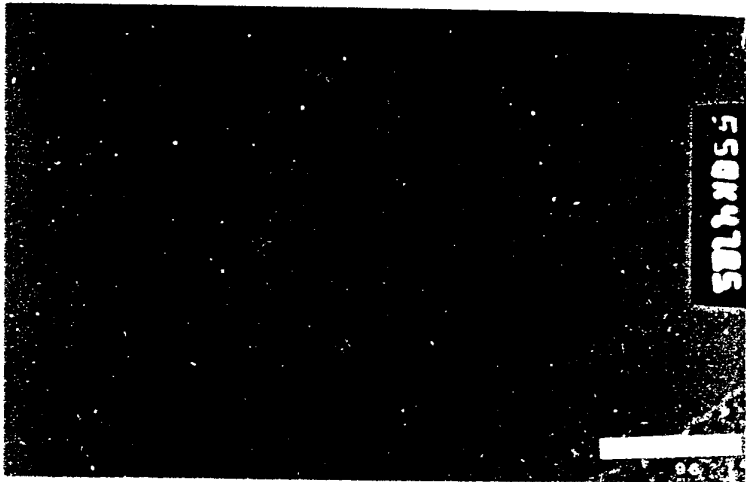




9.4



9.5



ESR4785

9.6

